ANNUAL TECHNICAL REPORT

DIVERTOR AND LIMITER TECHNOLOGY

PFC/RR 80-26

Editor: T. F. Yang

H. Becker
D. Blackfield
E. Erez
P. Gierszewski
J. L. Jones
L. M. Lidsky
J. Mc Murray
B. Mikic
D. B. Montgomery
E. J. Rapperport
N. Todreas
J. Tracey
A. Wan
M. L. Xue

T. Brogan (MPSCO)
Franklin Chang (Draper)
E. T. C. Cheng (GA)
J. Fisher (Draper)
D. Morgan (McD. D.)

TABLE OF CONTENTS

1.0 Summary

1.1 Overview

This report contains three major sections: (1) a review of the progress in the technology planning effort, and in the divertor concept development; (2) the combined technical conclusions and recommendations from the Divertor Technology Workshop at Albuquerque; and (3) individual contributions on specific topics.

The program has brought an awareness on the part of a wide spectrum of the experts in and outside the fusion community, and has generated a number of innovative concepts, such as a hypersonic gas jet target, phase-change solid-pellet targets, metal window pumping, and helium selective pumping (helium fly paper), high pressure cryosorption, and oscillating limiter concepts.

The major design achievement has been that a good bundle divertor configuration for ETF and INTOR has been found which can satisfy critical requirements for both engineering and physics.

The following sections expand on the specifics of these topics. Further details of the work in each area are given in the sections dealing with specific topics.

1.2 A Review of the Progress in FY80

The Divertor Developmental program was initiated in November, 1979, and ORNL contracted for the design and facricate of the ISX-B bundle divertor in August, 1979. The activities accomplished are listed in the following subsections:

1.2.1 Workshops

To inform the community of this project and to seek feedback, MIT has at various times arranged the following workshops:

- Target Miniworkshop, March 5, 1980, DOE
- Miniworkshop on ETF poloidal divertor
- Divertor Technology Workshop, April 10-11, 1980, MIT

1.2.2 Outside Activities

Full support of ETF divertor design, and participation in all levels of ETF Activities

MIT has also actively attended the following workshops to keep this program in line with other projects:

- INTOR Bundle Divertor Report
- Impurity control, Plasma Wall Interaction and Divertor Workshop on February 25-26 at DOE
- First Wall/Blanket Shield Workshop, March 1980
- Divertor, First Wall Material and Impurity Control Workshop, JEARI, Japan, March 17-20, 1980

- Sandia "Plasma"-Materials Development Workshop, June 24-25, 1980

1.2.3 Work Accomplished or in Progress

(1) Magnetic concepts development and divertor fabrication

The L-shaped bundle divertor concept has been proven. Many configurations using different combinations of L-shaped coils have been developed and studied. The ripple has been found to be reduced significantly so that the beam particles are contained. An engineering method has also been developed such that the divertor can be dismounted as a single unit.

The fabrication of divertor housing and winding for ISX-B has been finished and will be assembled and tested. The complete divertor assembly is anticipated to be shipped to ORNL in the spring of 1981.

In addition to these major accomplishments there is other on-going work listed as follows:

- Three versions of an internal poloidal divertor with minimized current have been obtained. The total current of each of these systems is about 25 MA-T as compared to as high as 100 MA-T for the external systems. An engineering concept for segmenting internal normal coils is in progress. The effort for next year is developing feasible engineering methods for maintainable internal divertor coil systems.
- An improved hybrid divertor configuration has been obtained and a detailed study is in progress.
- An improved concept of a mousetrap divertor has been conceived. A detailed study will be carried out when the engineering difficulties can be resolved.
- A study on hybrid divertor has been initiated, an extensive study will be carried out when the computational tools are ready.

(2) Divertor Shielding

A one dimensional shielding design study has been carried out by General Atomic and the minimal shielding requirement has been established. A three dimensional shielding Model for the bundle divertor is in the planning stage.

A survey of insulation materials is in progress. A follow-on test program on the irradiation and mechanical properties of G-10 insulation material done by MIT at Idaho for another project, is under consideration.

(3) Divertor Target and Limiter (MIT, MEPSCO, McD)

The following areas of work have been pursued at MIT and by outside contractors in order to gain an insight into future program planning.

- Solid target design study
- A general target characteristics and requirement study has been carried out by MIT.
- Active cooled limiter design study

- A specific limiter designed to be tested on Alcator has been carried out by McDonnell Douglas and is now in a second phase evaluation. Many unique configurations have been conceived by MIT, and a study is in progress.
- Gas Target (Draper Laboratory)
- A supersonic gas jet target has been conceived and studied by Draper Laboratory.
- An innovative oscillating limiter concept which can be cooled by helium and can stand high local heat load has been conceived.

(4) Plasma Simulation Sources

A number of forms of plasma sources have been evaluated. They have been narrowed down to decellerated low energy neutral beam and Hall accelerator. A design and small scale test of Hall accelerator is in progress.

(5) Bundle Divertor Modeling

A design window scheme has been developed for understanding material performance limits. An analytical method for modeling a bundle divertor has been developed and detailed computation is in progress.

2.0 Workshop Summary

2.1 Summary of Divertor Technology Workshop held at MIT in April

It is envisioned that the major elements of a divertor technology program will involve (1) development of concepts, (2) development of targets and pumps to handle the particle loads, (3) development of testing techniques to investigate concepts and proof-test components. These program elements will be integrated with existing or planned divertor experiments such as on ISX-B PDX and Doublet III, but will also investigate the independent plasma heat sources which might be appropriate for simulation of the condition in the divertor throat and target chamber.

A two-day workshop was called by MIT to discuss the technology issues involved. The goal of the workshop was better to define the needs of the divertor program, to assess the status of existing solutions, to reach some consensus for future directions and to gather the experts in the country to work together to solve technological problems related to the divertor and limiter.

The consensus of the workshop was that there are many important near term pilot scale programs which could be undertaken. The program should not be limited to the use of confinement experiments alone as test beds. Before components are put into a tokamak, screening is required, and it is particularly important in investigating novel target and pumping concepts, that some off-line facility be used for this screening. The near term recommendations are in the area of pilot-scale experiments to be done either on existing tokamaks or on largely existing facilities at "off-time". They involve areas such as material behavior, heat transfer experiments on various target concepts, and novel divertor and divertorless concept development.

2.1.1 Issues and Discussions

The particle and thermal handling problems for a typical 1000 mw reactor can be approximated by Table I. In the pessimistic case all the particles leaving the tokamak in a one confinement time have to be removed and only small back streaming is allowed. Because of high heat and particle fluxes high efficiency collectors and high heat transfer technology are needed. The material problems are also quite severe. The problems would be very much eased if 80% of the diffused particles could be recycled and a large fraction of the power can be radiated. This requires the realization of novel concepts such as gas target. In dealing with these problems, both older and new novel concepts have been discussed.

TABLE I

PARTICLE AND THERMAL HANDLING

For Typical 1000mw Reactor

PESSIMISTIC CASE	OPTIMISTIC CASE
$Q_p \cong$ 1500 Torr-liter/sec	Allow 80% Recycle
$Q_t \cong$ 200mw	Reduce the power by Impurity Radiation
$P_{vacuum} = 10^{-5}$ Torr	Operate at 10^{-3} Torr
Helium Back Streaming $\leq$ 1%	Pumping and Heat Loads can be Relieved
$A_{pumping} \simeq 1500m^2$ (For 10 $\ell/cm^2/sec$)	→ Gas Target
Target Area $\simeq 20m^2$	
Need High Efficiency Collector and High Heat Transfer Technology	

The Issues can then be listed as follows:

1. Can impurities and ash be handled in a divertorless concept?

2. What pressure can be maintained in a divertor chamber?

3. What is a practical heat flux to handle at a divertor target?

4. What surface materials should be used for the target?

5. Must the impurity control pump all the plasma components in order to remove ash and impurities?

6. Can a magnetic divertor concept be identified with acceptable engineering requirements and acceptable influence on injected alpha particles?

It was the general consensus that all the older known concepts suffer problems and all the new concepts have too many unknowns.

Thus, an impurity handling development program (whether it be divertor or divertorless) will have to develop concepts as well as components and an agressive program is required on an appropriate ETF time scale.

The discussions of the workshop were held in four separate groups: the solid target, novel concept, simulation and magnetic concept groups. Although magnetics form the central roll in divertor technology, it was not the major topic in the workshop because magnetics has been thoroughly discussed in various previous conferences. The summaries of the other three group discussions are given below.

2.1.2 Solid target/limiter

A summary of the solid target aspects has been established and listed in Table 2.

Three major development/design tasks have been identified as follows:

1. Thermal/mechanical test using a thermal source

This task would screen candidate configurations and materials on a macroscopic engineering basis (as distinct from surface physics consideration). The peak heat flux should be of order 1 kW/cm^2. The test target area should be about $0.25m^2$. Water and helium can be equally considered.

2. Surface Physics Development

This task would produce the engineering data on surface physics characteristics (gas retention, release, trapping reflection, sputtering and impurities) necessary to define the design options for solid targets.

3. Composite Test Using a Neutron Beam or Plasma Source

This test would be mounted on the design concept derived from the two programs above. The source would mockup the particle and thermal loadings characteristic of a reactor divertor. Consequently this test awaits development of a suitable source which could provide the necessary particle energy level over a suitable area with the desired reactor cyclic behavior.

TABLE 2

SUMMARY OF SOLID TARGET ASPECTS

PARTICLE HANDLING	STATE OF ART	DEVELOPMENT NEEDS
Retention Release Surface Chemistry Sputtering	Present data in the range 10^{14} - 10^{16}/cm^2 sec particle flux at > 1 kev	Perceived need in the range 10^{17} - 10^{18}/cm^2 sec from 0.1 - 10 kev Necessitate new source development Sputtering data for composite target and for beam with a spectrum of energies Study hydorgen diffusion process in target
MECHANICAL DESIGN Thermal Cycling Thermal Schock Irradiation Damage	1 kw/cm^2 thought to be acceptable	Establishment of upper heat flux, studies of target life and behavior at 1 kw/cm^2 over target area 50 cm X 50 cm

TABLE 2 CONTINUED

THERMAL DESIGN	Water Cooled 10 kw/cm^2 over 9 cm long Swirl tube 1.57 kw/cm^2 average and 2.9 kw/cm^2 peak over 25 cm long 4 kw/cm^2 over 6.5 cm tube axial flow jet nozzles at 10 kw/cm^2 for minutes MHD Generator at 1 kw/cm^2 steady state Helium Cooled .2 kw/cm^2 Liquid Metal limited	Two regimes of thermal hydraulic design: 1. 1 kw/cm^2 non boiling water 2. 2 - 5 kw/cm^2 for more challenging task

2.1.3 Alternative Concepts

The novel concepts being discussed are listed as follows:

1. Lithium pellet absorber
2. Lithium rain
3. High pressure cryopumping
4. Hypersonic gas target
5. Gas target and helium enrichment
6. Removal of helium with differential pumping method
7. Moving metal belt

   Reflect hydrogen and trap helium
8. Window pumping

   Reflection of helium and diffusion of hydrogen through the target
9. Electrotatic trapping
10. In-situ or external recoating

2.1.4 Plasma and thermal simulation sources

The plasma and thermal sources can be classified into generic source and surface heater. The generic sources are the most desirable but not yet available. The potential sources are:

1. Neutral beams

   There are high energy and high current pulsed beams available at ORNL and LBL. A low energy and high current beam has also been developed at the University of Wisconsin.

A suitable decellerating neutralizing cell could probably be used to give a very close match to the actual distribution spectrum at plasma edge.

2. Hall accelerators

The Hall accelerators have been studied for possible heating source for tokamaks. There seems no basic physics reason precluding steady state operation. There are many surface heat facilities, such as ARC Jets, E-Beams and radiant heat source available in the nation. In order to use such facilities, some simulator specifications have to be defined. A preliminary list is given below:

Heat flux

Ion temperature

Electron temperature

Species fraction

Operating time

Operating pressure

Finite size effects

Collination

Duct charge exchange

Cyclic pressures

Alpha-particle effects

Cold gas component

Magnetic geometry

The ideal test beds are of course the tokamak facilities. The tokamak devices with high heat and particle fluxes are ISX-B, PDX, Alcators, PLT and Doublet III.

PROGRAM RECOMMENDATIONS

1. The divertor technology program should be multifacited and make maximum use of existing facilities and experts groups throughout the country.
2. Miximum use should be made of existing divertor confinement experiments like PDX, PDX-Up-Grade and ISX-B to measure parameters of engineering importance such as divertor duct and chamber parameters and surface plasma effects at the targets. Non-diverted tokamaks, particularly high power density machines like Alcator, should increase their investigation of non-diverted impurity control.
3. A long pulse tokamak such as ISX-C, can provide the vital link required before ETF relevant divertor (or divertorless) concepts can be confirmed. The impurity control technology program should take part in the planning of that machine in order to maximize its usefulness to the technology program.
4. The program should not be limited to the use of confinement machines. Maximum use should be made of pilot scale experiments on existing or modifiable "off-line" facilities.
5. A pilot scale design and test program should begin immediately on one or more potential target configurations to establish realistic design limits.
6. A major activity to develop suitable surface coatings and to characterize those materials under realistic conditions must be undertaken. These activities can obviously build on the plasma surface material development programs, but would be more design specifics.

7. The program should encourage the development of novel concepts, which show potential to relieve the possible "Fatal Flaw" problems associated with current solid target concepts. Off-line facilities and small tokamaks will be particularly valuable in this aspect of the program.
8. Finally, the program should encourage the development of divertorless concepts.

2.2 "Plasma"- Material Workshop in Albequerque - Divertor Group Summary

In accordance with the theme of the workshop discussions, this group was primarily concerned with material aspects of divertor plates (neutralizing targets or collectors). Lithium pellet, lithium rain, hypersonic gas target, gas target, and other novel divertor target ideas discussed in the April Divertor Workshop at MIT were only mentioned briefly. The need for material development work as discussed at MIT Workshop is reconfirmed and specifics have been worked out in this discussion group.

An integrated divertor system consists of magnetic, vacuum and target components. It is difficult to single out the material issues. In particular, the effect of the plasma on the material of the plates are closely related to the vacuum condition in the divertor chamber. Lately, a number of proposed novel concepts have presented a very optimistic picture on the requirements of a target. The most attractive concept in the gas target, which may reduce the heat load on a metal plate, is serving as a neutralizer. The effectiveness of such a concept for both target plate protection and He management needs to be seen. However, the interaction of plasma with material always exists and the material cannot be eliminated altogether, especially in the divertorless case. In this discussion group some innovative ideas involved the use of material as both thermal and particle handling have also been proposed. Therefore, it is agreed that the development of material plates and the understanding of the characteristics under a wide expected range of conditions is urgently needed.

For the solid target ideas, the group concluded that the development effort should be approached in two phases. In the

initial phase, already in progress, the various issues should be studied for small samples and medium size tiles using existing or upgraded specialized facilities. The group identified three major areas of development needing attention during this phase.

1. Thermal-mechanical design
2. Concepts for hydrogen and helium management
3. Surface materials response

Phase II studies are required to bring together information gathered in these areas to produce engineering designs and to test these designs where possible under simultaneous heat and particle fluxes with appropriate pumping geometry. Large area test facilities for this phase have not yet been identified.

The three Phase I study areas are summarized below with appropriate test conditions. The interaction of these efforts is shown schematically in the block layout (Fig. 1). Although some interaction occurs between the areas, the group felt that at this stage they should be pursued in parallel. This is justified under the particle management concept which isolates the three -- a hot, non-retaining surface layer and auxillary H and He gas pumping. Improvements over this approach can then be pursued independently.

Phase I Program

1. Thermal/Mechanical Design

This task would screen candidate heat transfer configurations and structural materials on an engineering basis. It would test prospective designs for:

a) thermal fatigue and shock resistance,

b) internal erosion resistance in the coolant channels and

c) heat transfer correlations and critical heat flux or burnout conditions.

The latter is of concern for future particle management concepts where surface temperatures become important. It was generally felt that the heat transfer to a forced coolant is not too difficult for fluxes of 1 kW/cm^2 or less, over reasonably-sized tile areas. However, a review of existing correlation data indicated that gaps exist in the forced convection and nucleate boiling regimes, particularly for high flow velocities at modest pressures. Thus, the heat transfer correlation and critical heat flux should be measured where missing for a range of flows, pressures, swirls (internal roughenings) and coolant channel geometries. Although the primary coolant candidate is water, helium gas and liquid metal coolants should also be considered.

Special substrate structural materials of high thermal conductivity and failure resistance should be explored. Their thermal fatigue and shock resistance should be studied first at 1 kW/cm^2 for 10^3 - 10^4 thermal cycles, then at higher power densities to handle possible peak conditions. Sample tiles could be tested with areas of about 10 x 10 cm, then perhaps 50 x 100 cm tiles or arrays.

Novel cooling approaches were discussed as possible alternatives to force-convection. Spray jet concepts using the latent heat of vaporization of water to cool surface are in existence but their reliability is a question. Heat pipes have been studied for use in cooling laser mirrors with uniform heat fluxes of about 0.5 kW/cm^2.

Existing high heat flux facilities must be utilized for the development of these ideas as well as for more conventional heat transfer solutions.

2. Concepts for Hydrogen and Helium Management

Novel, innovative ideas and their development are needed to solve the particle management problem. Here the task is to store the hydrogen isotopes and helium ash at the collector plate, remove the helium and recycle the hydrogen fuel to the plasma. Possibilities for this gas management are:

a) stop, re-emit, and continuously pump both H and He from the system,

b) trap and outgas He from the plate between pulses (to be pumped along with some H),

c) trap H, but re-emit and pump He during pulses, then outgas H between pulses, or make H diffuse through the metal,

d) trap and bury He in the plate for later removal and processing outside the system, and

e) trap and remove He from the system, then desorb and recycle (as on a belt, disc, drum, etc.). -- He fly paper

Each concept requires specialized coatings, for the collector plate, with controlled trapping and re-emission properties. Development of concept-oriented coating materials and composites should be pursued. For many of these concepts, in-situ coating replenishment must also be considered.

Evaluation of management concepts can be done with small scale experiments. For these tests, simultaneous H and He ion fluxes are needed over small areas (about .5 x .5 cm).

Although uncertain, ion energies are postulated to be about 1 keV at fluxes of about 10^{17} cm^{-2} s^{-1}. No experimental facilities are known which produce these conditions.

3. Surface Materials Response

A key issue brought out in the initial presentations and echoed in the divertor working group was that of particle erosion. It was decided that one must be optimistic about the particle flux and require it to be a reasonable level. Additional issues pertaining to handling the particle load are:

a) erosion due to sputtering, blistering, chemical, and arcing effects,

b) retention, re-emission, and diffusion of H and He, and

c) radiation damage from H, He, impurities, and neutrons.

The task of this area is to evaluate existing and develop new cnadidate coating/cladding materials with regard to these issues. Testing can be done using small scale (.5 x .5 cm areas, or smaller) controlled experiments. However presently available test conditions of 10^{14} - 10^{16} cm^{-2} s^{-1} at 1 keV should be improved to the proposed fluxes of 10^{17} - 10^{19} cm^{-2} s^{-1} at .1 - 2 keV.

Phase II Program

In this program the near term goal to make available one or more reliable modules for ETF is emphasized. Studies are proposed to test the survival of prototype divertor collector plate designs under both the thermal and particle loads. Testing should be done over large areas in order to evaluate thermal/mechanical behavior.

Fluxes should be averaged over 10 x 10 cm to 25 x 100 cm areas, at 1 kW/cm^2 with 1 keV H and He, and in a vacuum environment of about 10^{-4} Torr. Possible facilities for this testing include modified neutral beam and plasma sources, and tokamaks. Impurity ash removal and fuel recycling would not be necessary in initial designs. In the advanced design the surface replenishment such as in-situ coating, the helium and impurity removed and possible fuel recycling should be considered.

Divertorless Approach

In the divertorless situation the particle and heat removal will be accomplished by specially designed limiter and/or first wall configurations. There is no distinguished line between limiter and divertor plate. The material problems and development needs are quite similar.

In principal, the divertor chamber can be outside the plasma column and thermal and particle problems can be handled externally. For the divertorless situation, all the thermal and particle loads have to be handled inside the torus. Frequent replacement is difficult. Modular life time and surface replenishment are important.

For comparison, the group gave some consideration to two divertorless approaches. The first was that of a rail limiter, which in the very worst case may be expected to experience 15 kW/cm^2, 10^{20} paritlces/cm^2 - s. In addition to posing a serious heat transfer problem, such an approach would require in-situ coating redeposition. The second case was that of allowing the plasma

to contact the entire first wall. Here fluxes are about 0.1 kW/cm^2, $< 10^{17}$ particles/cm^2- sec. Again in-situ recoating would probably be required for a reasonable life.

Conclusion and Recommendations

For quick reference the novel concepts, target thermal problems and issues given in the last three secions are condensed and tabulated in Tables 1 through 5. The expansion on novel concept is encouraged.

The group recommended small to medium size scale, controlled Phase I experiments in three areas: heat transfer/mechanical design, hydrogen/helium management concept evaluation, and surface materials response. These should be followed by larger scale, proof-test experiments on prototype designs. Overlap of the two phases is necessary.

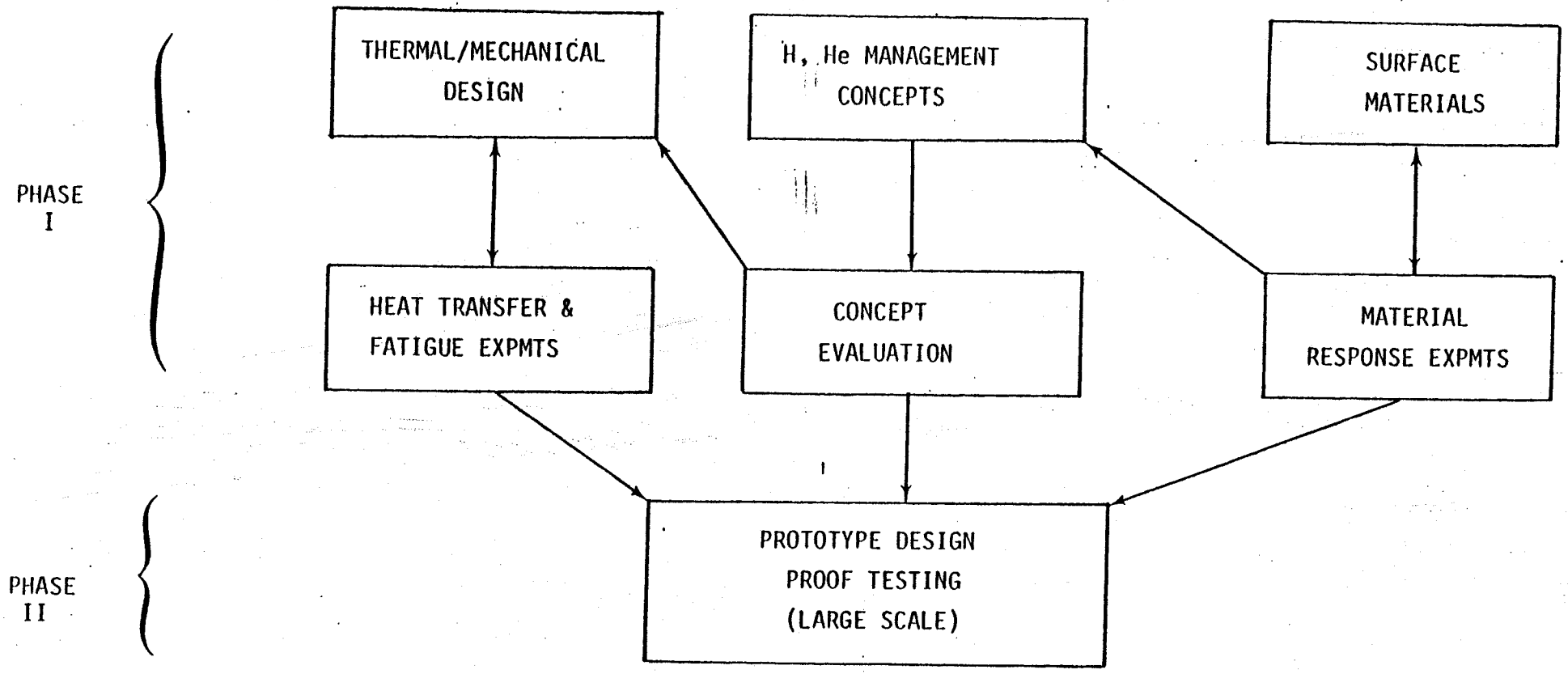

Figure 1. Divertor target or collector plate development plan

TABLE 1

NOVEL CONCEPTS

1. GAS TARGET AND HELIUM ENRICHMENT
   REMOVAL OF HELIUM WITH DIFFERENTIAL
   PUMPING METHOD
2. HYPERSONIC GAS TARGET
3. LITHIUM PELLET ABSORBER
4. LITHIUM RAIN
5. HIGH PRESSURE CRYOPUMPING
6. MOVING METAL BELT (HELIUM FLY PAPER)
   REFLECT HYDORGEN
   TRAP HELIUM
7. WINDOW PUMPING
   REFLECTION OF HELIUM, DIFFUSION OF HYDROGEN THROUGH METAL
8. ELECTROSTATIC TRAPPING
9. IN-SITU OR EXTERNAL RECOATING

TABLE 2

TARGET THERMAL PROBLEMS, ISSUES, AND RECOMMENDATIONS

1. FATIGUE (THERMAL SHOCK)
2. INTERNAL EROSION DUE TO COOLANT
3. CORRELATION

   TO ESTABLISH PHYSICAL COEFFICIENTS AND BURN OUT CONDITIONS

   - FOR RANGE OF FLOWS, PRESSURES, SWIRLING OR ROUGHENING
   - FOR WATER, HE, (LIQUID METALS?)
   - FOR 1 KW/CM^2, THEN HIGHER
   - FOR 10 CM X 10 CM SURFACE AREA THEN 50 CM X 50 CM OR 25 CM X 100 CM
   - FOR APPROPRIATE MATERIALS (CU, CU ALLOYS, TA, MO, N6 AND ALLOYS)
   - NEUTRON DAMAGE
4. NOVEL APPROACHES

   JET, HEAT PIPE, ETC.
5. ALTERNATIVE APPROACHES

TABLE 3

CONTROLLED EXPERIMENTS

CONDITIONS

NEED { 10^{17} - 10^{19}/cm^2-SEC; .1 - 10 KEV }

NOW { 10^{14} - 10^{16}/cm^2-SEC; > KEV }

ISSUES

- EROSION (SPUTTERING, BLISTERING, CHEMICAL, ARCING)
- RETENTION, REEMISSION (DIFFUSION)
- RECOATING (IN-SITU, EXTERNAL)
- RADIATION DAMAGE
- IMPURITIES PROBLEMS
- PARTICLES HE, H, D, T, HEAVY IONS

CONTROLLED EXPERIMENT	CONCEPT EXPERIMENT
FOR COLLECTING DATA SYSTEMATICALLY WITH LARGE FLUXES AND FLUENCES ON SMALL SAMPLES (.5cm x .5cm)	• STOP, RE-EMIT AND PUMP CONTINUOUSLY • TRAP, OUTGAS BETWEEN PULSES AND PUMP • TRAP AND BURY FOR LATER REMOVAL EXTERNALLY • TRAP AND REMOVE FROM SYSTEM • BELT, DRUM, RECOATING, ETC.

TABLE 4

PROOF TEST EXPERIMENTS - (NEAR TERM GOAL)

- CONDITIONS

  1 KW/CM^2, 10 CM x 10 CM - 25 CM x 100 CM

  1 KEV (H, HE), $\sim 10^{-4}$ TORR

- FACILITIES

  NEUTRAL BEAMS, PLASMA SOURCE

  TOKAMAKS:

ISX-B	DOUBLET-III
PDX-	ISX-C
PLT	EBT
ALCATOR	MICROTOR

- PARTICLE AND THERMAL LOADING CHARACTERISTICS OF REACTOR DIVERTOR (ALL PARTICLE COMPONENTS)
- SURVIVAL EFFECTS

  MECHANICAL, LIFE TIME, VACUUM INTEGRITY
- IN-SITU OR EXTERNAL REDEPOSITION OF SPUTTERED MATERIALS
- HE AND IMPURITY REMOVAL AND FUEL REGENERATION

  (ADVANCED SOLID TARGET SYSTEM)

TABLE 5

ISSUES (DIVERTORLESS APPROACH)

THE FOLLOWING EXTREME CASES ARE LISTED TO SHOW THE RELATIONSHIP BETWEEN DIVERTOR AND DIVERTORLESS AND THE DEVELOPMENTAL NEED.

1. MOST PESSIMISTIC CASE - RING LIMITER
   15 KW/CM^2, 10^{20}/CM^2-SEC
   REDEPOSITION
   IN-SITU COATING
   THICKWALL
2. MOST OPTIMISTIC CASE - FIRST WALL SURFACE
   $\sim$ 100 W/CM^2, $< 10^{17}$/CM^2-X
   INSITU COATING

RECOMMENDATIONS

PHASE I (SMALL SCALE)
- CONCEPT EVALUATION
- MATERIAL RESPONSE
- HEAT TRANSFER
- HE REMOVAL

PHASE II (LARGE SCALE)
- PROOF TEST
- PROTOTYPE

3.0 Divertor Magnetics

3.1 Bundle Divertor

It has been discussed by many authors [1,2,3,4] that bundle divertors can be greatly improved by varying the coil configurations. The designs of a bundle divertor for reactors have been discussed in detail in references [1] and [2] and were found to be feasible. However, there were still many shortcomings which needed to be resolved. Two of the major shortcomings were: that the ripple is too large, which enhances the loss of energetic particles; that the current required in the divertor coil is too large, and the divertor coils interfere with the TF coils, making the maintenance difficult. To alleviate some of these problems a short T-shaped coil configuration has been proposed by T. Yang [4] and a long T-shaped hybrid divertor has been proposed by H. Furth [5]. This divertor configuration is illustrated by Figure 1. As has been discussed in the 1979 U.S. INTOR report and in reference [4], the horizontal conductor elements will increase the divertor field required to cancel the toroidal field and will also enhance the radial component of the diverting flux lines. Such a divertor requires less current and thus produces lower ripple. Another method of reducing the ripple is to use an "X"-shaped four-coil arrangement like a small tokamak, proposed by R. Dory and John Sheffield [2]. All these configurations have been examined in this report. It is found that four coil configuration gives the lowest ripple but the associated engineering problems are too difficult. A compromised physics and engineering solution can be obtained from the two T-shaped coil configurations.

Magnetic Concept

Magnetic Configuration

The plasma parameters and TF coil number and size used in this study are listed in Table 1.

Table 1. Key parameters for INTOR and ETF used in this study.

	= INTOR	ETF
R_0	= 5.2 m	5.5 m
B_0	= 4.8 T	5.5 T
a	= 1.3 m	1.4 m
R_{TF}	= 10.5 m	11.5 m
$TF\sharp$	= 12	12

*R_{TF} (outer radius)

There parameters are chosen partly based on the INTOR and ETF space under consideration, and partly for computational convenience. They provide information and comparison for different sizes and field intensities and a flexible range when choosing final parameters. The coil configurations studied here are shown in Figure 2. The typical flux patterns for these coil configurations except (a) are shown in Figure 3. The magnetic configuration of coil type (a) is similar to Figure 3(c). Configuration 3(b) shows the T-shaped divertor with expander coils. It shows that flux can be led to the outside of the TF coils and expanded which makes the particle removal and thermal handling easier. The configuration (c) was considered to be desirable for lower ripple and energetic particle containment. The major disadvantage is that the magnetic intensity at the middle of the diverted flux loop, is 17 Tesla, i.e., the field becomes the strongest and the flux tightest at this point where expansion is needed most. The 17 Tesla field makes the expansion nearly impossible. An attempt has been made to expand the flux or reduce the field intensities by opening the outer legs as shown by configuration 3(c) and by changing the coil shape as shown by Figure 3(d). The gain is insignificant. The radially outward translational force in configuration 3(b) is approximately equal to 20 MN whereas it is nearly zero in configuration 3(c). In the configuration 3(c) the interaction of the divertor with the TF coil is negligible. From the engineering point of view it is nearly an independent structure since minimal structure is required to hold the divertor assembly in place. As will be discussed in the mechanical section, the divertor can still be designed as a plug-in unit for case (b). Lacking an adequate method to expand the flux, or to remove the particle and heat load in the very tight space in case (c) and (d), we will concentrate our effort in optimizing case (b). To determine the optimized design parameters, the field ripple on axis and the divertor current are plotted in Figures 4, 5, 6 as functions of height, width and length, while the coil position and separatrix are fixed. Figure 7 plots the ripple and the position of the separatrix as function of current. The design point for INTOR is shown by the dot. The

choice was made based on many engineering and physics considerations. For physics consideration one would like to make the ripple as small as possible. The ripple reduces linearly as the width reduces and the length increases. However, the current requirement increases in both cases. The ripple and current decrease with the height and there is obviously no lower bound. Therefore, physical contraints have to be considered for making the selection of parameters.

For the convenience of maintenance, the width of the divertor assembly was chosen to be smaller than the gap so that the whole assembly can be removed without interfering with the TF coils. The width and height are also the minimum required to allow 30 cm of shielding on each side, 30 cm of plasma duct, 50 cm of conductor pack, and 10 cm of structure. The amount of shielding chosen is based on the life time of 1 MW-Year. Anything less is dangerously optimistic.

The magnetic field intensitites along a field line of the midplane for the two T-coil case are shown in Figure 8. The ripples calculated from these fields are plotted as a function of major radius and shown in Figure 9. Figure 10 shows the ripple as a function of vertical distance z from the midplane for fixed radii. The ripple curves can be approximated by an exponential function

$$E(z,R) = E_o(R)e^{-z^2}/\alpha,$$

where $\alpha = 1.06$ for this particular case and $E_o(R)$ is the amplitude of the ripple given in Figure 10. The expanded ripple for T-coil with expander and for the four-coil type is also plotted in Figure 9. The ripple for the T-coil with expander is only 0.4 on axis and becomes positive at a smaller radius and is generally better than the four-coil case. The implication of this kind of ripple distribution on the particle confinement has to be studied. A preliminary calculation of an α-particle orbit and beam particles are given in the following section.

α-Particle Confinement

The α-particle orbits have been studied for four cases using the code FLOC developed by Fowler and Rome [6]. In Case 1,the current is 7.2 MA and the divertor height-to-width ratio is 0.58; the orbit is shown in Figure 11, and the banana orbit is not confined. In Case 2, the current is 8.3 MA and the height-to-width ratio is 0.5, but the coils are separated by 1.4 m. The banana orbit is again not confined as shown in Figure 11. In Cases 3 and 4, the height-to-width ratio is 0.5 and the coils are separated by 1.2 m, and the divertor currents are 11.2

MA-T and 6.72 MA-T respectively. In both cases the α-particles are confined as is shown in Figure 12. The time sequence of the banana shows that the banana steps toward the center of the machine. More has to be studied in order to draw a positive conclusion. However, it does illustrate that the α-particle can be confined for such a divertor system. The typical confined beam particle orbit is shown in Figure 13. The lower picture shows the variation of angular momentum of which is time average is nearly conserved.

Structural Concept of ETF Bundle Divertor

A prime requirement of the structure is the necessity to provide easy demounting of the bundle divertor from between the TF coils for servicing requirements.

Four "L"-shaped saddle magnet coils, each approximately 50 cm square in cross-section, 2.4 meters high, 1.2 meters wide, and 1.2 meters long are arranged to form a bundle divertor for the INTOR. These coils may be constructed of OFHC water-cooled copper conductors run at a current density of less than 6000 a/cm^2 in the conductor. The substantial forces generated by these windings are delivered to their surrounding structure in three dimension. Hence, the structure conceived is made extremely stiff in all three dimensions.

Forces

The net horizontal plane forces delivered by the divertor coils to their containment structure is given in Figure 14. This figure shows an indicated net radial force of about 30 MN on the whole assembly.

In addition to this net radial force, each pair of coils has substantial opposing forces in the perpendicular circumferential direction, and also in the perpendicular axial direction (out of plane). These forces have been examined in preliminary fashion as have the interactive forces on the adjacent four TF coils.

Structure Concept

The basic structure containing the bundle divertor coil forces consists of two thick 304L stainless steel plates (approximately equal to 15 cm thick) top and bottom, with built-up box beams (keyed and/or welded) of 304L stainless steel. A mid-plane section of a plan view is shown in Figure 13. The box beam sections shown in Figure 15 are schematic in nature, but they do have a geometry that keeps the bending stresses below 20,000 psi, consistent with the ASTM Boiler and Pressure Vessel Code, Section VIII, Division 2.

The four bundle divertor coils are envisioned as being sandwiched between the stainless steel plates mentioned above, with suitable intermediate tie-downs and strong-back cross-beams, to form a large, rigid monolithic assemble which fits between two adjacent TF coils as shown in Figure 16. Keyed joints (demountable) will be made between the monolithic assembly at its edges, and mating plates attached to the two TF coils to support the approximately 16 million pound net radial thrust of the divertor asssembly. The keyed joints are designed to permit remote removal of the keys and shim plates, which would then permit the radial movement of the entire monolithic divertor assembly outward from its operating position on rails, rollers, or other means.

The stainless steel plates which remain with the TF coil assemblies will have low thermal conductivity compressive links of G-10 in order to effect a satisfactory load link between the TF coils at liquid helium temperature and the divertor at ambient temperature. This compressive load link will have an intermediate liquid nitrogen cooled metallic intercept station to reduce the heat loss along the load path.

Conductor Consideration

Water-cooled copper conductors have been considered for use in theINTOR and ETF bundle divertor. Preliminary examination indicates that the 8.5×10^6 amp. turns required for each divertor coil can be achieved using a conventional square O.D. conductor (2.3 cm on a side) with a round cooling hole (1.3 cm). For the 400 turns per coil envisioned, the current in each conductor would be approximately 21,250 amperes at a current density of about 5400 amps/cm^2 in the conductor (3400 amps/cm^2 average within the coil envelope).

Half-turn (360 cm) cooling with a water flow velocity of 4.6 m/sec (approximately equal to 36.3 litres per minute per half turn) gives rise to a temperature increase of about 21°C to the cooling water at a pressure differential of about 0.79 Atm between inlet and outlet.

Alternatively, full-turn (7.2 m) cooling could be utilized with a water flow velocity of 9.2 m/sec (approximately equal to 72.3 litres per minute per turn) with the same 21°C temperature rise inlet to outlet and a pressure differential of about 5.5 Atm inlet to outlet.

Each front coil, therefore, requires approximately 70 MW of electric power for its operation and about 28,766 litres of water per minute to remove this power. The power requirement for half height coil and current 6.72 MA-T would be approximately 33 MW.

Nuclear Shielding Study

A one-dimensional ANISN calculation has been done to estimate the shielding thickness needed for the normal conduction operation. The one-dimensional shield model is shown in Figure 17. The dose rate on the insulation material (epoxy-base material such as G-10) as a function of shield thickness for three shield material combinations, 10% H_2O (B) + 50% W, 30% H_2O (B)+ 70% W and 50% H_2O (B)+ 50% W have been obtained. The results show that the 10% H_2O (B)+ 90% W shield is the best material combination. The neutron flux, nuclear heating and dose rate are plotted in Figures 18, 19, and 20, as functions of thickness for the best case.

The dosage on the insulator can be expressed as

$$D(x) = D(o)e^{-0.14008t - 3.3333\times 10^{-4}t^2},$$

where D(o) = 2.5 $\times 10^{11}$ Gray/year at MW/m^2 wall loading and t is the shield thickness with unit measure of cm. The lifetime of the insulation for three thicknesses for the dose limits of 10^7 and 10^9 Grays are listed in Table 2. Since there is 10 cm structure and 30 cm shielding, it is fair to say that the divertor can operate for 1 MW-Yr/m^2. If the duty factor is 50%, the divertor lifetime would be one year for 2 MW/m^2 wall loading. Since the divertor can be designed as a plug-in unit, a one-year replacement schedule should be very reasonable.

Table 2. Magnet Lifetime (MW-YR/m^2) for Dose Limits of 10^7 and 10^9 Grays.

Shield Thickness	Insulation Dose Limits
cm	10^7 Gray	10^9 Gray (MIT test)[7]
30 cm	0.004	0.4
40 cm	0.02	2
50 cm	0.1	10
60 cm	~ 1	100

Summary and Discussion

The coil dimensions, current and power consumption are listed in Table 3.

Table 3. Dimensions and Currents for Selected Bundle Divertor for INTOR

height = 1.40 m	I_1 = 6.72 MA-turns
length = 1.20 m	I_2 = 4.8 MA-turns
R_1 = 7.3 m	coil cross-section = 50 × 50 cm
R_2 = 10.2 m	Average j = 2.6 ka/cm^2
	= 0.56 ka/cm^2/Tesla

The current required for ETF is 8.3 MA-T and R_1 = 7.6 m. This divertor is feasible from an engineering and physics standpoint; the power consumption and lifetime are reasonable, and the replacement is easy. The most significant achievement of this concept is the drastic reduction in size and outboard forces. This fact can be demonstrated by the comparison of INTOR and ETF with a similar reactor design DTHR( ) as is shown in Figure 21. DTHR uses conventional two coil divertor whose size is more than double that of INTOR and ETF. Further optimism and detailed study of particle confinement are in progress.

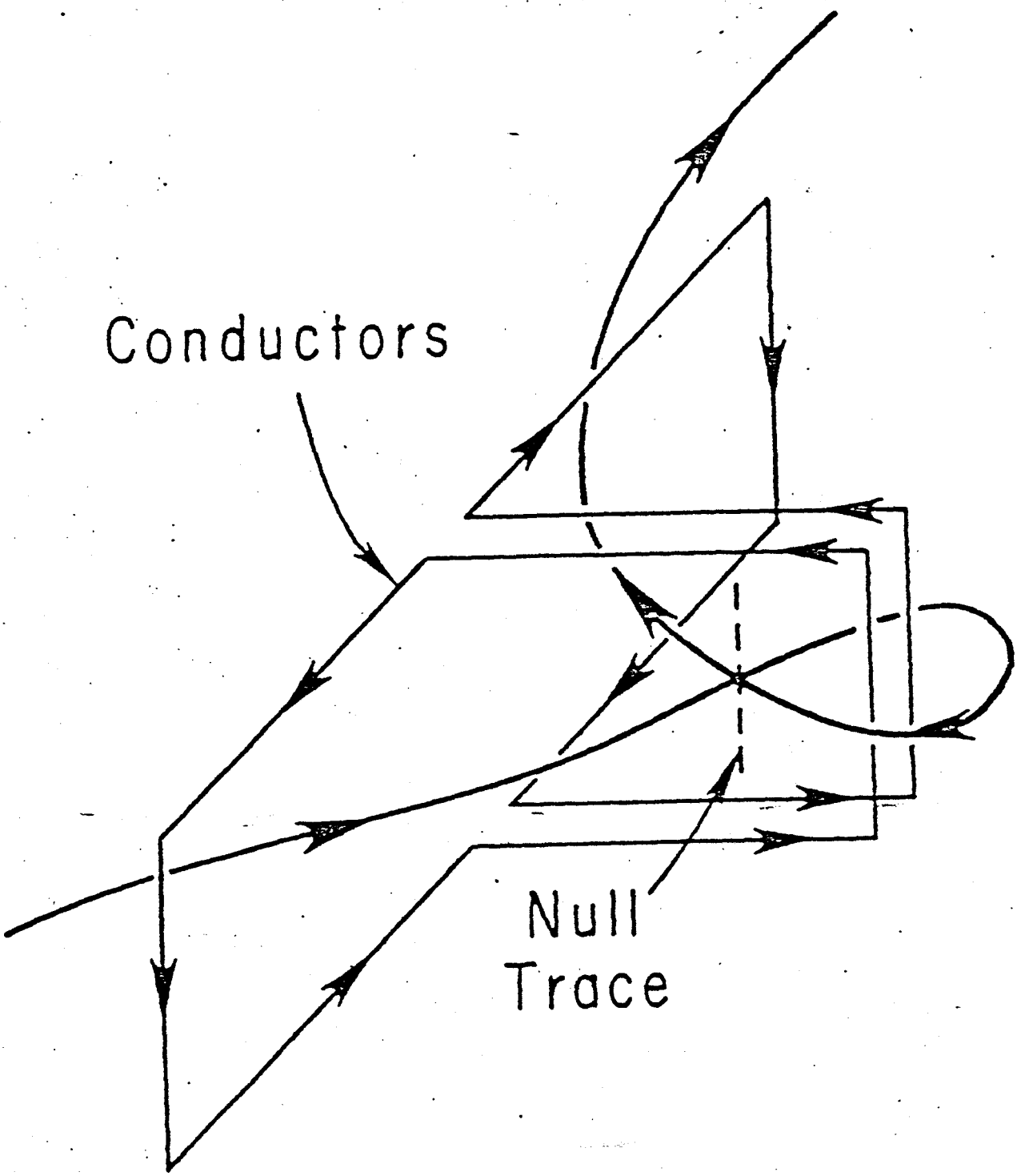

Fig. 1 Schematic of a T-shaped bundle divertor coil.

(a)

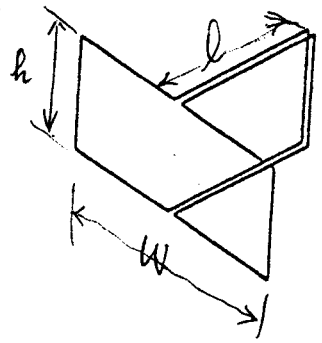

(b)

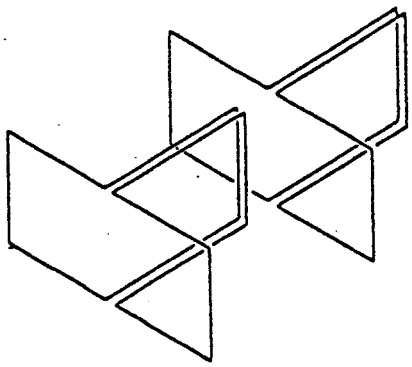

(c)

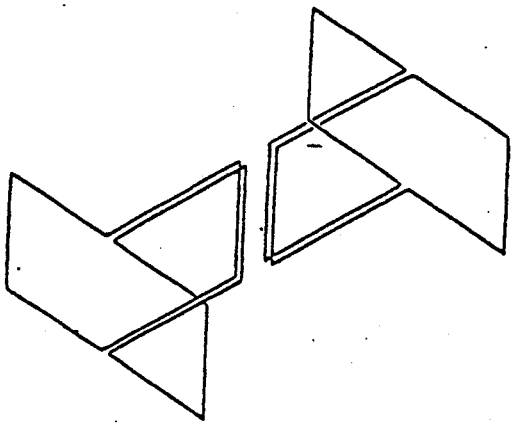

(d)

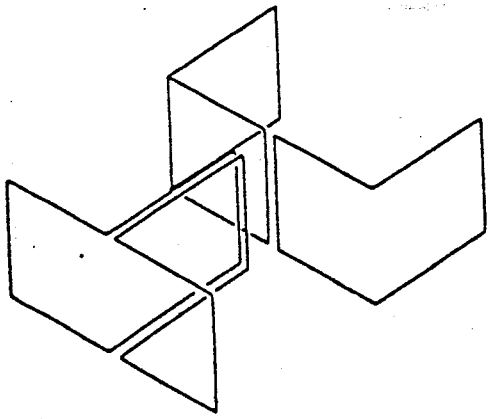

Figure 2 Divertor Coil Configurations

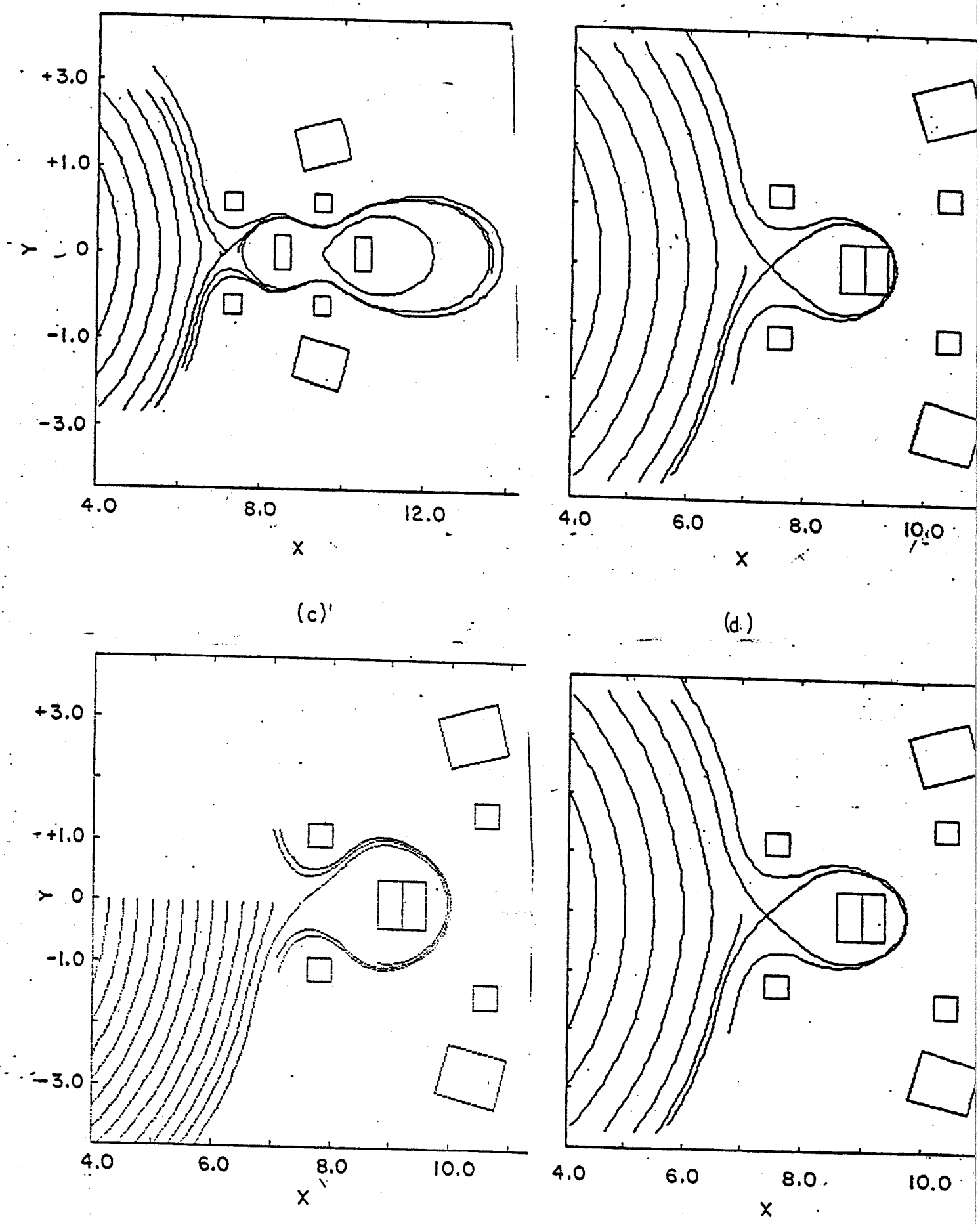

Figure 3 Magnetic Flux Configurations for the coil type (b), (c), (d) and (e) in Figure 2.

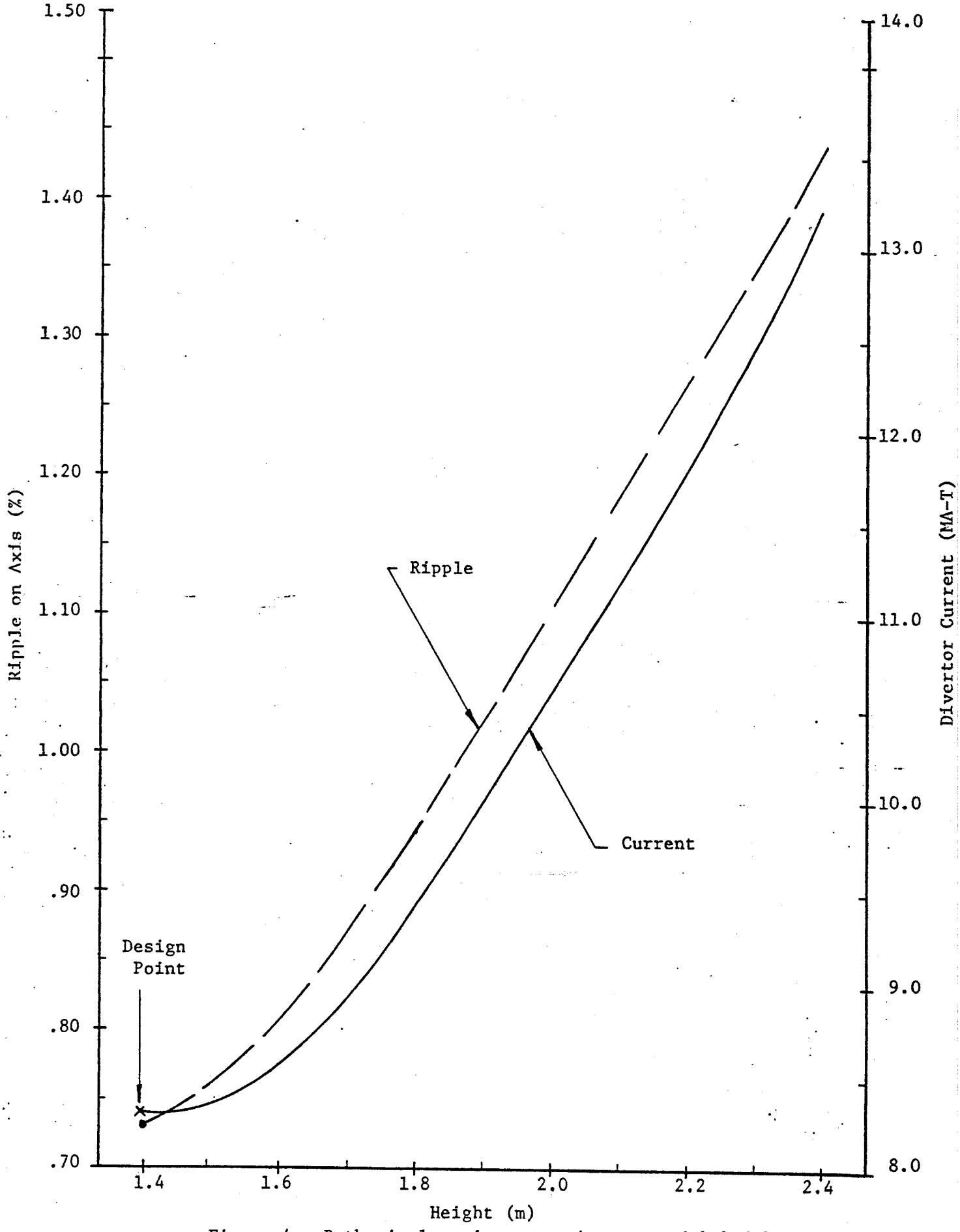

Figure 4 Both ripple and current increase with height.

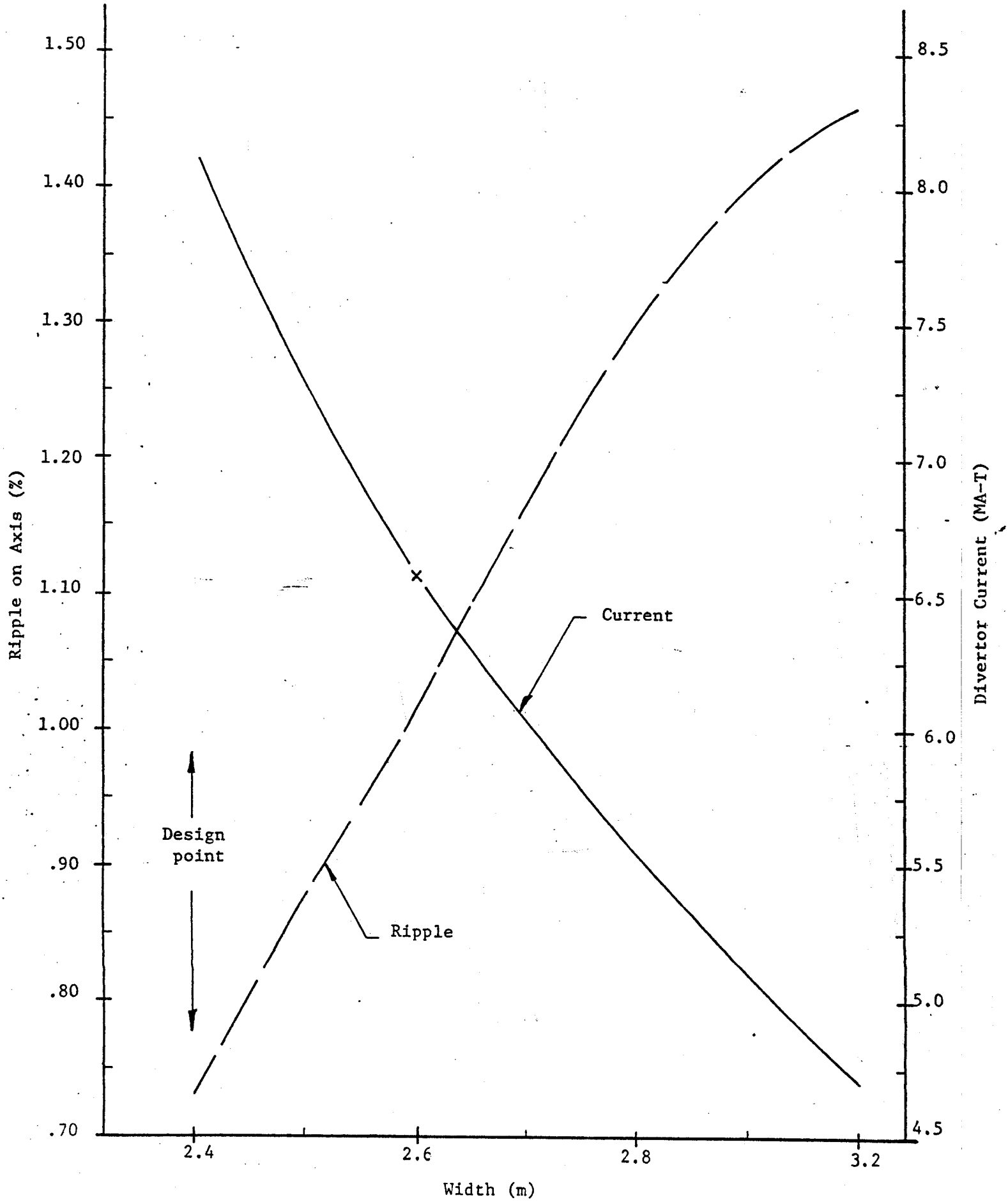

Figure 5 Ripple and current as functions of width
(Ripple increases while current decreases with width)

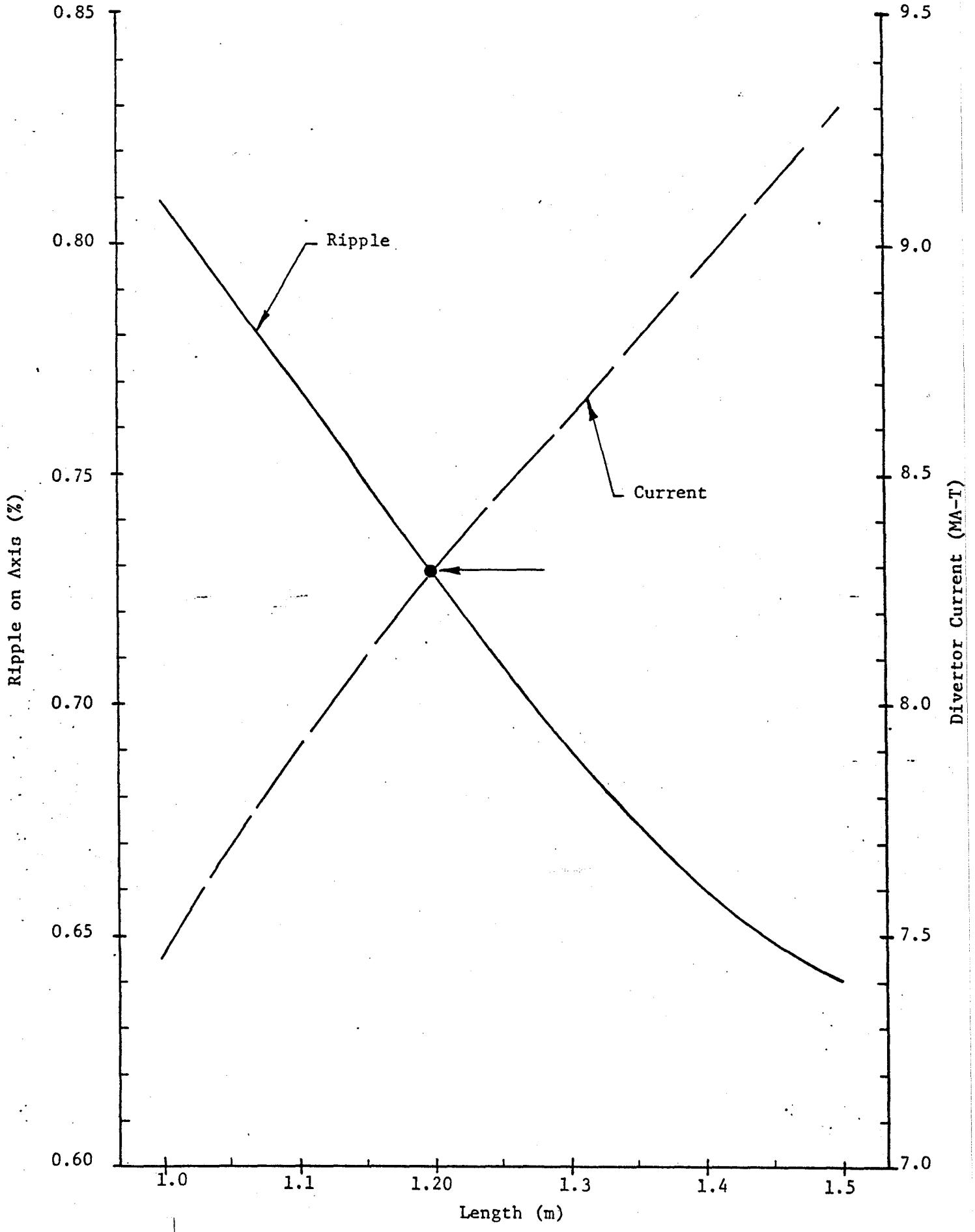

Figure 6 Ripple and current as functions of length

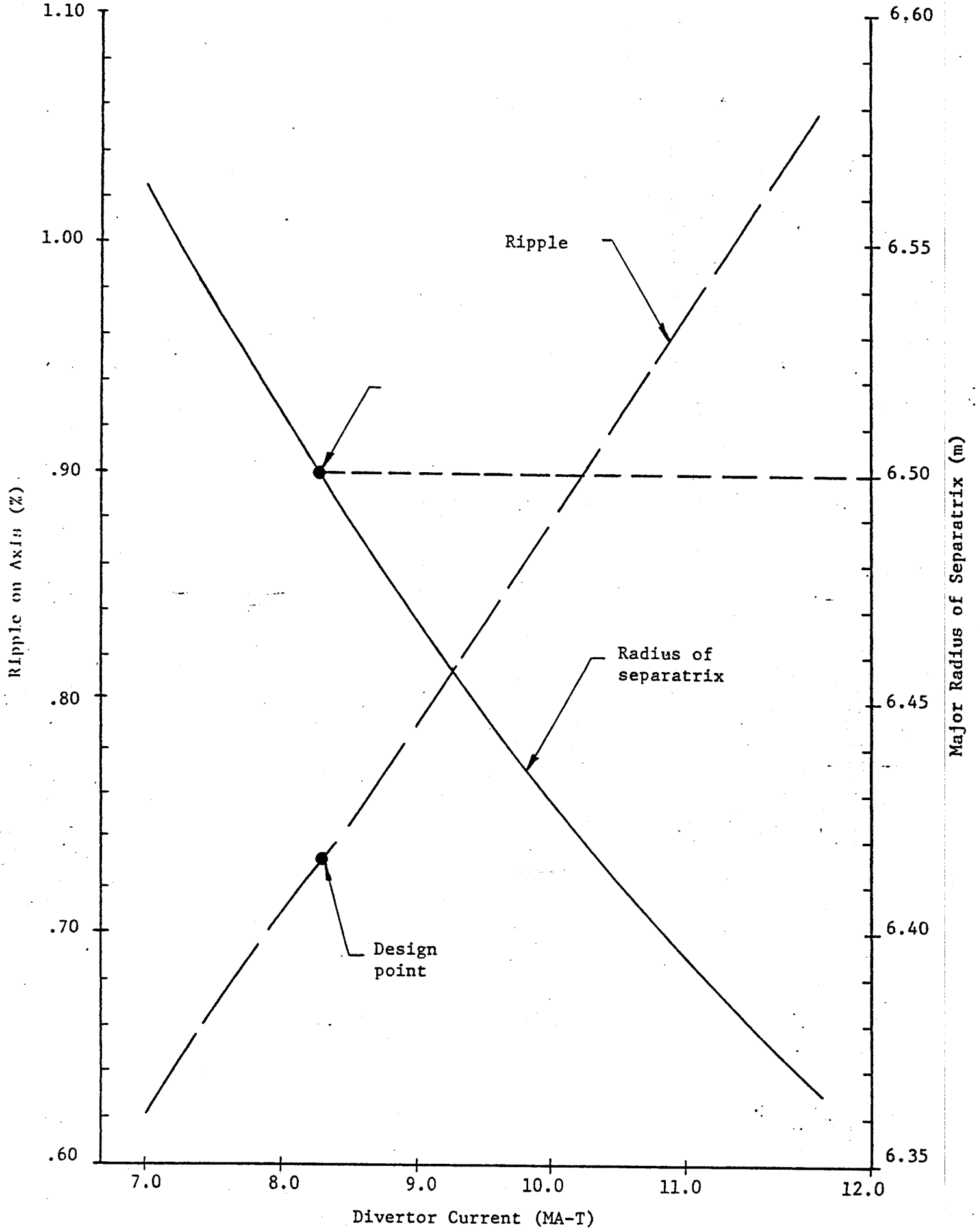

Figure 7 Ripple and radius of separatrix as function of current.

dxpetf5bf1
frame: 3

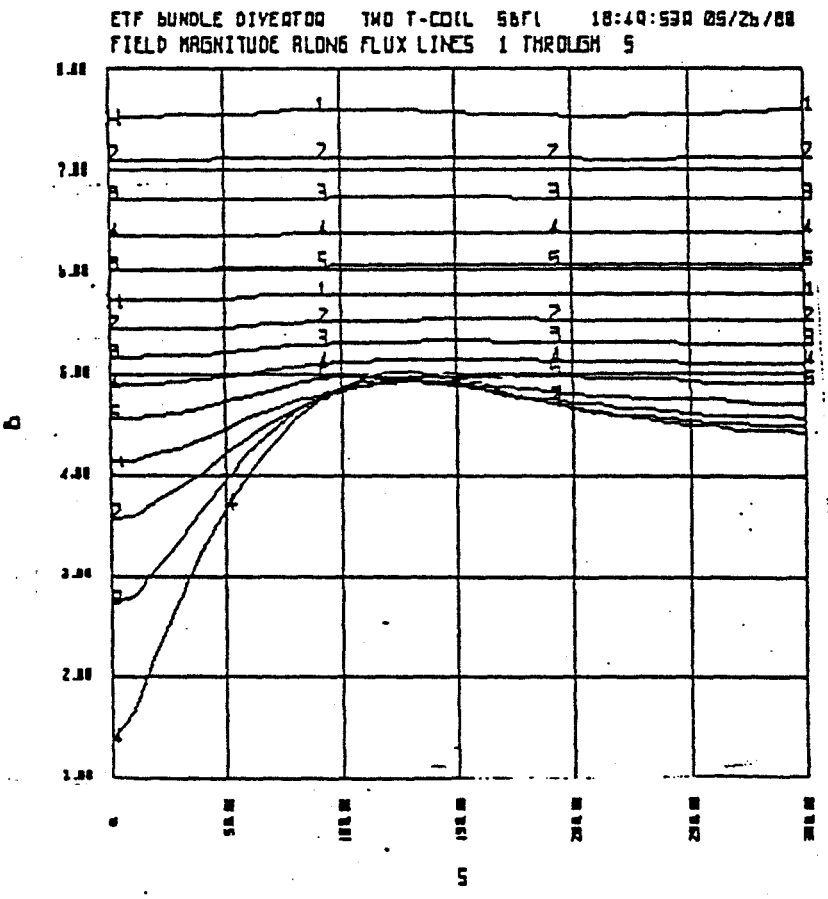

Figure 8 Field Intensities along the Field Line for Configuration 3C.

$$\left|\Delta B\right| = \left|\frac{B_{max} - B_{min}}{B_{max} + B_{min}}\right|$$

ALONG FIELD LINES

R	%
-75	.254
-50	.360
-25	-.095
0	-.398
25	-.837
50	-1.54
75	-2.88
100	-5.43

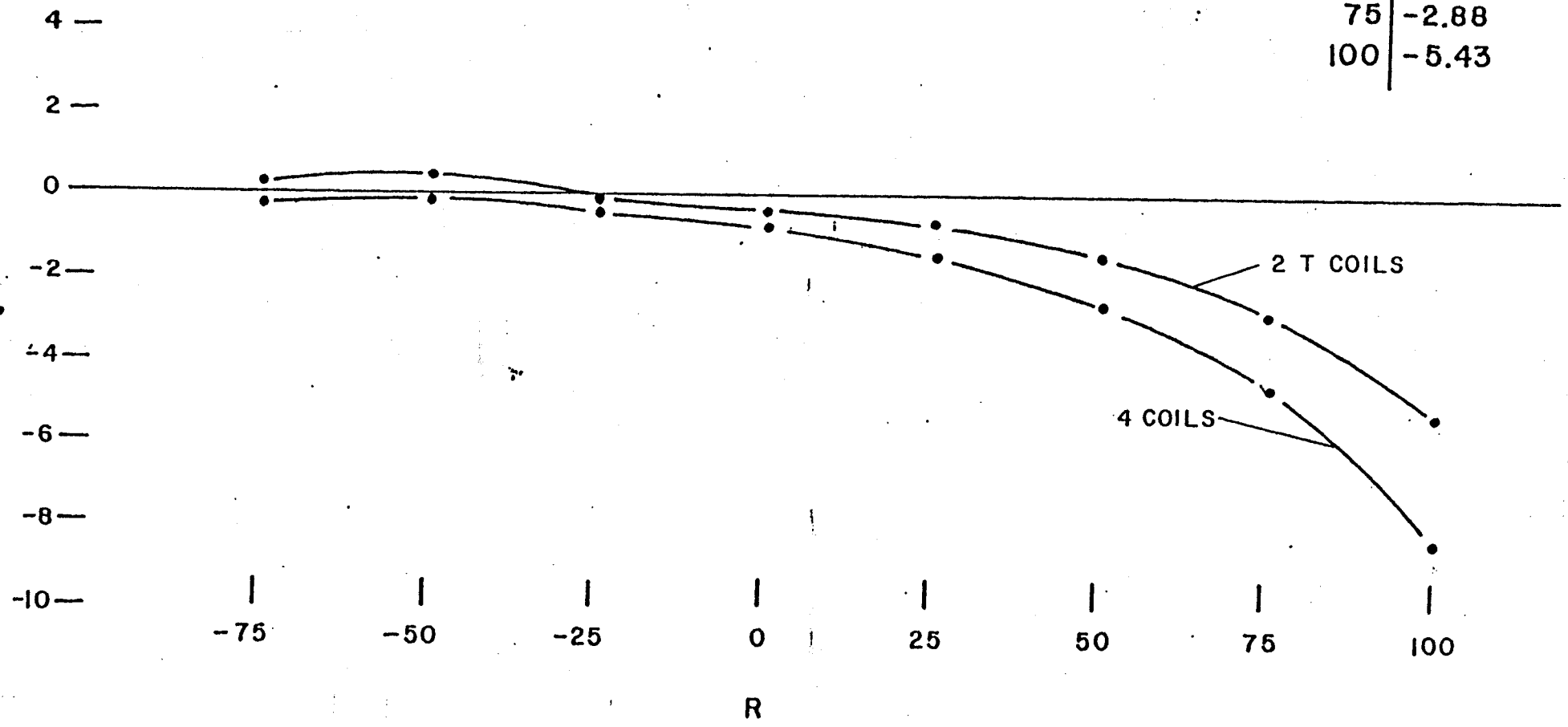

Figure 9 Comparison of ripple for 4 coils and one T with expansion coils.

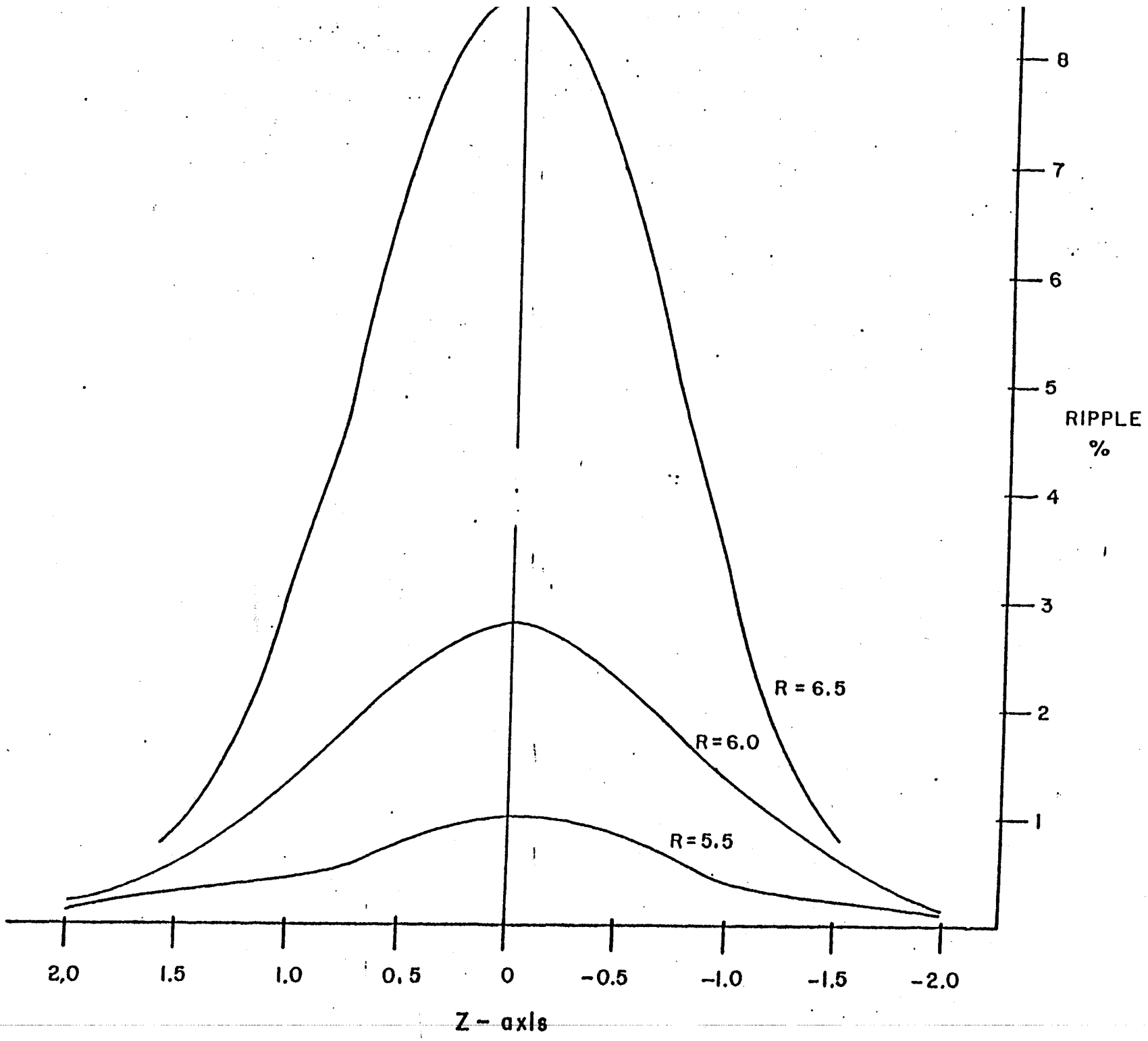

Figure 10 Ripple Distribution in the

dxplotssiv
frame: 3

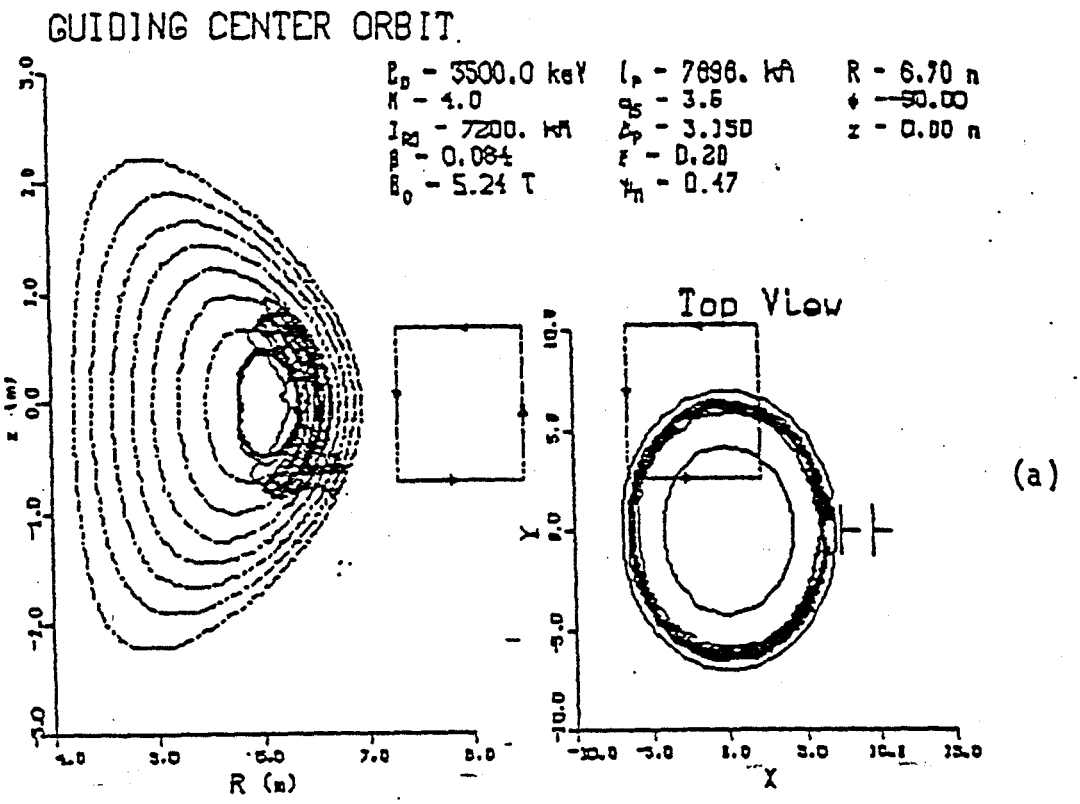

(a)

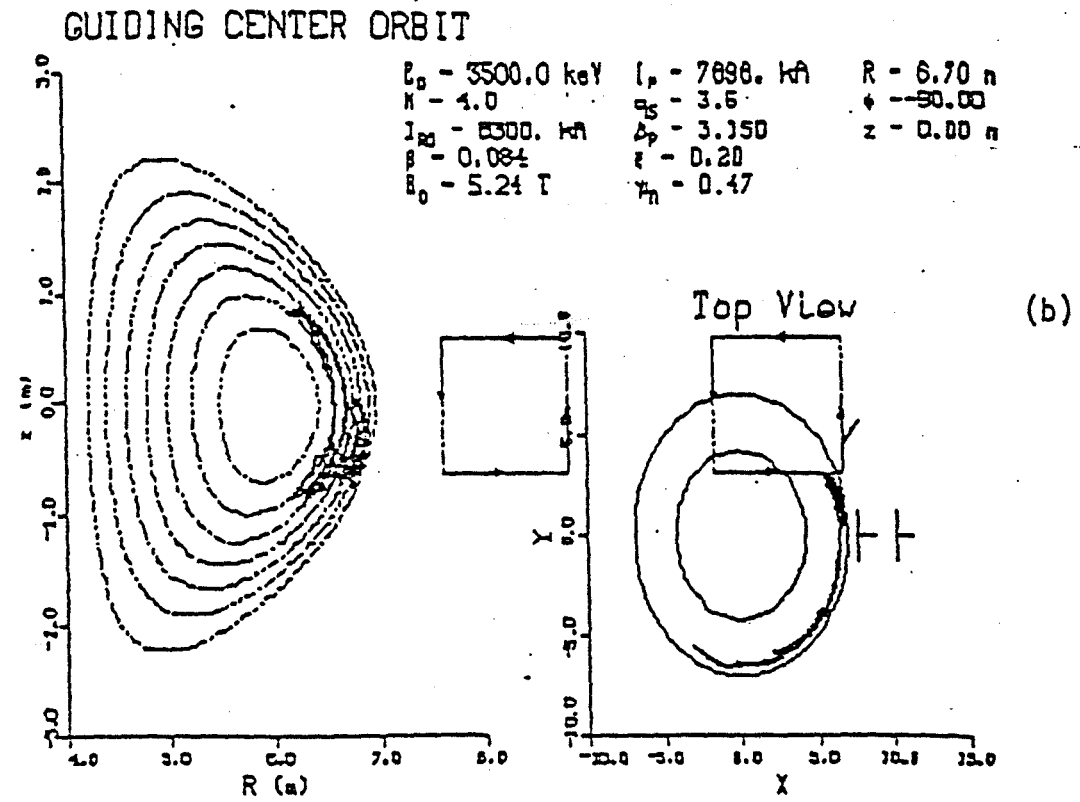

(b)

Figure 11 Unconfined α-particle orbits.

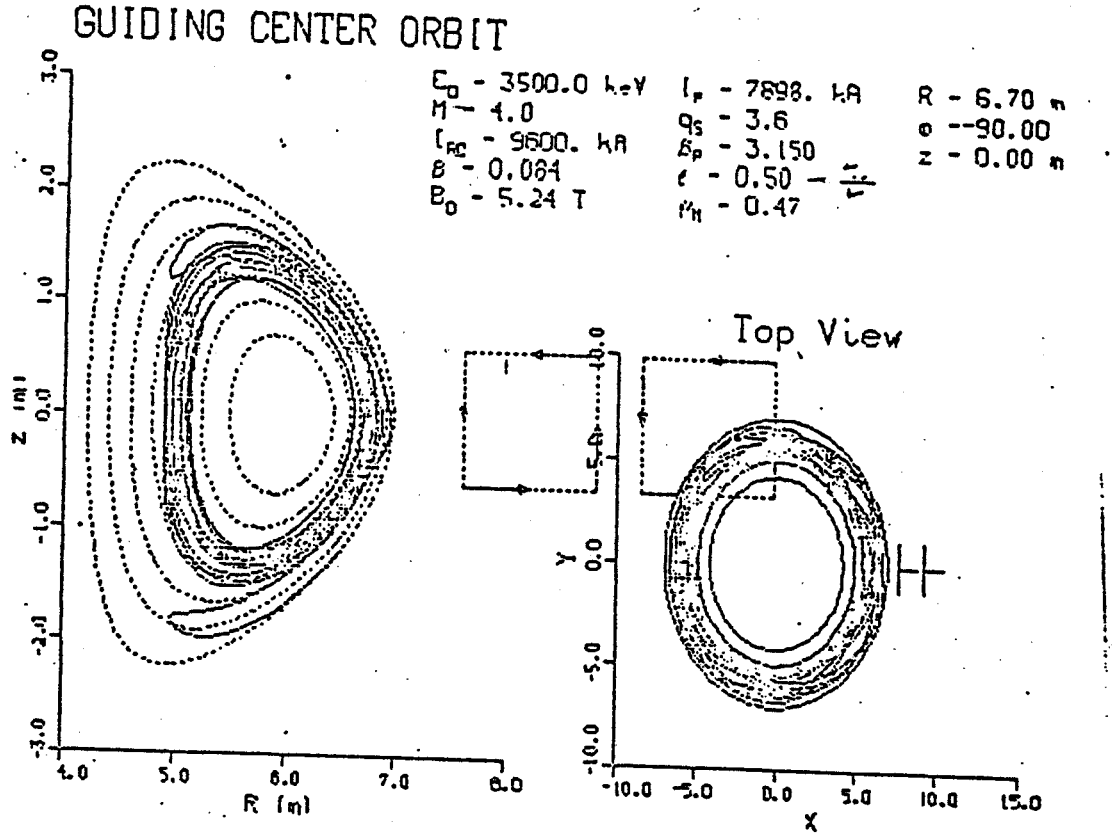

(a)

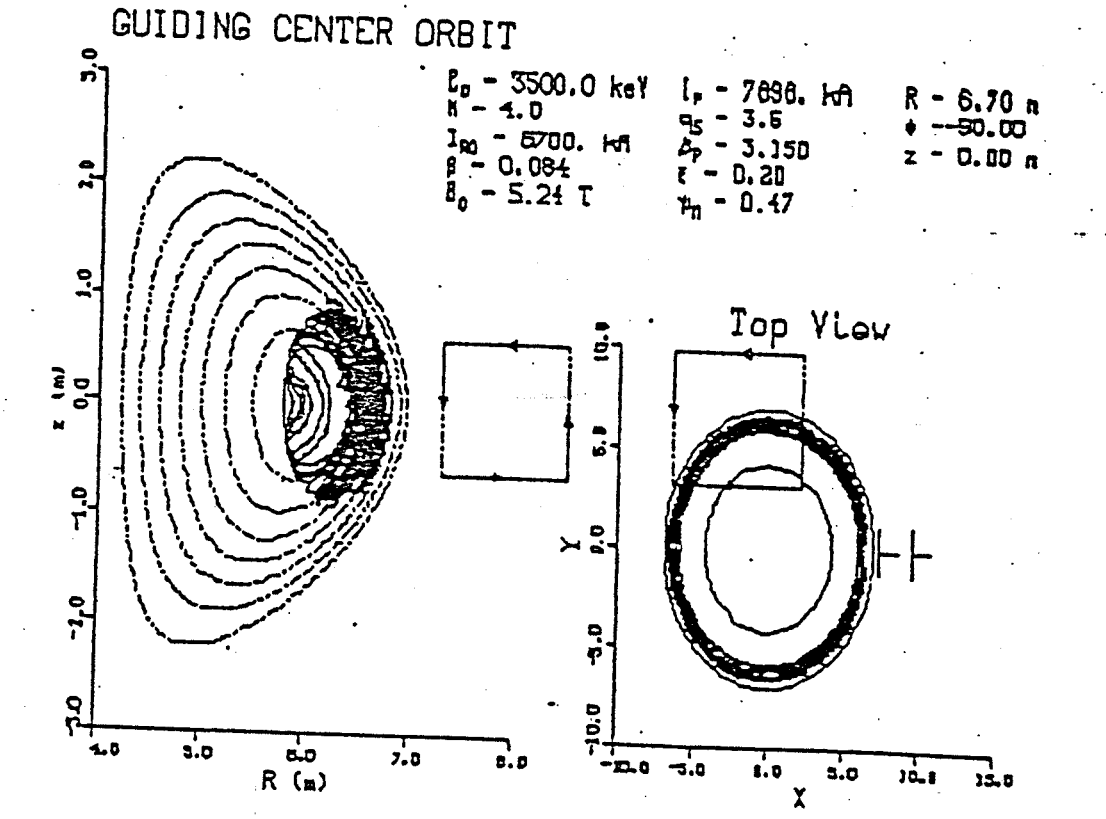

(b)

Figure 12 Confined α-particle orbits

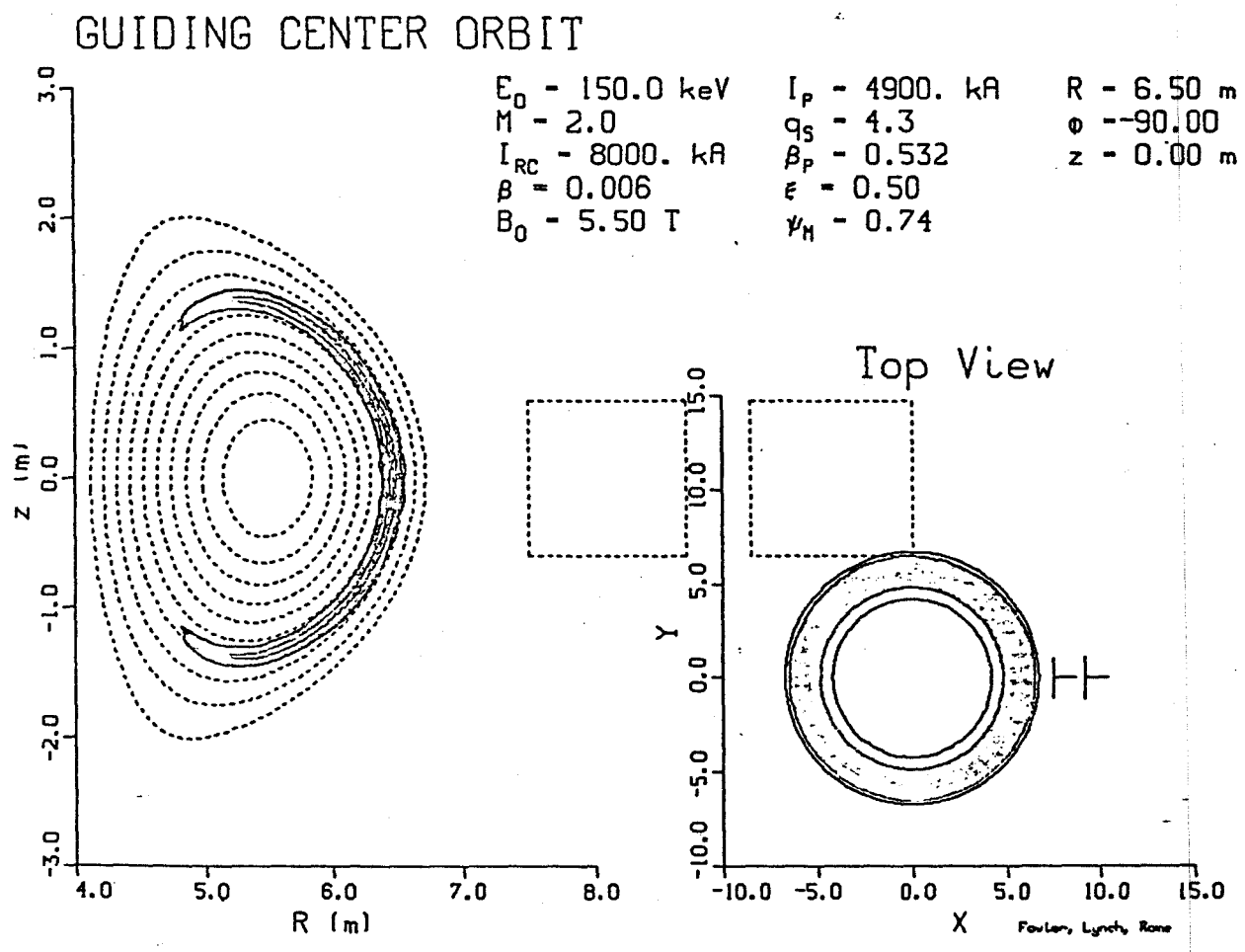

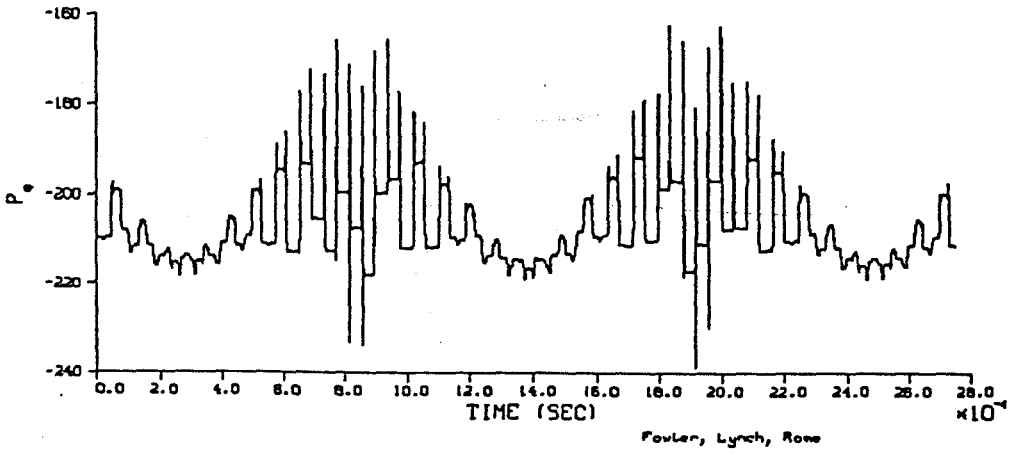

Figure 13 Typical confined beam particle

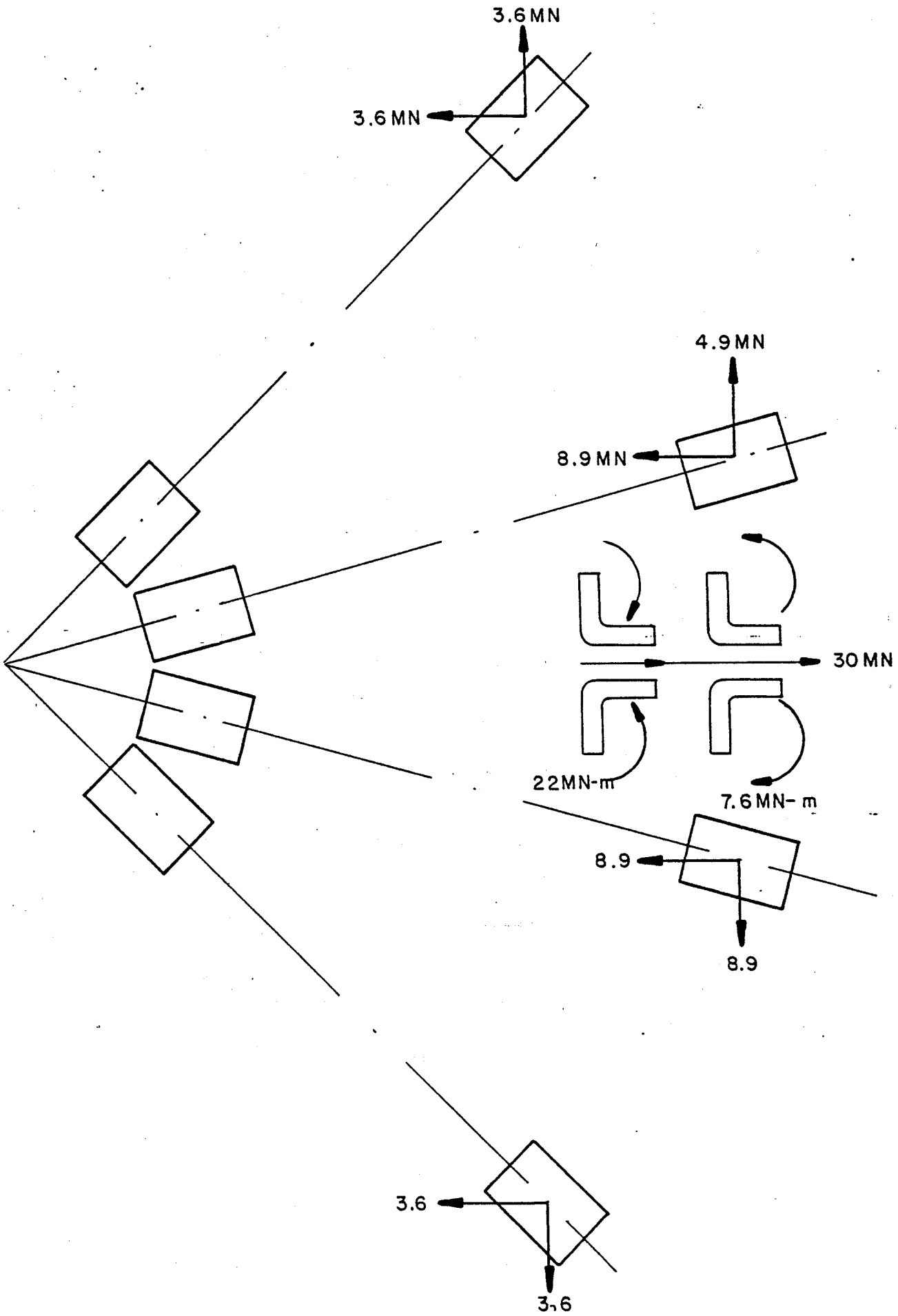

Figure 14 Preliminary summation of forces acting on energized bundle divertor coils of INTOR.

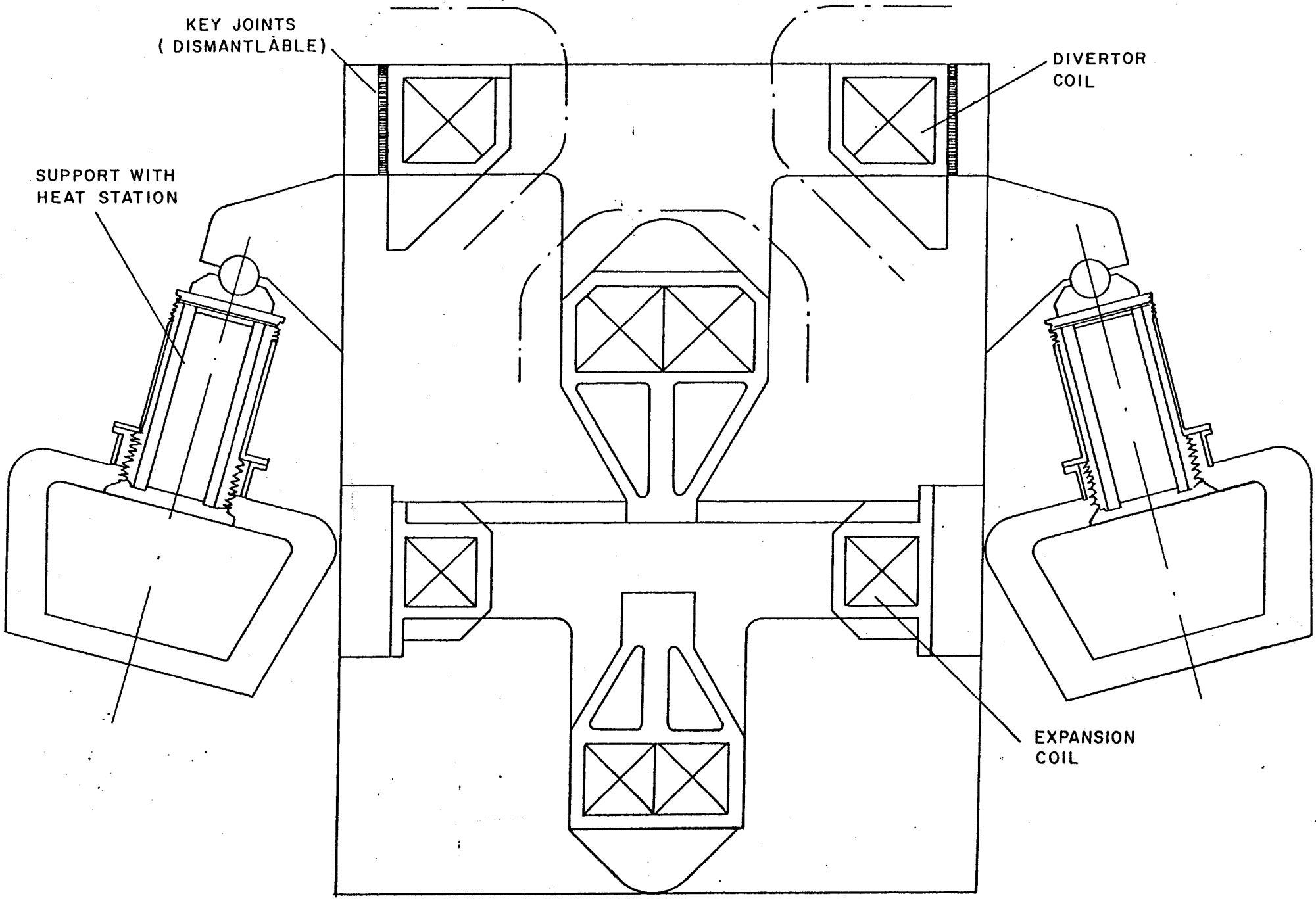

Figure 15 INTOR and ETF bundle divertor coils with support structure - mid plane section

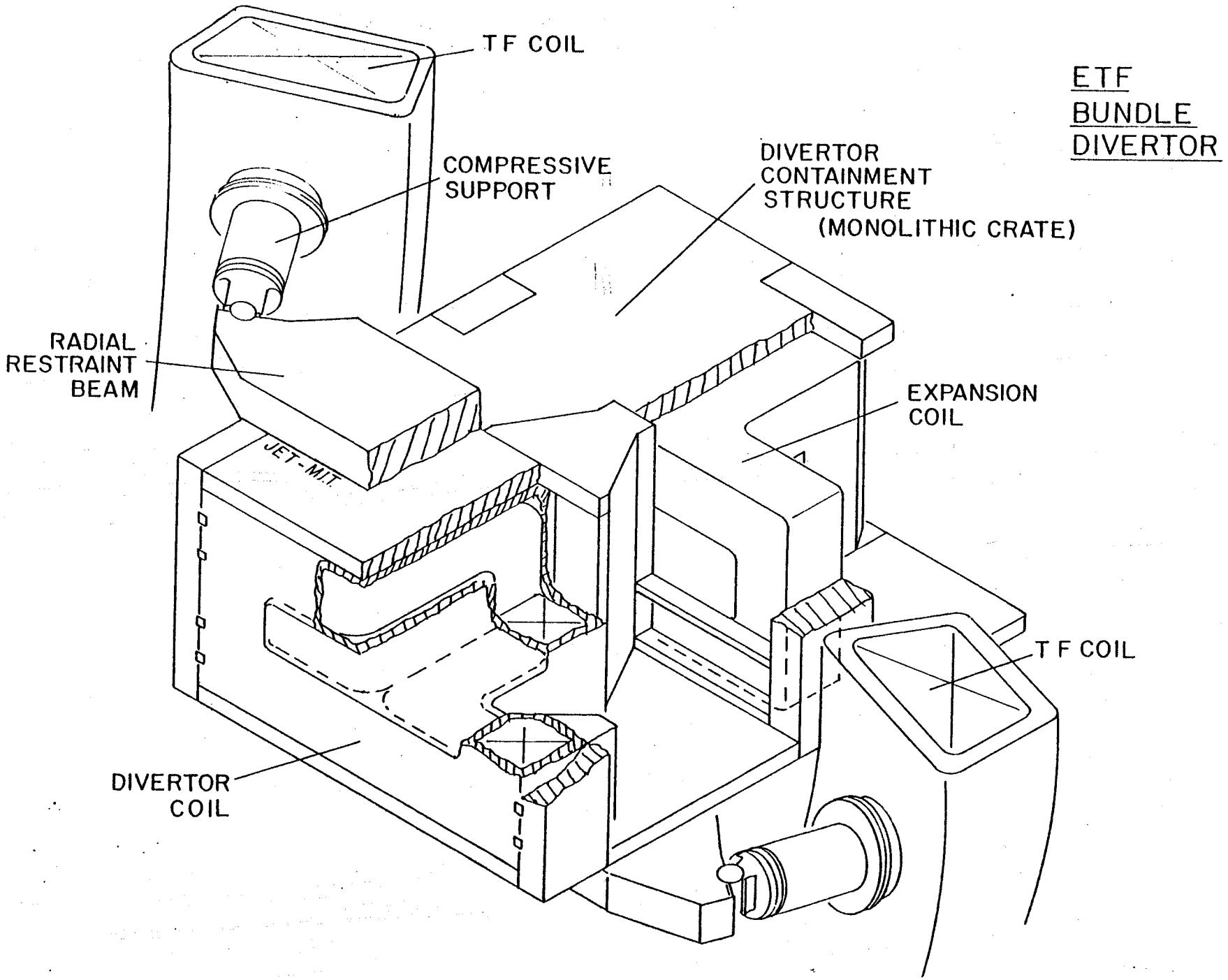

Figure 16 INTOR and ETF bundle divertor assembly

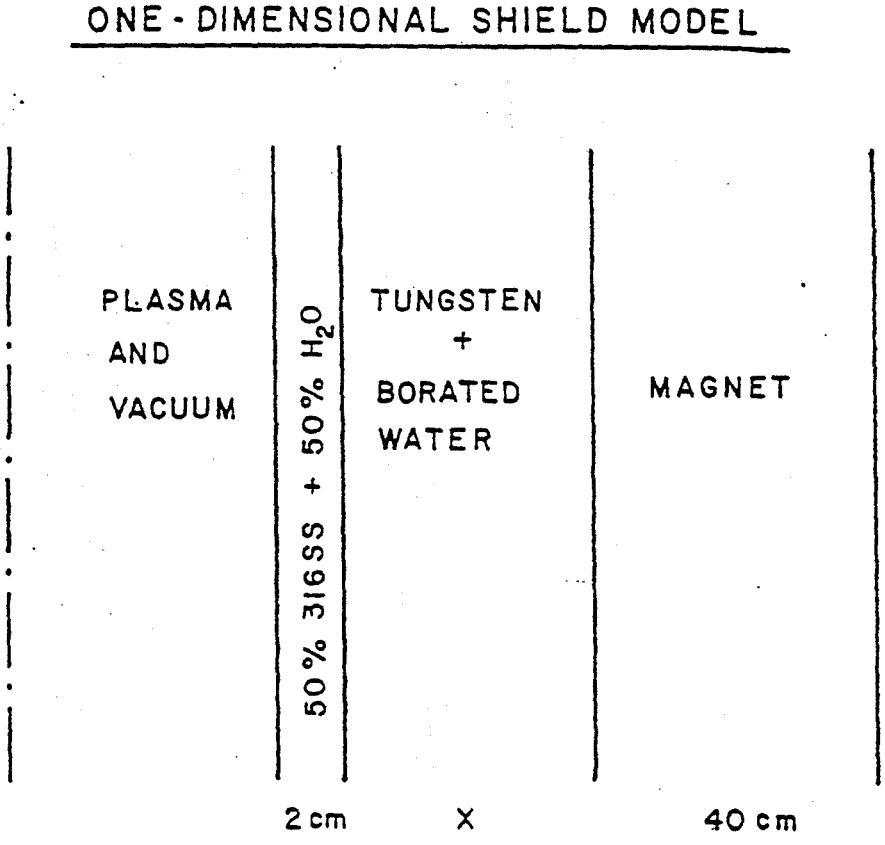

Figure 17 One-dimensional shield model

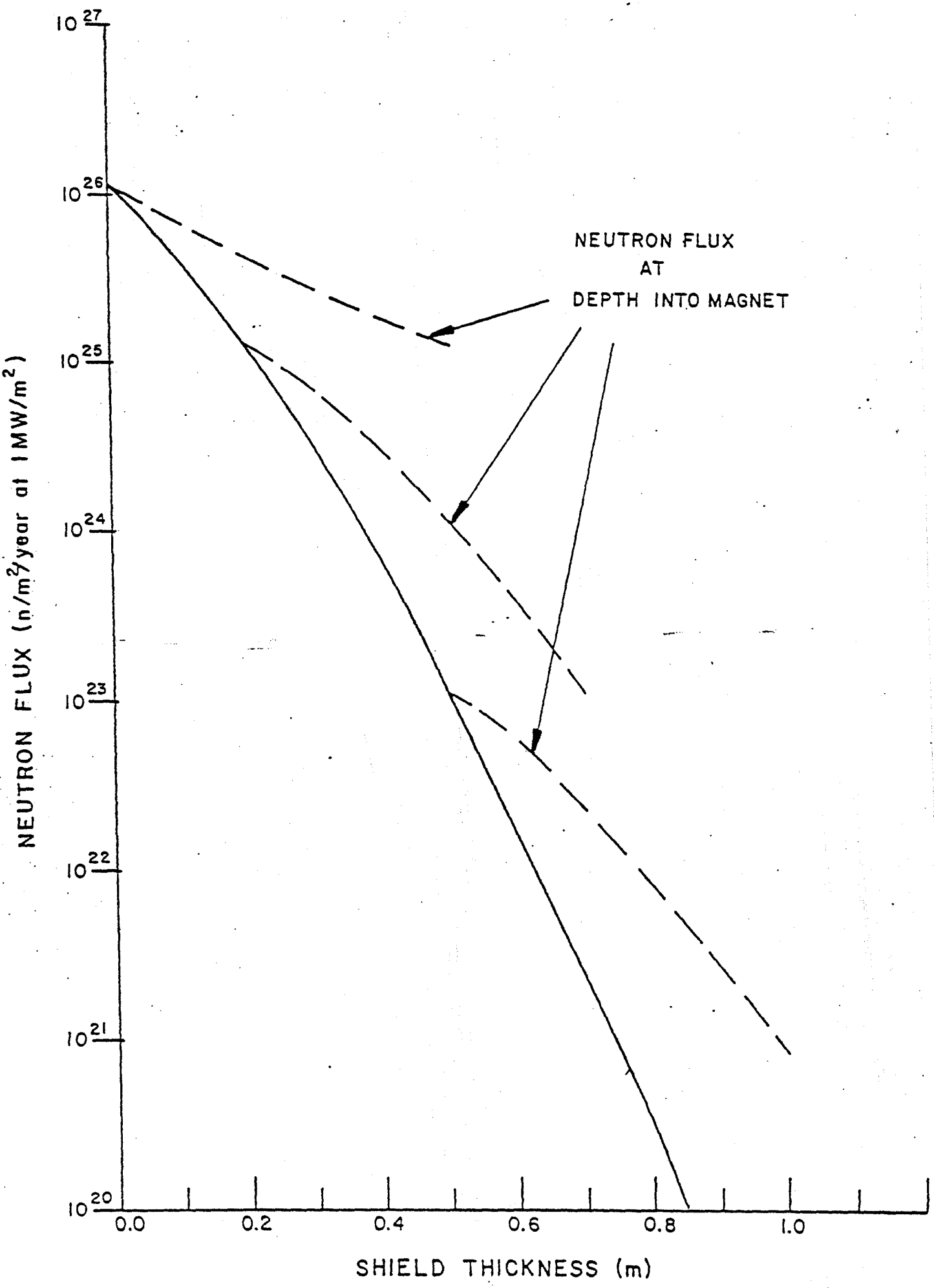

Figure 18 Neutron flux as function shield thickness

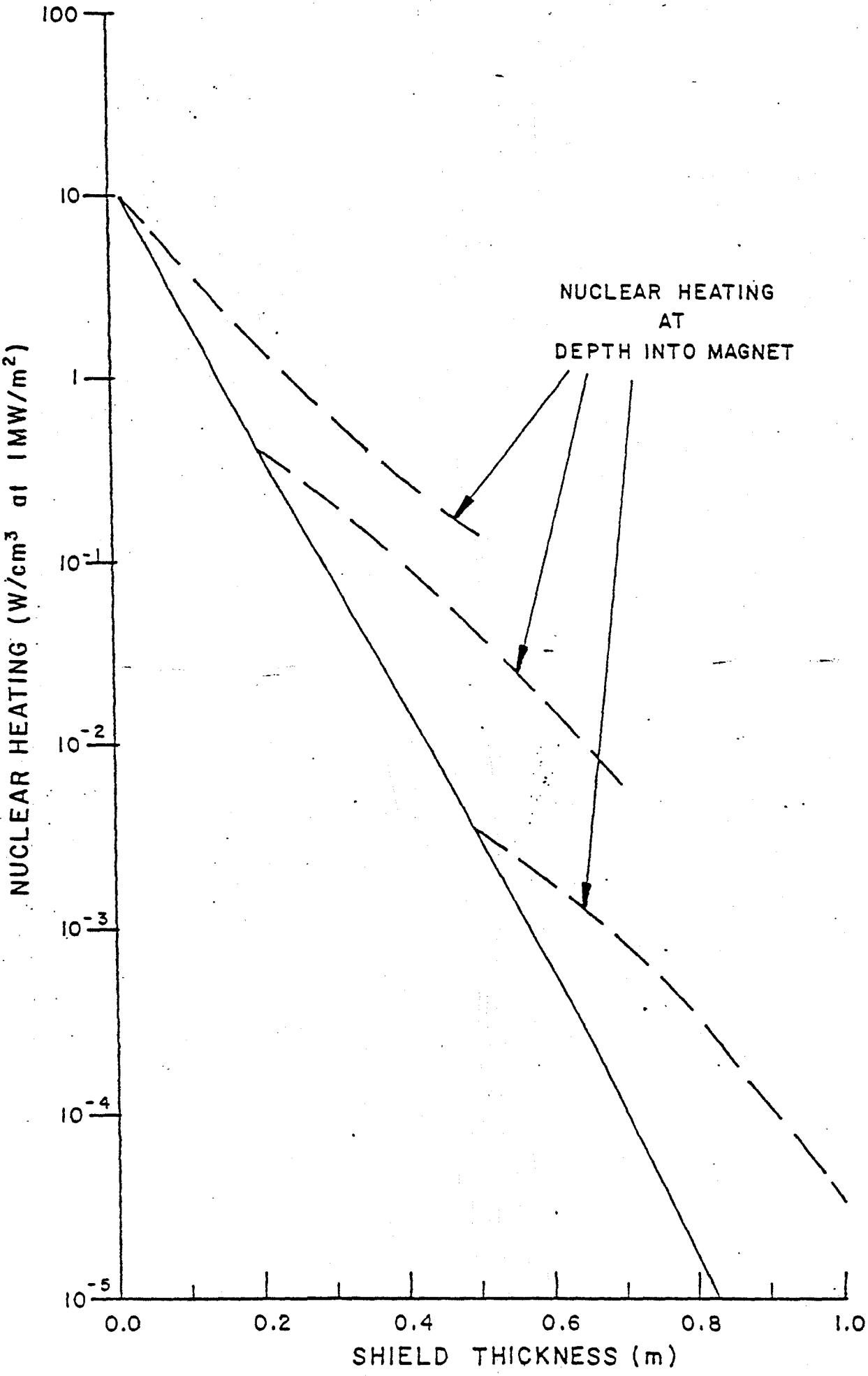

Figure 19 Nuclear heating as function of shield thickness

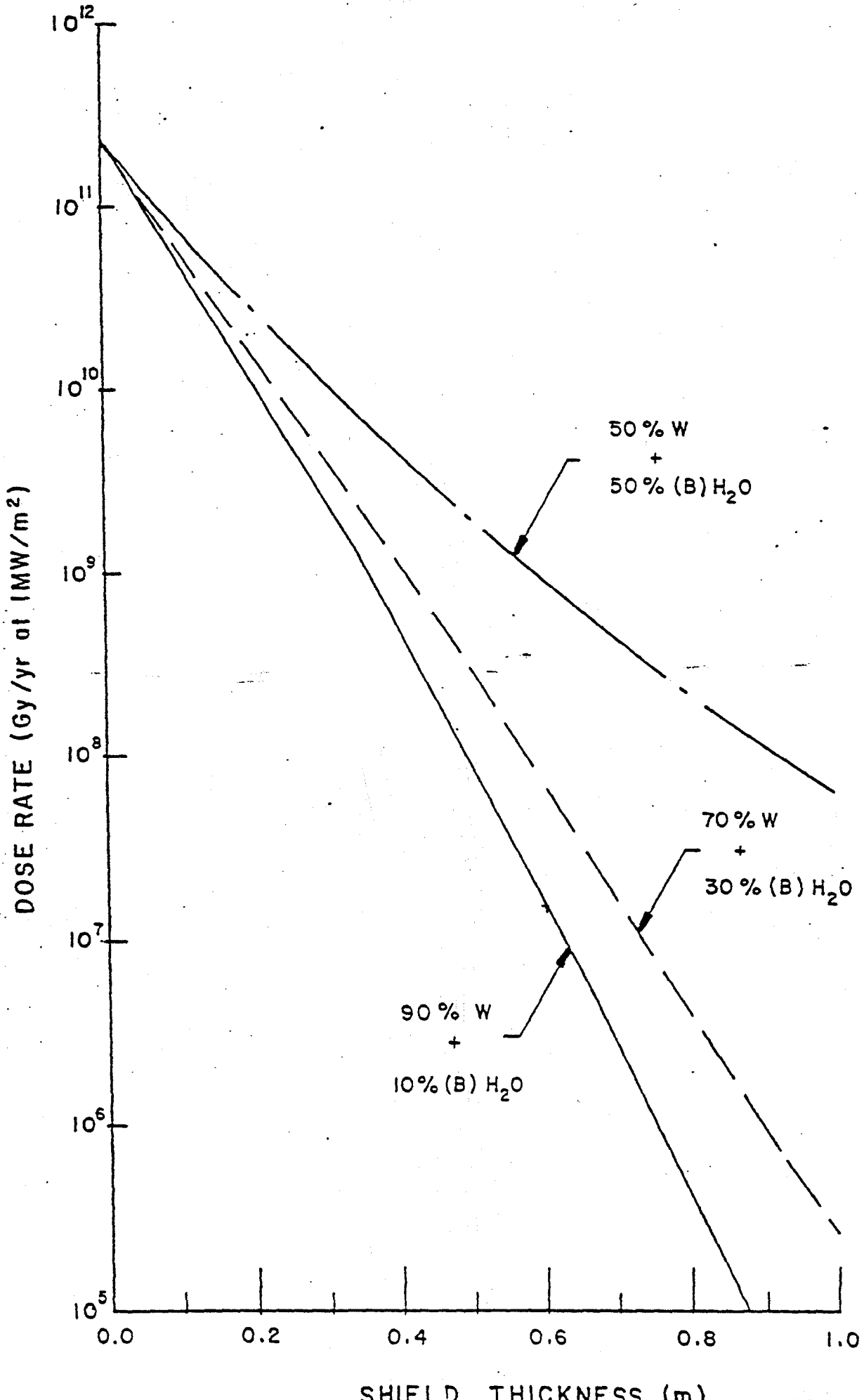

Figure 20 Dose rate as function of shield thickness

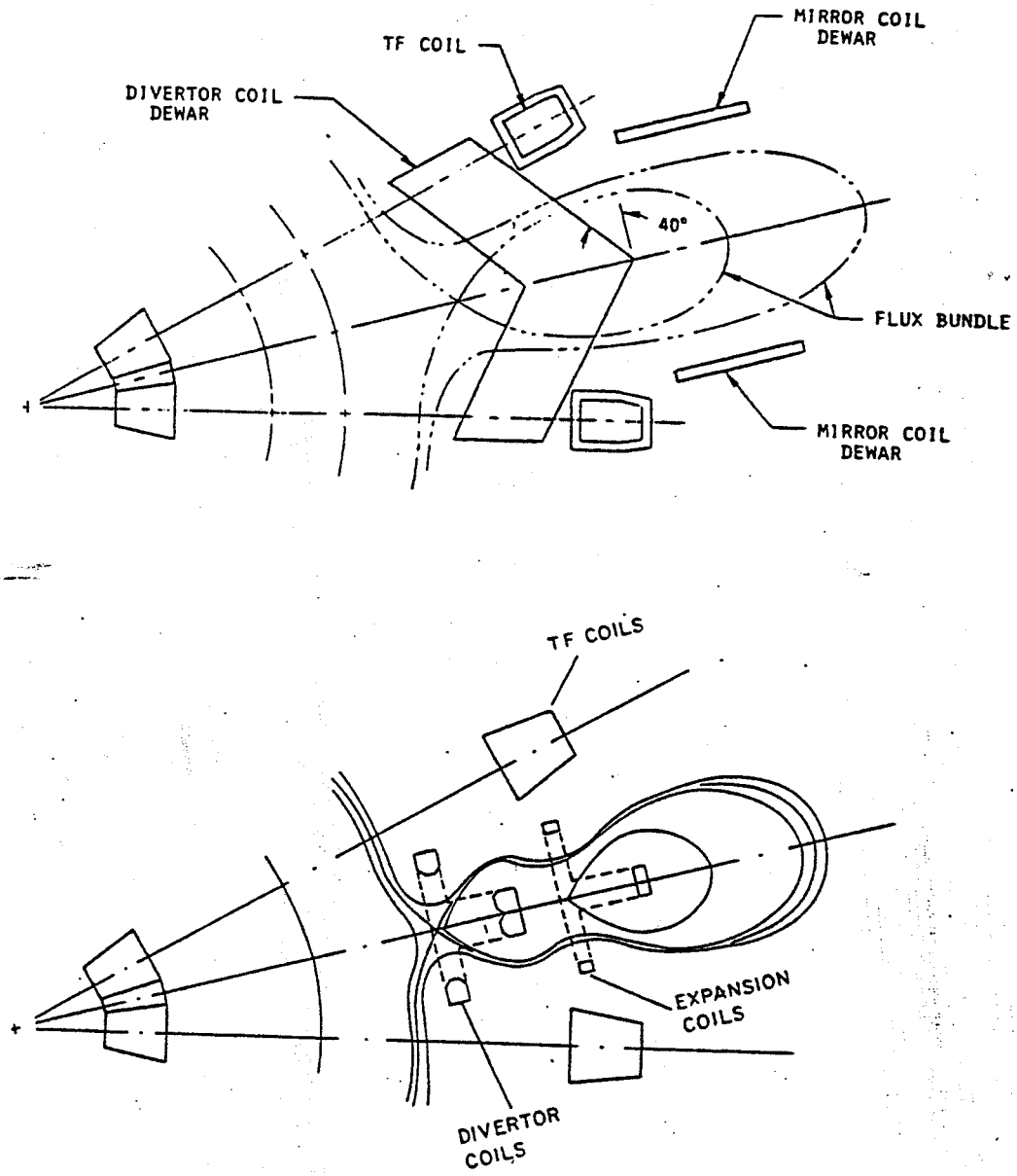

Figure 21 Comparison of two circular coil divertors and two T-shaped coil divertors

3.2 Hybrid Divertor

The concept of hybrid divertor is illustrated by Figure 1. The hybrid draws the edge field lines out in the form of broad, thin edge, which can be brought through a roughly horizontal slit into a separate chamber. The potential benefits include lower coil current densities, lower stresses, lower field ripple, and much greater room for radiation shielding. The drawback for putting the hybrid at the side of the torus is the coils have to be tilted about 3°, equivalent to the pitch angle of the magnetic flux, to avoid the field lines being intercepted by the structure. The way to avoid this is to put the hybrid on the outer lobe of the external poloidal divertor as is illustrated by Figure 2. The preliminary results are shown in Figures 3, 4, 5, and 6. Figures 3 and 4 show the cross-sectional and side views of magnetic fluxes of the axisymmetric plasma. Figures 5 and 6 are the fluxes with hybrid divertor on the top. The magnetic fluxes are brought out from the plasma and into the outer lobe. Figure 6 shows that lines 2, 3, and 4 and leaving the tokamak. The divertor coils are extended 120° in the toroidal direction. The current is only 2 MA-T.

The particle handling with axisymmetric external poloidal divertor will have the difficulty at the inner lobe where the pumping path is blocked. The scrape-off layer is thicker at the inner side of the plasma than the outer side, which will reduce the shielding space. Hybrid divertor will alleviate these problems. The vacuum system and thermal handling will be much easier when the plasma is diverted to the outer lobe.

The optimization and detailed study are in progress.

HYBRID POLOIDAL-BUNDLE DIVERTOR
(DIVERTOR COILS ON THE OUTSIDE OF PLASMA)

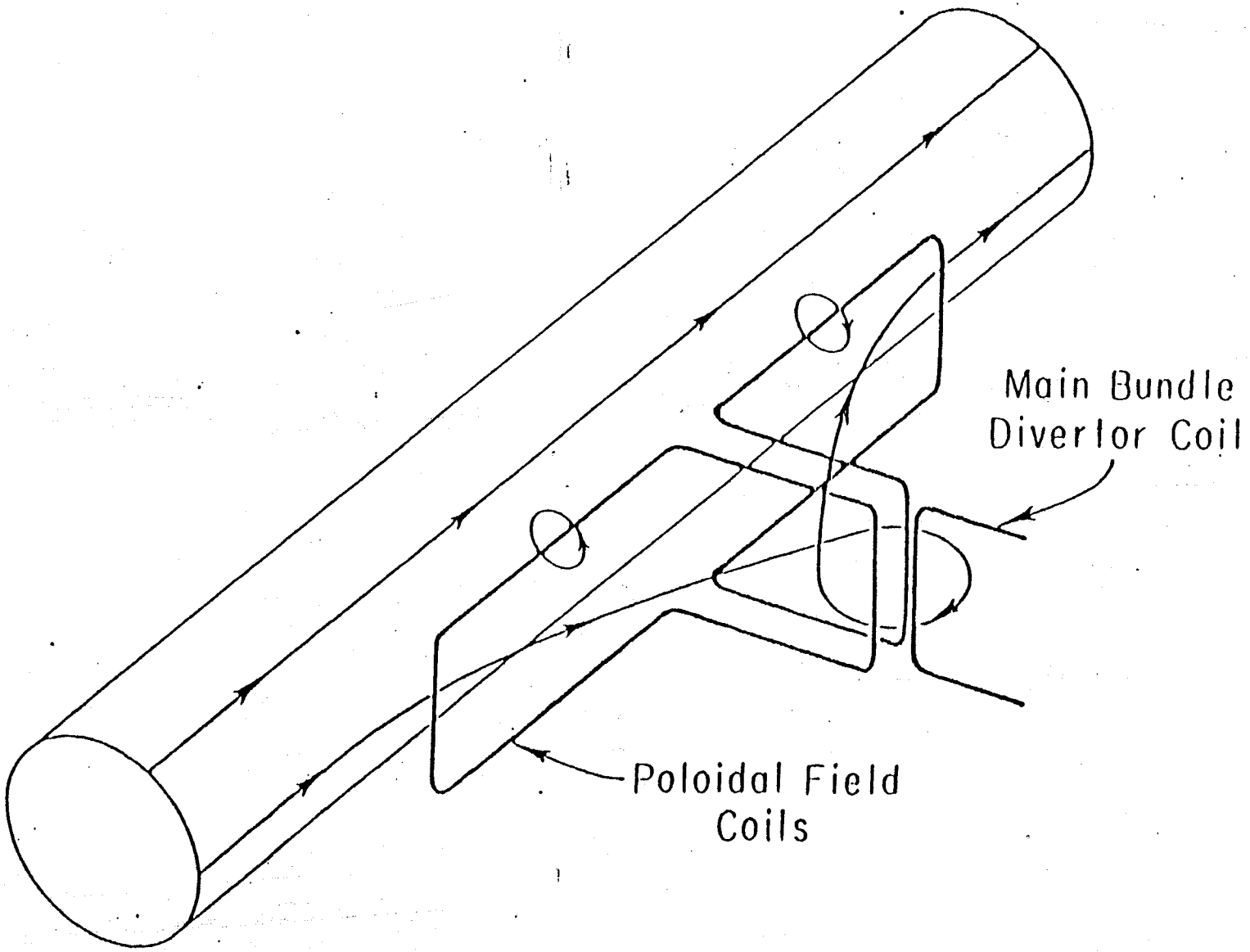

PPL 7936/3

DIVERTOR COILS PLACED ON THE TOP OF THE TORUS

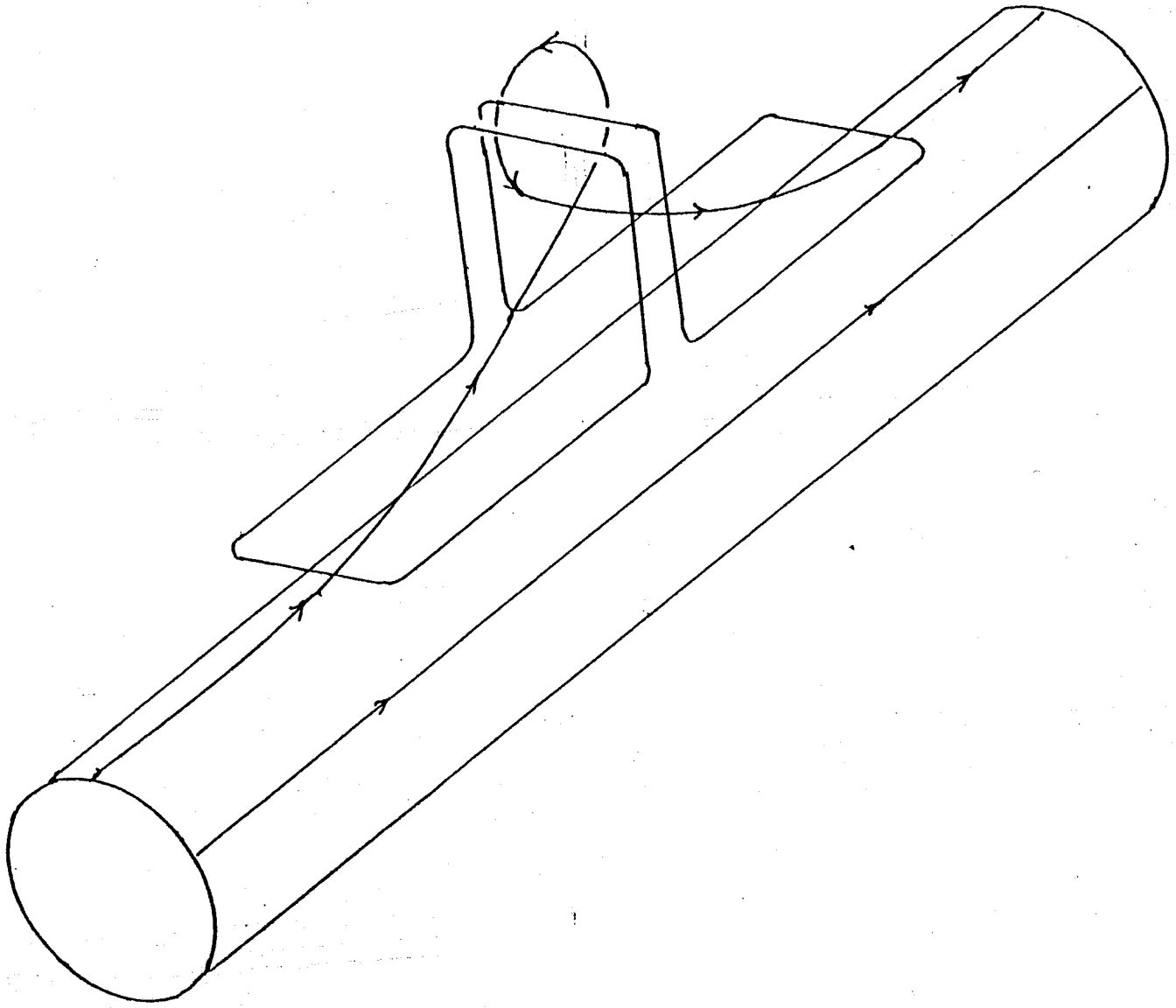

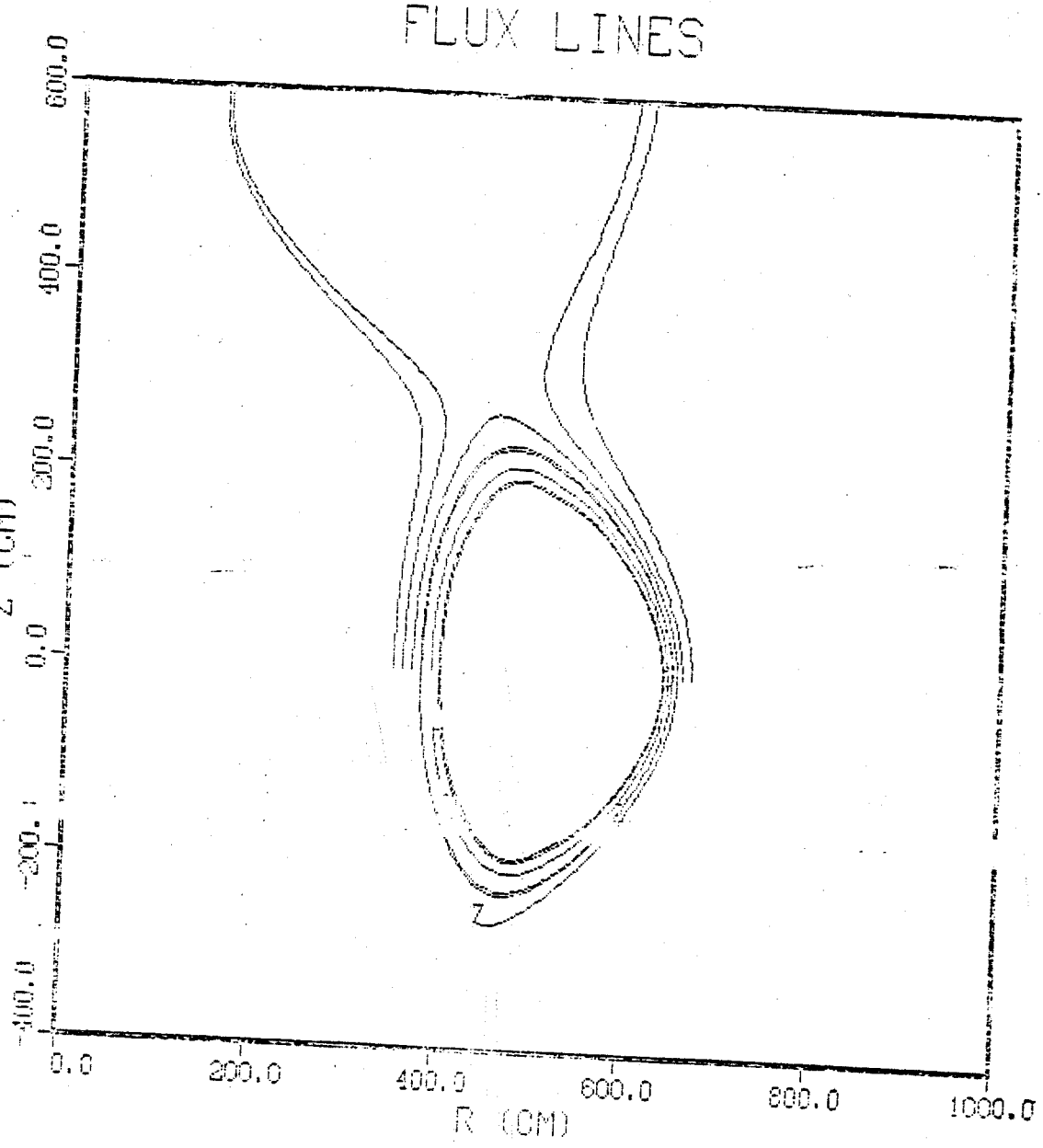

AXISYMMETRIC PLASMA WITH SEPARATRIX OUTSIDE THE WALL

SIDE VIEW OF THE MAGNETIC FLUXES. LINE 1 IS LEAVING THE MACHINE WHILE LINES 2 AND 3 ARE CONTAINED.

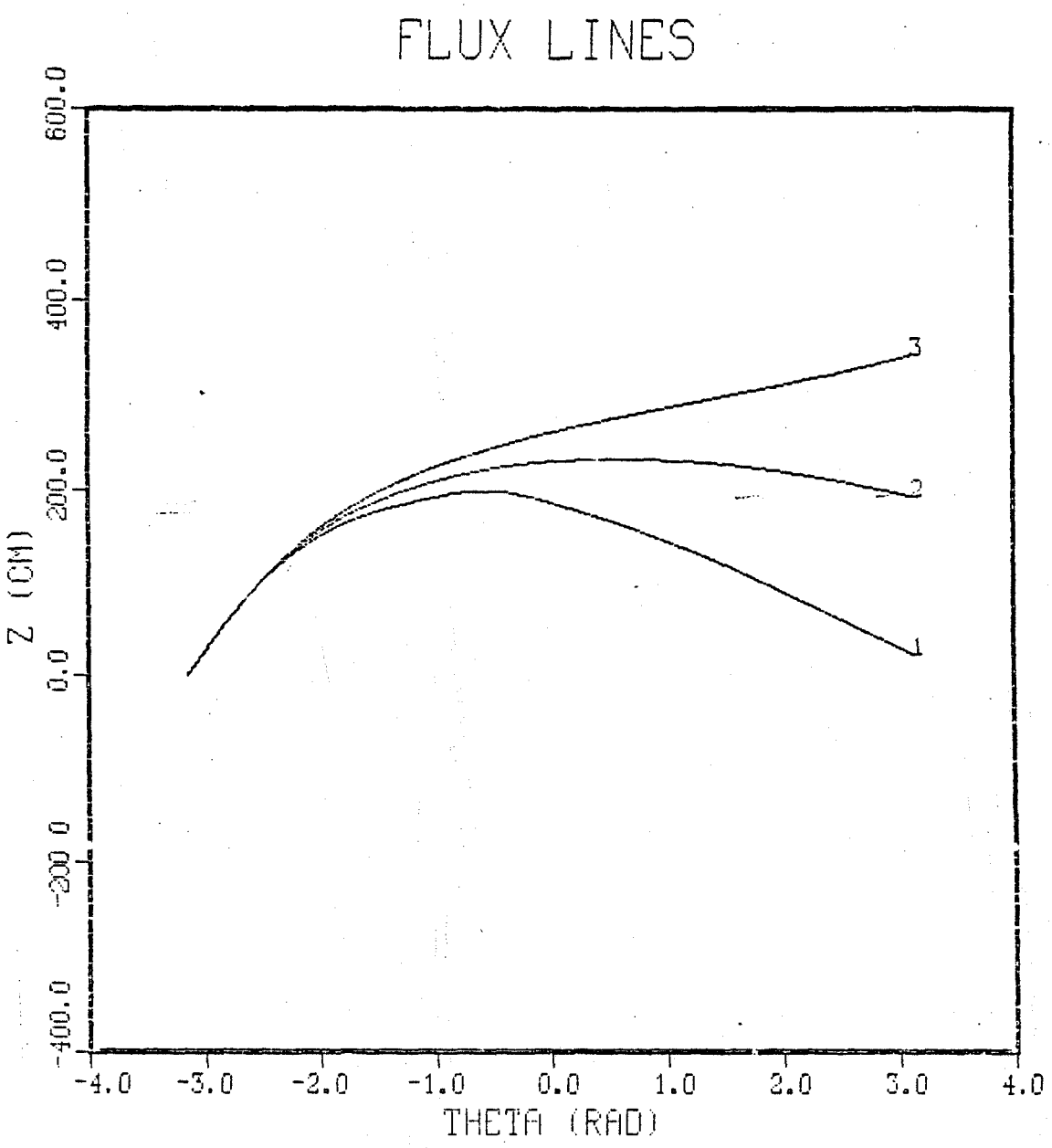

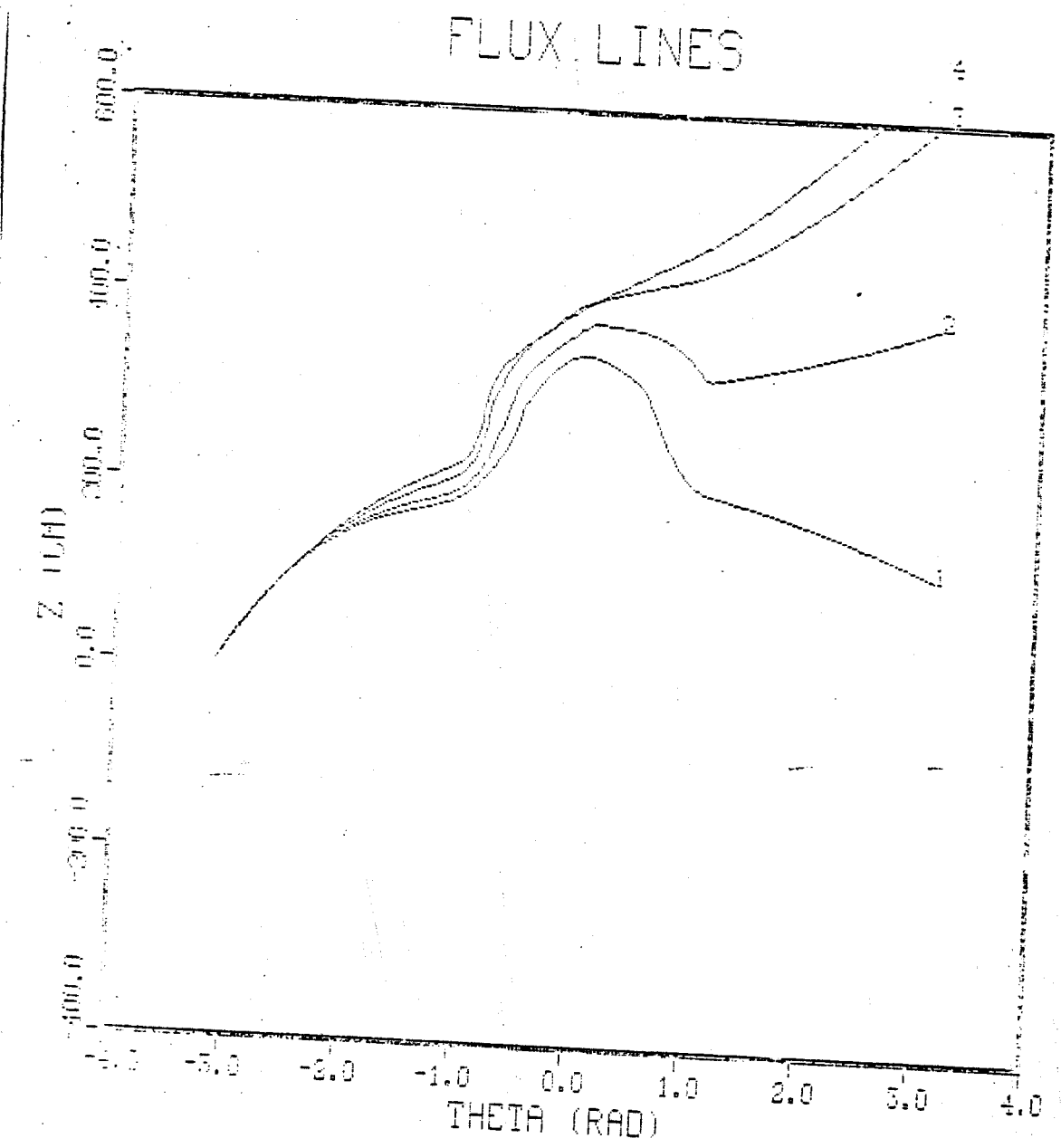

LINE 2 IS DIVERTED BY THE BY THE HYBRID DIVERTOR AND IS ALSO LEAVING THE MACHINE

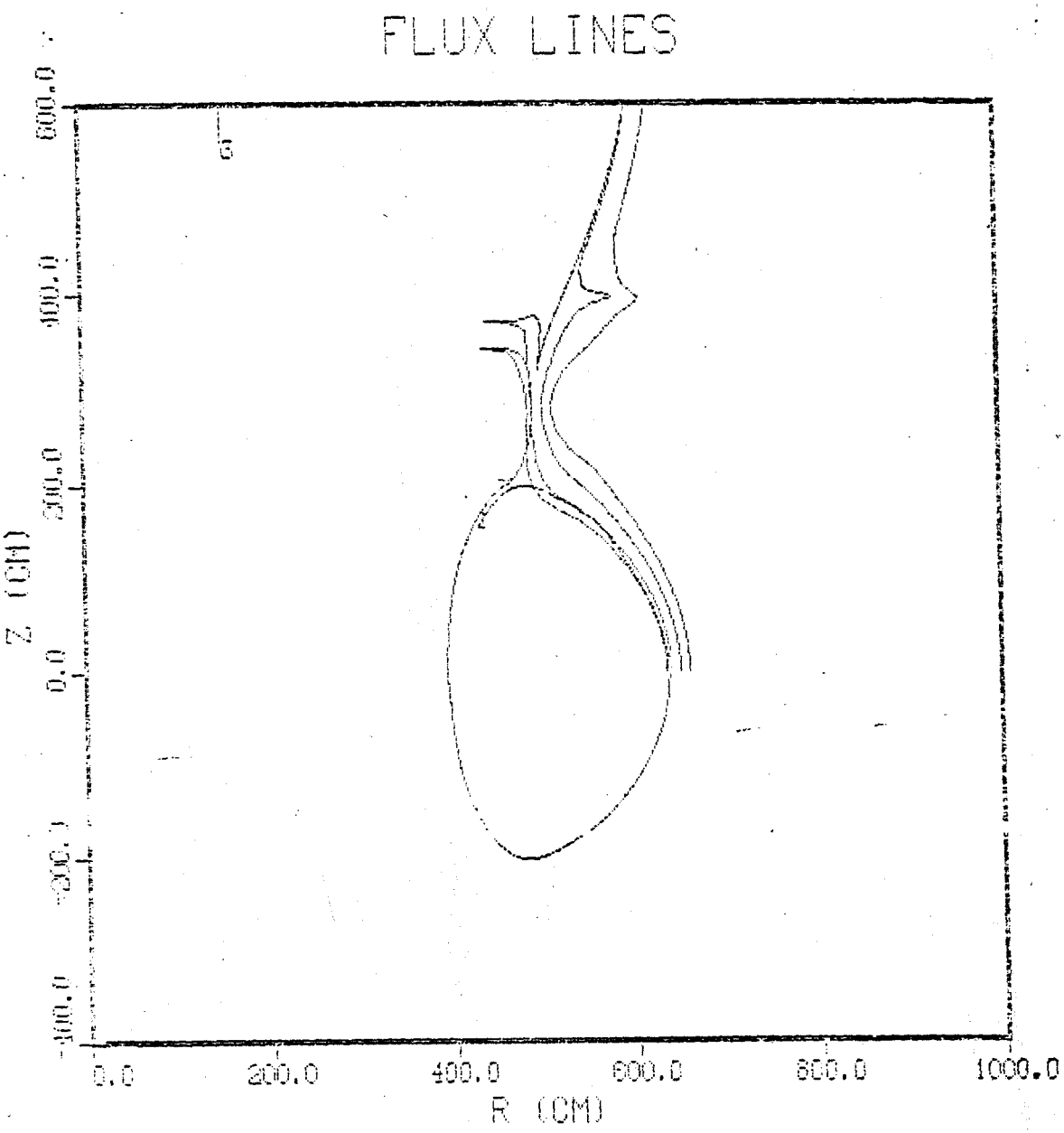

PLASMA IN THE SCRAPE-OFF LAYER IS DIVERTED INTO THE OUTER BRANCH OF THE SEPARATRIX(AT LARGER MAJOR RADIUS) WHICH SOLVES THE BLOCKAGE OF THE PARTICLE HANDLING AT THE INNER BRANCH FOR POLOIDAL DIVERTOR

4.0 Divertor Target and Limiter Study

4.1 Design Window Study

Solid divertor target design demands consideration of two vital functions, survival and particle handling. These two functions can be pursued separately in the development stage, and may even be distinct in final design. Emphasis has thus far been placed on target survival, a prerequisite for particle handling.

Major constraints on survivability are heat removal, sputtering rate, and fatigue life. Analysis of existing divertor design work and known sputtering data suggests that acceptable design options may be defined using a design window approach.

Several divertor target designs have been produced to date, including those of Grumman, General Atomic, and Westinghouse, which seek to accomodate peak heat loads of nearly 3 kw/cm^2. Each is subject to some doubt as to survivability. Based on input from the Divertor Workshop at MIT, April 1980, and the Plasma Materials Workshop at Sandia, June 1980, a design heat load of 1 kw/cm^2 was selected as reasonable for the divertor target plate. While experimentation with higher heat loads should continue, analytic treatment of erosion and fatigue life suggest that higher loads would cause very early material failure.

Development of a region of acceptable design conditions requires treatment of all three survival constraints, as well as input of the (presently somewhat uncertain) expected plasma conditions. Further evaluation of particle handling techniques is necessary to incorporate the particle handling function into the design window. Treatment of the survival constraints according to the design

window equations of Fig. 1 and the procedure detailed below leads to the graphical design regions depicted in Figures 2 and 3. Regions within the curves and below the material lines are acceptable. Existing design points can be plotted on such graphs to evaluate their suitability, and specific configurations may be selected from within the design window.

The base design consists of parallel tubes arrayed so that particle flux is received on only one side. Water coolant boasts the broadest range of correlated behavior and has been used to date in developing the procedure.

Heat removal options are limited by critical heat flux, fluid pressure drop, and temperature rise in the fluid. Critical heat flux correlations exist for heat fluxes up to 12 kw/cm^2 without swirl flow and 7 kw/cm^2 with swirl flow. A ratio of pump power to thermal power equal to 2% is taken as the pressure drop design limit. Subcooled boiling pressure drop introduces some uncertainty in the pumping power and CHF boundaries at high heat and mass fluxes. For a conservative treatment, design heat load is here limited to $q"_{CHF}/1.3$. Particle trapping considerations may determine the acceptable fluid temperature rise, though a rather arbitrary allowable $\Delta T_{1-2} = 200^{o}F$ has here been assumed. For any given tube length, diameter, inlet pressure, and inlet temperature, application of appropriate CHF and friction factor correlations and an energy balance permit a plot of design window boundaries on a graph of heat flux (q") versus mass flux (G). The effect of varying diameter can be shown graphically, Fig. 4, while length effects may be treated as in Appendix C.

Fatigue life dictates a maximum tube thickness which varies inversely with heat flux. Major axial thermal stress due to tube connections and supporting structure may be minimized with careful design, but through-thickness cyclic thermal strain is unavoidable. Maximum tube thickness based on this through thickness thermal strain may be plotted versus heat flux, Figs. 5 through 9. In most cases this fatigue curve establishes limits on the maximum thickness allowable under a specified heat load. For two materials evaluated (TZM and Vanadium) the temperature of the outer fiber would exceed that for which reliable fatigue data can be projected. Limiting thickness based on this temperature would be overly conservative (since inner fibers can easily contain the coolant pressure) so allowable heat loads are taken as 75% of that predicted by the known fatigue curves in such cases.

For survival the "thin" tubes desirable for fatigue life must be thick enough to withstand projected sputtering rates. For a given lifetime, this limits the allowable heat flux and provides a third boundary on the design window. Sputtering analysis for a 1 kw/cm^2 heat flux and capacity factor = 1 is presented in Appendix A. Reconciling the sputter rate with the wall thickness limit (due to fatigue) results in either a maximum heat load for 1 year's service or a maximum lifetime for a 1 kw/cm^2 heat load, as detailed in Appendix B. (Also listed is the maximum heat load for 1 month's service.) For this analysis, sputtering varied linearly with heat load, and a target capacity factor of .28 was assumed, consistent with a 90 second burn/15 second rejuvenation cycle.

This analysis establishes the heat flux limits for each material which are graphed on Figures 2 and 3. For TZM, heat load is limited to .6 kw/cm^2 for 1 year life and 2.2 kw/cm^2 for 1 month life. Other material limits are lower, as shown.

FIGURE 1. DESIGN WINDOW EQUATIONS

THERMAL-HYDRAULICS

1. CRITICAL HEAT FLUX

Axial Flow $$q_c'' \leq \frac{1400\ (G)^{.5}}{(D)^{.05}\ (L)^{.15}}$$

Swirl Flow $$q_c'' \leq \frac{398\ G^{.645}(1+(\pi/2y)^2)^{\frac{1}{2}}D^{.24}}{L^{.44}}$$

High Heat Flux $$q_c'' \leq .83\ (1+\frac{G\ \Delta t_{sub}}{\rho\ (1000)})$$

2. ENERGY BALANCE

$$T_{1-2} = \frac{4Lq''}{Dc_pG}\ ,\quad Re = \frac{GD}{\mu} = \frac{4Lq''}{\pi\mu c_p\ \Delta T}$$

3. PRESSURE DROP

$$f_{iso} = .184/Re^{.2} = .184\,\mu^{.2}/(GD)^{.2}$$

$$1\phi\ \text{Axial}\ \Delta p = f\frac{L\ G^2}{2D\ g_c} = \frac{.184\,\mu^{.2}\ L\ G^{1.8}}{2\ D^{1.2}\rho\ g_c}$$

$$1\phi\ \text{Swirl}\ \Delta p = .00089\ \frac{L\ G^2\ \mu_i^{.18}}{2\ D^{2.2}\rho\ g_c\ y^{.6}\ \mu_b^{.18}}$$

4. PUMPING POWER RATIO ($W_p \leq .02$)

$$W_p = \frac{\text{Pumping Power}}{\text{Thermal Power}} = \frac{\dot m\ \Delta p\ /\rho}{\dot m\ c_p\ \Delta T}$$

$$= \frac{\Delta p}{\rho\ c_p\ \Delta T} = \frac{.184\pi\mu^{.2}\ G^{2.8}}{8\ D^{.2}\rho^2\ g_c\ q''\ (778)}$$

MECHANICAL LIFE

1. SPUTTERING THICKNESS LIMIT

$$t \geq \frac{M}{N_a\rho}\ S_i\ J_i\ C \quad + \text{Primary Stress t}$$

2. PRIMARY STRESS THICKNESS LIMIT

Thin Wall $$t \geq pD/2\sigma_m$$

Thick Wall $$t \geq D/2\ \left(\left(\frac{\sigma_m}{\sigma_m-2p}\right)^{\frac{1}{2}} - 1\right)$$

3. FATIGUE THICKNESS LIMIT

$$t \leq \frac{2\ k\ (1-\nu)\Delta\epsilon_{max}}{\propto q''}$$

4. CORROSION TEMPERATURE LIMIT

$$T_c - T_{inlet} \geq q''/h + \Delta T_{1-2}$$

5. MECHANICAL TEMPERATURE LIMIT

$$T_{lim} - T_{inlet} \geq \frac{q''\ (R+t)}{k}\ \ln(1+2t/D) + q''/h + \Delta T$$

6. HEAT TRANSFER COEFFICIENT

$$1\phi\ \text{Axial}\quad h = k/D\ (.023\ Pr^{.4})(D/\mu)^{.8}\ G^{.8}$$

$$1\phi\ \text{Swirl}\quad h = \frac{2.18\ c_p\ G}{y^{.9}}\ \frac{.023(1+(D/L)^{.7})}{Pr^{.667}\ Re^{.2}}$$

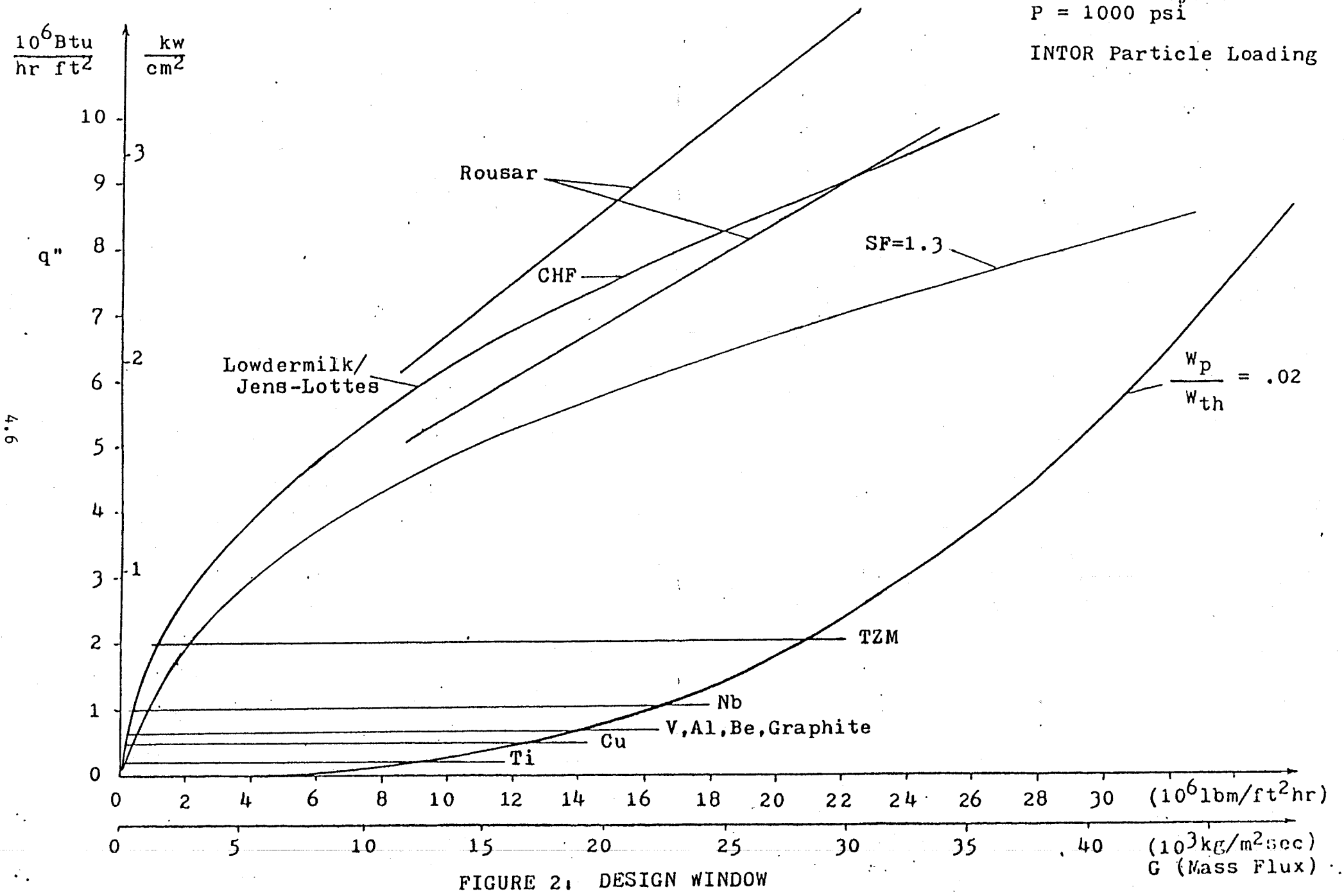

FIGURE 2: DESIGN WINDOW

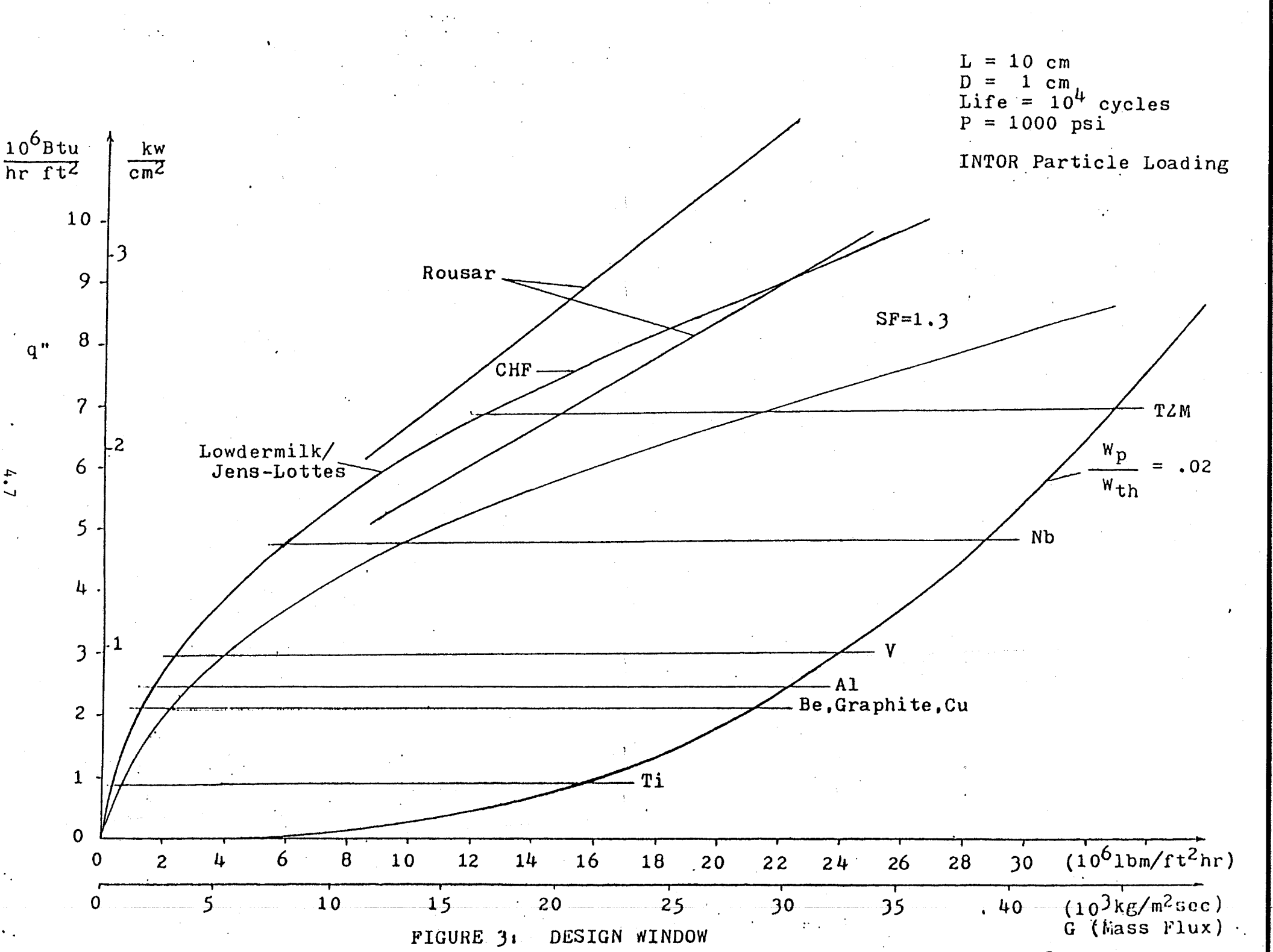

FIGURE 3: DESIGN WINDOW

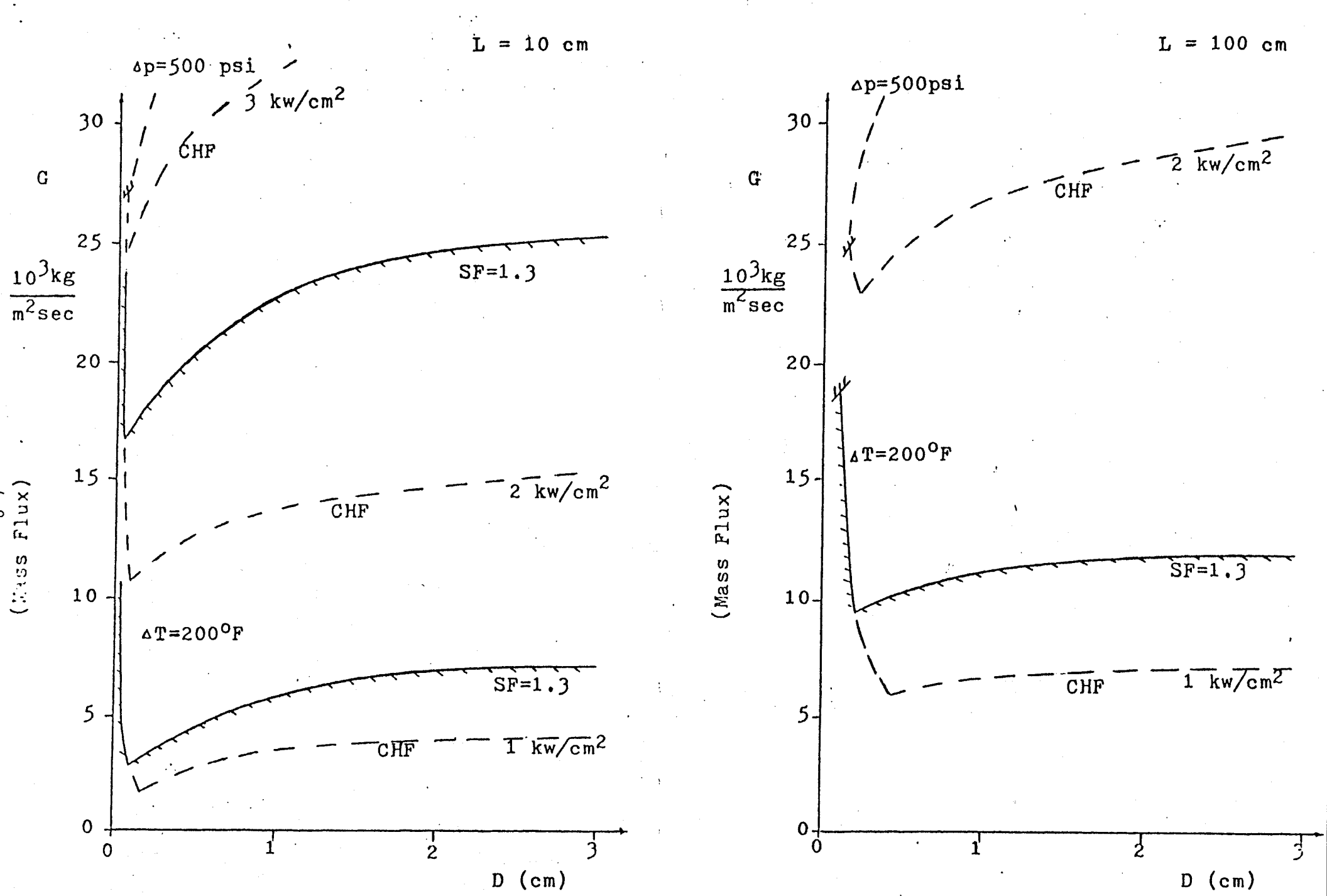

FIGURE 4: Permissible operating regimes for various fluxes (above solid lines) for 10 cm and 100 cm tube lengths

FIGURE 5

MAXIMUM HEAT FLUX VS. THICKNESS
(Region Below Curves Acceptable)

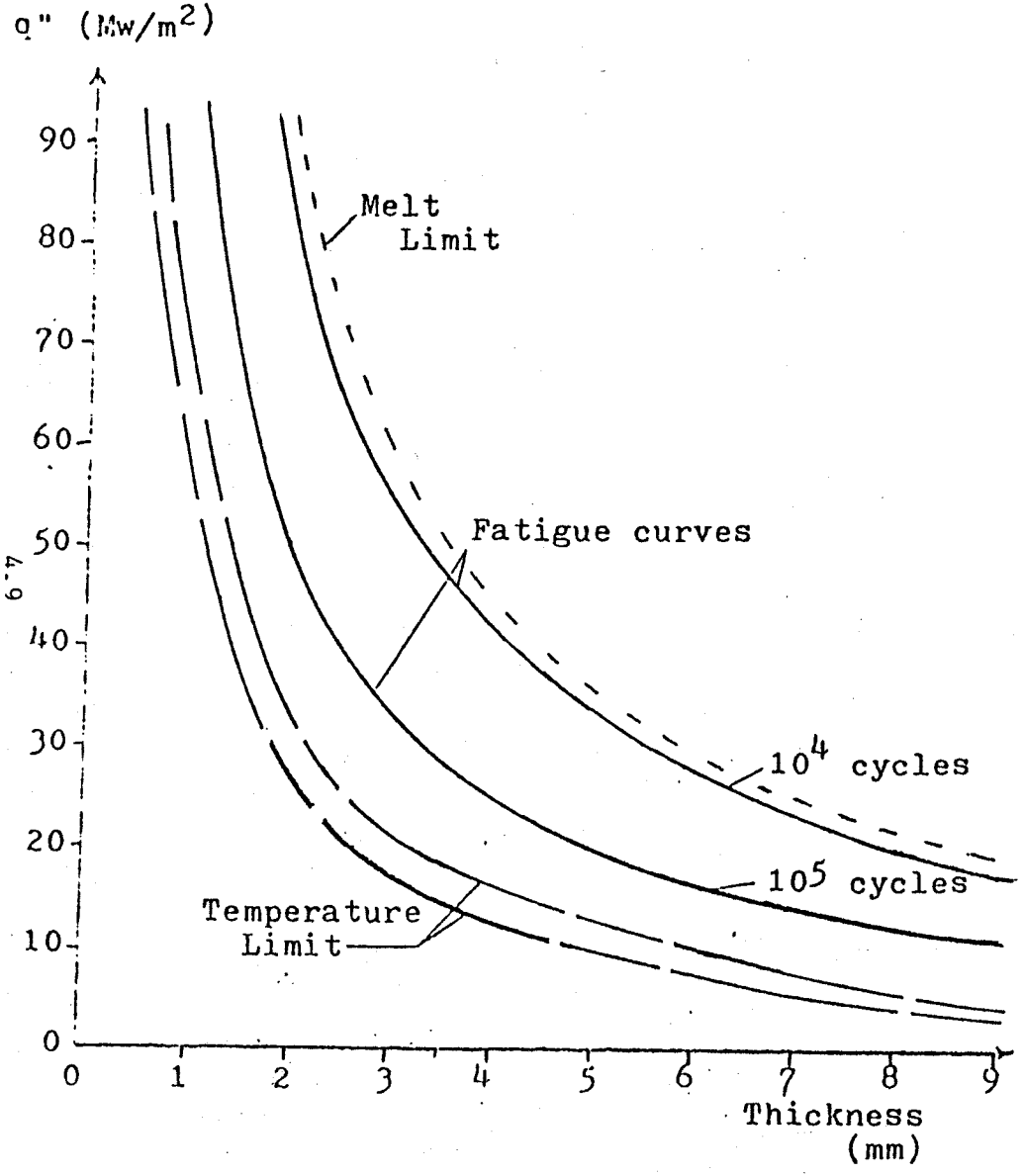

TZM Molybdenum Alloy

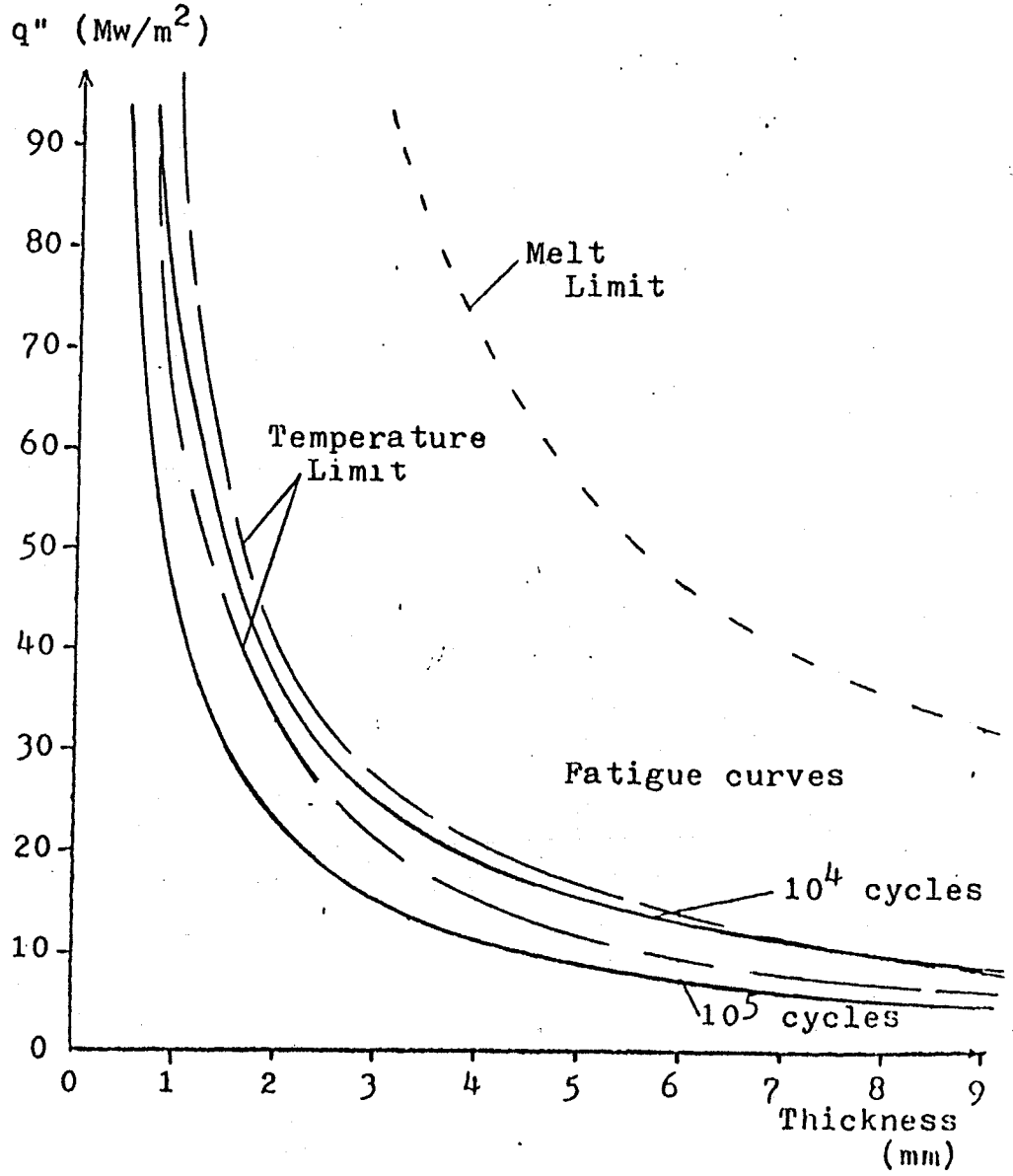

ZAC-2, Copper Alloy

MAXIMUM HEAT FLUX VS. THICKNESS
(Region Below Curves Accept ble)

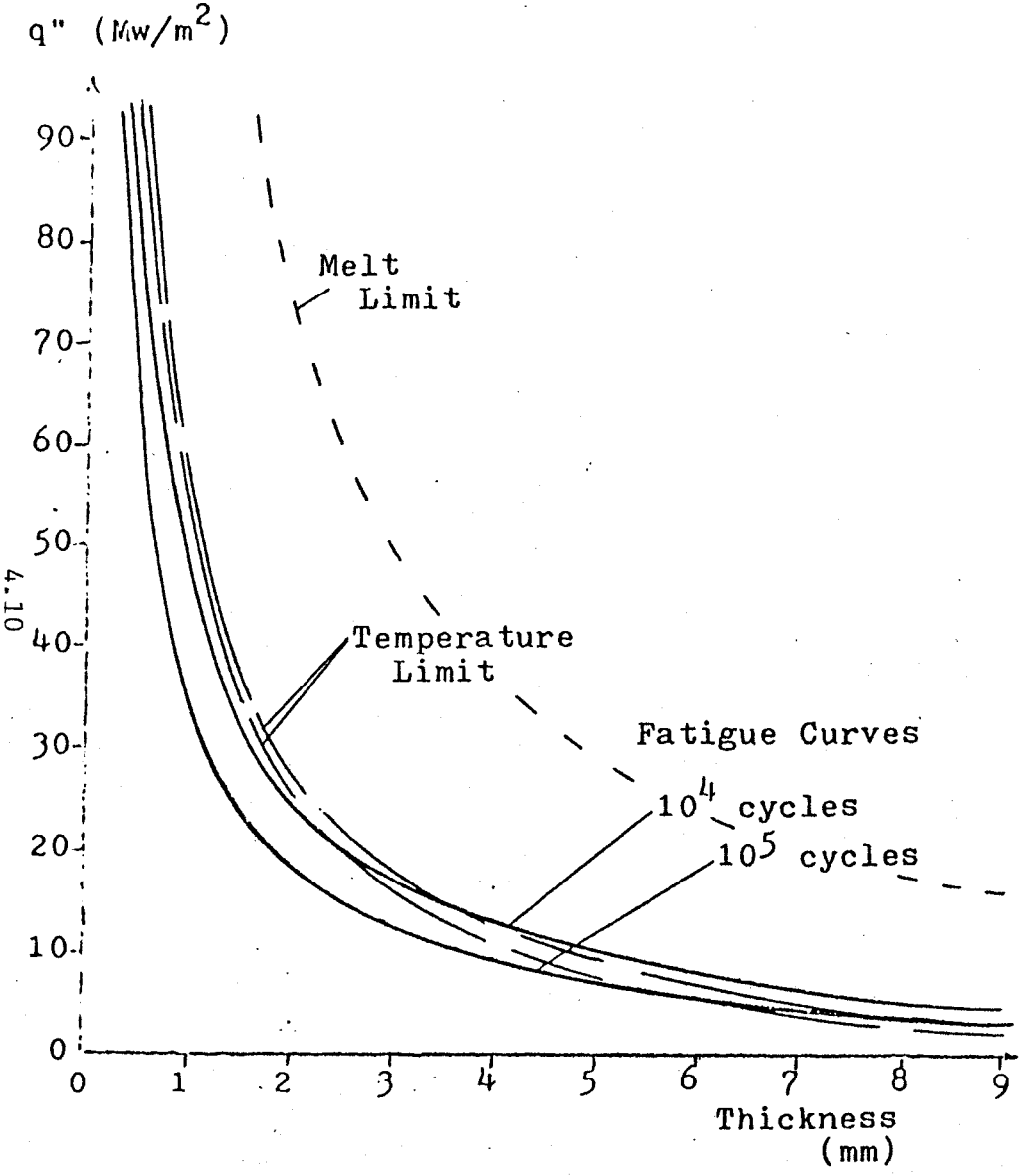

Al-4Mg-1Mn Aluminum Alloy

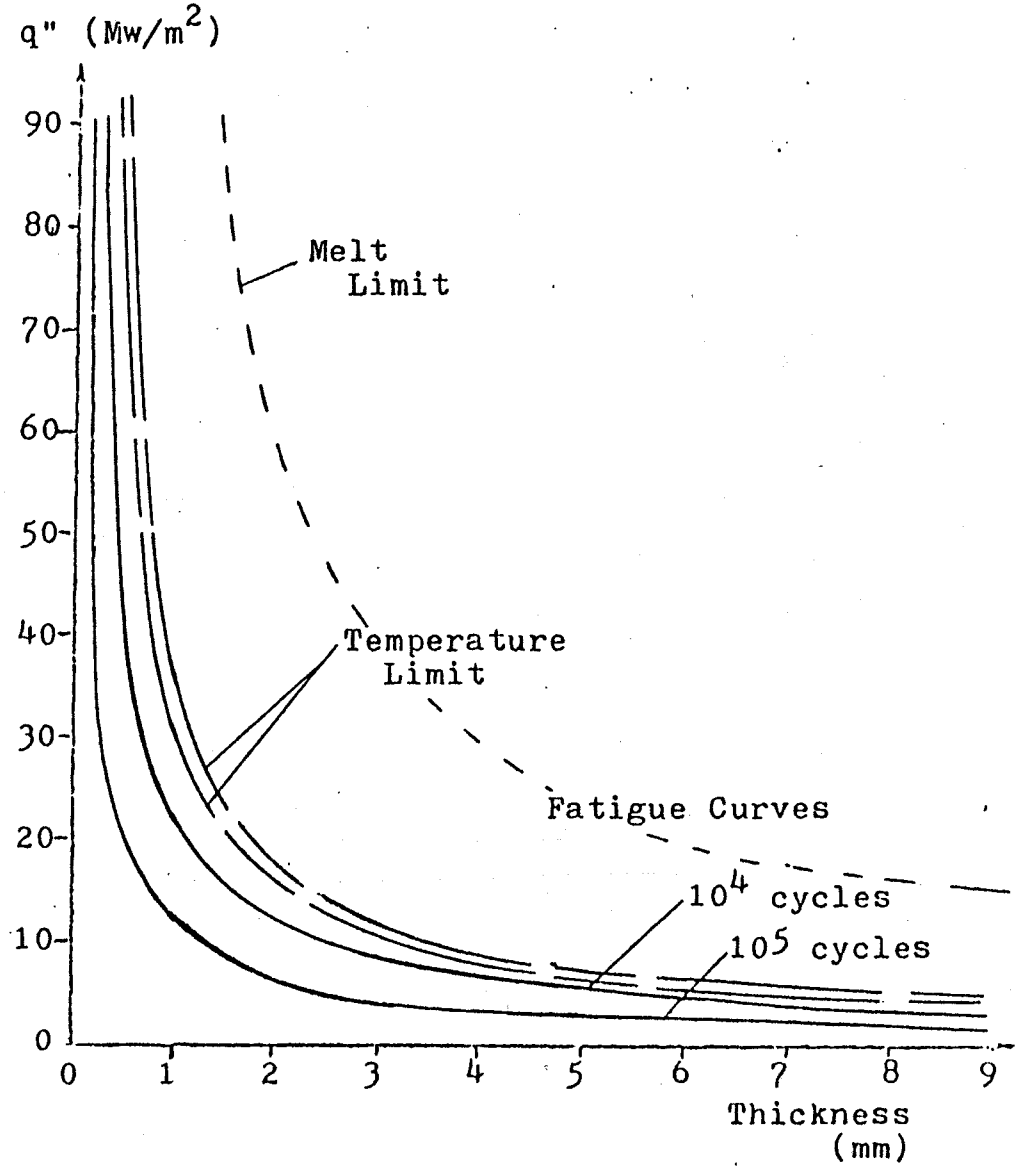

D-43 Niobium Alloy

FIGURE 7

MAXIMUM HEAT FLUX VS. THICKNESS
(Region Below Curves Acceptable)

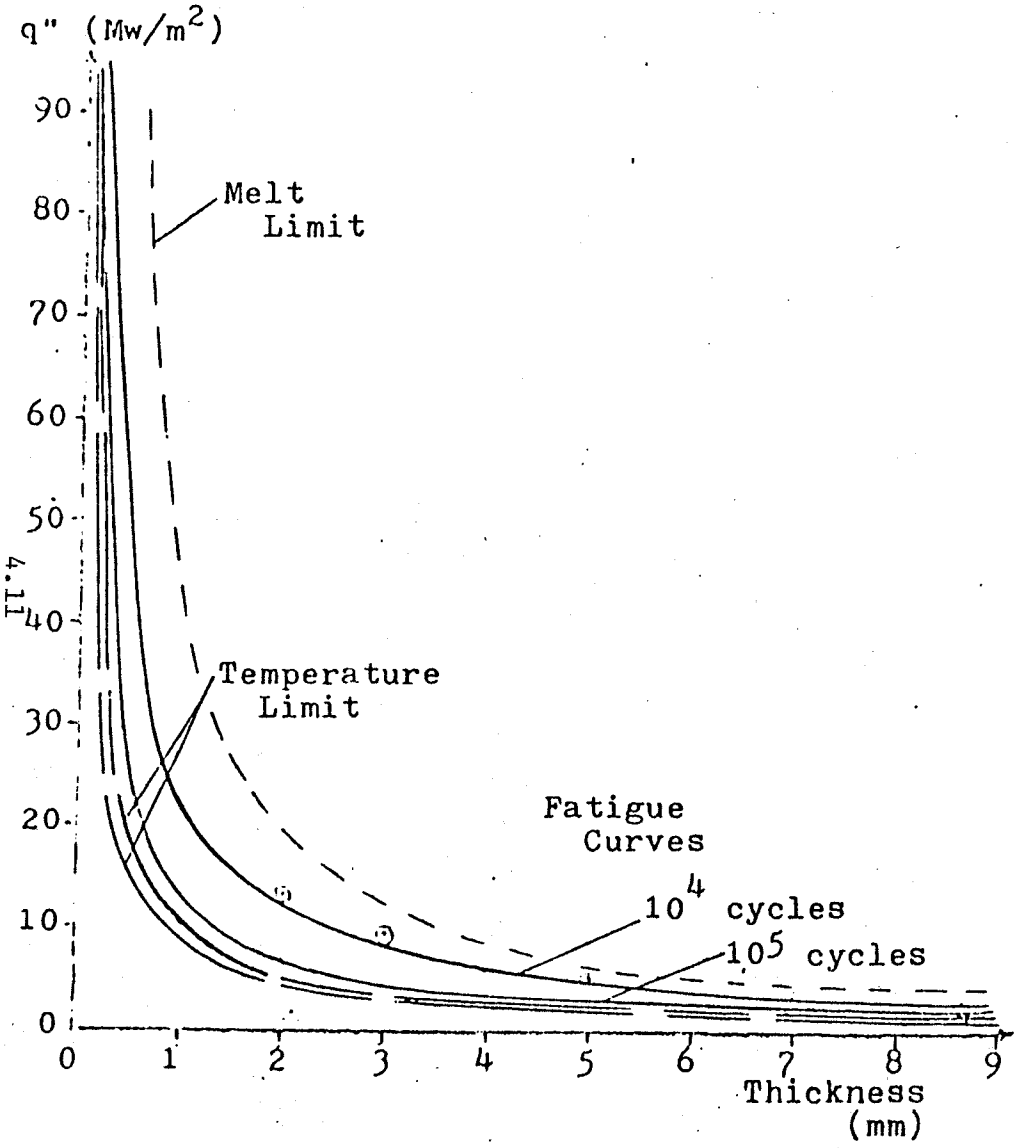

Vanadium Alloy

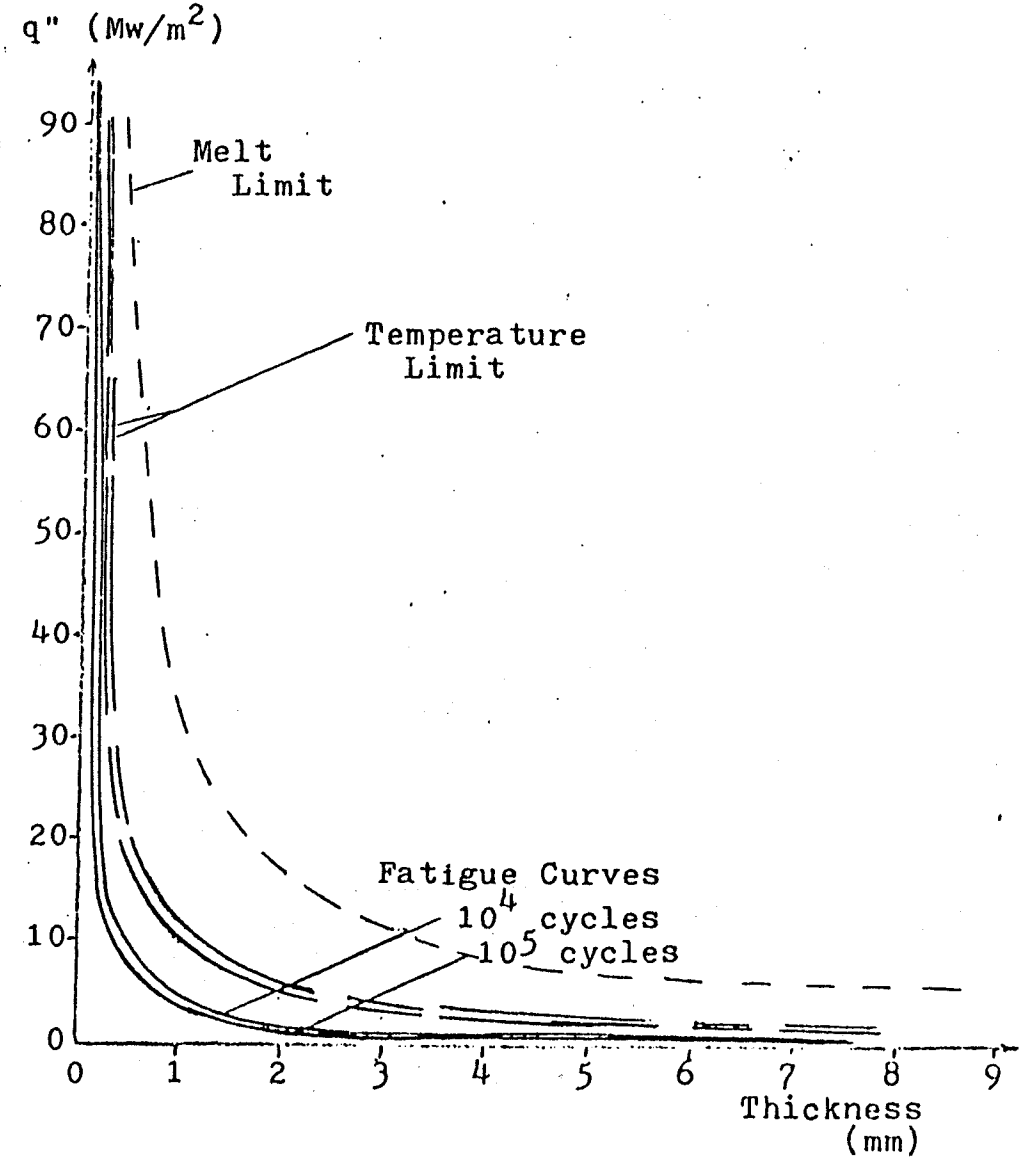

Ti-6Al-4V Titanium Alloy

MAXIMUM HEAT FLUX VS. THICKNESS
(Region Below Curves Acceptable)

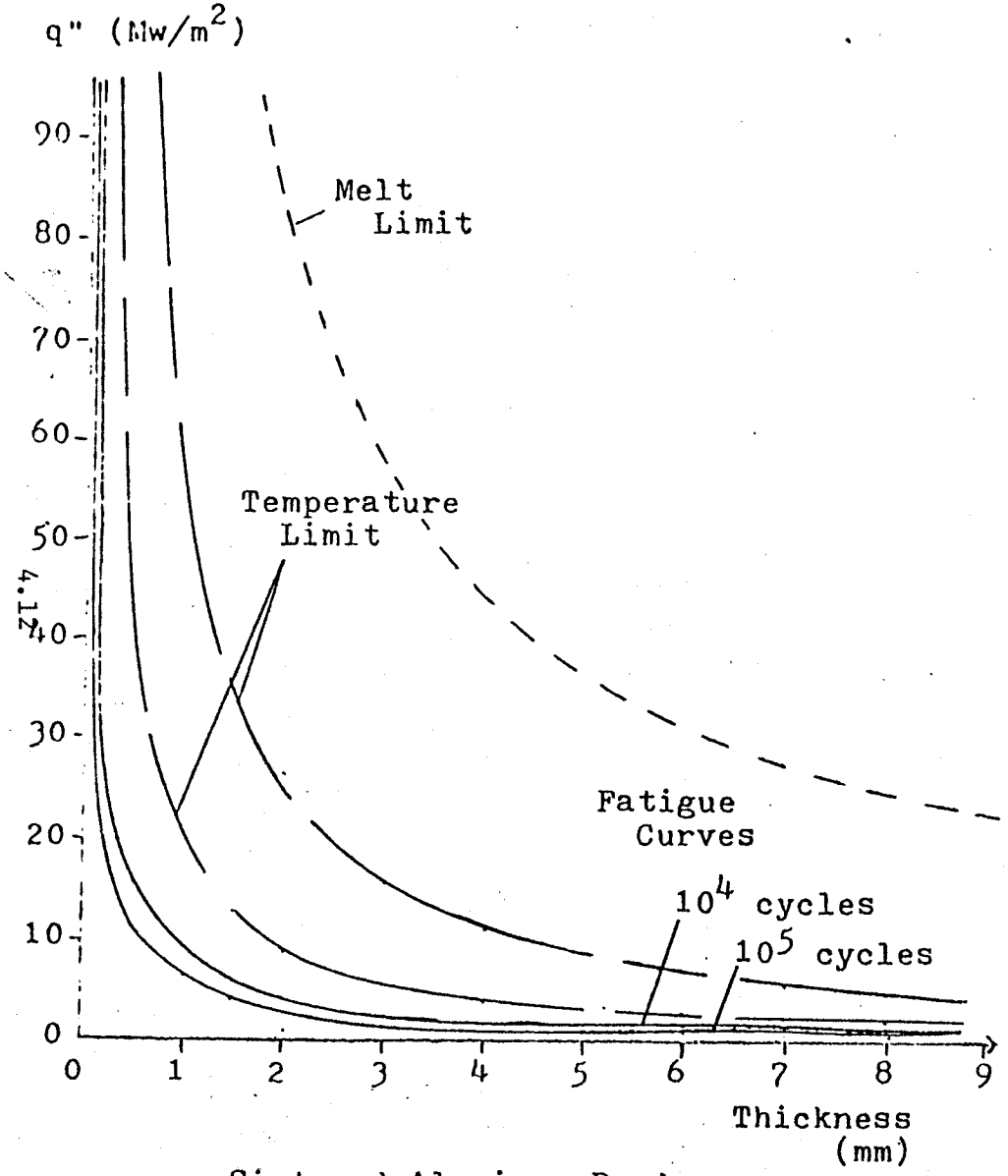

Sintered Aluminum Powder

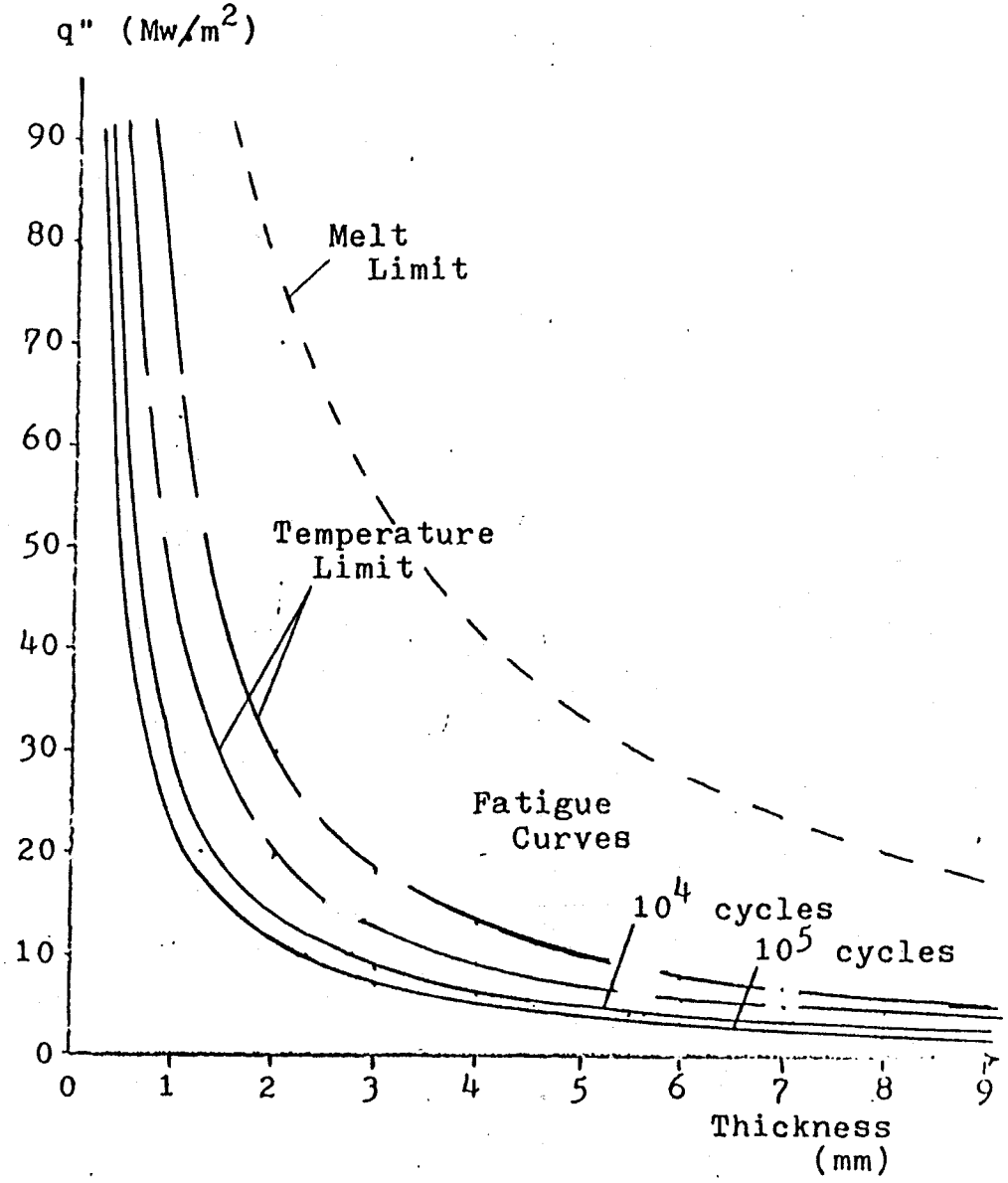

Beryllium

MAXIMUM HEAT FLUX VS. THICKNESS
(Region Below Curves Acceptable)

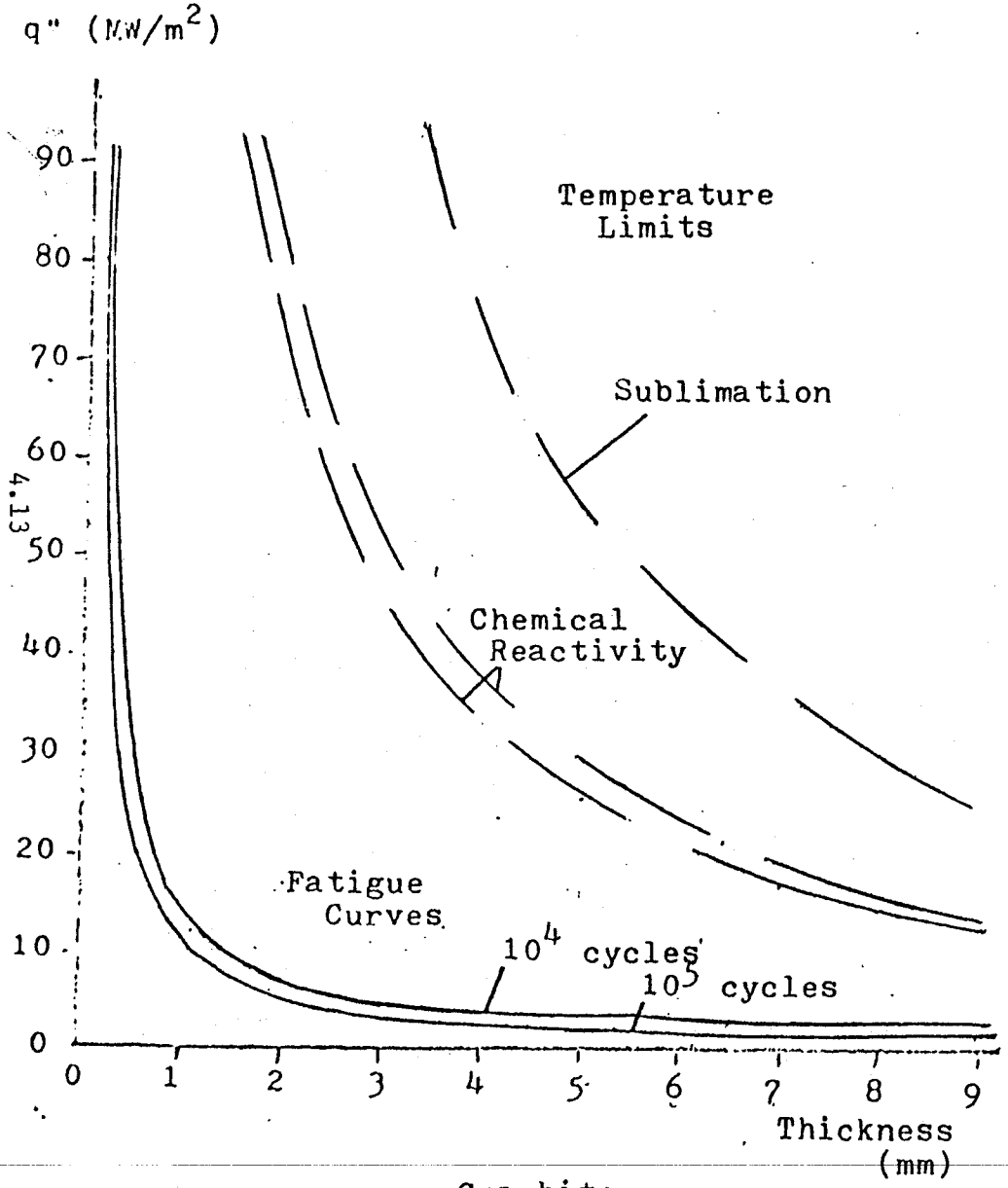

4.13

Graphite

SPUTTERING ANALYSIS

1. To develop comparative values of sputtering rate, independent of target capacity factor, take as base case a 1 kw/cm^2 heat load applied continuously for one year. Base plasma parameters on PPPL calculations for the INTOR poloidal divertor considering 99% recycling at the plate. An ETF sized bundle divertor would receive lower heat and particle load, so data should be conservative.

$$P = 2.9\ N\ k\ T_i$$

Divertor Power, P = 90 MW ; T_i = 1.3 keV.
Particle Current = 1.5×10^{23} particles/sec.
For 1 kw/cm^2 heat load, target consists of 9 m^2.
Particle flux = 1.66×10^{22} particles/m^2-sec.

2. Sputtering rate estimated by following equation:

$$\frac{\Delta t}{\Delta \tau}\left(\frac{mm}{yr}\right) = \frac{M}{N_a \rho} S_i J_i C$$

M = target atomic wt. S_i = sputtering coefficient
N_a = Avogadro's Number J_i = ion flux
ρ = target density C = capacity factor

S_i for 1 keV D^+ ions from ORNL 5207; ORNL 5207/R1.
(Correction to 1.3 keV, according to Bohdansky, is factor = 1.07)
C = 1.0 for continuous operation.

3. Results for 10 Mw/m^2 flux, 1.3 keV mean particle energy, continuous operation:

Cu - 626 mm/yr	V - 101 mm/yr	Mo - 54 mm/yr
Al - 371 mm/yr	Ti - 98 mm/yr	Nb - 40.4 mm/yr
Be - 154 mm/yr	C_{gr} - 96 mm/yr	W - 7.9 mm/yr

4. Plasma Contamination Constraint

a. Max impurity concentration for ignition: $\sigma_{max} = 50 \times 10^{-.12}$
b. ETF plasma 6.4×10^{22} particles.
c. Sputtering rate = $J_i S_i$
d. Assume 1% of sputtered material gets to plasma. (99% is pumped or condensed.)

$$\text{Plasma burn time limit} = \frac{\text{max impurity allowed}}{\text{sputtering rate @ 10 Mw/m}^2}$$

e. Results:

W - .0082 sec	Nb - 3.79 sec	Al - 234 sec
Mo - 1.94 sec	V - 71.5 sec	Be - 2178 sec
Cu - 2.46 sec	Ti -117. sec	C_{gr} - 2610 sec

5. A sputtering/plasma contamination figure of merit may be computed:

$$M = \frac{\text{burn time}}{\text{sputter rate}} \qquad \left(\frac{\text{mm-sec}}{\text{yr}}\right)$$

W - .00104	Nb - .088	Ti - 1.19
Cu - .0035	Al - .632	Be - 14.19
Mo - .0361	V - .712	C_{gr} - 27.38

The larger the value of M, the more suitable is the material for the target surface.

POSSIBLE DESIGN POINTS

	For 1 Year Life			For 1kw/cm^2 Heat Flux	
	L= 10cm	L= 100cm		L= 10cm	L= 100cm
TZM Tube	single coat			single coat	
	.6 cm	.8 cm	Dia.		
	1.9 x 10^6	4.0 x 10^6	G($\frac{lbm}{hr\ ft^2}$)		
	.6 kw/cm^2	.6 kw/cm^2	q" max	NOT POSSIBLE	
	9.5 mm	9.5 mm	thickness		
	21 °F	44 °F	ΔT_{1-2}		
	.3 psi	9 psi	ΔP_{1-2}		
	.000009	.00006	W_p		
	monthly recoat/replacement			frequent recoat	
	.6 cm	.8 cm	Dia.	.6 cm	.8 cm
	4.5 x 10^6	8.2 x 10^6	G($\frac{lbm}{hr\ ft^2}$)	4.5 x 10^6	8.2 x 10^6
	1.0 kw/cm^2	1.0 kw/cm^2	$q"_{max}$	1.0 kw/cm^2	1.0 kw/cm^2
	1.8 mm	1.8 mm	thickness	12.2 mm	12.2 mm
	13 °F	55 °F	ΔT_{1-2}	13 °F	55 °F
	.9 psi	30 psi	ΔP_{1-2}	.9 psi	30 psi
	.00004	.0003	W_p	.00004	.0003
	1 month	1 month	coating life	9.8 months	9.8 months
luminum Tube	single coat			single coat	
	.6 cm	.8 cm	Dia.		
	.5 x 10^6	.9 x 10^6	G($\frac{lbm}{hr\ ft^2}$)		
	.2 kw/cm^2	.2 kw/cm^2	$q"_{max}$	NOT POSSIBLE	
	20 mm	20 mm	thickness		
	24 °F	73 °F	ΔT_{1-2}		
	.02 psi	.4 psi	ΔP_{1-2}		
	.000003	.000023	W_p		
	monthly recoat/replacement			frequent recoat	
	.6 cm	.8 cm	Dia.	.6 cm	.8 cm
	2.4 x 10^6	5.5 x 10^6	G($\frac{lbm}{hr\ ft^2}$)	4.5 x 10^6	8.2 x 10^6
	.8 kw/cm^2	.8 kw/cm^2	$q"_{max}$	1.0 kw/cm^2	1.0 kw/cm^2
	8.3 mm	8.3 mm	thickness	6.4 mm	6.4 mm
	20 °F	50 °F	ΔT_{1-2}	13 °F	55 °F
	.4 psi	9 psi	ΔP_{1-2}	.9 psi	30 psi
	.000015	.00012	W_p	.00004	.0003
	1 month	1 month	coating life	22.5 days	22.5 days

POSSIBLE DESIGN POINTS

	For 1 Year Life			For 1kw/cm^2 Heat Flux	
	L= 10cm	L= 100cm		L= 10cm	L= 100cm
Niobium Tube	single coat			single coat	
	.6 cm	.8 cm	Dia.		
	.5 x 10^6	.9 x 10^6	G($\frac{lbm}{hr\ ft^2}$)		
	.3 kw/cm^2	.3 kw/cm^2	q" max	NOT POSSIBLE	
	3.7 mm	3.7 mm	thickness		
	36 °F	110 °F	ΔT_{1-2}		
	.02 psi	.4 psi	ΔP_{1-2}		
	.000002	.000015	W_p		
	monthly recoat/replacement			frequent recoat	
	.6 cm	.8 cm	Dia.	.6 cm	.8 cm
	4.5 x 10^6	8.2 x 10^6	G($\frac{lbm}{hr\ ft^2}$)	4.5 x 10^6	8.2 x 10^6
	1.0 kw/cm^2	1.0 kw/cm^2	q" max	1.0 kw/cm^2	1.0 kw/cm^2
	1.8 mm	1.8 mm	thickness	2.3 mm	2.3 mm
	13 °F	55 °F	ΔT_{1-2}	13 °F	55 °F
	.9 psi	30 psi	ΔP_{1-2}	.9 psi	30 psi
	.00004	.0003	W_p	.00004	.0003
	1 month	1 month	coating life	66 days	66 days
Copper Tube	single coat			single coat	
	.6 cm	.8 cm	Dia.		
	.5 x 10^6	.9 x 10^6	G($\frac{lbm}{hr\ ft^2}$)		
	.16 kw/cm^2	.16 kw/cm^2	q" max	NOT POSSIBLE	
	27 mm	27 mm	thickness		
	20 °F	58 °F	ΔT_{1-2}		
	.02 psi	.4 psi	ΔP_{1-2}		
	.00004	.00028	W_p		
	monthly recoat/replacement			frequent recoat	
	.6 cm	.8 cm	Dia.	.6 cm	.8 cm
	2.2 x 10^6	4.8 x 10^6	G($\frac{lbm}{hr\ ft^2}$)	4.5 x 10^6	8.2 x 10^6
	.7 kw/cm^2	.7 kw/cm^2	q" max	1.0 kw/cm^2	1.0 kw/cm^2
	12.5 mm	12.5 mm	thickness	11 mm	11 mm
	19 °F	46 °F	ΔT_{1-2}	13 °F	55 °F
	.3 psi	6 psi	ΔP_{1-2}	.9 psi	30 psi
	.000011	.00009	W_p	.00004	.0003
	1 month	1 month	coating life	23 days	23 days

POSSIBLE DESIGN POINTS

	For 1 Year Life			For 1kw/cm^2 Heat Flux	
	L= 10cm	L= 100cm		L= 10cm	L= 100cm
Titanium Tube	single coat			single coat	
	.6 cm	.8 cm	Dia.		
	.5 x 10^6	.9 x 10^6	$G(\frac{lbm}{hr\ ft^2})$		
	.08 kw/cm^2	.08 kw/cm^2	q" max	NOT POSSIBLE	
	2.3 mm	2.3 mm	thickness		
	10 °F	29 °F	ΔT_{1-2}		
	.02 psi	.4 psi	ΔP_{1-2}		
	.000008	.000056	W_p		
	monthly recoat/replacement			frequent recoat	
	.6 cm	.8 cm	Dia.	.6 cm	.8 cm
	.5 x 10^6	.9 x 10^6	$G(\frac{lbm}{hr\ ft^2})$	4.5 x 10^6	8.2 x 10^6
	.08 kw/cm^2	.08 kw/cm^2	q" max	1.0 kw/cm^2	1.0 kw/cm^2
	1.3 mm	1.3 mm	thickness	.5 mm	.5 mm
	36 °F	110 °F	ΔT_{1-2}	13 °F	55 °F
	.02 psi	.4 psi	ΔP_{1-2}	.9 psi	30 psi
	.000002	.000015	W_p	.00004	.0003
	1 month	1 month	coating life	6.6 days	6.6 days
Vanadium Tube	single coat			single coat	
	.6 cm	.8 cm	Dia.		
	.5 x 10^6	.9 x 10^6	$G(\frac{lbm}{hr\ ft^2})$		
	.2 kw/cm^2	.2 kw/cm^2	q" max	NOT POSSIBLE	
	6.0 mm	6.0 mm	thickness		
	24 °F	73 °F	ΔT_{1-2}		
	.02 psi	.4 psi	ΔP_{1-2}		
	.000003	.000023	W_p		
	monthly recoat/replacement			frequent recoat	
	.6 cm	.8 cm	Dia.	.6 cm	.8 cm
	4.5 x 10^6	8.2 x 10^6	$G(\frac{lbm}{hr\ ft^2})$	4.5 x 10^6	8.2 x 10^6
	1.0 kw/cm^2	1.0 kw/cm^2	q" max	1.0 kw/cm^2	1.0 kw/cm^2
	2.5 mm	2.5 mm	thickness	2.5 mm	2.5 mm
	13 °F	55 °F	ΔT_{1-2}	13 °F	55 °F
	.9 psi	30 psi	ΔP_{1-2}	.9 psi	30 psi
	.00004	.0003	W_p	.00004	.0003
	1 month	1 month	coating life	32 days	32 days

POSSIBLE DESIGN POINTS

	For 1 Year Life			For 1kw/cm^2 Heat Flux	
	L= 10cm	L= 100cm		L= 10cm	L= 100cm
eryllium Tube	single coat			single coat	
	.6 cm	.8 cm	Dia.		
	.5 x 10^6	.9 x 10^6	G($\frac{lbm}{hr\ ft^2}$)		
	.2 kw/cm^2	.2 kw/cm^2	q" max	NOT POSSIBLE	
	8.9 mm	8.9 mm	thickness		
	24 °F	73 °F	ΔT_{1-2}		
	.02 psi	.4 psi	ΔP_{1-2}		
	.000003	.000023	W_p		
	monthly recoat/replacement			frequent recoat	
	.6 cm	.8 cm	Dia.	.6 cm	.8 cm
	2.2 x 10^6	4.8 x 10^6	G($\frac{lbm}{hr\ ft^2}$)	4.5 x 10^6	8.2 x 10^6
	.7 kw/cm^2	.7 kw/cm^2	q" max	1.0 kw/cm^2	1.0 kw/cm^2
	3.3 mm	3.3 mm	thickness	3.0 mm	3.0 mm
	19 °F	46 °F	ΔT_{1-2}	13 °F	55 °F
	.3 psi	6 psi	ΔP_{1-2}	.9 psi	30 psi
	.000011	.00009	W_p	.00004	.0003
	1 month	1 month	coating life	22.8 days	22.8 days
Graphite Tube	single coat			single coat	
	.6 cm	.8 cm	Dia.		
	.5 x 10^6	.9 x 10^6	G($\frac{lbm}{hr\ ft^2}$)		
	.2 kw/cm^2	.2 kw/cm^2	q" max	NOT POSSIBLE	
	5.5 mm	5.5 mm	thickness		
	24 °F	73 °F	ΔT_{1-2}		
	.02 psi	.4 psi	ΔP_{1-2}		
	.000003	.000023	W_p		
	monthly recoat/replacement			frequent recoat	
	.6 cm	.8 cm	Dia.	.6 cm	.8 cm
	2.2 x 10^6	4.8 x 10^6	G($\frac{lbm}{hr\ ft^2}$)	4.5 x 10^6	8.2 x 10^6
	.7 kw/cm^2	.7 kw/cm^2	q" max	1.0 kw/cm^2	1.0 kw/cm^2
	2.1 mm	2.1 mm	thickness	1.8 mm	1.8 mm
	19 °F	46 °F	ΔT_{1-2}	13 °F	55 °F
	.3 psi	6 psi	ΔP_{1-2}	.9 psi	30 psi
	.000011	.00009	W_p	.00004	.0003
	1 month	1 month	coating life	20.3 days	20.3 days

PUMPING POWER VS. LENGTH

Competing influences on pressure drop as a function of length result in a minimum pumping power. The length at which this minimum occurs may be a desirable tube design length. On one hand, longer tubes reduce manifold friction losses but require higher flow rates to avoid CHF. On the other, shorter tubes demand more manifolding but can operate below CHF at lower flow rates.

Modelling the manifolding for each tube by two tee joints and two 90° elbows of large radius, the tube pressure drop depends on tube length plus the equivalent lengths of tees and elbows.

$$\frac{\Delta p}{\text{tube}} = f \frac{G^2}{2\rho} \left(\frac{L(\text{tube}) + 2L_{eq(\text{tee})} + 2L_{eq(\text{elbow})}}{D} \right)$$

Common values are $L_{eq(\text{tee})}/D = 60$; $L_{eq(\text{elbow})}/D = 20$.

From the CHF correlation and the Safety Factor of 1.3:

$$G = \left[\frac{q'' \, D^{.05} \, L^{.15}}{1400 \; / \; 1.3} \right]^2$$

Substitution and differentiation leads to a minimum pumping power when $L = 30.5\ D$. For diameters between .6 cm and .8 cm, this suggests an <u>optimum length</u> between <u>18.3 cm</u> and <u>24.4 cm</u>.

4.2 Limiter Concepts

In the major tokamak devices the limiters are often damaged by high heat load from the plasma. The heat load tends to concentrate on a small local area. The problem will become more severe for a power producing reactor because the heat load would be much higher. The present major devices such as ISX-B, Alcators, PLT, PDX and Doublet have a total heat load in the range of hundreds of kW to 6 MW. Doublet III will reach 18 MW and TFTR will have 40 MW. The heat load for a prototypical reactor will be about 200 MW for 1000 MW of thermal power[1]. Therefore, limiters will be subjected to a very high heat load if the plasma is not diverted.

Lately there is emphasis on mechanical divertors or pumping on a limiter. The first criterion for such a method to work is to be able to design a reliable limiter which can survive the high heat load of the plasma. To spread the heat uniformly a limiter of large surface area which closely matches the boundary of the plasma is necessary. A toroidal bumper or belt limiter has been discussed by many groups. However, there is still a peaked local heat load even on a limiter surface perfectly matched to the plasma boundary. Thus, a uniform heat load condition is almost impossible to achieve, let alone the other abnormal operations, such as disruptions or run-away electrons. We have found that an oscillating limiter system is a possible answer for solving the high heat load problem. The unsteady heat transfer analyses show that a cooled surface can sustain a much higher heat load under transcient conditions.

4.2.1 Oscillating Limiter Concept

As has been discussed in the introduction, local heat is very difficult to avoid. A large surface limiter system covers more than fifty percent of the first wall. It is also very difficult to replace any damaged part. Remote controlled maintainance is necessary which will greatly reduce the machine availability. Therefore, it is important to find a method to design a feasible local limiter which can sustain the heat load and can be replaced with reasonable ease. We thus discovered that the oscillating limiter method might be the solution.

A straight forward oscillating limiter concept can be illustrated by Fig. 1, which is the cross-sectional view of a tokamak plasma. The end of the limiter driving shaft is attached to a spring. The limiter can be driven by a cam shaft. Such a limiter system is closely in analogue to the piston system of an internal combustion engine. Only one segment is in contact with the plasma while all the others are back near the wall. The half circle limiter system is illustrated by Fig. 2. The lower picture shows the top view of the tokamak. The upper figures are the expanded plasma cross-sections at AA and BB. The limiters at AA are in contact with the plasma. They will be subjected to a transcient heat for 50 ms or less and thus called exposure period. The limiters at BB and

other locations are away from the plasma and will be cooled by water or helium and thus called cooling period which is 0.5 sec. The limiters are driven by a simple mechanism on the top and bottom. When the shafts are pushed in, the limiter pair will be separated from the plasma. On the other hand, the limiter pair will move toward the plasma when the shafts are pulled away. Since there is only 2 cycles per sec for each limiter pair, the driving mechanism would be simple. The thermal hydraulic analyses for water and helium cooling are as follows. The heat transfer problems in the transcient exposure period and cool down period can be treated separately. During the exposure period the heat load is very high and time is short so that we can conservatively and conveniently neglect the heat removal by the coolant. The surface temperature rise can be calculated from[2]

$$\Delta T = 4q\frac{\delta}{\lambda}\sqrt{F}\sum_{n=1}^{\infty} ierfc\frac{(2n-1)}{2\sqrt{F}}. \tag{1}$$

Here $F = \frac{a\tau}{\delta^2}$, $a = \frac{\lambda}{\rho c_p}$ and λ is the heat conductivity, ρ is the density, C_p is the specific heat, δ is the wall thickness of the limiter and τ is the exposure time. We choose Mo as the sample material. Other materials with high melting point will work equally well as long as they meet other requirements, such as low Z and erosion resistance. For sputtering, erosion and protection against disruption and run-away electrons, the wall thickness is chosen to be no less than 3 mm. We also assume that the heat load of 10 kW/cm^2 which is reasonable for both TFTR and prototype reactors. This means that the needed limiter area is 0.33 m^2 for reactors which can be easily designed. The surface temperature rising would be $\Delta T = 1410$°C for 50 ms and 25 ms respectively. The average temperature rises are 554°C and 277°C. The question is now whether it can be cooled in 0.5 sec during the cooling down period by either water or helium. Since the cooling of helium is of great interest because it is safe, we will use helium cooling as a sample case to analyze the thermal characteristics. The analysis method using water as coolant is similar.

During the cooling down period, the limiter has been moved back 5 cm where the heat load will be reduced by a factor of nearly two orders of magnitude because of the exponential decay in heat flux from the plasma boundary[3]. This heat load can be neglected as compared with the cooling rate. A reasonable choice of the helium pressure is 60 atm and the mean velocity would be 400 m/sec. Assuming the equivalent diameter of the cooling path is $d_{eq} = 2$cm, then Prandtl number $\simeq 0.72$, Reynolds number $= \frac{\rho v d}{\mu} = 1.1 \times 10^6$, and the Nusselt number Nu $= 0.023 \times (\mathrm{Re})^{0.8}\,(\mathrm{Pr})^{0.4} \simeq 1373$. The heat transfer coefficient becomes

$$a = \frac{Nu\lambda}{d} = 1.37 \text{ Watt/cm}^2\ ^\circ\text{k}$$

To remove the total heat within 0.5 sec, the average heat transfer rate is

$$q_{av} = 0.5 \text{ kW/cm}^2 .$$

Thus the mean temperature difference between the helium and the wall is 364°C. The thermal characteristics for both water and helium cooling are shown in Figs. 3 and 4 and tabulated in Table 1. Figure 3 shows the input heat as function of time. The design points are indicated by the arrows. Figure 4 shows the temperature variation during the exposure (on) and cooling down (off) periods. The maximum temperature is well below the melting point. The limiter can be cooled down in 0.5 sec. The temperatures cooled down to 764°C and 200°C for He and water coolants respectively. Cooling down to lower temperature is not necessary and is not efficient. This temperature range is close to that of the enviroment inside the reactor chamber. The cooled down temperature is higher and the exposure time is shorter for He because of the much lower heat transfer coefficiency.

Conclusion

We can draw a definitive conclusion from this preliminary analysis. The oscillating limiter concept is feasible for a tokamak reactor, using either water or helium as a coolant. The advantage is that the helium can be used as coolant so the danger of water leakage can be eliminated. The limiters are at discrete local positions, thus easy maintenance is possible. Further investigation of fatigue problems, detailed mechanical and maintenance design studies are warranted.

Table 1

Thermal Characteristics of the Oscillating Limiters Designed

Using near TFTR Parameters

TFTR Parameters

thermal power	W = 40 MW	first wall loading	18 W/cm^2
major radius	R_o = 2.48 m	first wall area	110 m^2
minor radius	a = 0.85 m	wall total loading	$18 \times 110 \times 10^4 = 20 \times 10^6$ W
plasma current	I_p = 1 MA	limiter loading	40 — 20 = 20 MW
mean temperature	T = 6 keV	limiter max. heat load	10 kW/cm^2
area of each limiter	0.2 m^2 = 0.8 m × 0.25 m		

Thermal Characteristics

material of limiters	Mo	Mo
thickness of limiters	3 mm	3 mm
exposure time	50 msec	25msec
max. surface temperature	1640°C	1764°C
coolant:	water	Helium
average wall temperature rise	553°C	277°C
velocity:	10 m/s	400 m/s
cooling period:	0.45 sec	0.475 sec
total limiters number	10	20

Figure Captions

Fig. 1. Cross-sectional view of toroidal plasma with simplified oscillating limiter system. The limiter surface is in contact with plasma sequentially following the movement of the controlled rods. There are four sets or more of such limiters distributed around the torus.

Fig. 2. A simplified diagram of a separated oscillating limiter system. The pictures on the top show the cross-sectional views at AA and BB in the figure at the bottom which shows the top view of tokamaks. Each limiter touches the plasma for a short time, then retreats several cm for a longer time to cool down.

Fig. 3. Thermal characteristics of the oscillating limiters. The upper curve is the maximum surface temperature of plates as a function of thickness δ under transcient heat load q. Here $a = \frac{\lambda}{\rho c_p}$ is the physical property of the materials, the ratio of surface temperature rise to the input heat, and t is the exposure time. The lower curve shows the typical history of surface temperature of limiter in a working cycle using water or helium as coolant.

References

1. Stacey, W. M., Jr. et al, U. S. INTOR Report, Nov. (1979)
2. Rohsenow, W. M., Hartnett, J. P., Handbook of Heat Transfer, McGraw-Hill Book Company, 3–67 (1973)
3. Hayzen, A., Private Communication (1980)
4. Kutateladze, S. S., Borishanski, V. M., A Concise Encyclopedia of Heat Transfer, Ch. 12, Pergamon Press (1966)

4.2.2 Alcator Limiter Study Concepts

Purpose

The purpose of this plan is: to develop a limiter or limiters (subjected to high heat and particle fluxes at plasma edge) for long pulse operation of tokamak fusion devices; to study the particle removal with the limiters; and to study and develop the methods for protections against disruptions and other abnormal operation, such as run-away electrons and arcing.

Alcator A has a peak heat of 5 kW/cm^2 and high particle flux, and as such is an ideal test facility. Access is adequate for small scale tests.

Limiter Types

Active cooling methods will be developed for the conventional poloidal ring type limiter. The complete or partial toroidal rail types will be designed and studied. Innovative ideas will be investigated.

The conventional methods and two conceived innovative ideas are described in the following.

1) Conventional ring type

The present limiters for Alcators are poloidal rings made of molybdenum and are inertially cooled after pulses. For the purpose of comparison, a ring type, water-cooled limiter has been designed by McDonnell Douglas. The preliminary results are shown in Figure 1. The surface of the limiter is a 2 mm molybdenum shell bonded onto an array of copper tubes. The initial design study of such a limiter is underway and will be evaluated. If judged to be feasible, it will be fabricated for testing. In this conventional method, the water temperature will rise at the exit ends, and thus will reduce the heat removal efficiency. A spray cooling method is proposed here and is illustrated by Figure 2. The surface can be coated with molybdenum or graphite or other materials. The pumping from the back side can be tested.

2) Innovative concepts

Three innovative concepts have been conceived, the spring-like coiled limiter, a series of coiled tops, and oscillating limiters (Section 4.3.1). The coiled limiter is shown in Figure 3. The advantage of the coil limiter is that the plasma will reach the front as well as inner surfaces of the tubes as is illustrated by Figure 3b. This not only increases the surface area, but also reduces the thermal stress. It will be tested if the neutrals inside the coil can be pumped out at the ends. One can vary the pitch of the spring to determine the most

effective cooling and particle removal. Because the plasma may pass through the space in between turn, two or more coil limiters may be needed. It is also possible to use a secondary cooling as is shown by Figure 3d with counter flow coolant. It is like a heat exchanger. The primary water will be recooled at each turn so that the temperature over the entire length of the limiter will be nearly uniform and the heat removal will be more effective.

The coiled top-like limiter is illustrated by Figure 4. The tops will be mounted on a duct and water lines will be connected to a manifold. The neutrals scattered into the duct can be pumped away.

The application of the coil limiters to a reactor is illustrated by Figure 5. The whole first wall can be lined with these springs. They do not have to be closely fitted together and can be easily replaced.

The purpose of the above discussion is to demonstrate that innovative methods are conceivable. Alcator-A is a valuable facility in which to carry out the testing of these methods.

Testing Plan

The testing plan is briefly outlined as follows:

- A valid concept will be designed, evaluated and tested.
- The test on the actively cooled limiters will always begin with low power. The power will be raised gradually to highest possible level.
- If the test is successful at normal operation, the limiters will be punished with simulated abnormal operations such as disruption, runaway electrons, etc.
- The limiter will be subjected to many thousands of pulses to test the fatigue
- Coating of different materials with various thicknesses will be tested. Pumping techniques will be tested.
- After the successful limiters are identified, the tests will be repeated by covering the first wall area as much as possible with these limiters

LIMITER CONCEPT 1:
FORMED SKIN/COOLANT TUBES

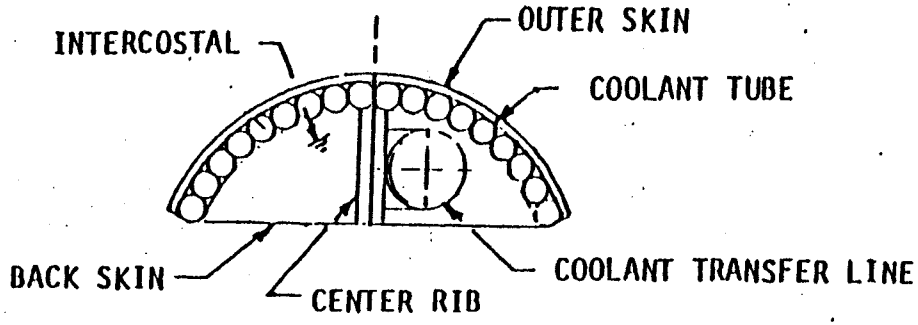

MATERIALS

	SKIN	TUBES	STRUCTURE
(a)	Cu	Cu	Mo; ST STL
(b)	Ta-10W	Cu	
(c)	Mo	Cu	

THERMAL HYDRAULICS

FOR 5 KW/CM^2 PEAK HEAT FLUX:

CLNT	SKIN MATERIAL	SKIN T_{MAX}
H_2O	Cu	250 °C
H_2O	Ta-10W	650 °C
H_2O	Mo	400 °C

FABRICATION

- SKIN FORMED OVER PATTERN
- TUBES, SKIN, STRUCTURE BRAZED AS UNIT
- COATING COULD BE ADDED TO SKIN

Figure 1. Water-Cooled Limiter Design

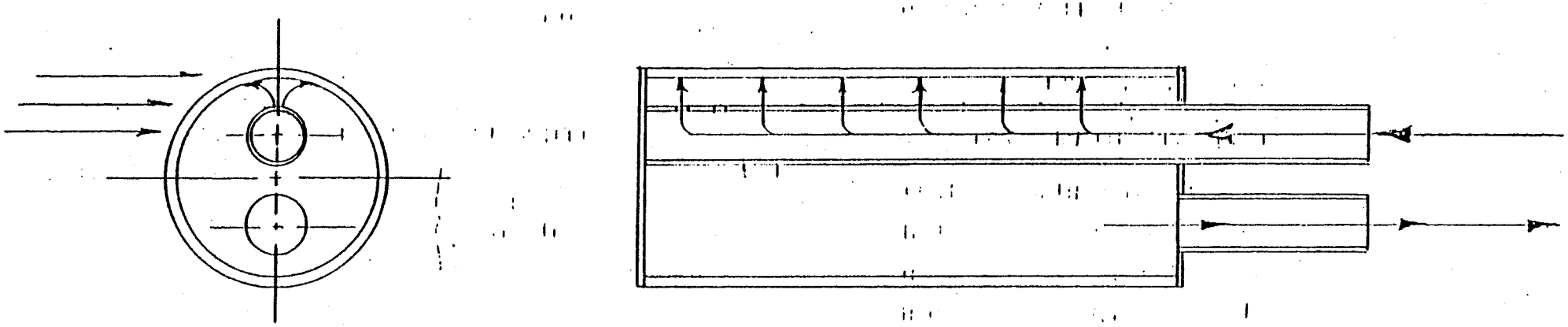

Figure 2. Sketches to Illustrate Different Cooling Methods

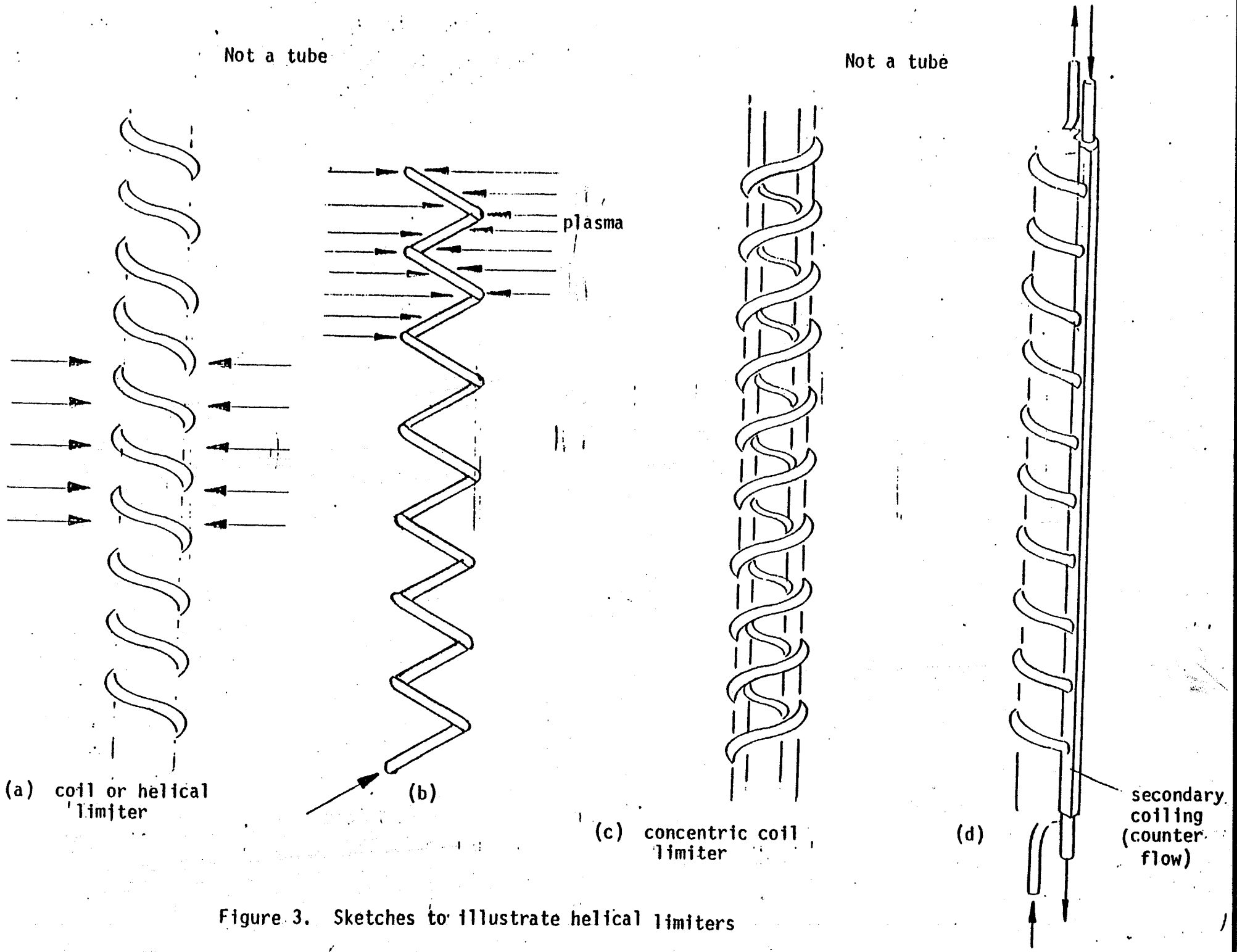

Figure 3. Sketches to illustrate helical limiters

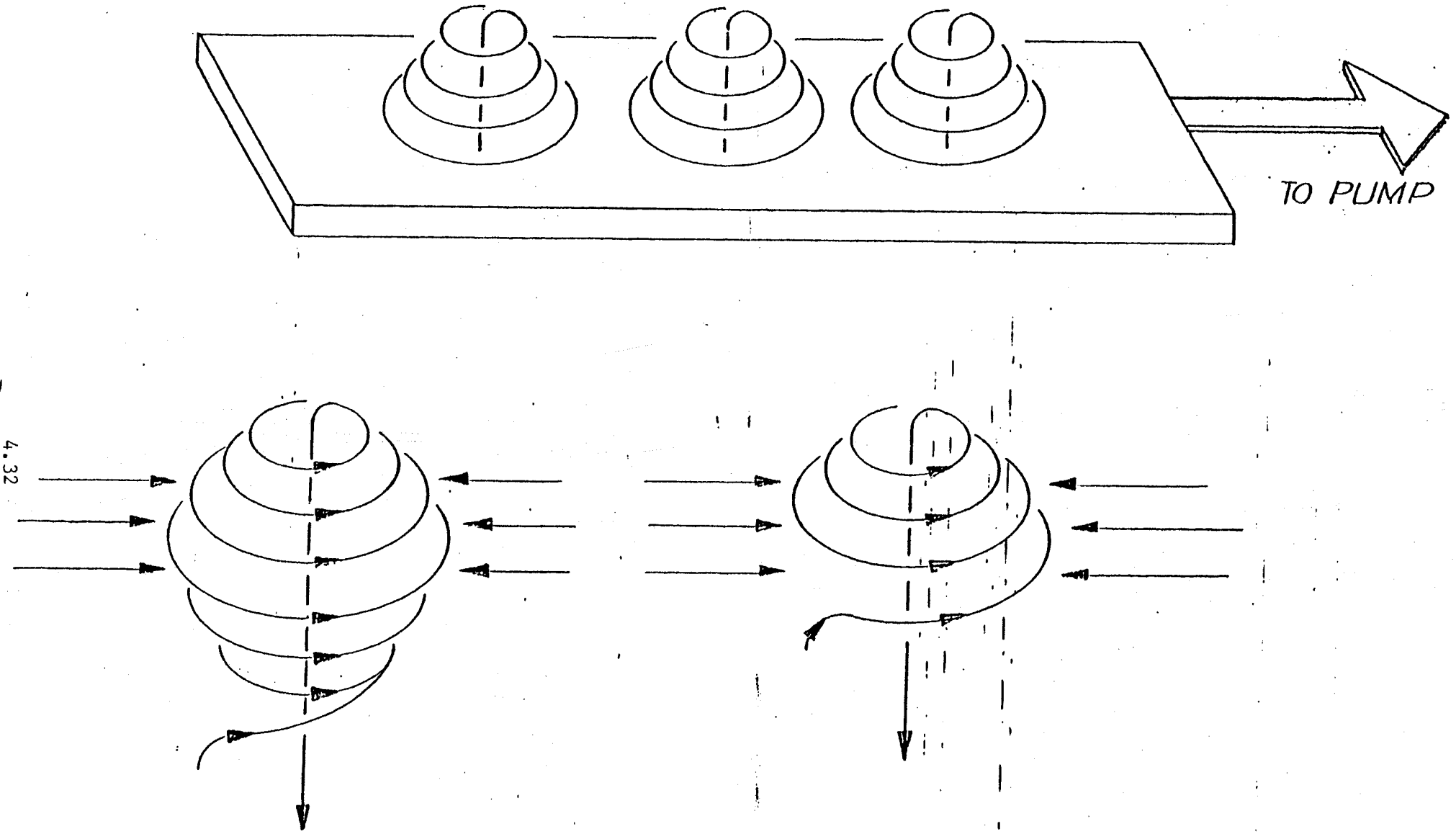

Figure 4. Sketches to illustrate coiled top limiters

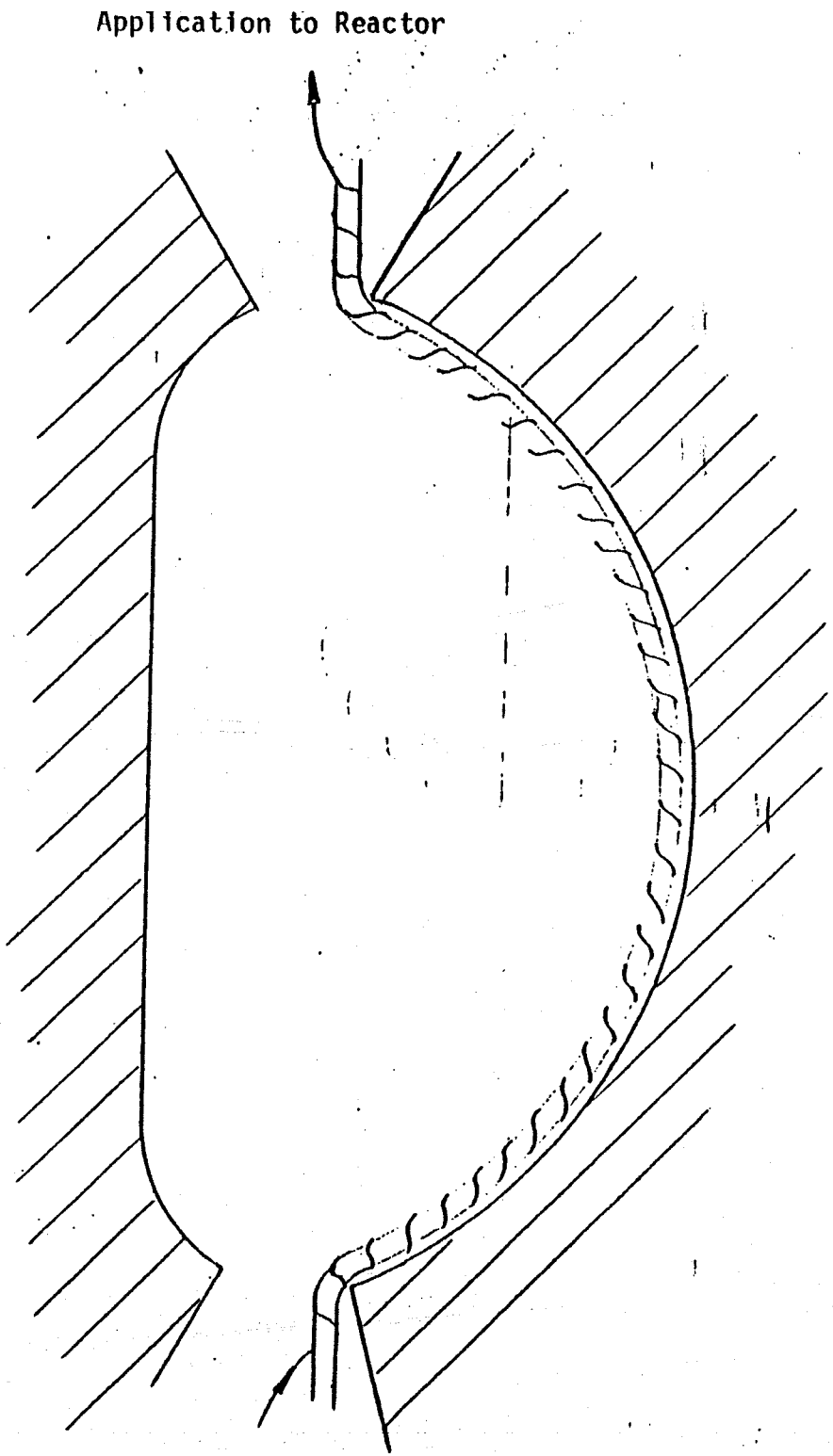

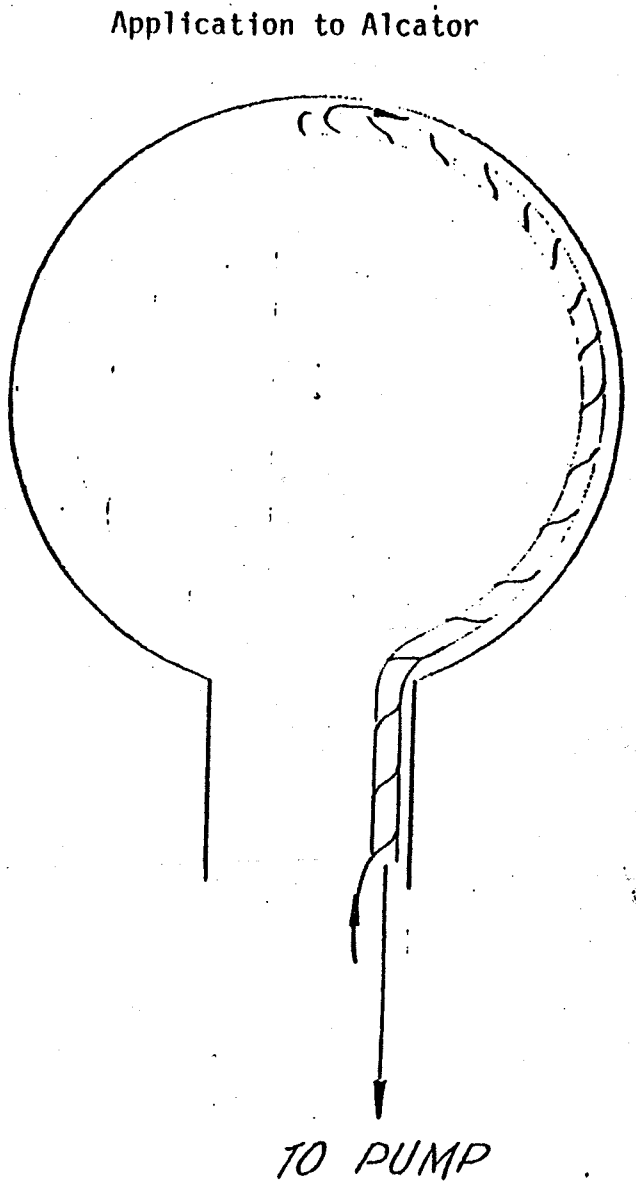

Figure 5.. Sketches to illustrate the Application to Alcator and the Reactor

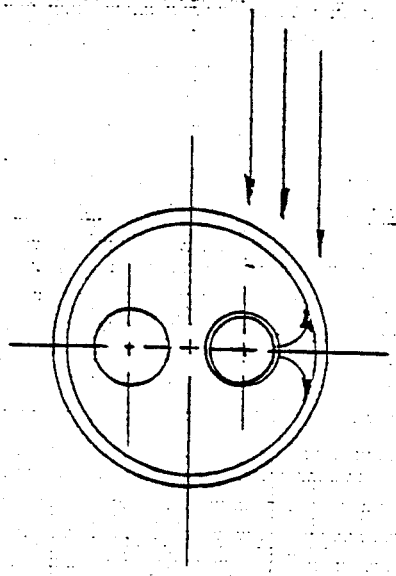

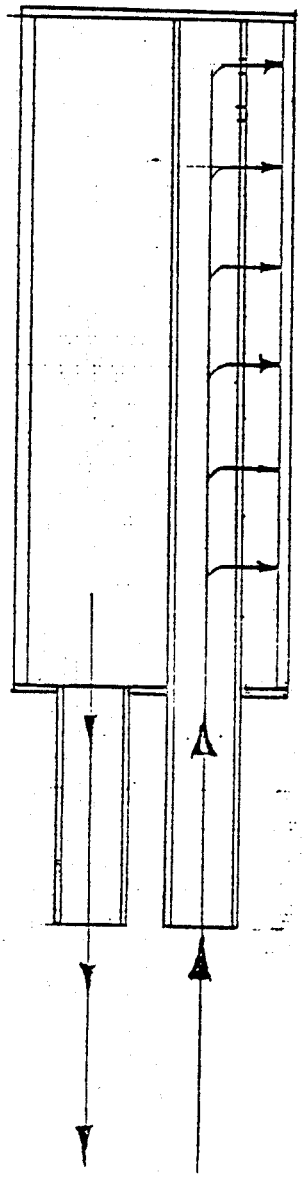

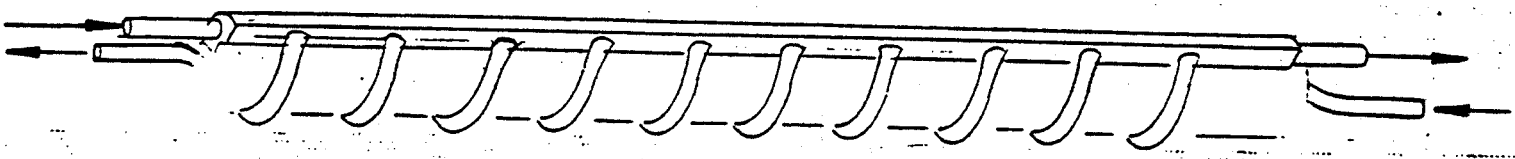

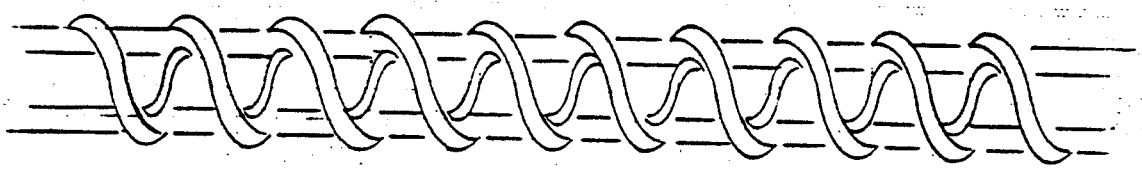

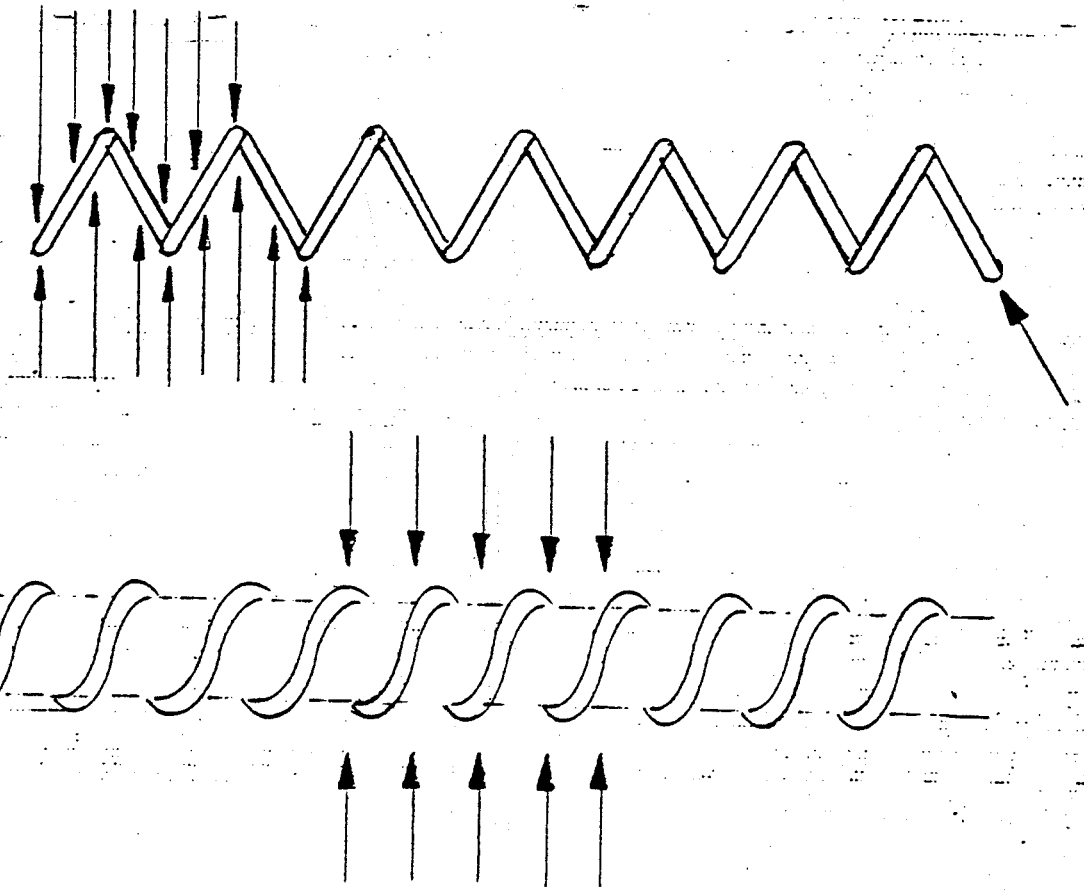

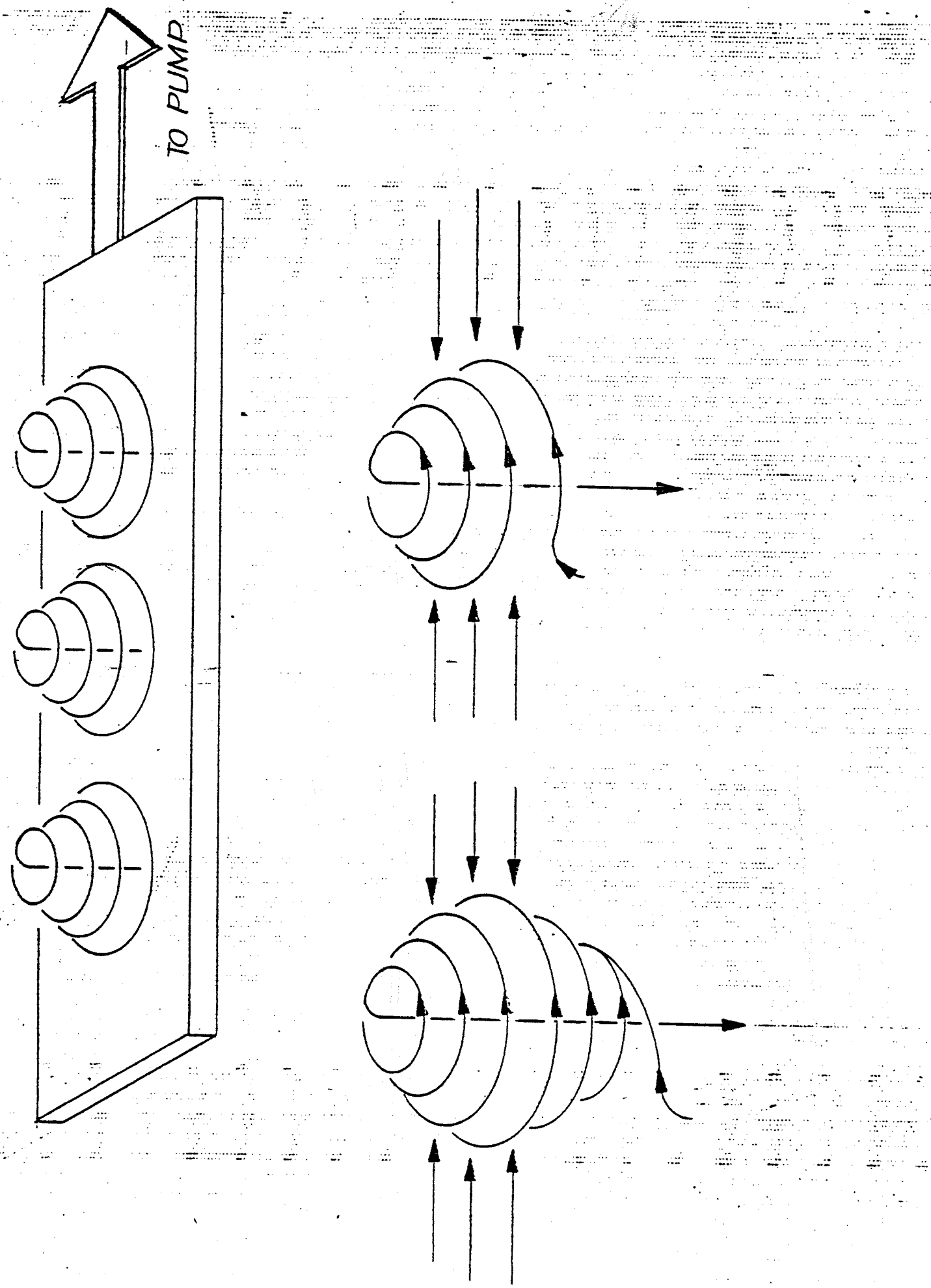
TO PUMP

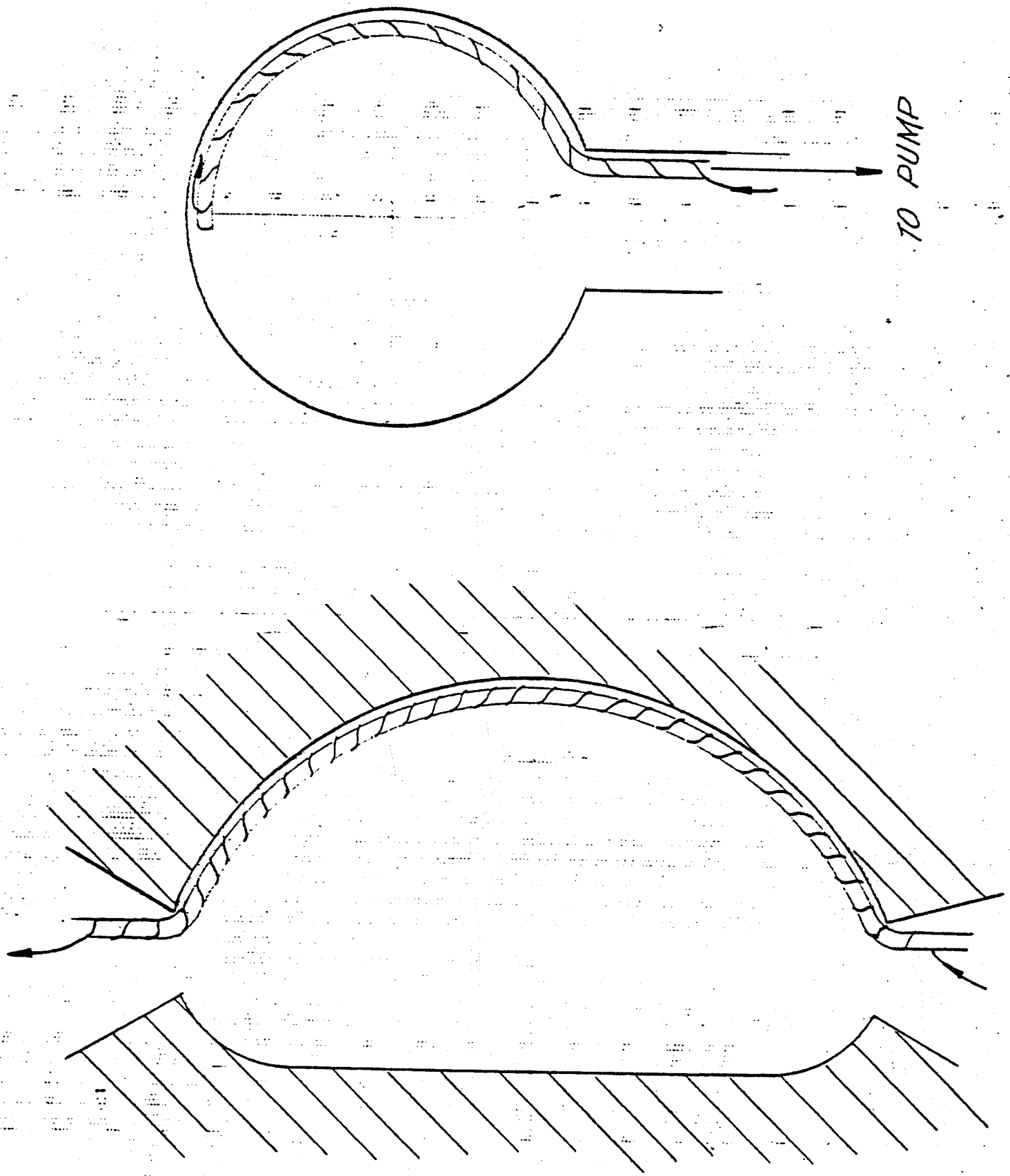
TO PUMP

LIMITER CONCEPT 1:
FORMED SKIN/COOLANT TUBES

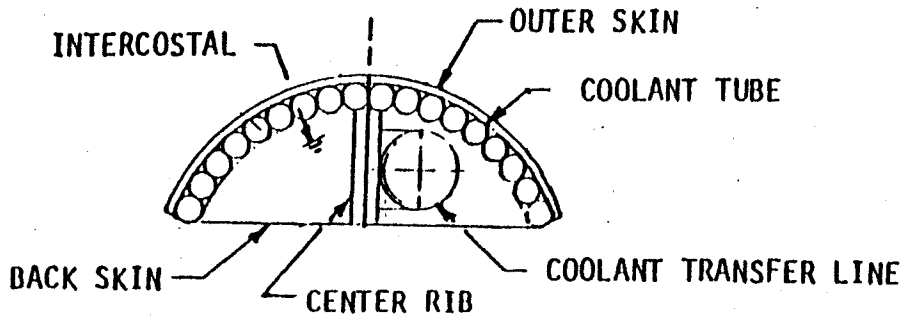

MATERIALS

	SKIN	TUBES	STRUCTURE
(a)	Cu	Cu	Mo; ST STL
(b)	Ta-10W	Cu	
(c)	Mo	Cu	

THERMAL HYDRAULICS

FOR 5 KW/CM^2 PEAK HEAT FLUX:

CLNT	SKIN MATERIAL	SKIN T_{MAX}
H_2O	Cu	250 °C
H_2O	Ta-10W	650 °C
H_2O	Mo	400 °C

FABRICATION

- SKIN FORMED OVER PATTERN
- TUBES, SKIN, STRUCTURE BRAZED AS UNIT
- COATING COULD BE ADDED TO SKIN

4.3 Divertor Target Concepts

4.3.1 Solid Target for Bundle Divertor

There was considerable contention at the Divertor Workshop regarding a value of maximum heat transfer rate which should be "specified" for use in bundle divertors. A lot of this contention was due to the fact that many of the workers were thinking only in terms of boiling heat transfer (see below). The suggested values for the limiting heat transfer rates varied from less than 100 W/cm^2 to in excess of 10 kW/cm^2, a range of 100:1. In a later bundle diverter heat transfer conceptual design, we will attempt to show that the limiting value should be somewhere in between, but shaded toward the higher figure. The limiting heat transfer rate for normal operation could be highly dependent on the magnification of local heat transfer rate which might occur during an upset. As far as we can tell, no systematic study of upset has been conducted. It is examined in a preliminary way here. It should also be noted that the limiting value may depend not only on the peak rate, but also the distribution.

Even if it is accepted that maximum heat transfer rates shaded toward the upper end of the limits discussed above could be sustained, there is no reason to deliberately utilize a diverter geometry in which these maximum rates must be handled. The mere ability to handle such rates is no advertisement for designs which deliberately push the limit. If satisfactory (in terms of overall reactor operation) bundle diverter designs with heat transfer rates near the lower values can be developed, they should be utilized. On the other

hand, if significant advantage, again in terms of overall reactor operation, is obtained by going to designs utilizing higher heat transfer rates, there is no reason for rejecting these designs on the basis of heat transfer alone.

Boiling vs Forced Convection (Highly Subcooled Single Phase) Heat Transfer

Consideration of the use of boiling heat transfer to handle the type of heat loads which have been postulated for bundle diverters was a surprise to most of the people whose normal work involves such heat loads. It certainly was a surprise to this writer. In the design of heat transfer apparatus with heat transfer rates between 0.3 and, say, 5 kW/cm^2, every effort is made to suppress boiling completely by utilizing forced convection alone (or highly subcooled single phase flow in the language of the usual heat transfer situation). Above 3-5 kW/cm^2, some nucleate boiling and swirl might become necessary. Use of film or bulk boiling at 0.3-5 kW/cm^2 would simply not be considered in the great majority of cases.

The use of forced convection heat transfer with boiling suppression allows close control of the surface temperature, and provides a means by which an upset margin can be available.

If satisfactory diverter designs with indicated heat loads in the 100 W/cm^2 or below range can be devised, then it may be advantageous to consider boiling heat removal or a gaseous coolant. The consequences of upset in such a system, however, need to be considered very carefully.

Coolant Selection

The potential diverter coolants discussed at the meeting included water, liquid metal, helium and hydrogen. The gases, presumably, would be utilized for designs with modest heat loads.

The objections to water as a coolant were based on the fact that, in the event of a leak or burnthrough, the system would be saturated with water

vapor. Because of the lower vapor pressure of liquid metals, presumably the immediate consequence of a leak in the liquid metal cooling system might be somewhat less than with water. However, particularly in case of a burn-through, the leak in either case is likely to be a massive one, requiring shutdown of the system. In the case of water as the coolant, the contaminant can be removed by pumping the system dry. In the case of a liquid metal leak, it would be necessary to disassemble the system to remove contaminant. On the surface, at any rate, it appears that the consequences of a leak in the liquid metal cooling system are far more severe than with water.

The use of hydrogen as a coolant for a diverter with modest heat loads was dismissed out of hand by the moderator. However, it is a fact that hydrogen is a far superior coolant than is helium, and that high pressure hydrogen is used as a coolant in the largest synchronous generators in modern power plants. The use is favored over helium simply because of the better heat transfer characteristics of hydrogen. It is even possible that a small hydrogen leak in a reactor could be ignored.

Upsets

The consequence of a reactor upset on the integrity of the diverter heat transfer design was mentioned at some of the sessions and in private discussions. From the point of view of the heat transfer design, the consequence of an upset appears to be a local increase in heat transfer rate not leading to significant increase in bulk rise in the coolant. Heat transfer design of the diverter must be capable of handling such an upset without burnthrough, a strong argument against the use of boiling heat transfer or gaseous coolant. Typical thermal diffusion time to the coolant is 0.02 sec.

In order to provide an adequate diverter design, it will be necessary for the reactor designer to specify the intensity of upsets which must be handled because, in many cases, the upset will dominate the cooling system design.

Conceptual Heat Transfer Design of a Bundle Diverter

In order to illustrate some of the factors that are involved in a bundle diverter heat transfer design, a conceptual heat transfer design of a bundle diverter, based on the design presented in Reference 1, is provided.

In the bundle diverter system described in Reference 1, the cooling system is arranged as shown in Figure 1 (Fig. 6-1 of Ref. 1). Each tube on the collector plate receives a fixed heat transfer rate along its entire length, which is a function of the radial position. For example, the tube on the inside receives a heat flux of 0.32 kW/cm^2 along its entire length, while the tube furthest from the reactor receives a heat flux of 0.007 kW/cm^2. Thus, in order to achieve efficient water utilization and maintain collector surface temperature within bounds, it is necessary to adjust the flow in each tube appropriate to its own heat transfer rate. Additionally, the coolant pressure will be fixed by the requirements of the inside tube, and will be substantially greater than that required by the outside tubes. The flow to each tube would be regulated by an orifice at the tube exit.

A more economical and efficient coolant system performance is obtained by directing the water flow radially outward along the collector plates, as is done with the shield tube. In this case, the water flow is from the region of high heat transfer toward the region of low heat transfer, and all the coolant passages see exactly the same heat transfer situation. Each tube receives an equal water allocation and requires the same inlet and exit header pressures. Thus, no orifices in the tube exits are required to balance the flow. This is the coolant geometry selected for the conceptual design.

---

1. T.F. Yang, et al, Westinghouse Fusion Power Systems Dept. Report No. WFPS-TME-104, Nov. 1978.

Additionally, the total thermal input to the diverter per the heat load distribution of Figure 1 is 47 MW, rather than the 240 MW stated on Pages 3-1 and 3-3 of Ref. 1. The heat load distribution has been modified to provide a total load of 240 MW with a peak of 3.2 kW/cm^2 impinging normally on the diverter by assuming an exponential decrease of heat transfer with radius. When this is done, the nominal heat transfer rate can be expressed as:

$$\dot{q} = 10.1 \times 10^6 \, e^{-\frac{x}{140}} \, Btu/ft^2 \, hr$$

where x is the distance along the radius from the inside edge of the diverter. At x = 120", the maximum radius $\dot{q} = 4.9 \times 10^6$ Btu/ft^2 hr.

The collector plate heat transfer rate is a factor of ten below the normal heat flux, so that on the collector plates:

$$\dot{q} = 1.01 \times 10^6 \, e^{-\frac{x}{140}} \, Btu/ft^2 \, hr$$

and $\dot{q} = 0.43 \times 10^6$ Btu/ft^2 hr at the maximum radius.

The overall arrangement of the cooling system for the diverter is indicated in Figure 2.

A. Collector Plate Design

For the collector plates:

$$\dot{q} = 1.01 \times 10^6 \, e^{-\frac{x}{140}} \, Btu/ft^2 \, hr$$

and $\dot{q} = 0.43 \times 10^6$ Btu/ft^2 hr at the extreme radius.

For reasons to be discussed, Nickel 200 is selected as the material of construction for the collector plates. The water passage geometry is as shown in Figure 3, and is arranged to handle the heat transfer input profile given above.

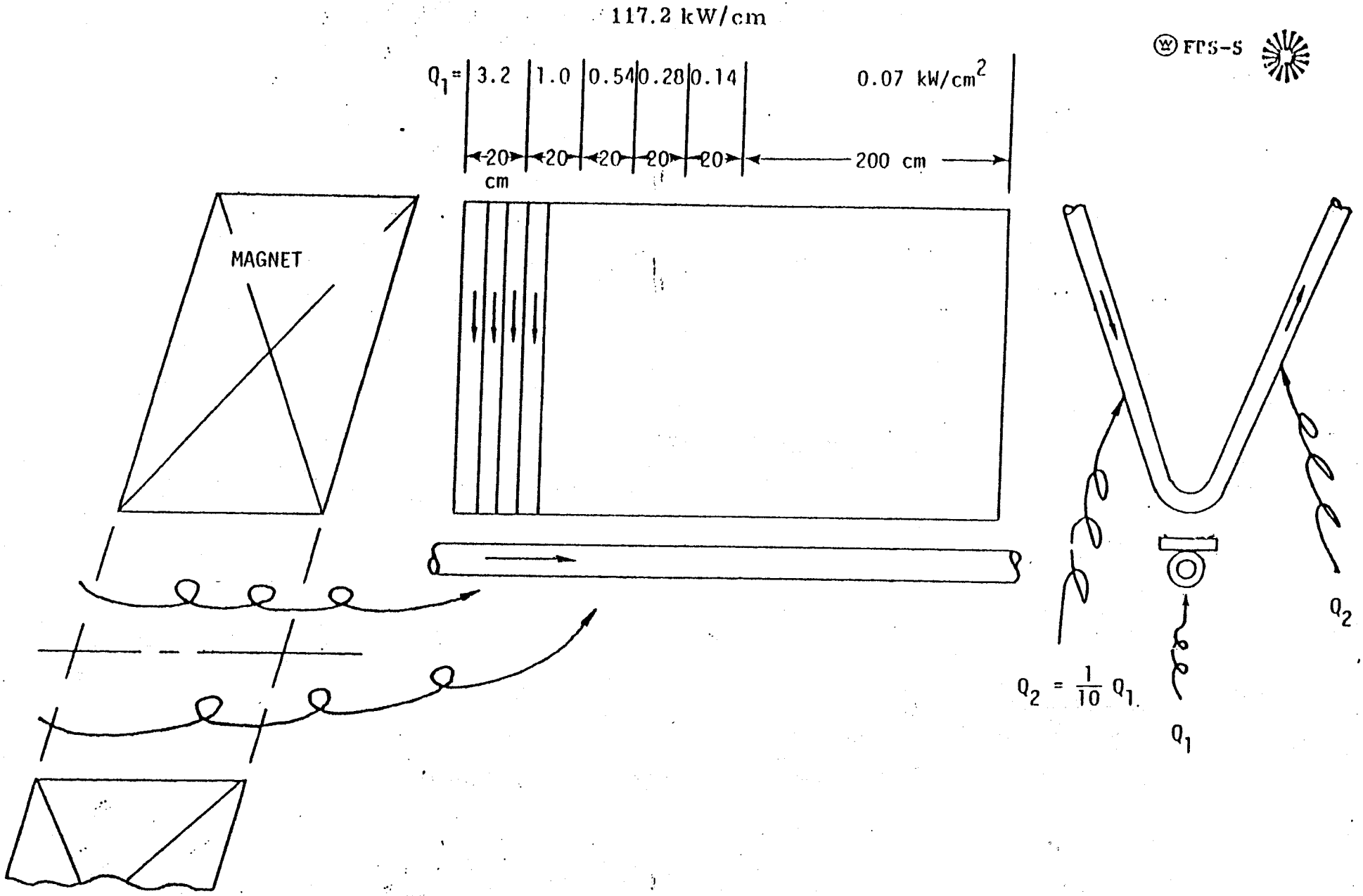

6-1. Bundle Divertor Particle Collector Tubes.

Figure 1

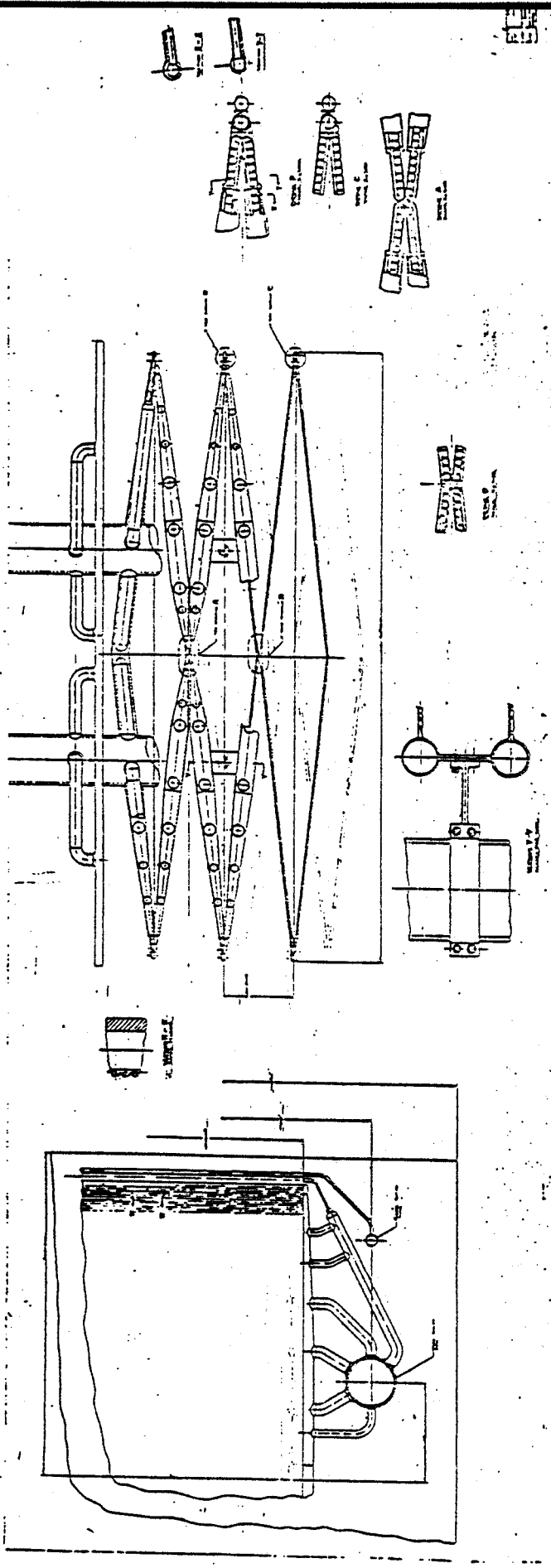

Figure 2

For 280 MW to diverter, 65.1 KW/cm of collector

$$\dot{q} = 1.01 \times 10^6 \, e^{-x/140} \quad \text{(x in)}$$

$\dot{q}$: Btu/ft^2 hr

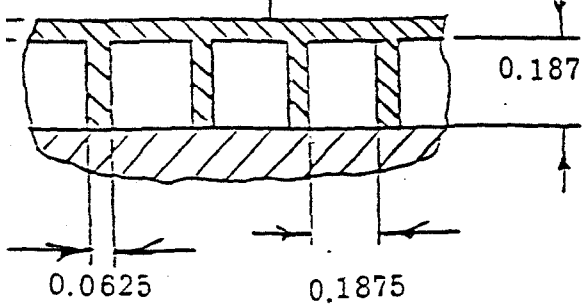

$\dot{q}_2 = 0.43 \times 10^6$ Btu/ft^2 hr (136 W/cm^2)

Material Ni 200

1.5 gpm/passage

$$\dot{q}_{eff} = 1.34 \times 10^6 \, e^{-x/140}$$

H = 39.2 Btu/sec passage

At x = 120, $\dot{q}_{eff} = 0.569 \times 10^6$ Btu/ft^2 hr

Figure 3
Collector Cooling Geometry

The individual cooling passages are 0.1875" square. Ribs of 0.062" width separate passages.

At the 120" station, two conditions must be fulfilled: (1) the maximum panel surface temperature must not exceed 300C, and, (2) there must be no nucleate boiling in the coolant.

The subscript notation used for the calculation is:

1,2 = inlet and exit (X=120") stations
b = bulk
f = film
s = surface
c = saturation
T_{f_2} = film temperature at exit
p_{c_2} = saturation pressure at T_{f_2}

As shown in Figure 3, in the interest of conservatism, the effective heat transfer rate to the water, $\dot{q}_{eff}$, is increased over the surface rate by 4/3, to account for the rib.

A flow rate of 1.5 gpm/passage is selected and the exit pressure is maintained at 1.25 p_{c_2}. Table 1 summarizes the features of the design. A 30 atm system, with a flow rate of 10,714 gpm at a pressure drop of 20 psi, will do the job. The required horsepower at 80% efficiency is 150.

It should be noted that the surface temperature is nearly constant along the entire length of the passage.

From a heat transfer viewpoint, this design is not challenging.

TABLE 1

Collector Plate Cooling Summary

$\rightarrow Q$	=	1.5 gpm/passage
$\rightarrow T_i$	=	60C (140F)
ΔT_{bulk}	=	196 F
T_2	=	336F
ΔT_{f_1}	=	206F
ΔT_{f_2}	=	88F
ΔT_{fS_1}	=	134F
ΔT_{fS_2}	=	57F
T_{S_1}	=	480F (249C)
T_{S_2}	=	481F (250C)
T_{f_2}	=	424F
P_{sat_2}	=	322 psia
$\rightarrow 1.25\ P_{sat_2}$	=	402 psia
ΔP	=	20 psi
$\rightarrow P_1$	=	422 psia = 407 psig = 28 atm $\rightarrow$ Use 30 atm system
$\rightarrow Q_{tot}$	=	10,714 gpm

Upset on Collector Plate

Upsets lead to local increases in $\dot{q}$. The local increase in $\dot{q}$ does not alter bulk rise appreciably. Because of the very small heat sinking capacity of the structure, the upset cannot be handled by a momentary increase in coolant flow; the system must always be operating at conditions which will tolerate the upset in steady state.

Upsets may be provided for in three ways, either singly or in combination. These are increased bulk (and system) pressure, transition to nucleate boiling, and increased flow rate.

1) Increased System Pressure: At the exit, p_{c_2} = 322 psia at $\dot{q}$ = 0.42 x 10^6 Btu/ft^2 hr (136 W/cm^2). The single phase limiting $\dot{q}$ may be increased by increasing system pressure. A limiting practical pressure level which will not lead to serious mechanical complication is, say, 1000 psi at which $T_{f_2} \leq$ 454F to avoid nucleate boiling. T_2 is still 336 F. Therefore,

$$\dot{q}_2 = \frac{545 - 336}{88} \; 155 = 368 \text{ W/cm}^2$$

is the maximum value of $\dot{q}$, or 2.4 times the normal value which can be handled without boiling with pressure suppression alone. No increase in pump horsepower is required if pressure suppression alone is adequate. The surface temperature goes to 716F (380C), which is well below the annealing temperature of 200 Ni.

2) Increased Flow Rate: Increased flow rate is effective as it both reduces bulk rise and film drop. Table 2 below gives some idea of the benefits to be gained by flow increase, both alone and combined with increase in system pressure to 1000 psi. The horsepower requirements are also noted. They increase as the 3rd power of flow rate. For these calculations, water inlet temperature has been increased at higher flow rates in order that T_{2_s} does not drop below 200C. This, of course, partially negates the

effect of increasing flow rate, and illustrates the interplay of various design requirements. The surface temperature is not maintained in the 200-300 C range at an upset location, but care is taken that the surface temperature does not reach the annealing temperature.

TABLE 2

Collector Plate Limiting Heat Transfer to Avoid Boiling

T_s min = 200C (392F)

Design Exit $\dot{q}$ = 136 W/cm^2

420 psi suppression pressure

Q (gpm)	HP	T_1	$\dot{q}_{2\ limiting}$ W/cm^2	T_{2_s}
10714 (design)	150	140F (60C)	175	481
15000	412	140	343	593
20000	976	178	429	629
25000	1906	207	491	655

1000 psi suppression pressure

Q	HP	T_1	$\dot{q}_{2\ limiting}$ W/cm^2	T_s
10714	150	140	320	716
15000	412	140	557	777
20000	976	178	700	837
25000	1906	207	817	886

As seen from Table 2, increased flow, together with pressure suppression of boiling, could permit the design to handle local upset heat levels as much as six (6) times the design value without departing from single phase forced convection cooling, and without overheating the surface. There is not much that could go awry with such a design as long as no boiling occurs and the reserve of nucleate boiling (the reserve would need to be determined by test) is still available. Therefore, the design of

the collector plates is straightforward even when significant upset heat loads are taken into account. The only real penalty for handling upset is increased pump horsepower.

Nonetheless, it is seen that the upset conditions dominate the design. Without upset, the design is trivial.

Construction of Diverter Collector Plates

Nickel 200 is selected as the material of construction of the diverter plates. The nickel may be clad or plated on the collection surface with a material designed to optimize particle collection.

The selection of nickel is based on (1) excellent ductability and elongation giving a good fatigue life; (2) annealing temperature above the 600C level, which is used to bake out the collected particles during the purge cycle; (3) excellent weldability and particularly suitable for electroforming, which appears to be a desirable method of fabrication of the plates; (4) good thermal conductivity; (5) good strength at the maximum temperature achieved during the collection cycle.

Plate fabrication is a straightforward process using the electroform technique for water passage closure. The collecting surface plate is first machined to produce the water passage. The grooves are then filled with a wax material, and the entire surface rendered electrically conducting. The passage closure is then electroformed. The final process is to mill or place the 0.020" deep grooves in the collection surfaces to increase the collection area of the plate. The plate is now ready for assembly with the water manifolds, and the final assembly into the complete diverter.

B. Front Shield Tube Heat Transfer Design

The heat transfer design of the front tube is another matter when upset is considered. Suffice to remark initially that the normal operating conditions of the shield tube push the simple forced convection concept about as far as it can go if the diverter actually absorbs 240 MWt, rather than the 46 MWt with a $\dot{q}$ distribution, as given by Fig. 6-1 of Ref. 1. If 240 MW is to be absorbed and substantial upsets handled, some nucleate boiling, probably combined with modest swirl, will be needed in order to handle any upset. If only 40 MWt is absorbed, forced convection alone can provide good upset margin, but never as good as for the collector plates. With nucleate boiling and swirl, testing is required in order to verify any design. Since particle absorption and surface effects are not important for the shield tube, resistance heating (possibly augmented by arcjet) is a suitable test procedure.

Basic Design for Normal Conditions

The heat transfer to the shield tube is given by:

$$\dot{q} = 10.1 \times 10^6 \, e^{-\frac{x}{140}} \cos \theta \ \text{Btu/ft}^2 \ \text{hr}$$

where θ is the angle between the normal to the diverter flow and any point on the tube. Consider here only the peak heat transfer at $\theta = 0$, so that

$$\dot{q} = 10.1 \times 10^6 \, e^{-\frac{x}{140}} \ \text{Btu/ft}^2 \ \text{hr}$$

Select a hard drawn copper tube, 0.400" (1cm) O.D. x 0.025 wall, or 0.350" I.D. The yield strength is 40,000 psi. The effective value of $\dot{q}$ to the coolant, $\dot{q}_e$, is increased over that to the surface, so that:

$$\dot{q}_e = 11.54 \times 10^6 \, e^{-\frac{x}{140}} \ \text{Btu/ft}^2 \ \text{hr}$$

and, at x = 120", $\dot{q}_e = 4.9 \times 10^6$ Btu/ft^2 hr. The total heat input per tube is 651 kW, or 617 Btu/sec.

After some preliminary calculations, a flow of 35 gpm is selected, with an inlet temperature of 40C (104F). The bulk temperature rise, ΔT, is 132F. We first calculate the exit pressure to assure boiling suppression, then check that conditions are satisfactory at the inlet. Table 3 summarizes the design. It is seen that it is straightforward.

Upset

Unfortunately, the design does not have good margin for upset in forced convection, 10 or 20% at most. Even the profile of Fig. 6-1 of Ref. 1 does not relieve the inlet. If the flow per tube is increased to 45 gpm and the peak system pressure to 2000 psi, about the highest that can be considered, the tolerable forced convection upset conditions at the inlet and exit are summarized in Table 4. Margins between 1.6 and 2.7 are noted depending on location. The inlet could not sustain the upset for very long or the tube would anneal and probably burst.

Even under optimum operating conditions, the design of the shield tube does not provide an upset margin in forced convection comparable to that which is obtained with relative ease for the collector plates.

There are several methods which can be utilized, either singly or in combination, to improve the upset margin.

1) Increased Tube Size: For a given peak pressure, higher coolant velocity, heat transfer coefficient, and limiting upset rates may be achieved if the shield tube diameter is increased. This has the disadvantage of increasing the part of the diverter which is not absorbing.

2) Reliance on Nucleate Boiling: The extent to which nucleate boiling can be relied on to increase the upset margin could only be established by test.

TABLE 3

Front Shield Tube Heat Transfer Design

Normal Operation

$\dot{q}$	$10.1 \times 10^6 \, e^{-\frac{x}{140}}$ Btu/ft^2 hr
Tube	0.400 O.D. x 0.025 wall ⟶ 0.350 I.D.
$\dot{q}_{e1}$	11.54×10^6 Btu/ft^2 hr
$\dot{q}_{e2}$	4.9×10^6 Btu/ft^2 hr
Heat absorbed = 617 Btu/sec	
T_1	104F (40C)
Q	35 gpm
ΔT	132F
h_f	28209 Btu/ft^2 hr ^oF

Exit

T_2	236F
ΔT_{2_f}	174F
T_{2_f}	410F
p_{2_c}	277 psia
p_2	$1.2 \, p_{2_c}$ = 332 psia
T_{2_s}	463F
Δp	878 psia

Inlet

p_1	1210 psia	
T_{c_1}	56F	
ΔT_{1_f}	409F	
T_{1_f}	513F	Inlet O.K.
T_{1_s}	620F	(below annealing for CDA107 copper)

Overall Design

Q	630 gpm
p_o	1300 psia
p_f	250 psia
Δp	1050 psi
HP	(η = 0.8) = 465

TABLE 4

Front Shield Tube - Forced Convection

45 gpm - 2000 psi upset conditions

	Inlet	Exit
Pressure = psi	2000	612
T_b = F	104	207
h_f = Btu/ft^2 hr	34752	34752
T_c = ^oF	635	488
ΔT_f	531	281
$\dot{q}_{max}$ = 10^6 Btu/ft^2 hr (kW/cm^2)	18.35 (5.1)	8.52 (2.7)
$\dot{q}_{max}/\dot{q}_{local}$ normal	1.6	2.7
T_s	805	567

3) Nucleate Boiling and Swirl: A modest amount of swirl not leading to significant pressure drop in this situation could lead to very significant improvements in upset capability. Swirl would not only cause nucleate bubbles to move away from the surface, but would also convert them into regions of lower heat transfer. Again, test would be required in order to establish the upset capability.

Recommendation

Designs for forced convection in normal operation, with whatever margin can be had, and utilize swirl and nucleate boiling (and possibly larger tube size) to improve the upset capability. Testing is required to establish the capability.

Testing: A combination of resistance and arcjet heating would provide a realistic test of the shield tube under normal and upset conditions. The resistance heating would simulate normal heat loads along the long tube. The arcjet would be directed at local areas to simulate upset conditions.

4.3.2 A Supersonic Gas Target for a Bundle Divertor

One major and yet unresolved problem in magnetic fusion is controlling the level of impurities in the plasma. A leading concept for dealing with this problem is the magnetic divertor. Such a device extracts particles from the vicinity of the reactor wall, "diverting" them along magnetic field lines into an exhaust chamber before they can contaminate the inner plasma or damage the reactor wall. The exhaust plasma flows into the exhaust chamber via a divertor channel. Figure 1 shows a typical divertor system.

One of the major engineering difficulties which divertor designers face is the actual extraction of large quantities of plasma heat (10 Mw in a typical power reactor) in an exhaust chamber of reasonable dimensions. For example, if the exhaust plasma is allowed to hit a cooled neutralizing plate and then is pumped out, the cooled surface area must be $10^2 m^2$, and the chamber must be able to remove about 10^{22} particles per second. This assumes a maximum allowable heat load of 1 kW/cm^2. The magnitude of the heat transfer and particle pumping problems can be easily appreciated.

These two basic difficulties can be greatly reduced by use of a gaseous target. For example, if a divertor exhaust chamber were filled with neutral gas, and the high energy plasma stream were allowed to impinge upon it, then the back plate of the divertor chamber would be protected from over-

heating and sputtering because the plasma energy would be absorbed by the target gas. The target, on the other hand, could be made to circulate through a heat exchanger and remove the heat from the divertor region by forced convection. A scheme for energy removal such as this would greatly simplify the divertor exhaust chamber design, since it would allow for a much more compact device. Also, the system would operate at a considerably higher target pressure than a solid collector scheme, and in turn would tend to reduce the pumping requirements as well.

One of the potential problems with this scheme is the backflow of neutral gas from the chamber into the divertor-channel. This backflow could produce a low temperature, high density plasma which would lead to enhanced cross-field diffusion and localized hot spots along the divertor walls. Eventually such a situation could lead to divertor choking or other assorted consequences of varying seriousness. However, the backflow problem may be ameliorated by an effect which may play an important role in this type of divertor arrangement: momentum transfer. In general, the plasma exiting the divertor channel is a reasonably well collimated stream of ions and electrons, having a relatively low static pressure but a very high dynamic pressure. The pressure of this exhaust plasma is highly anisotropic. The momentum associated with the speed of the flow could be used to advantage by letting it plug the entrance of the exhaust

chamber and thus reduce the flow of gas back into the channel [1].

The Physics of the Interaction

When a typical plasma ion interacts with a gaseous target, a wide variety of reactions are likely to occur. Figure 2 shows a plot of the most important types of reactions, of which the most influential one is charge exchange. The second most important one is the stripping reaction, which is responsible for reionizing charge exchanged neutrals. For target densities of interest in this concept (i.e., $10^{23}/m^3$), the charge exchange mean free path is about 0.1mm for 4 keV ions, and the stripping mean free path is about 1mm. There is little energy and momentum transfer in these interactions; the incident ion must make many such collisions before thermalizing with the background gas.

Physically, the situation is as follows: the energetic ion first enters the gas target area. As soon as it travels the 0.1 mm into the gas it charge exchanges with the background. As a neutral, the particle travels about 1mm more before it becomes ionized once again by the stripping reaction described earlier. There is little energy and momentum

exchange as these events go on. The particle "flips" back and forth between the neutral and ionized states many times. It penetrates several centimeters before it has lost all of its energy and momentum. Thus an interaction region will be established at the exhaust chamber entrance. Upstream of this region there will be mostly high temperature plasma, while downstream there will be mostly neutral gas. Typically, the region thickness will be related to the mean range, about 20 cm for the conditions of interest. Figure 3 shows a schematic of what this region may look like.

An important parameter is the mean range, R, a measure of how far the incident particles really penetrate before they lose all of their energy and momentum to the gas. Figure 4 shows mean range data for hydrogen ions in hydrogen gas (these data were obtained at 15°C and 1 atm, and must be scaled for the lower densities of interest in this work). Table I shows typical penetration depths for 10 Kev ions in molecular hydrogen and nitrogen at various temperatures. Assuming a linear variation with density, the mean range at arbitrary conditions, R(T,P), is given by

$$R(T,P) = R_0 \, n_0/n(T,P) \qquad (1)$$

where T and P are the gas temperature and pressure, and n_0 is the gas density and R_0 is the mean range at known conditions. Using the ideal gas law,

$$R(T,P) = 2.64\ (273+T(^{0}C))\ R_0/P(torr) \qquad (2)$$

Given the value of R_0 from the nuclear data and a desired value of R, Eq. (2) can be used to determine the pressure and temperature that are consistent with that particular particle penetration depth.

The basic condition for establishing a stable boundary is that the total momentum delivered by the plasma stream must be balanced by the static pressure exerted by the gas. In looking at Fig. 3, it is evident that for a given plasma flux and fixed target conditions, there will be only one value of R where this condition is truly satisfied. The model in Fig. 3 can be approximated by an interaction region in the shape of a right circular cylinder, as shown in Figure 5. The area over which the gas exerts pressure depends on R and also on the channel diameter, d. The incoming plasma stream provides a total force, F1, which must be balanced by the static pressure force, F2, exerted by the target gas. For equilibrium,

$$F1 = F2 \qquad (3)$$

But

$$F1 = np \cdot mp \cdot Vp^2 \cdot A1 \qquad (4)$$

where

np = plasma density

mp = mass of plasma particles

Vp = ion speed

A1 = divertor channel cross sectional area

and

$$F2 = P \cdot A2 \qquad (5)$$

where

P = target gas pressure

A2 = area bounded by interaction region.

From Figure 5,

$$A1 = \pi d^2/4 \qquad (6)$$

and

$$A2 = \pi d^2(1+4R/d)/4 \qquad (7)$$

where d is the divertor channel diameter and R is the mean range for plasma ions in the target. Thus Eq. (3) becomes

$$P = 2\ np\ k\ Tp/(1+4R/d) \qquad (8)$$

and in the appropriate units, Eq. (8) becomes

$$P(\text{torr}) = \frac{2\times760\times1.602\times10^{-16}\ (np(m^{-3})Tp(kev)/(1+4R/d))}{1.01325\times10^{7}} \qquad (9)$$

where Tp is the plasma temperature. The plasma density can be further related to the geometry of the system, namely d, if the total particle flux out of the divertor is held constant. For example, if the total flux is $1.25\times10^{23}\ s^{-1}$ [2], then

$$np = 5.74\times10^{17}/\ d^{2}\ Tp^{.5} \qquad (10)$$

and this result can be incorporated in Eq. (9).

Basic Design Criteria

Eqs. (9) and (10) give the engineering requirement on the temperature and pressure of the target gas. Combined with the results of Eq. (2), they can be used to determine the basic design criteria for the formation of the interaction region. These combined results are shown in Figs. 6 and 7. In Fig. 6, one family of curves represents the valueof R required by the pressure balance; the other family represents the actual value of R for given temperatures and pressures. In order for the boundary to be physically possible,

the two curves must match at at least one point. In Fig. 6 the curves do not match at high gas temperatures (i.e., 500°C to about 50°C). At low temperatures, the curves match for small diameter plasma channels (i.e., 5 cm). The higher temperature targets are accessible if the plasma channel diameter is further reduced; this is shown in Fig. 7. For example, a channel diameter of 3.5 cm can be used with a target gas at 100°C. It must be noted that the channel diameter d refers to the actual plasma cross section and not to the diameter of the physical pipe enclosing it. This latter diameter will be somewhat bigger to account for profile effects and the like. Note that reducing the exit diameter creates a magnetic mirror at the divertor channel exit. This is an undesirable situation, and it may be preferable to operate with low temperature targets; moreover, low initial temperatures are a natural consequence of the present concept, as will be shown later.

If the rate of plasma leakage into the divertor varies with time, the diameter of the plasma stream exiting into the exhaust chamber could be magnetically controlled (i.e., to yield a constant flux) in order to maintain the required matching condition. This is a desirable feature, since the total leakage rate into the divertor will not be constant in time but will vary, especially during startup and shutdown.

Power Dissipation and Pumping Requirements

The amount of plasma energy entering the exhaust chamber is very high. For example a flux of 1.25×10^{23} s^{-1} of ions at 4 keV each will yield a heat load on the gas of

$$W = \frac{1.25 \times 10^{23} \cdot 4 \cdot 1.6 \times 10^{-16}}{\pi d^2 (1+4R/d)/4} \qquad (11)$$

which produces a value of 3.5×10^5 W/cm^2 for R = 20 cm and d = 3.5 cm. The mass flow rate required to remove that much energy while increasing the target temperature an average of 200°C is given by

$$m' = \frac{Q}{Cp \cdot \Delta T} \qquad (12)$$

where $Q = 1.25 \times 10^{23}(s^{-1}) \times 4(keV) \times 1.602 \times 10^{-16}(J/keV) = 80$ MW is the total heat transfer rate, $\Delta T = 200^{\circ}C$, and Cp = 3.41 cal/gm K = $3.41 \times 4.184 \times 10^3$ J/kg K. Substitution of these numbers into Eq. (12) shows that 28.07 kg/s is required to maintain the 200°C temperature change at the target.

The volumetric flow rate consistent with m' is very high because of the low pressure required. If N'=m'/m, where N' is the number flow rate and m is the mass per gas particle, then the volumetric flow rate V' is given by

$$V' = N' k T/P(N/m^2) \qquad (13)$$

The conversion factor is $P(N/m^2) = 101325\ P(torr)/760$. These numbers yield a volumetric flow rate of about 10^4 m^3/s at a pressure of 10 torr; this corresponds to a pumping rate of 10^7 l/s. This unfortunate situation is one of the basic problems that must be solved for adequate particle and heat removal in any divertor.

~~4.1 NOZZLE FLOW~~

It may be possible to eliminate the pumping problem by pumping at relatively high pressures while allowing a low pressure region to form only near the target; such a pressure discontinuity suggests the existence of a shock which, in this case, could be used to advantage. The low pressure region, on the other hand, would be consistent with that required by the plasma gas interface described earlier. The required flow rates could then be attained with lower volumetric pumping speeds (as seen by the pumps) than the 10^7 l/s value quoted earlier. This effect can be achieved in principle by isentropically accelerating the flow near the target with a Laval nozzle.

An interesting arrangement is depicted in Fig. 8. The plasma exits supersonically into the exhaust chamber at low pressure (i.e., a few torr). The target pressure profile is then highly peaked and the low pressure end is made to match the low pressure requirement at the divertor channel exit. The plasma will interact with neutrals at the required low

gas pressure, and the energy deposited will be convected away by the bulk flow.

The maximum mass flow rate results from having sonic conditions at the throat. Downstream from the throat it is desired to reduce the pressure to that of the divertor exit, and to speed up the flow and thus maintain the high mass flow rate. Therefore, the nozzle must have both converging and diverging sections. The target temperature will also be lowered by the expansion at the nozzle exit; this is a desirable effect since it will allow a wider plasma channel and therefore reduce the mirroring effect at the divertor channel exit.

Nozzle Design

Consider the converging diverging nozzle shown in Fig. 8. The flowing gas is accelerated to high Mach numbers and is then made to blend with the plasma stream at the nozzle exit. The flow at the nozzle throat will be sonic. The flow velocity there is given by

$$V^* = c = (\gamma k T^*/m)^{.5} \qquad (14)$$

where the superscript (*) refers to properties at the throat, and $\gamma = 1.4$ is the ratio of the specific heats. Let $T^* = 500K$ be the temperature at the throat; further assume a

stagnation pressure of 1 atm, and set the molecular mass m at $2 \times 1.67 \times 10^{-27}$ kg for pure deuterium gas. Then,

$$V^* = 1.70 \times 10^3 \text{ m/s} \tag{15}$$

From the isentropic data tables it is found that

$$T^*/T_0 = 0.8333 \qquad (M^* = 1) \tag{16}$$

so that

$$T_0 = 600\text{K} = 327^\circ\text{C} \tag{17}$$

The subscript ($_0$) denotes stagnation properties. The throat area A* can be obtained from continuity, that is

$$m' = \rho^* V A^* \tag{18}$$

and

$$p^* = n^* k T^* \tag{19}$$

But

$$\rho^* = n^* m \tag{20}$$

so that

$$p^* = \rho^* k T^*/m \tag{21}$$

From the isentropic data tables,

$$p^*/p_0 = .52828 \tag{22}$$

so that

$$p^* = 401.49 \text{ torr} \tag{23}$$

which yields

$$\rho^* = 2.59 \times 10^{-2} \text{ kg/m}^3 \tag{24}$$

This results in

$$A^* = .637 \text{ m}^2 \tag{25}$$

or a throat diameter d* of 0.901 m.

This flow must be expanded to a pressure, pe, of approximately 10 torr; therefore, the pressure ratio

$$pe/p_0 = 0.01316 \tag{26}$$

which corresponds to an exit Mach number Me of 3.5. The area and temperature ratios pertaining to exit conditions are obtained from isentropic data. Thus

$$Ae/A^* = 6.7 \quad (27)$$

and

$$Te/T_0 = 0.289 \quad (28)$$

resulting in an exit area of $4.268 m^2$, an exit diameter de = 2.331m, and an exit temperature Te = 173.4K. Also,

$$\rho e/\rho_0 = .045 \quad (29)$$

and

$$\rho^*/\rho_0 = .63394 \quad (30)$$

so that $\rho_0 = 4.09 \times 10^{-2}$, and $\rho e = 1.84 \times 10^{-3}$.

Transition Region Between Nozzle and Diffuser

Refering once again to Fig. 8, the plasma leaving the nozzle exit does so at very high velocity. For an exit temperature of 142.8K, the exit velocity is 1700 m/s, which corresponds to a Mach number of 3.5. At this point, and nearly tangential to the flow, the plasma streams are allowed to enter and deposit their energy on the target gas. The static

pressure at these entry ports is below 10 torr, as required by the plasma gas boundary discussed earlier. Under these conditions, the plasma stream will penetrate several centimeters into the target. The plasma energy raises the bulk temperature of the flow, and a fraction of it can be recovered downstream with a heat exchanger.

As the flow is being heated by the plasma, it is also made to slow down in the duct (which acts as a supersonic diffuser). The heat transfer is highly localized near the source; however, it is expected that substantial mixing will occur as the flow moves downstream. The heating will, of course, be higher upstream. For the present analysis, it is assumed that the heat transferred per unit mass to the flow drops linearly with distance along the duct.

The addition of heat is sufficiently high to reduce the Mach number for both converging and diverging ducts; however, the variation of duct area with distance can be tailored to optimize the flow conditions. It is desirable to have a low Mach number since the shock losses increase as M^3; however, the flow must be supersonic to prevent choking.

By fixing the back pressure, a stable shock can be obtained downstream of the diffuser throat. This situation allows a significant pressure increase as the flow suddenly decelerates to subsonic conditions. Because of the entropy increase and various other inefficiencies, the pressure

downstream of the shock is only a fraction of the initial value; hence, a suitable compressor will be required to complete the cycle. On the other hand, the pressure increase across the shock will be a very important contribution and will ease the compressor size requirements considerably. At the same time, the temperature downstream from the shock will be sufficiently high to allow additional energy recovery.

The length of the duct is mainly determined by the heat transfer behavior within the gas. It is desired that sufficient mixing occur in a reasonable distance such that the temperature will be rendered essentially uniform in the radial direction immediately before the shock. Such mixing depends on a large variety of flow parameters such as Reynolds number, wall friction, and boundary layer effects, which need to be determined experimentally. For the present calculations, a diffuser length of 5 m has been assumed.

When the effects of wall friction are included, it will also be necessary to modify the contour of the duct walls to provide some compensation for friction-induced deceleration. If the Mach number can be maintained near 1 for most of the duct length, then frictional effects will be minimized. Fig. 9 shows the nozzle/diffuser/expander region with the flow characteristics at the various stages.

Consider the geometry shown in Fig. 9, where a converging diffuser is used to slow down the flow coming out of the nozzle. The system is in steady state, with exit velocity and temperature denoted by Ve and Te respectively. The mass flow rate is a constant denoted by m'.

Let l be the length of the diffuser and assume that the heat Q (in Watts) from the plasma is added in a linearly decreasing manner over l. The power per unit length W(x) is given by

$$W = \frac{2\,Q\,(1 - x/l)}{l} \qquad W/m \qquad (31)$$

The amount of energy received by the element of mass dm in time dt is given by

$$dE = \frac{2Q\,(1 - x/l)\,dx\;dt}{l} \qquad J \qquad (32)$$

But since dt = dm/m' and dq = dE/dm, then

$$dq = \frac{2Q\,(1 - x/l)\,dx}{l\,m'} \qquad J/kg \qquad (33)$$

The fractional area change, assuming a linearly varying diffuser, is given by

$$dA/A = 2a\,dx/(r_0 + ax) \qquad (34)$$

where a is the slope of the diffuser walls and r_0 is the initial radius of the duct (i.e., de/2).

For one-dimensional flow with heat addition but without friction, the fractional change in velocity is related to the Mach number, the fractional area change, and the amount of heat added, as follows [3]:

$$\frac{dV}{V} = \frac{1}{M^2-1}\left(dA/A - dq/Cp\ T\right) \qquad (35)$$

where Cp is the heat capacity at constant pressure and T is the temperature of the fluid. The second term in Eq. (5) can be obtained from energy conservation. The amount of heat dq added to the flow must go into both random and directed flow energy; that is

$$\frac{dq}{dx} = Cp\frac{dT}{dx} + V\frac{dV}{dx} \qquad (36)$$

where V is the flow velocity. The flow temperature can be obtained by integrating Eq. (36); that is,

$$T = \frac{1}{Cp}\left(q + (Ve^2 - V^2)/2 + Cp\ Te\right) \quad K \qquad (37)$$

where Te and Ve are initial values of temperature and velocity respectively. Using the definition of Mach number

$$M^2 = V^2\ m/\gamma\ k\ T \qquad (38)$$

where m is the mass of the gas molecules, γ the ratio of specific heats, and k is the Boltzmann constant. The final result is

$$\frac{dV}{V} = \frac{dx}{(M^2-1)}\left(\frac{2a}{(r_0 + ax)} - \frac{2Q(1 - x/l)}{l\ m'\ Cp\ T}\right) \qquad (39)$$

Integrating Eq. (33) one obtains the heating per unit mass as a function of the distance x.

$$q(x) = 2\ Q\ x\ (1 - x/l)/l\ m' \qquad J/kg \qquad (40)$$

Diffuser Design

Eq. (39) is highly nonlinear and has been solved numerically. The results are presented in Figs. 10 and 11, where fluid velocity, temperature, and Mach number are plotted as functions of the distance x, for various input parameters.

Figure 10 shows the actual results for a converging duct with a linear slope of 5%; the Mach number decreases from 3.5 to 1.2, the velocity decreases, and the temperature increases from 142K to about 600K. Figure 11, on the other hand, shows the results for a diverging duct. In that case, the Mach number decreases initially and increases slightly toward the diffuser exit. This is a temperature effect; that is, the cooling due to the expansion of the flow near the

end is sufficiently strong to overcome the heating from the plasma stream.

Figures 10 and 11 illustrate how the diffuser contour can be tailored to minimize the amount of frictional and shock losses that will be present. For example, by reducing the velocity of the flow, the frictional losses are also reduced; at the same time, by operating at low Mach numbers (although still greater than 1), the shock losses are also reduced. In the present frictionless design, the converging diffuser is more attractive. In the real case, the frictional effects may have to be compensated for by using a diverging duct. One alternate solution is to prescribe a fractional change in velocity or Mach number and solve the equations for the resulting fractional area change along the duct.

Diffuser Exhaust Design

At the diffuser exit, a throat will exist which is wider than the isentropic throat consistent with the conditions upstream. The flow will therefore not become sonic there. Instead, the walls of the duct will be made to diverge and the back pressure will be fixed such that a normal shock will be established slightly downstream from the throat. Under these conditions, the shock will be stable to small disturbances in the flow and will not be swallowed upstream

[4]. The presence of the shock will introduce a sudden deceleration of the gas and its kinetic energy will be partly recovered as pressure downstream from the shock. The basic design proceedure is outlined as follows.

Assuming a linearly converging duct with slope a = -0.05, the diffuser exit radius is 0.92m, corresponding to a diffuser exit area Ad = 2.66 m^2. The exit Mach number at that point is 1.225. The throat area Ad* consistent with this Mach number is 2.57 (from isentropic data). Let the shock exist downstream from the throat, at a point where the duct area is As = 3 m^2. At that point

$$As/Ad^* = 1.17 \tag{41}$$

and immediately before the shock, the Mach number is

$$Mx = 1.5 \tag{42}$$

The static pressure at the diffuser exit is given by

$$pd = m' \; K \; Td/Vd \; Ad \; m \tag{43}$$

where d refers to diffuser exit. This gives

$$pd = 87.09 \text{ torr} \tag{44}$$

and from isentropic data

$$pd_0 = 216.79 \text{ torr} \quad (45)$$

The pressure ratio before the shock is

$$psx/pd_0 = 0.2724 \quad (46)$$

so that the static pressure behind the shock is

$$psx = 59.05 \text{ torr} \quad (47)$$

and from normal shock data, at Ms = 1.5

$$py/px = 2.4583 \quad (48)$$

where y denotes conditions after the shock; hence

$$py = 145.17 \text{ torr} \quad (49)$$

In principle, one seeks to obtain the highest possible pressure beyond the shock, since this would mean that a smaller compressor would be required to bring the gas to its initial pressure to complete the cycle. In the present design, a pressure of 145.17 torr is obtained. This amounts to about 20% of the 1 atm required. A suitable compressor is needed to close the cycle.

Since gas downstream from the shock will be hot, some form of heat removal must be supplied; this requires a heat exchanger in series with the compressor. A fraction of the heat removed could be recovered via a conventional thermal cycle and used to help meet the compressor power requirements.

Conclusions

Some potential difficulties are envisioned. First, the flow may be drastically affected by the addition of heat from the plasma stream; second, the heat will be transferred from the edge of the jet where the interaction region is via thermal conduction, a process which may be too slow to reach into the central region of the flow. That problem has not been evaluated, and a suitable flow-mixing model needs to be incorporated in the design. This model is expected to have an impact on the design of the supersonic diffuser, particularly its desired length.

Beyond the shock, further increases in pressure may be attained by cooling the flow; however, such pressure gains may be somewhat offset by the presence of the heat exchanger as a source of impedance.

An important aspect which has not been evaluated is the heat transferred to the diffuser walls, particularly near

the divertor exhaust ports. The materials problems and cooling requirements in these regions await further study.

The effects caused by the presence of a boundary layer and other frictional effects need to be evaluated as they directly impact the pump size and power requirements of the system.

Finally, other operational problems such as tritium recirculation, helium and impurity recovery, and the entire transient and control related aspects of such a device must be delineated in the context of a full-scale power reactor.

REFERENCES

Aspects of the Gaseous Neutralizer Princeton Plasma Physics Laboratory Poster Session 4P-1 APS Meeting, Boston, MA (November 1979).

SANDERSON, A.D. and Stott, P.E., A Bundle Divertor For a Fusion Reactor, Culham Laboratory Report CLM-P 530(April 1978).

KUETHE, A.M. and SCHETZER, J.D., "Foundations of Aerodynamics", John Wiley & Sons, Inc., (1959).

SHAPIRO, A., "The Dynamics and Thermodynamics of Compressible Fluid Flow" Vol. I, The Roland Press Company New York, (1953).

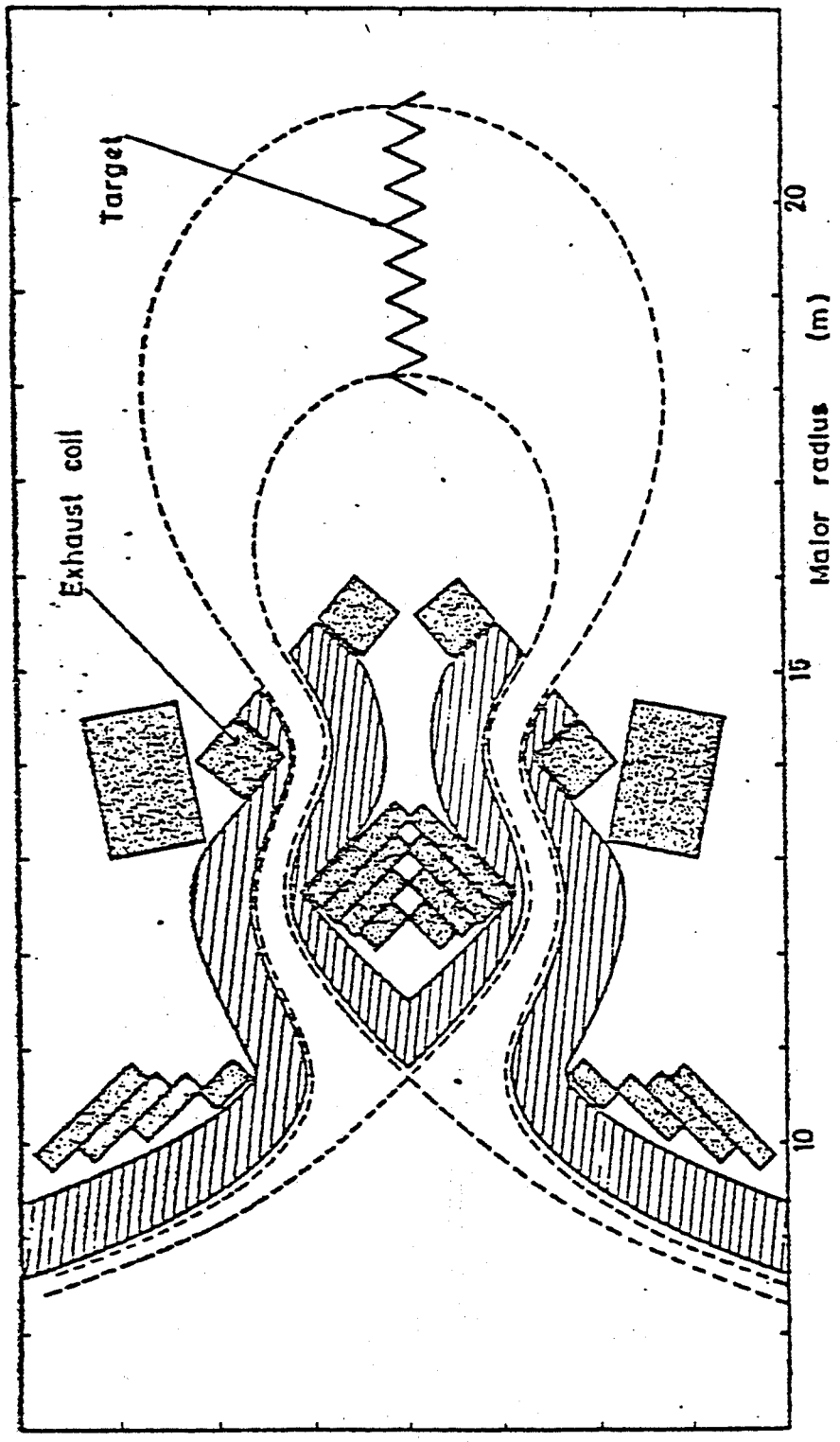
Target
Exhaust coil
10
15
20
Major radius (m)

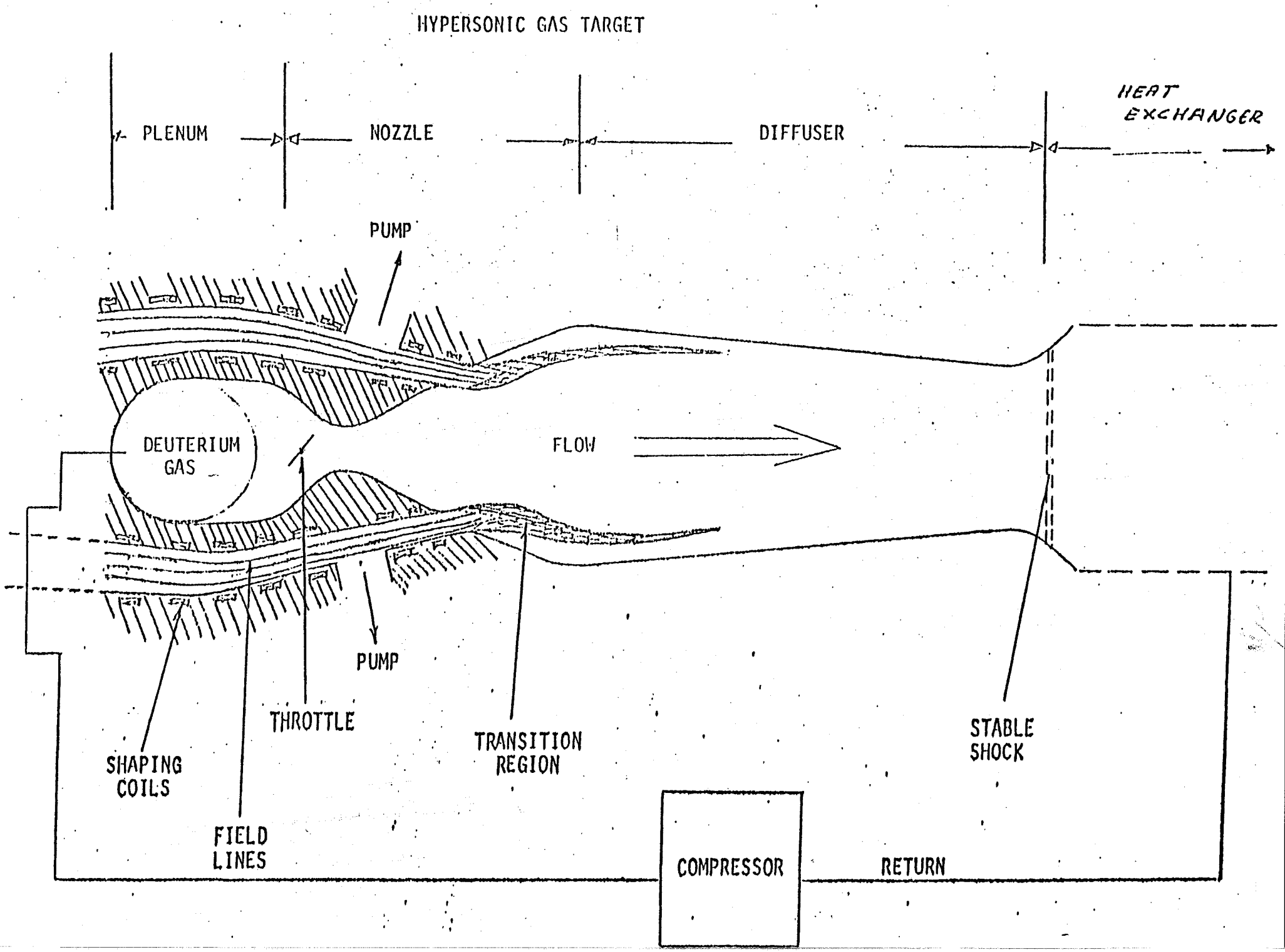
HYPERSONIC GAS TARGET
PLENUM
NOZZLE
DIFFUSER
HEAT EXCHANGER
PUMP
DEUTERIUM GAS
FLOW
PUMP
SHAPING COILS
FIELD LINES
THROTTLE
TRANSITION REGION
STABLE SHOCK
COMPRESSOR
RETURN

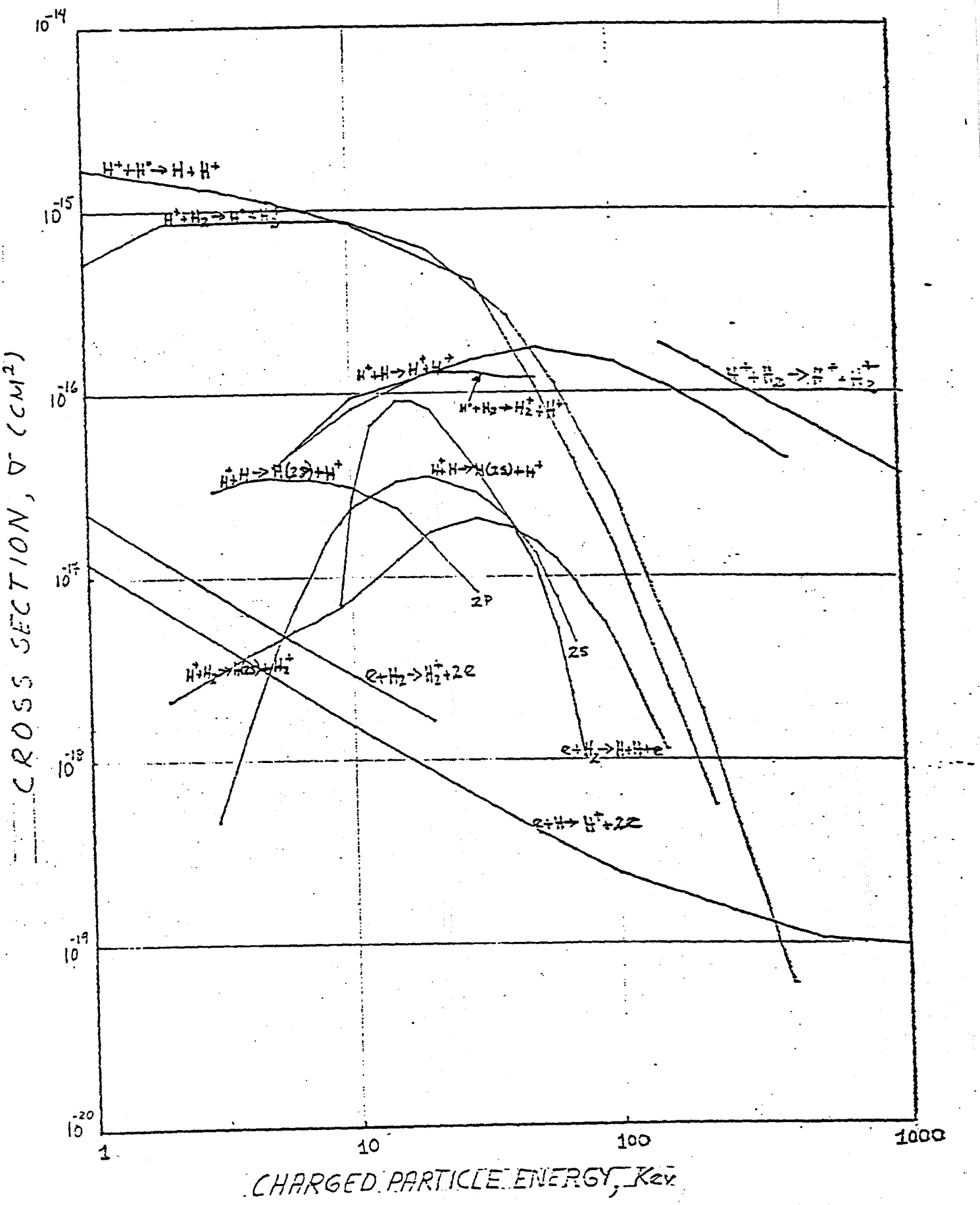
10^{-14}
10^{-15}
10^{-16}
10^{-17}
10^{-18}
10^{-19}
10^{-20}
CROSS SECTION, σ (CM²)
$H^+ + H^* \rightarrow H + H^+$
$H^+ + H_2 \rightarrow H^* + H_2^+$
$H^+ + H \rightarrow H^* + H^+$
$H^+ + H_2 \rightarrow H_2^+ + H^+$
$H^+ + H \rightarrow H(2s) + H^+$
$H^+ + H \rightarrow H(2s) + H^+$
2P
2S
$H^+ + H_2 \rightarrow H(2s) + H_2^+$
$e + H_2 \rightarrow H_2^+ + 2e$
$e + H_2 \rightarrow H + H + e^-$
$e + H \rightarrow H^+ + 2e$
1
10
100
1000
CHARGED PARTICLE ENERGY, Kev

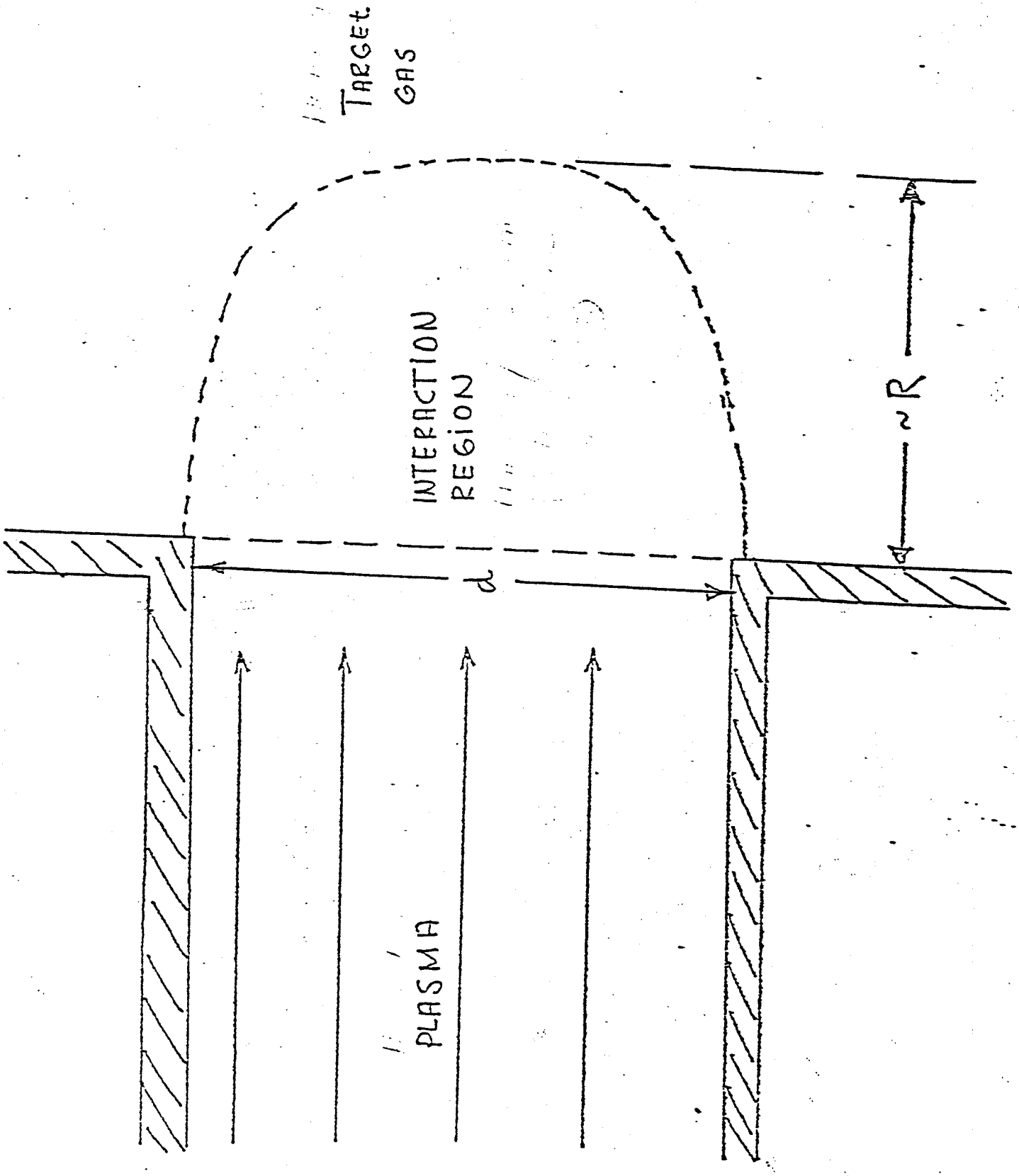
TARGET GAS
INTERACTION REGION
d
≈ R
PLASMA

RANGES OF H^+ AND H_2^+ IN H_2

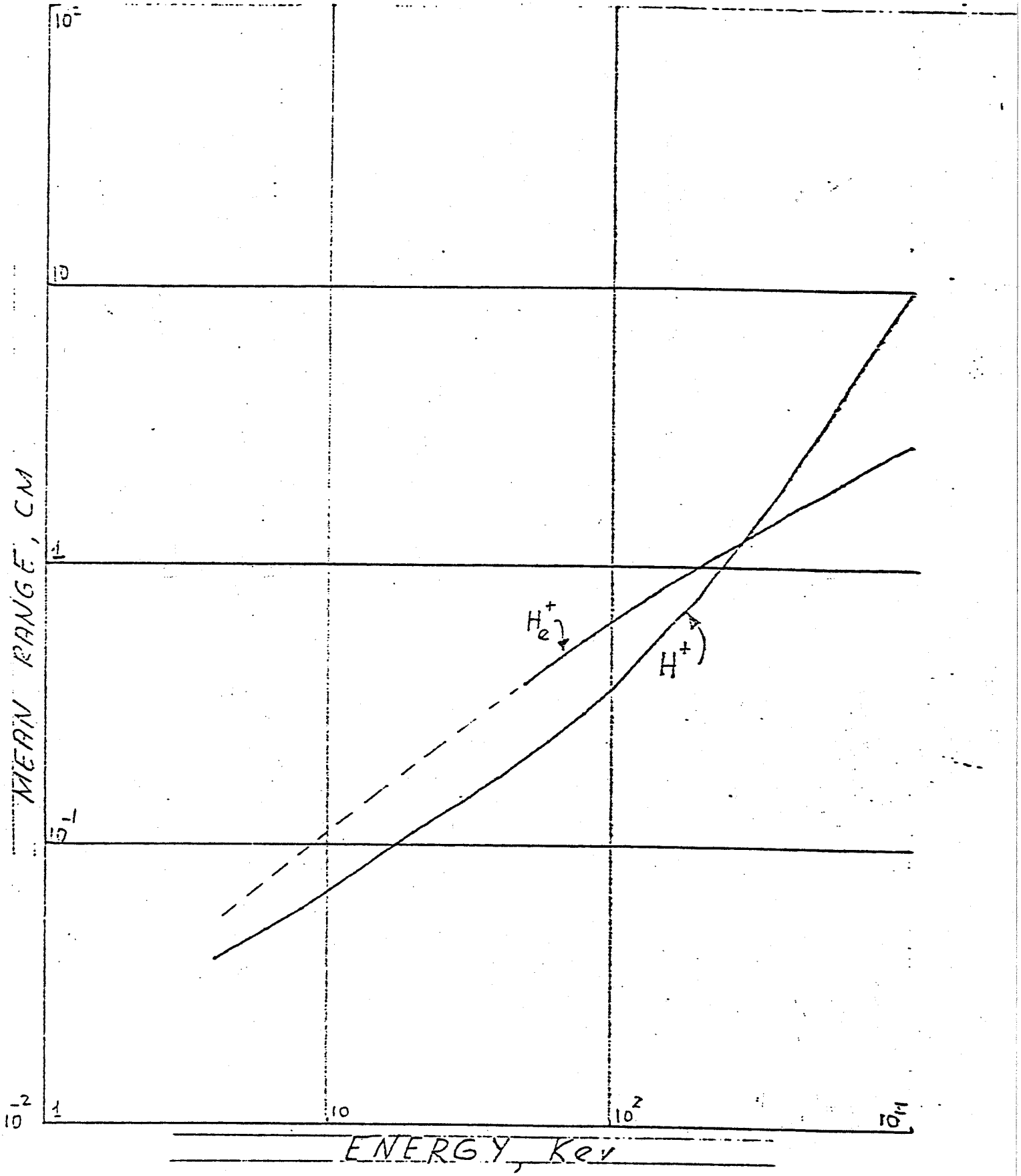

TABLE I

TARGET PRESSURE (MM Hg)

TARGET GAS TEMPERATURE °C

MEAN RANGE, R FOR 10 Kev H IONS IN HYDROGEN & NITROGEN	0.5	1	10	100
1000	H_2 469.7 cm	235	23.5	2.35
	N_2 154.0 cm	77.2	7.72	0.772
500	286	143.0	14.3	1.43
	93.8	46.9	4.69	0.47
100	138	68.9	6.89	0.69
	45.2	22.6	2.26	0.23
10	104.4	52.2	5.22	0.52
	34.4	17.2	1.72	0.17

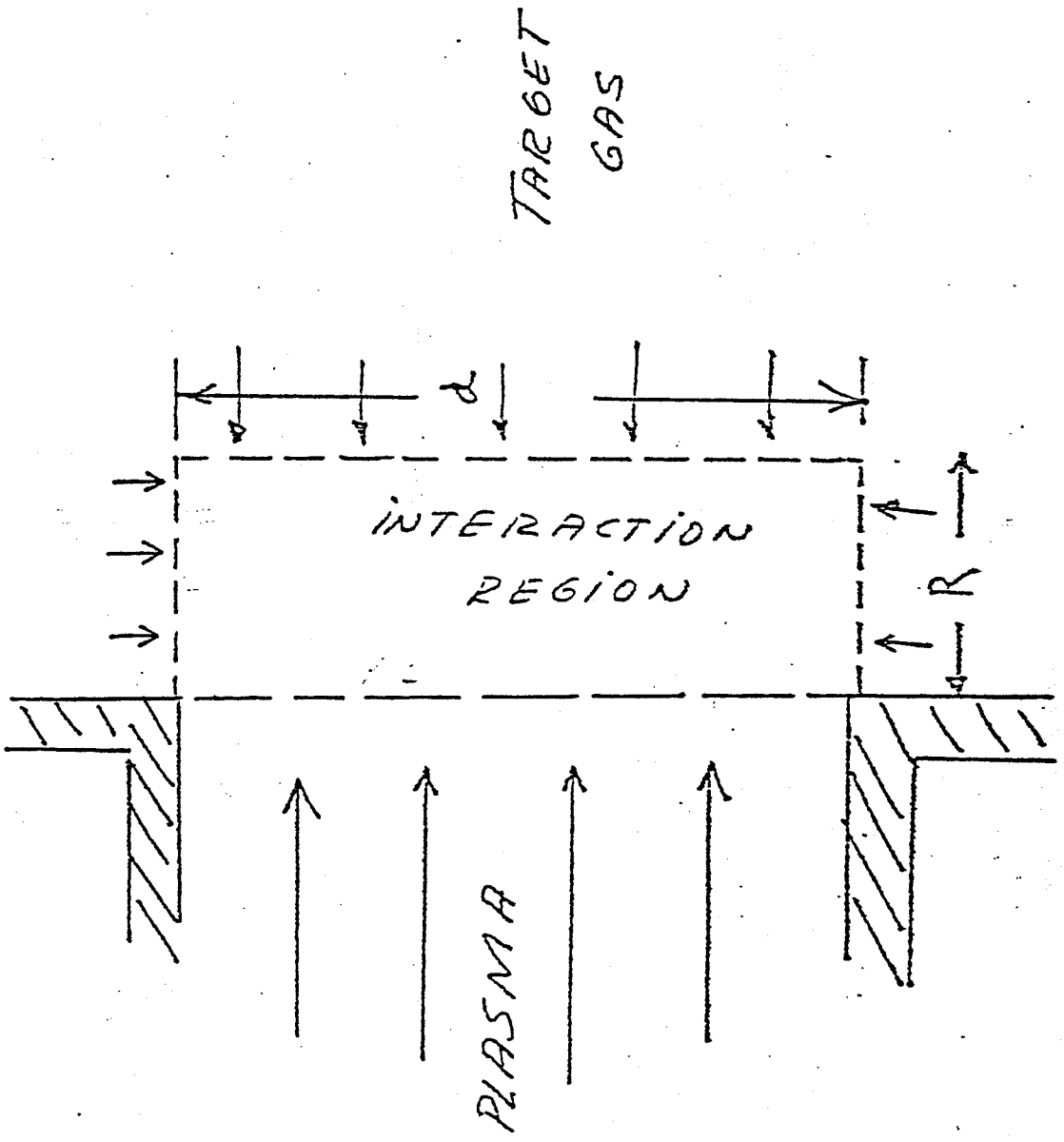
TARGET
GAS
d
INTERACTION
REGION
R
PLASMA

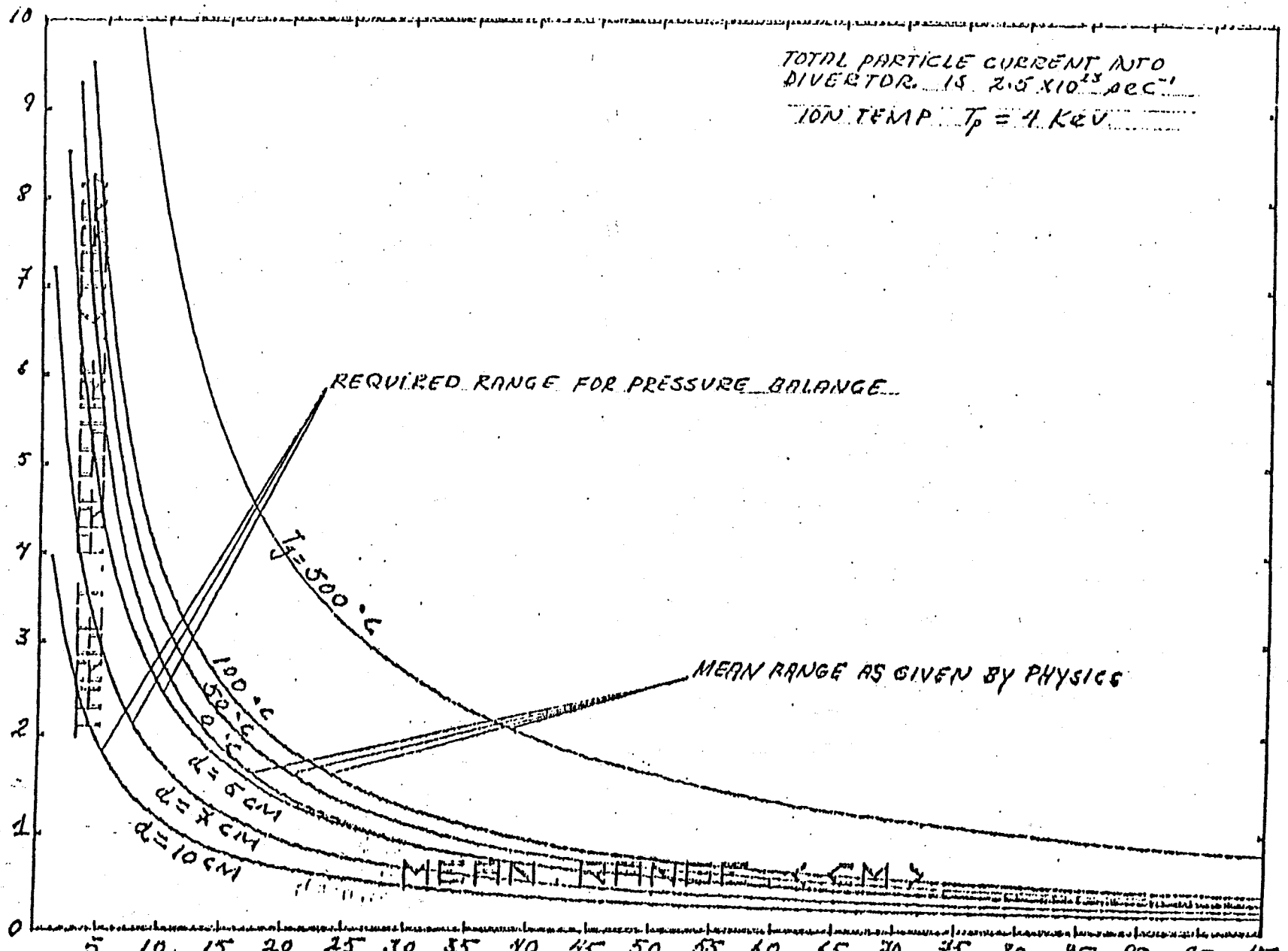
TOTAL PARTICLE CURRENT INTO DIVERTOR IS 2.5 X10^23 sec^-1
ION TEMP T_p = 4 KeV
REQUIRED RANGE FOR PRESSURE BALANCE
MEAN RANGE AS GIVEN BY PHYSICS
T_J=500°C
100°C
50°C
0°C
d = 5 CM
d = 7 CM
d = 10 CM
MEAN FREE PATH (CM)
0
1
2
3
4
5
6
7
8
9
10
5
10
15
20
25
30
35
40
45
50
55
60
65
70
75
80
85
90
95
100

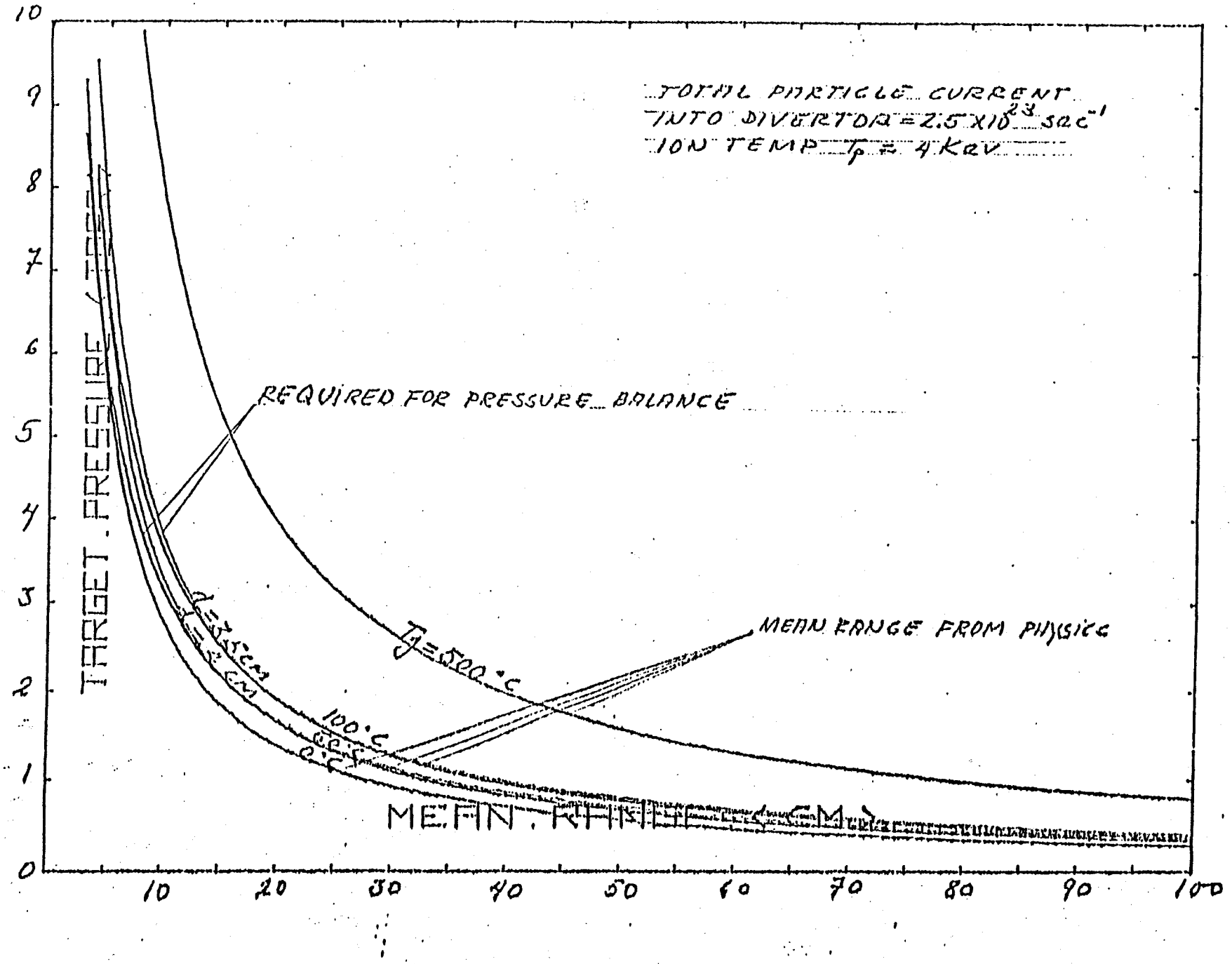
TOTAL PARTICLE CURRENT INTO DIVERTOR = 2.5 X 10^23 sec^-1
ION TEMP T_p = 4 KeV
REQUIRED FOR PRESSURE BALANCE
MEAN RANGE FROM PHYSICS
T = 500 °C
100 °C
0 °C
TARGET PRESSURE (TORR)
MEAN FREE PATH (CM)
0
1
2
3
4
5
6
7
8
9
10
10
20
30
40
50
60
70
80
90
100

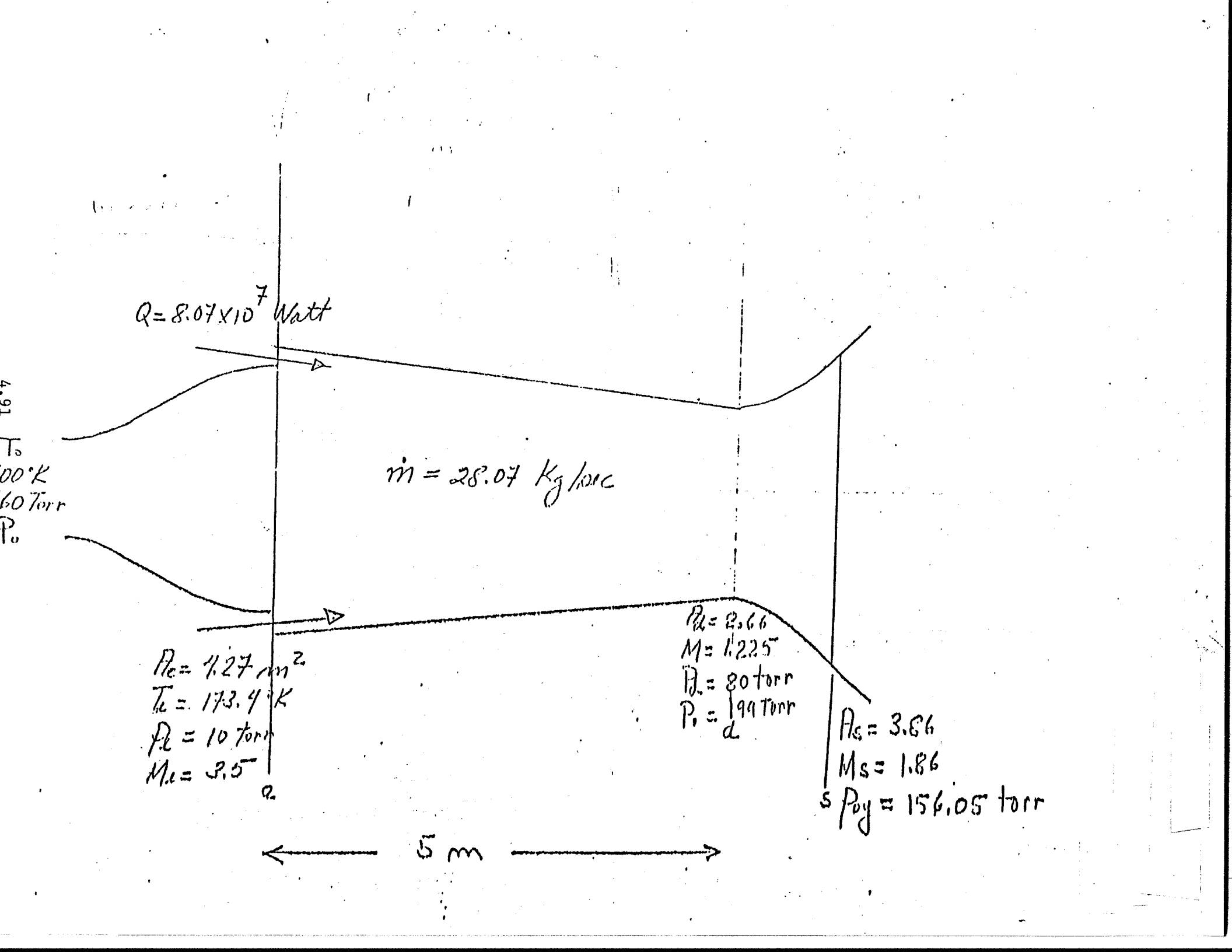
Q = 8.07 x 10^7 Watt
ṁ = 28.07 Kg/sec
T₀
00°K
60 Torr
P₀
Aₑ = 1.27 m²
Tₑ = 173.4 °K
Pₑ = 10 Torr
Mₑ = 3.5
e
Aᵈ = 2.66
M = 1.225
Tᵈ = 80 torr
Pᵈ = 99 Torr
d
Aₛ = 3.66
Mₛ = 1.86
s
Pₒᵧ = 156.05 torr
5 m

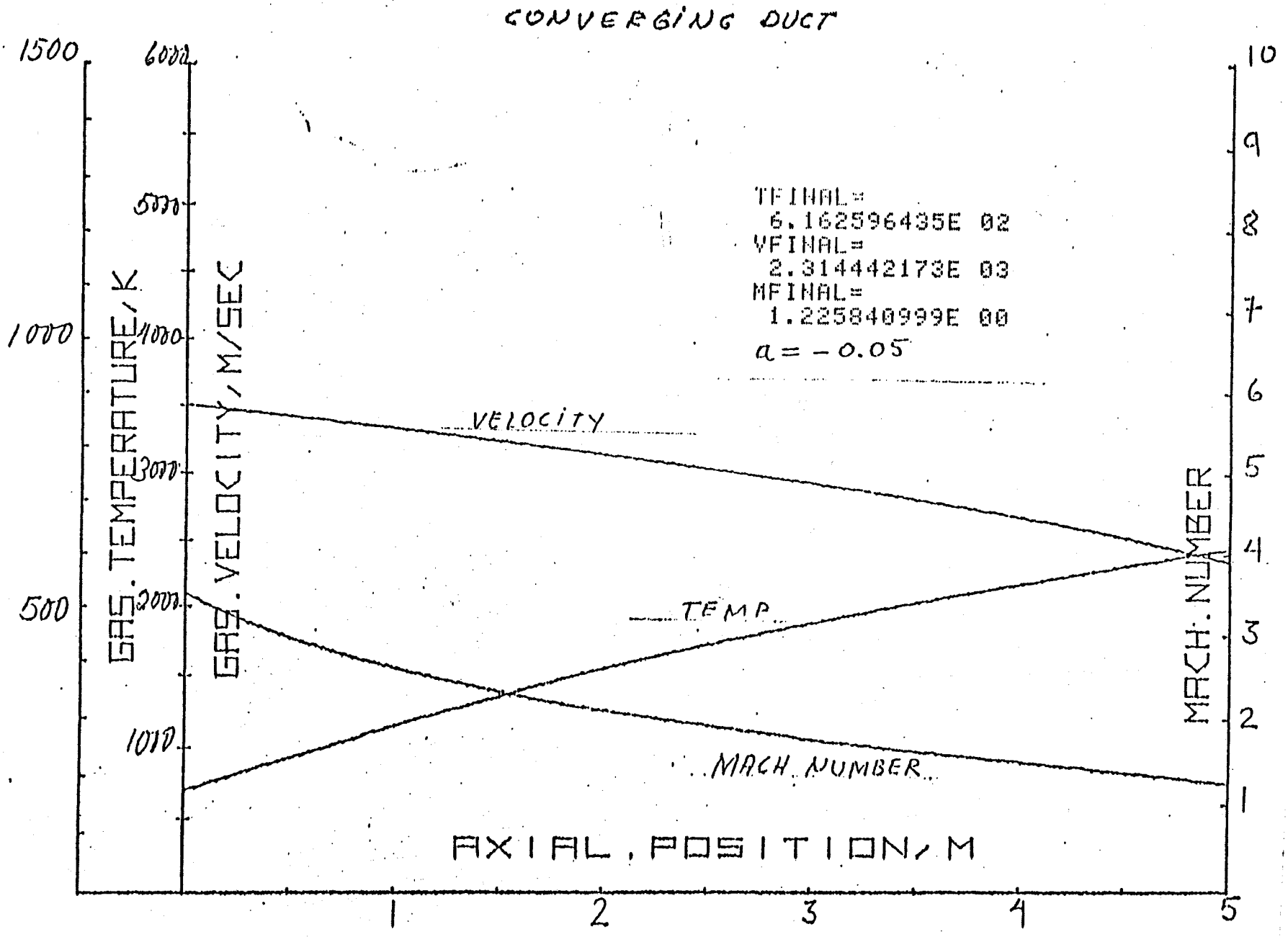
CONVERGING DUCT
TFINAL=
6.162596435E 02
VFINAL=
2.314442173E 03
MFINAL=
1.225840999E 00
a = -0.05
VELOCITY
TEMP
MACH NUMBER
GAS. TEMPERATURE, K
GAS. VELOCITY, M/SEC
MACH. NUMBER
AXIAL, POSITION, M
1500
1000
500
6000
5000
4000
3000
2000
1000
10
9
8
7
6
5
4
3
2
1
1
2
3
4
5

DIVERGING DUCT

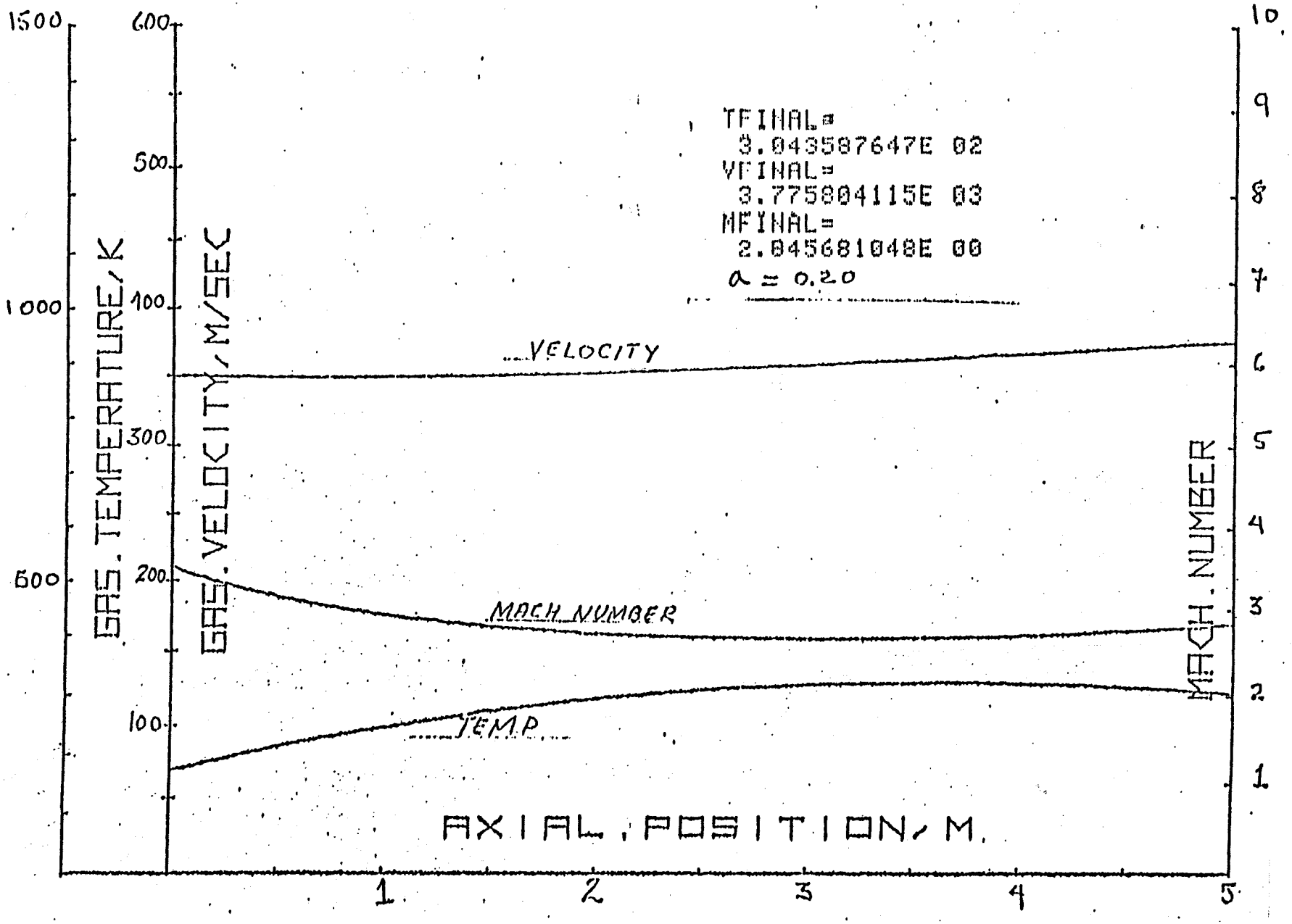

4.3.3 Poloidal Divertor Collector Systems

Introduction

A single null poloidal divertor was considered as the design option for INTOR in the previous study phase. The target in the divertor chamber was a solid tungsten plate with or without protective lithium film. Since there is no experimental program to test the target and pumping methods at this stage, it is imperative that we should try to look into as many alternative concepts as possible. Each concept can thus be tested out at an early stage of INTOR so that a workable solution can be assured. Three new target concepts and external fuel recycle methods are proposed and discussed in this report. To improve the erosion rate or the target life time, the use of a two null divertor which can operate alternatively as two single null divertors is also suggested. Since there is plenty of space behind the divertor chamber and the shielding does not have to be in contact with the divertor target, the shielding does not present a problem whether it is a single or double null divertor system.

Wall Erosion Problems

The plasma conditions in the scrape-off layer and on the divertor target for INTOR are listed in Table 1 [1,2]. These are the results of transport modeling by considering 99% recycle. The particle flux to the divertor can be estimated consistently from sheath model [3,4]. The total energy of the impinging ions on the target for T_i = 190 eV and T_e = 250 eV at the plasma edge is

$$\varepsilon_i = 2\ kT + Z\ (\frac{kT_e}{2})\ \ln\ (\frac{T_e m_i}{T_i m_e}) = 1.4\ \text{keV}. \qquad (1)$$

Normalized to the total particle and power load the particle flux on the target can be calculated from

$$\Gamma = \frac{Q}{2.9\ \varepsilon_i} \qquad (2)$$

The erosion rate for several material for various energy and particle fluxes can be quickly estimated from the erosion rate graphs given by Cecchi [4] and listed in Table 2. The sputtering erosion for a solid target is a severe problem. To limit the erosion rate to less than 1 mm/year it is necessary to operate the divertor at 0.1 kw/cm^2 level of power load. Such designs will be discussed in the next section.

Table 1. Divertor plasma conditions for 99% recycle.

Power to the divertor	80 MW
Total particle load	$1.5 \times 10^{23} s^{-1}$
Ion energy on target	1.4 keV
Plasma edge ion temperature	190 eV
Plasma edge electron temperature	250 eV
Availability	0.25

Table 2. Erosion rate of divertor target for 99% recycle.

Power density	1 kw/cm^2	0.1 kw/cm^2
W	7 mm/yr	0.6 mm/yr
Mo	11 mm/yr	1.0 mm/yr
V	5.5 mm/yr	0.6 mm/yr
TZM	11 mm/yr	1.0 mm/yr

3. DIVERTOR TARGET CONCEPT

Three alternative target design options are proposed here in addition to the flate plate with protective lithium film. The target will be assembled from a module of 10 cm x 10 cm tube array as shown in Fig. 1. The tube can be aligned parallel to the magnetic field or transverse to the magnetic field as shown by Figs. 2 and 3. The tube array is constructed such a way that every other tube

is set back to leave a gap in the longitudinal direction between the tubes to allow the plasma to pass through. Therefore, the neutrals will be scattered to the back side of the target and pumped away. Since only 1% of pumping is required, it is very easy to obtain 1% of transmission coefficient from such a design. The tube grill like target will be sitting inside the gaseous chamber. The volume of particles to be pumped can be regulated by the gas pressure. The great advantage of this method is that the inner branch of the divertor (at smaller radius) is no longer obstructed.

Because of the high erosion rate, the target has to be operated at a low power level in order to survive a reasonably long period of time, following which, the target surface would be replenished. For the tubular construction, the total surface is $\frac{\pi}{2}$ times larger than the flate plate which was 70 m^2 given in the previous design. Therefore, total area per divertor is about 110 m^2, the erosion rate for 0.25 machine availability is less than 1 mm/year for a molybdenum target. The power density is less than 0.1 kw/cm^2, thus the thermal hydraulic design is simple. The tube can even be cooled by steam and a reasonably amount of thermal energy can be recovered.

The second target design method is shown by Fig. 4. Since each branch of the divertor plasma resembles a beam, the targets are placed on both sides of the plasma slab and contoured in such a way that they are nearly tangential to the flux. Since the targets are not intersecting the separatrix where the plasma is peaked, the power and particle flux on the targets are nearly uniform. Because of the grill-like structure of the target, the plasma will reach the off-set tubes and the scattered neutrals can be pumped from the backside. The total target area is almost double the previous design. The target life time will double to two years and the thermal load is reduced to 0.05 kw/cm^2.

The third method is to use straight forward gaseous targets. The plasma will be slowed down by the gas, dispersed, neutralized, and radiate some of it's power. The gas may be hot, but the chamber wall will be thermally shielded by tube arrays. The life time and thermal performance of the wall shield should be better than the second case since the gas temperature is lower and more evenly distributed.

Divertor Operation Methods

As discussed in the introduction, the shielding space is not a problem. The use of a double null divertor gains many advantages over the use of a single null divertor. The PDX experimental result shows that the power load to the divertor is equally distributed to inner and outer branches of the single null divertor [6]. Because the target area is smaller in the inner branch, the power density would be higher. For the double null divertor, approximately 90% of the power flows to the outer branch which has a larger area. Then the advantage of using the two null divertor is that the power and particle densities will be more evenly spread. The total target area will also be doubled; therefore, 1 mm of target thickness will last 4 years.

To pump 1% of the total particle flux of 1.5×10^{23}/sec, there is still 1.5×10^{21} particles/sec to be pumped. The tritium through-put would be 7.5×10^{20} particles/sec which still gives very large tritium inventory. It would be better to find a way to recycle the tritium inside the tokamak. A method to accomplish this is to put a D & T getter pump inside as shown by Fig. 6 or use the getter as D & T filter. He and a fraction of other impurities can be removed by an external pump. D & T can be released later as fuel. The advantage of the getter pump is that the impurities will not be released during the remission process and the fuel is free of impurities and He. Each divertor can be operated as divertor and gas puffing fueling alternatively. Both divertors will use the same pumping facility with the pumping path controlled by a gate valve.

Revisiting of the High Efficient Divertor

In the past year, because of the concern of excessive pumping requirement and tritium inventory, it was considered desirable to recycle the fuel and keep the plasma edge cool. The diffusion at the plasma edge has to be enhanced due to the large recycling. This greatly increases the particle load on the target. From the scaling law of the bulk plasmas diffusion coefficients [7]

$$D = 500 \cdot (\frac{v}{a})^3 + 1.25 \times 10^{17}/n_e \qquad (3)$$

we can estimate the bulk plasma confinement time for INTOR to be about 3 sec. The particle leakage flux would be 1.5×10^{22} which is one order of magnitude less than the recycle case. The plasma edge temperature is usually about 3 keV and electron temperature is higher than the ions. The total ion energy on the target is as high as 15 keV due to the effect of sheath potential. This again reduces the sputtering yield by a factor of 10. The combined effect of less particle flux and higher energy will reduce the erosion rate by two orders of magnitude. With regard to the target life time, it is better to operate the divertor at high efficiency. The tritium through-put is about 7.5×10^{21}/sec, which is 10 times larger than the recycle divertor. These issues and pumping problems are under study.

Thermal Consideration

For a heat flux of less than 0.1 kw/cm^2, the thermal hydraulic design of the target is well within the state of the art. Here we would like to investigate the possibility of using superheated steam as a coolant so that the thermal energy can be recovered. Let us consider a tube 20 cm long with an inner diameter of 1 cm and wall thickness of 3 mm. To drive a steam turbine directly, a suitable choice of steam pressure is 100 atm and mean temperature is 400°C. For a through

the tube velocity of 40 m/sec, the heat transfer coefficient is 4.64×10^{-4} kw/cm^2°C [8]. The heat flux at the inner wall is 0.16 kw/cm^2, thus the temperature difference between the inner wall and steam is 350°C. The temperature increase at the exit end of the tube can be calculated from the equation

$$\rho V C_p \frac{dT}{dx} \frac{\pi d^2}{4} = \pi D \cdot q \qquad (4)$$

we obtain ΔT = 35°C. The thermal characteristics are given in Table 3. It can be concluded that the superheated steam cooling and thermal energy recovery are feasible.

Table 3. Thermal characteristics for molybdenum tube cooled by superheated steam.

Tube length	20 cm
Wall thickness	3 mm
Steam pressure	100 Atm
Steam velocity	40 m/sec
Steam temperature	400°C
Exit temperature	435°C
Inner wall temperature	810°C
Outer wall temperature	840°C

Conclusion

The preliminary analysis shows that a divertor system can be designed with a target life of 4 years at a power density of 0.1 kw. The benefit of this power density level is that a molybdenum target can be cooled by superheated steam and thermal energy recovery is possible.

REFERENCES

[1] SINGER, E. C., R. A. Hulse, and D. E. Post, INTOR Topical Report, (June, 1980) and private communication.

[2] HOMEYER, W. G., D. K. Sze, C. P. Wong, R. L. Creedon, INTOR Topical Report, (June, 1980)

[3] SCHMIDT, J. A., private communication.

[4] GORDINIER, M., Univ. of Wisconsin, Ph.D. Thesis, UWFDM - 356 (1980).

[5] CECCHI, J. L., PPPL - 1668 (1980).

[6] MEADE, D., V. Arunasalam, C. Barnes, K. Bell, M. Bol, et al, IAEA 8th Int'l Conf. on Plas. Phys. and Contr. Nucl. Fus. Research Brussels (1980), to be published.

[7] ENBANK, H. et al, IAEA 7th Int'l Conf. on Plas. Phys. and Contr. Nucl. Fus. Research, Vol. 1, 167 (1979).

[8] KUTATELADZE, S. S., V. M. Borishanski, A Concise Encyclopedia of Heat Transfer, Ch. 12, Pergamon Press, First Edition, 1966.

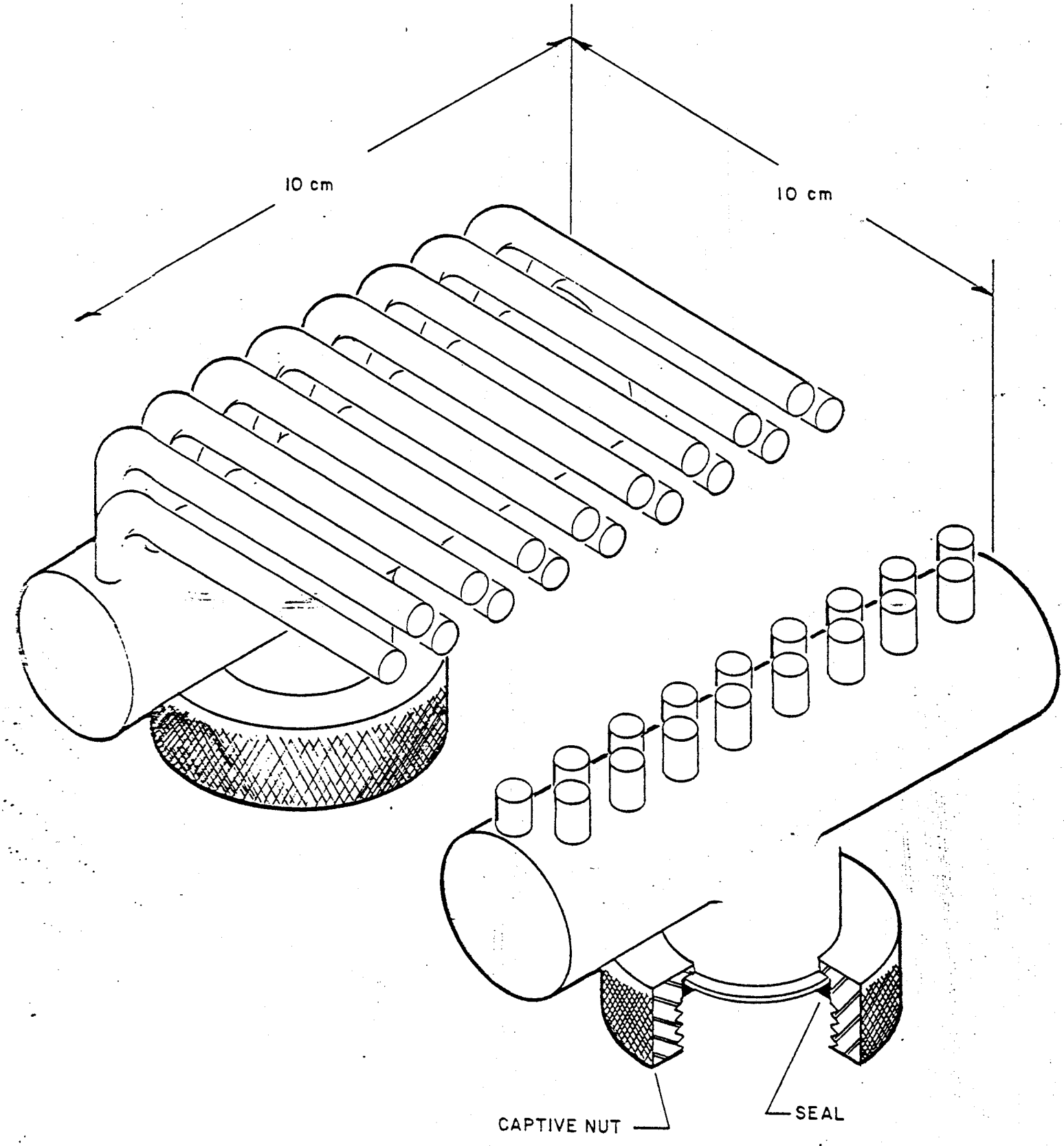

Fig. 1 Divertor target module.

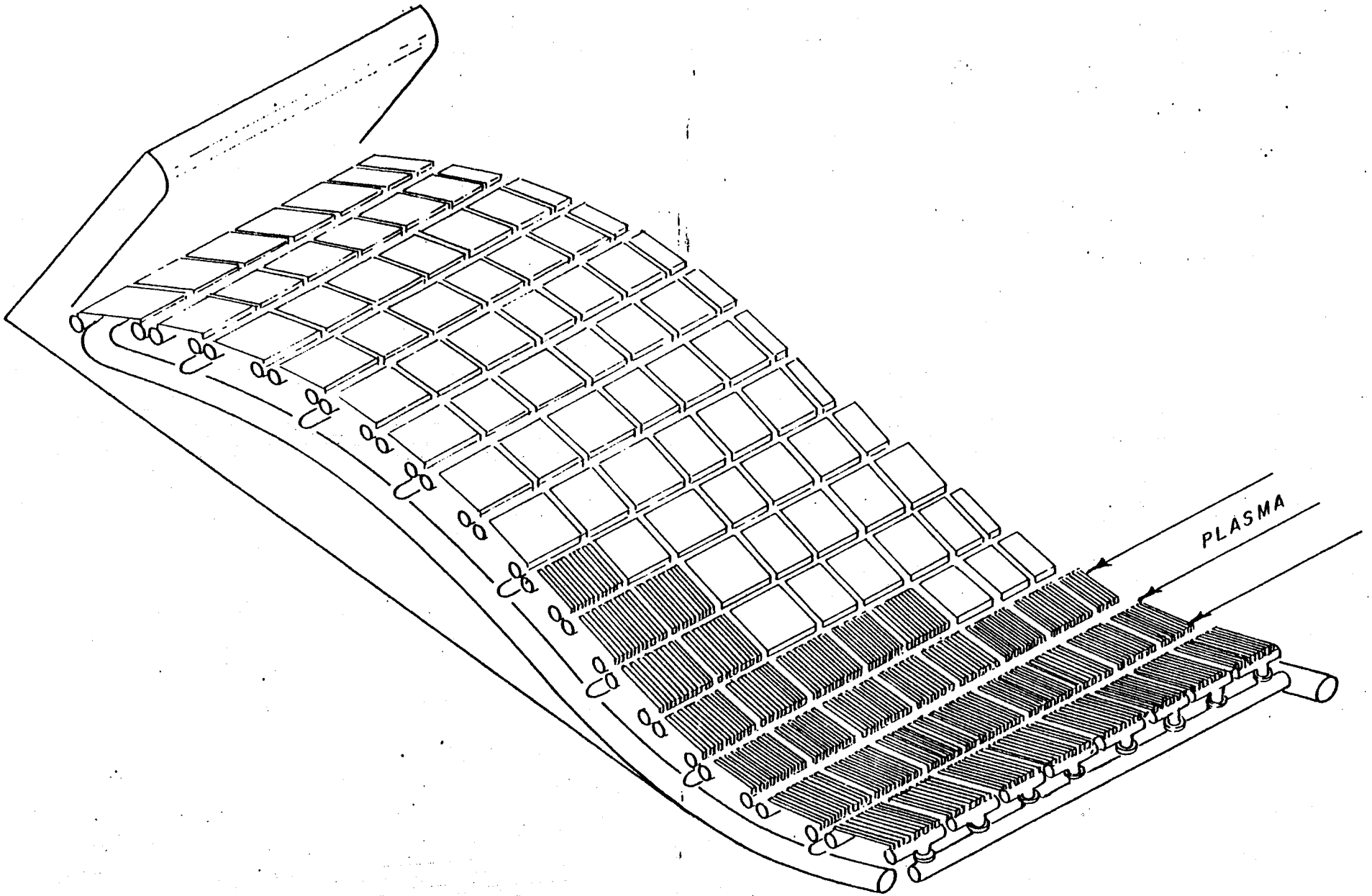

Fig. 2 A section of divertor target assembled from the modules where the tubes are oriented in the transverse direction.

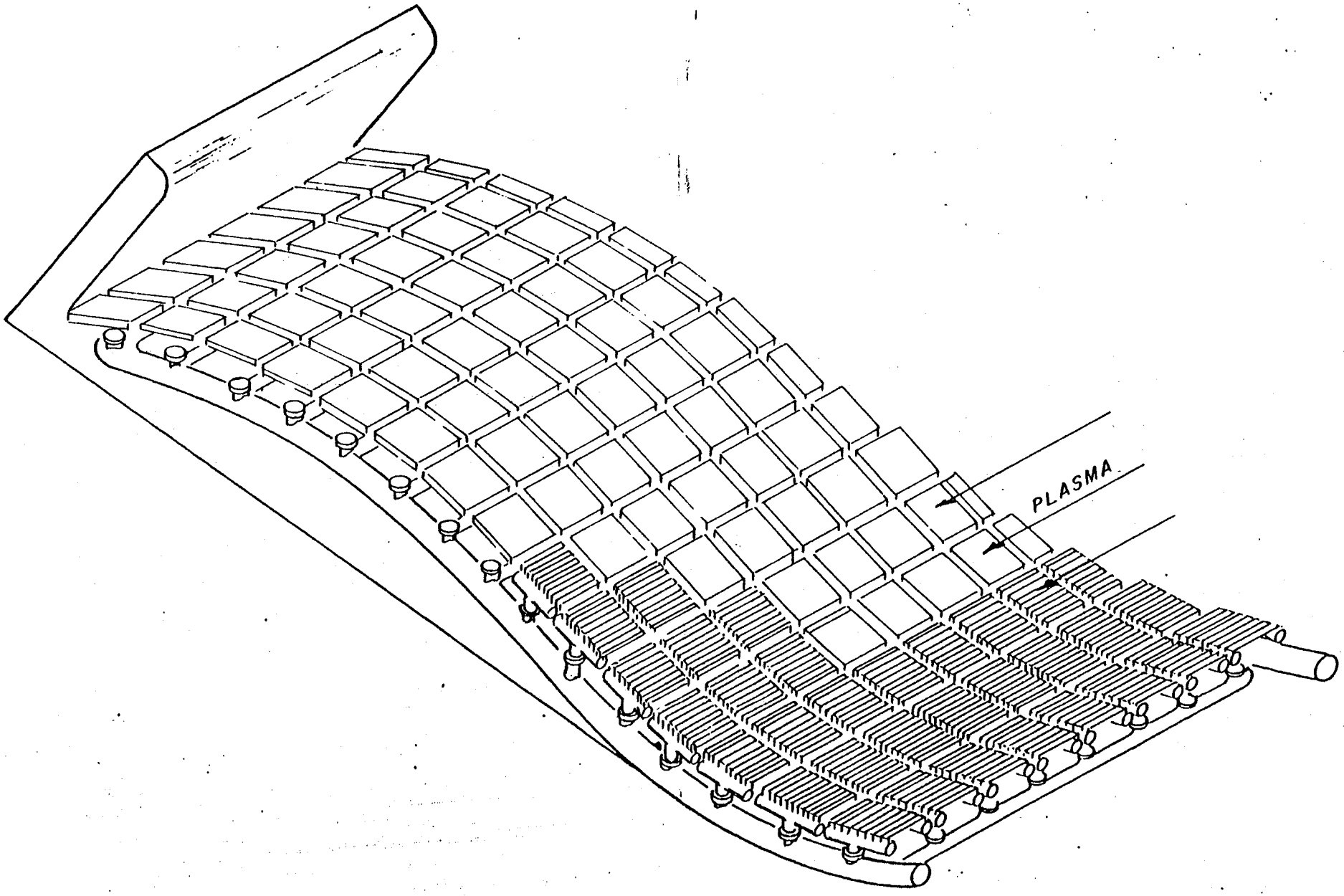

Fig. 3 A section of divertor target assembled from the modules where the tubes are oriented in the parallel direction to the plasma.

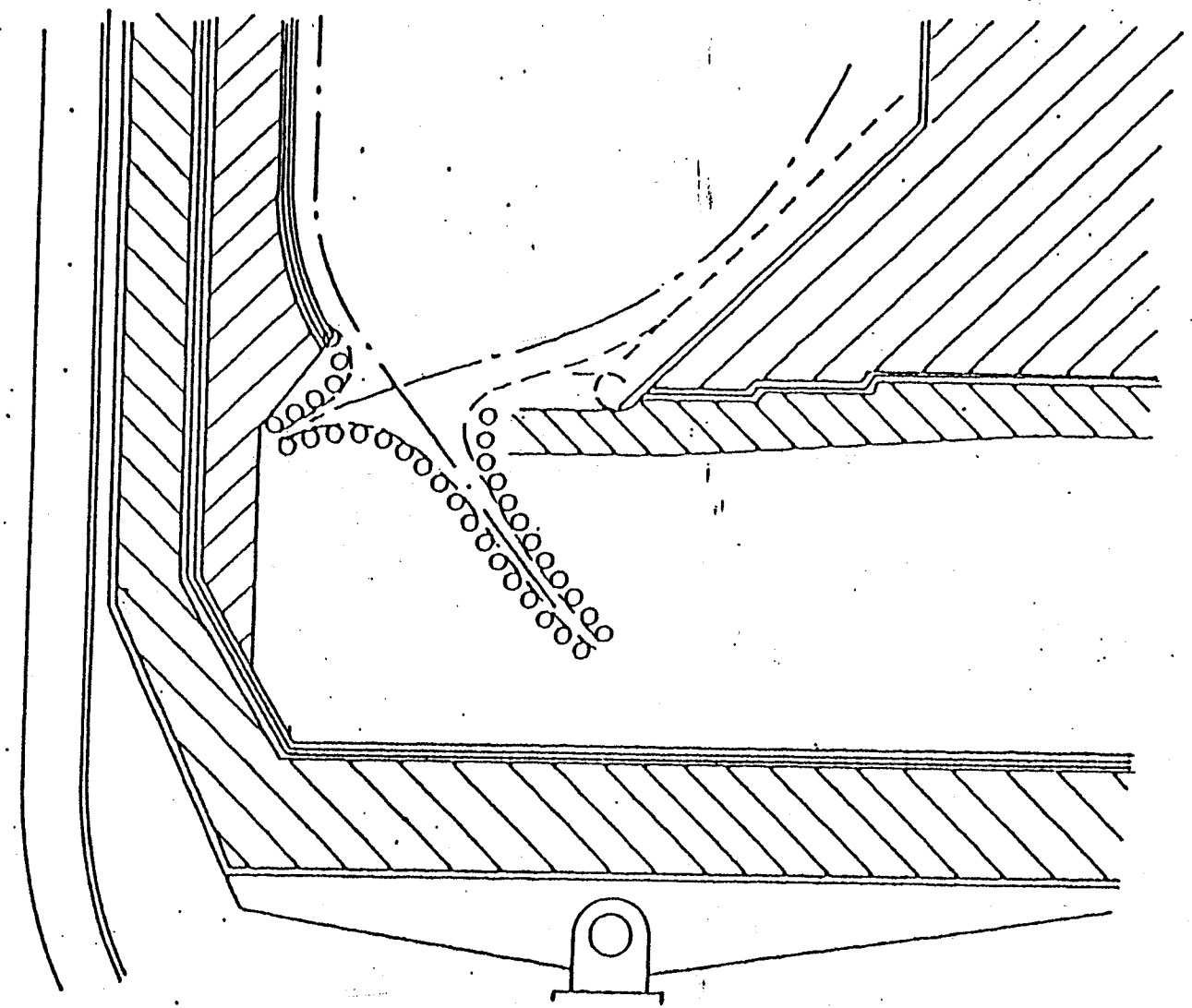

Fig. 4 The targets are placed on the sides of the plasma slab on each branch of the divertor.

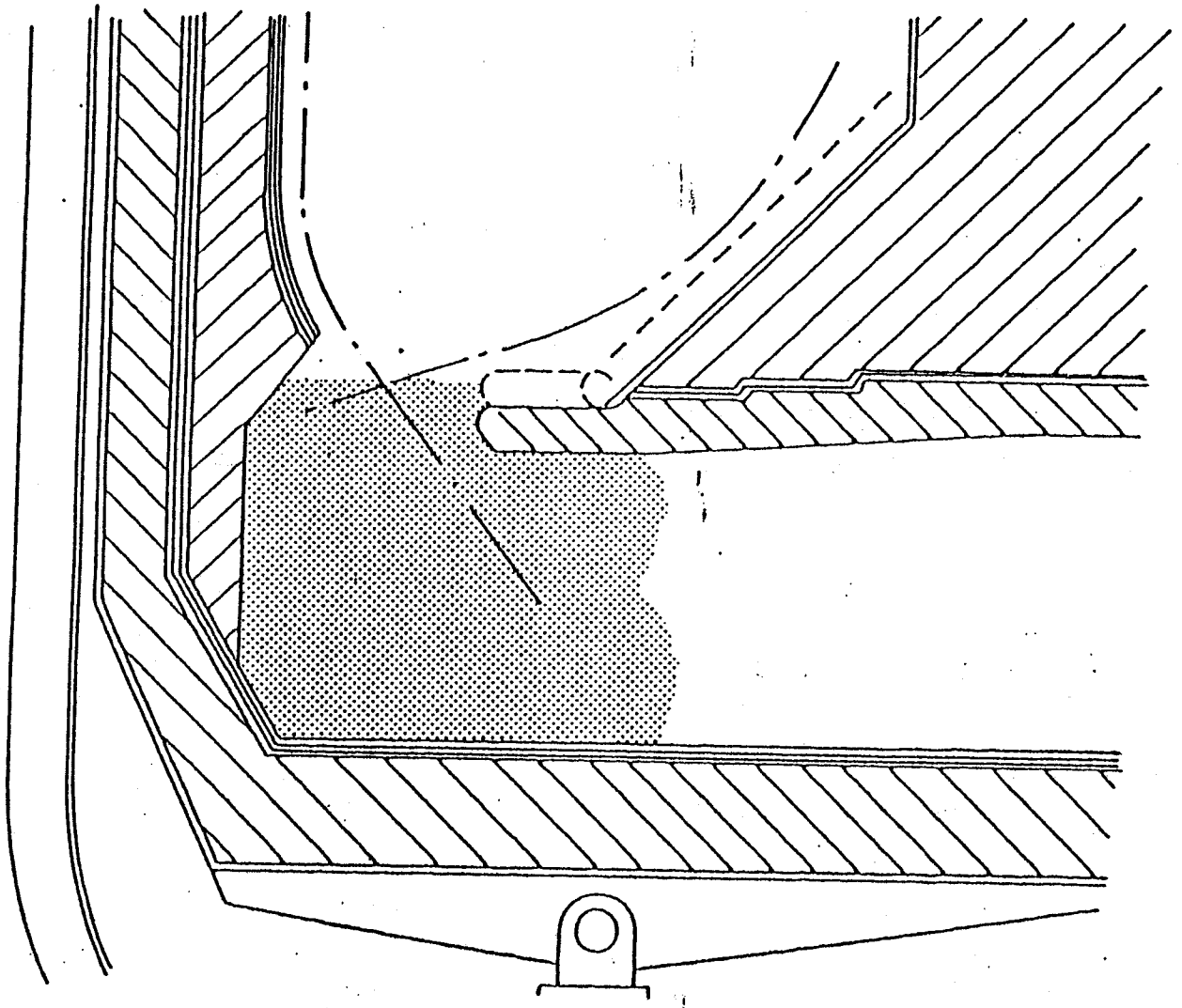

Fig. 5 Gaseous target and the chamber wall is thermally shielded by water cooled tube modules.

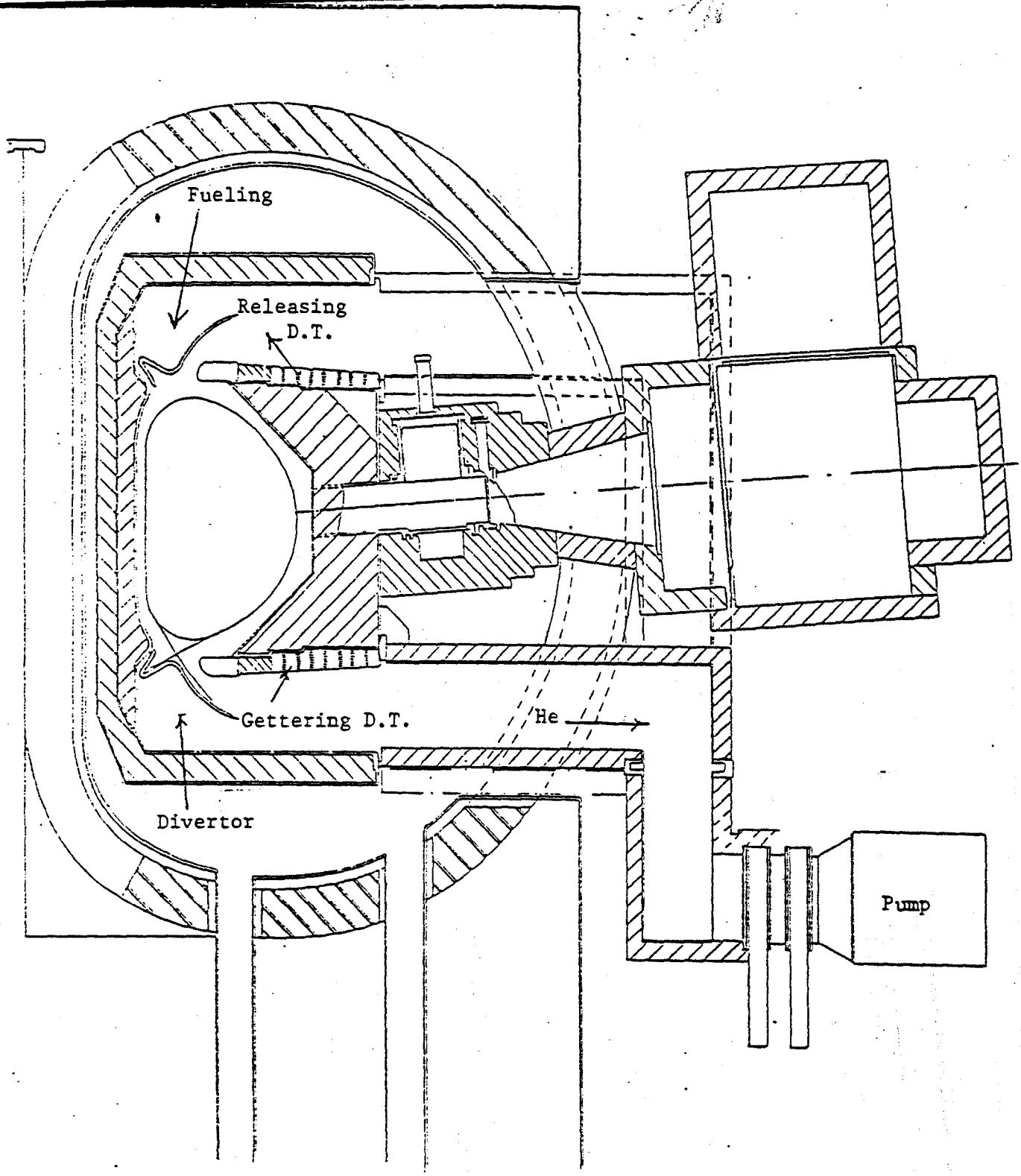

Fig. 6 The proposed operational methods for double divertors. The divertor on the top is releasing D & T fuel into the plasma where the one at the bottom is pumping. During the pumping phase the D & T fuel is trapped and only He ash is removed.

5.0 Divertor Shielding, Insulating Materials and Coils

5.1 Shielding Considerations

It has been demonstrated previously that by improving the magnetic designs, bundle divertors that are technically feasible can be developed for tokamak reactors.[1] Unlike a poloidal divertor, a carefully designed bundle divertor can be demounted for maintenance and the particle and thermal handling systems can be placed at the outside of the TF-coils. The major difficulty of designing a bundle divertor coil is the very high current required in the divertor coil. The coil current required increases exponentially with the distance of the coil from the plasma. The divertor components in the region at the front legs of the divertor coils, as shown by the shaded area in Fig. 1, suffer the most critical radiation damage. Therefore, the space in front of the divertor coils is at a premium and the shielding design is critical. It is the purpose of this work to search for an optimum combination of shielding materials for best radiation protection of the divertor coils in the minimal possible space. The available shielding space is only about 0.4 m in the design shown in Fig. 1 which is chosen as a preliminary optional divertor for INTOR.[2]

The radiation damage characteristics and the radiation exposure limit for superconducting and normal magnets have been discussed in detail in Refs. 3 & 4. For a superconducting magnet, the magnet insulation, stabilizer and superconductors suffer severe radiation damage characterized by mechanical and electrical property degradation of the insulation due to radiation dose, resistivity increase of the stabilizer due to atom displacement, and critical temperature and current density changes in the

---

*Work supported by Department of Energy; GA Contract DE-AT03-75ET51011, MIT Contract DE-AC02-80ER-52057.

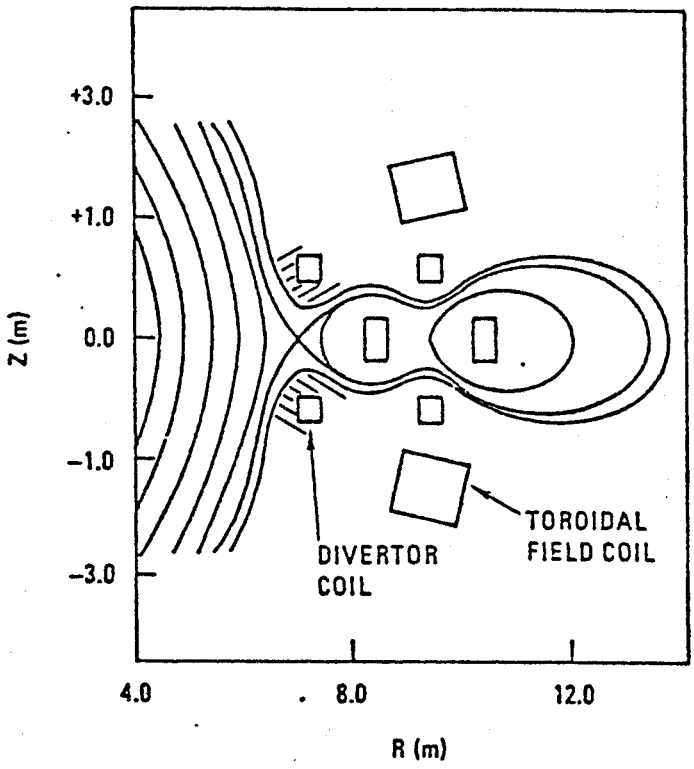

Fig. 1. Schematic of the INTOR bundle divertor

superconductor due to neutron transmutation and atom displacement. The superconductor damage is very small in the currently considered radiation enviroment. The conductivity in the stabilizer may be partly recovered if the magnet is annealed. Hence, the most critical damage is the insulation radiation damage which is unrecoverable. For a normal magnet, radiation damages are characterized by the insulation property changes due to dose degradation and resistance increase in the conductor due to atom displacement. DPA damage may be annealed out and it appears that the most critical damage again is the insulation dose damage.

Various shielding materials and combinations of shielding materials such as 316SS + B_4C and W + B_4C, have been studied for regular fusion reactor shield designs.[5] Tungsten appears to be the best shielding material. Recently shield combinations of tungsten with advanced materials such as TiH_2 and ZrH_2 have been proposed for the Engineering Test Facility divertor shielding design.[6] We report here a preliminary shielding requirement study

performed using a one-dimensional model. However, more detailed and particularly multi-dimensional calculations are needed in the design phase study. Several neutronics calculations to estimate the shielding thickness needed for the normal coil divertor design were performed. The one-dimensional discrete ordinate transport code ANISN was employed with P_3S_6 approximation, in cylindrical geometry. The calculational model consists of a 20 mm stainless steel first wall where 50% of the space is filled with water for cooling, a variable thickness of shield and a 0.4 m 40% SS + 60% Cu zone representing the copper coil and structure. Three combinations of shielding materials are considered: 10% H_2O(B) + 90% W, 30% H_2O(B) + 70% W, and 50% H_2O(B) + 50% W. The borated water is employed both as neutron absorber and coolant. A density factor of 0.9 is used for tungsten to account for the packing effect.

The results show that the 10% H_2O(B) + 90% W shield is the best material combination. The radiation dose on the insulation material can be expressed as

$$\overline{D(t)} = D_o e^{-14.01\ t\ -\ 3.33\ t^2}$$

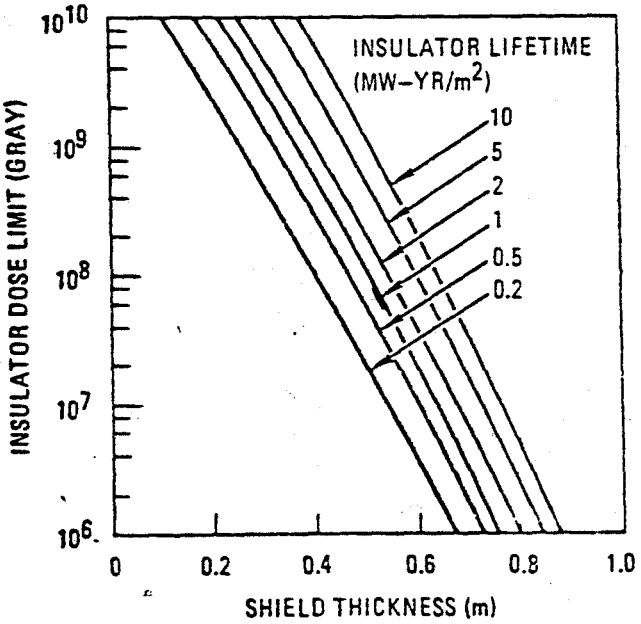

Fig. 2. Lifetime of insulation material as a function of dose limit and shield thickness

where D_o, which is 2.5×10^{11} Gy/year at 1 MW/m^2 wall loading, is the dose on the insulator if there is no shield between the first wall and divertor coils, and t is the shield thickness in meters. Note that the dose attenuation coefficient is not linear. It depends somewhat on the effective neutron energy which is the result of neutron moderation in the shield. The lifetime of the insulation material is depicted in Fig. 2 as a function of dose limit and shield thickness. Considering a magnet lifetime of 1 MW-yr/m^2, the minimum shield thicknesses required would be 0.63 m and 0.37 m, respectively, if the dose limits on the insulator are 10^7 Gy and 10^9 Gy, depending on type and form of the insulator. Recent irradiation tests[7] indicate that G-10 epoxy/E-glass insulation is capable of 10^9 Gy with good mechanical property retention. With an overall shield thickness of 0.4 m which allows space for the divertor structure, and a reactor duty factor of 50%, the divertor lifetime would be one year at 2 MW/m^2 wall loading. Since the divertor can be designed as a plug-in unit, a one year replacement schedule should be reasonable.

REFERENCES

1. T.F. Yang, *et al.*, "Design of an Advanced Bundle Divertor for the Demonstration Tokamak Hybrid Reactor," Proc. of 8th Symp on Engineering Problems of Fusion Research, November 13–16, 1979, San Francisco, California.
2. U.S. INTOR Report, to be published (1980).
3. M.A. Abdou, Nucl. Tech. 29, 7 (1976).
4. G.A. Carlson, *et al.*, "Definition and Conceptual Design of a Small Fusion Reactor," Electric Power Research Institute Report ER-1045, Sec. 6.3.3 (April 1979).
5. E.T. Cheng, "The Reflector-Shield Concept for Fusion Reactor Designs," Trans. Am. Nucl. Soc. 34, 49 (1980).
6. B.A. Engholm, General Atomic Company - ETF, private communication.
7. H. Becker and E. Erez, Plasma Fusion Center, Massachusetts Institute of Technology, private communication.

5.2 Insulating Materials

A survey of the radiation damage on the insulating materials is shown in Table 1. Some material can survive the dosage of 2×10^9 to 3.8×10^{11} rad. The highest tested dosage is 3.8×10^{11} rad on thin sheets of G-10[(1)]. Therefore, high strength insulating materials exist. For the special bundle divertor application, the use of such material is important and further development is needed. Assuming a safety of 4 from the testing result of G-10 in the last row, a dosage of 10^{11} rad is chosen for the shielding requirement assessment. The radiation testing of G-10 was conducted by MIT at both Idaho National Laboratory and MIT reactor facility. To qualify the quoted data, the testing procedure is described in the following.

Disks were cut from thin sheets of G-7, G-10 and G-11 CR*. They were irradiated in the Advanced Test Reactor at Idaho National Engineering Laboratory. The radiant flux was calculated from a standard code used at INEL and is stated to be within 20 percent of actual values. The total fluence was 1.6×10^{19} n/cm^2 for neutron energies greater than 0.1 Mev, 10^{20} n/cm^2 for the total neutron spectrum and 3.8×10^{11} rads of gamma radiation. That dose is somewhat higher than the fluence expected in ITR.

The specimen temperature was reported to be 120 F. All specimens were found to be highly radiactive after months of cooldown. Consequently, testing was conducted in a hot cell.

The compression fatigue tests were conducted in the same manner as for the unirradiated samples (Figure 1). The results appear in Table 2. In addition the G-10 data are plotted on the graph of Figure 2. All tests were stopped arbitrarily at 200,000 cycles if no failure had been observed.

---

* Diglycidyl ether of bisphenol A reinforced by E-glass.

It is clear that the observed strengths are much greater than reported previously for rods irradiated at 4.9 K (Ref. 6) for which G-10 CR static compression values of about 69 MPa were obtained. The INEL results also exceed the ITR requirements. The stress level of 345 MPa is more than twice the ITR requirement. Furthermore, 200,000 cycles corresponds to 20 times the required life.

If it is assumed that the low temperature fatigue strength is twice the RT value, which matches the ratio for static ultimate compression of G-10 rods, then the 77K fatigue curve would be as shown on Figure 2. The observed survivability of the 77K specimens is consistent with that curve.

Reference:

E. A. Erez and H. Becker, "Radiation Damage in Thin Sheet Insulators", ICCM Conference in Geneva, August, 1980.

Table 1

MATERIAL	RADIATION	TYPE OF TESTING	COMMENTS
UNFILLED EPOXY RESINS	$2. \times 10^{3}$ RAD RT	MECHANICAL PROPERTIES	NO CHANGE THE MOST SUITABLE ARE AROMATIC EPOXY RESIN.
FIBER-GLASS EPOXY LAMINATES	1×10^{10} RAD RT	MECHANICAL PROPERTIES	USABLE AS A SUPPORT AND STRUCTURE COMPONENTS.
UNFILLED EPOXY RESINS	3.2×10^{9} RAD RT	MECHANICAL PROPERTIES	25% DAMAGE
GLASS-FIBER EPOXY COMPOSITES	2.65×10^{10} RAD RT	MECHANICAL PROPERTIES	25% DAMAGE
GLASS-FIBER AND MINERAL FILLED EPOXY	5×10^{10} RAD RT	MECHANICAL PROPERTIES	25% DAMAGE
FIBER-GLASS EPOXY WITH Al_2O_3 FILLER	10^{10} RAD RT	COMPRESSION STRENGTH	NO CHANGE

Table 1 (cont.)

MATERIAL	RADIATION	TYPE OF TESTING	COMMENTS
SIXTEEN FIBER-GLASS EPOXIES WITH DIFFERENT HARDENERS	2×10^{10} RAD, GAMMA, AIR, RT	FLEXURAE STRENGTH AND MODULUS RT	GLYCIDYE AMINE RESINS ARE EXCEPTIONALLY STABLE TO RADIATION. AROMATIC AMINE HARDENERS GIVE RESINS MORE STABLE TOWARDS RADIATION.
G-10 FIBER-GLASS EPOXY	1.4×10^{17} N/CM^2 + 2.2×10^{8} RAD + ALPHAS RT	FLEXURAL STRENGTH RT	DECREASE ON 30%
EPOXY RESINS	10^{9} RAD 77°K	FLEXURAL STRENGTH AND MODULUS 77°K	NO CHANGE
FIBER-GLASS EPOXY COMPOSITES	10^{10} RAD OR 2.4×10^{9} RAD + 2.4×10^{16} N/CM^2 FAST NEUTRON FLUENCE 5 K	FLEXURAL AND COMPRESSIVE STRENGTH 77 K	RETAIN SUFFICIENT STRENGTH.

Table 1 (cont.)

MATERIAL	RADIATION	TYPE OF TESTING	COMMENTS
KAPTON (POLYIMIDE)	10^{10} RAD GAMMA 305°K	TENSILE STRENGTH RT	DECREASE ON ≈ 10%
VESPEL (POLYIMIED)	4×10^{9} RAD	TENSILE STRENGTH	NO SIGNIFICANT CHANGE
	10^{11} RAD 448°K		EMBRITTLED BUT STILL FORM STABLE
VESPEL SP1	5×10^{8} RAD 77°K	TENSILE STRENGTH AND MODULUS 77°K	SLIGHTLY INCREASE
AROMATIC EPOXY RESINS			SLIGHTLY DECREASE
EPOXY RESINS, FIBER-GLASS EPOXIES AND VESPEL	1.1×10^{9} RAD 3.0×10^{17} NVT 8.0×10^{8}R GAMMA 5 K	COMPRESSION STRENGTH AT 77°K STRESS-STRAIN CURVES AT 4 K	VESPEL AND FIBER-GLASS EPOXY SHOW HIGHER STRENGTH ANG NO CHANGE IN STRESS-STRAIN CURVES AFTER IRRADIATION.
FIBER-GLASS POLYIMIDE	10^{10} RAD NUCLEAR REACTOR	FLEXURAL STRENGTH RT	NO DETERIORATION REPORTED.
G-10	3.8×10^{11} RAD GAMMA 10^{20} N/CM^2	COMPRESSION STRENGTH RT STRESS LEVEL 345 MPA 200,000 CYCLE	

Table 2

Results of INEL Compression
Fatigue Tests of Irradiated Insulators

For all Specimens D = 11.1 mm
(See Figure 1 for test arrangement)

Material	Thickness (mm)	Temperature	Max. Applied Stress (MPa)	Number of Cycles
G-7	0.30	RT	207	10,000 F *
G-11	4.00	RT	207	10,000 F
G-10	0.50	RT	207	200,000 S
			241	200,000 S
			276	21,900 F
			310	3,570 F
			345	460 F
		77 K	207	20,000 S
			241	40,000 S
			276	36,000 S
			310	30,000 S
			345	30,000 S

* Paired disks broke, singles survived

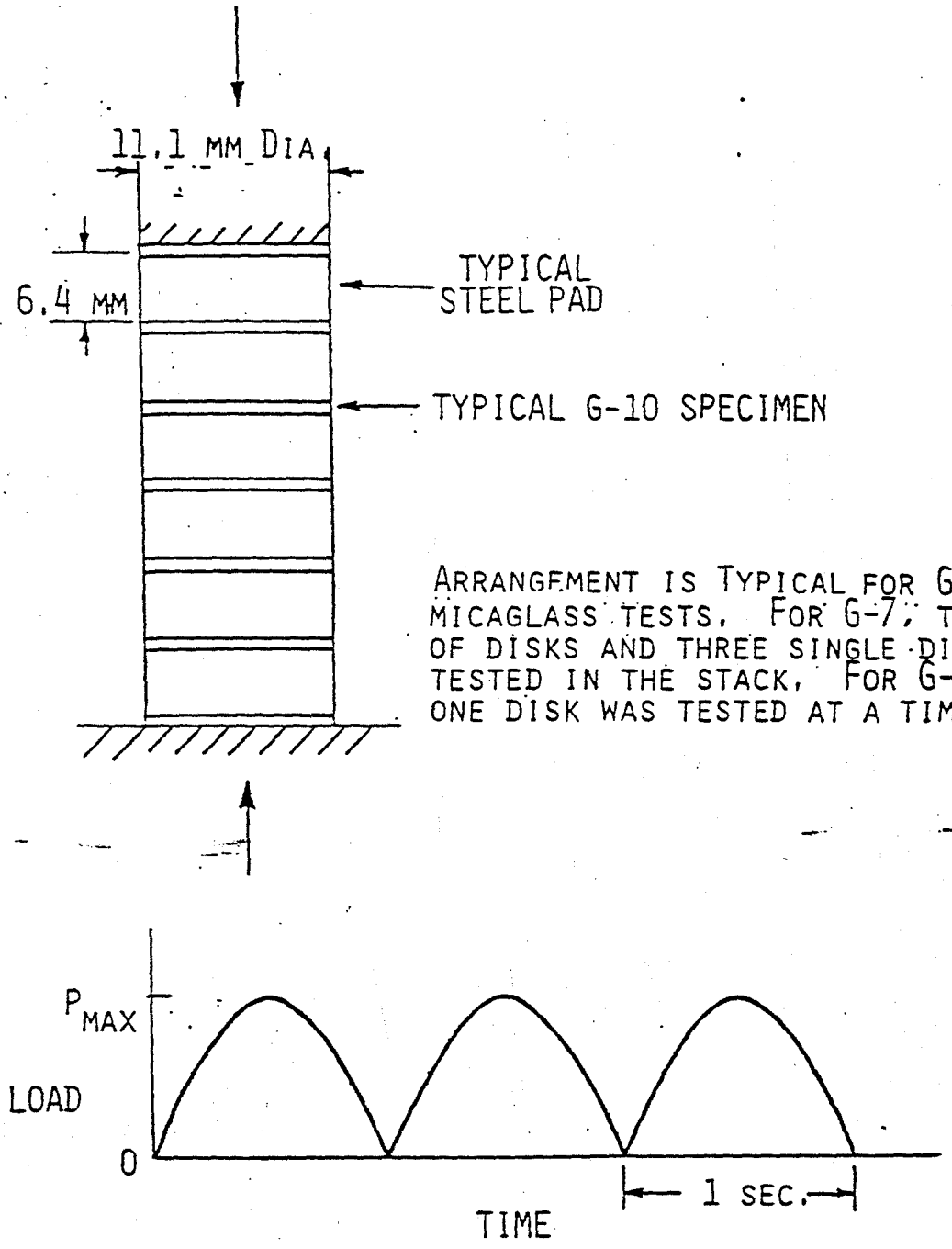

FIGURE 1 TEST FIXTURE SCHEMATIC AND LOADING CYCLE

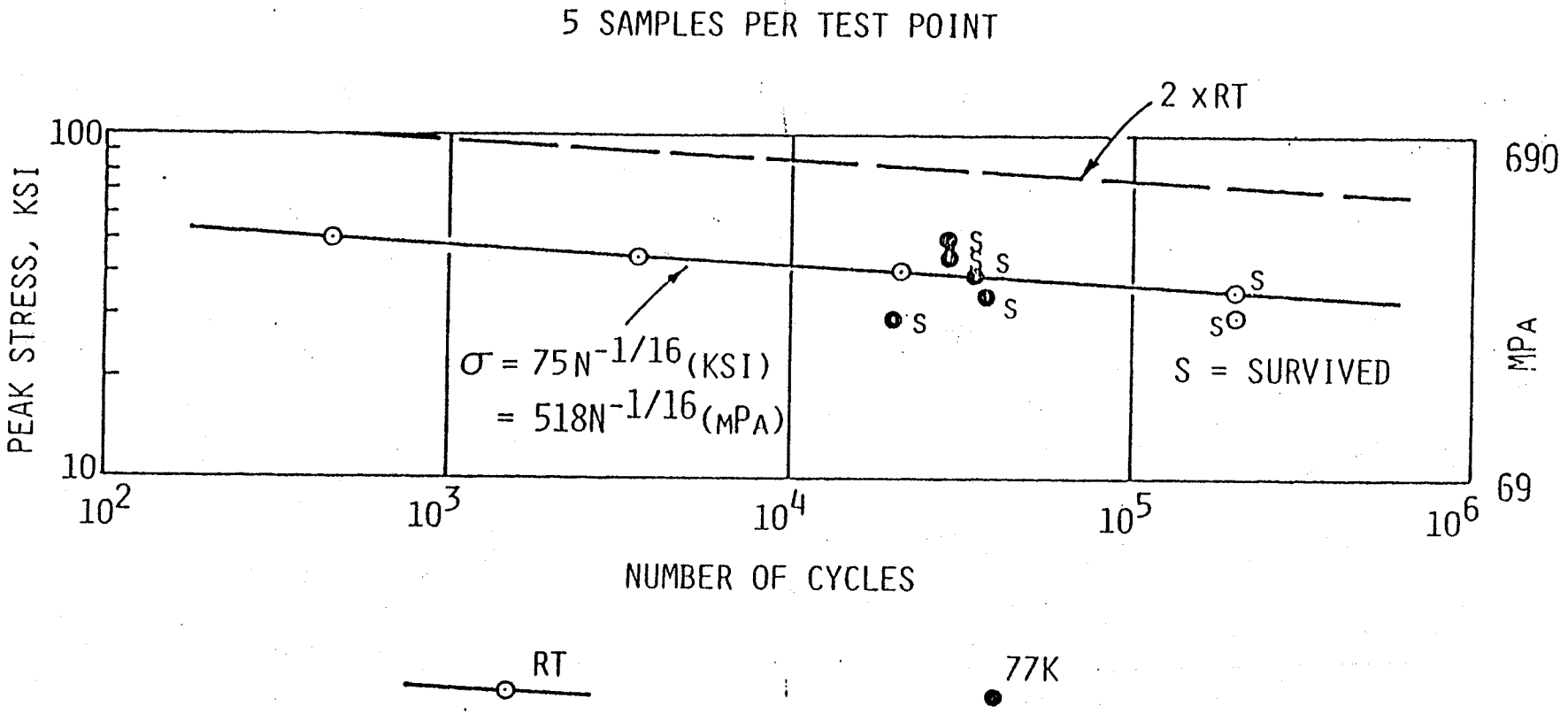

FIGURE 2 IRRADIATED G-10 COMPRESSION FATIGUE TEST DATA

5.3 Cryogenic Normal Coils

The size of the bundle described in Section 3.1 is small. It might be possible to operate the normal copper coils at cryogenic temperature to reduce the power consumption. This preliminary analysis will determine the optimum operating temperature.

The resistivity of copper and aluminum increases with temperature. Minimizing resistive dissipation losses in magnet coils thus favors operating at the lowest possible temperature. However, maintaining the coils at low temperatures requires transporting heat from the operating temperature and rejecting it, ultimately, at ambient conditions. The energy required for this is at least as much as an ideal refrigerator consumes operating between the two heat sinks, and decreases as 1/T as the operating temperature increases. Combining resistive losses and refrigeration power, there is an overall minimum power operating point.

The resistive power per unit volume is $j^2\rho$, where j is the current density (A/m^2) and ρ is the resistivity (Ω-m). The refrigeration power per unit volume is $(j^2\rho)\left((T_o/T)-1\right)/\eta$, where $j^2\rho$ is the heat transferred from the operating temperature T to atmospheric conditions at T_o, with mechanical efficiency η. The <u>total</u> power per unit volume is

$$P_{total} = j^2\rho + j^2\rho\left(\frac{T_o}{T} - 1\right)\frac{1}{\eta} \qquad (1)$$

Since j is fixed by the magnetic field strength requirement, the task is to minimize the figure of merit

$$M = \rho\left[1 + \frac{1}{\eta}\left(\frac{T_o}{T} - 1\right)\right] \qquad (2)$$

For present purposes, take T_o = 293 K (20 C) and η = 0.3. In fact, η has a small temperature dependence given as (G. C. Haselden, "Cryogenic Fundamentals", Academic Press, New York, 1971),

$\eta \sim$	0.1 to 0.3	for T $\sim$ 4.5 K
	0.2 to 0.4	20. K
	0.4 to 0.5	80. K

Figures 1 and 2 summarize copper and aluminum resistivity data for 0 < T < 100 K. Resistivity is strongly dependent upon factors such as impurity and defect content. This and experimental error account for the scatter in the data.

Figure 3 shows the figure of merit of Eq. 2, plotted as a function of temperature, using the estimated curves of the resistivity temperature data of Figs. 1 and 2. Note that the exact minimum is sensitive to the estimated shape of the resistivity curves, themselves in some doubt. Nonetheless, copper and aluminum are seen to be comparable, with M $\sim$ 1 $\mu\Omega$-cm at T $\sim$ 25 K. The minimum point compares reasonably with that in Fig. 4 for high purity aluminum extracted from the NUWMAK reactor study report (University of Wisconsin). Their refrigeration factor F is presumably similar to the present figure of merit M.

FIGURE 1:
COPPER RESISTIVITY

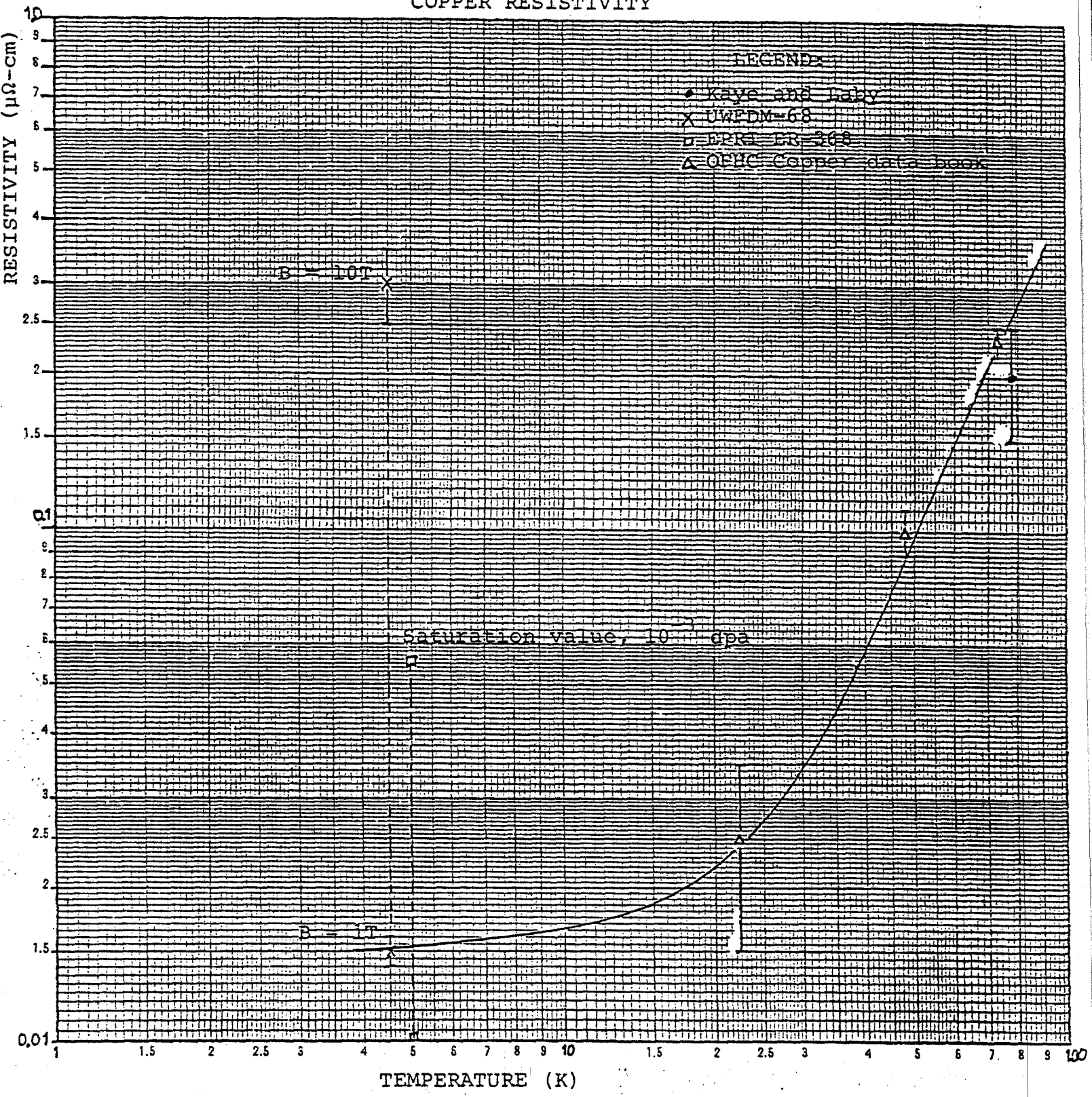

FIGURE 2:
ALUMINUM RESISTIVITY

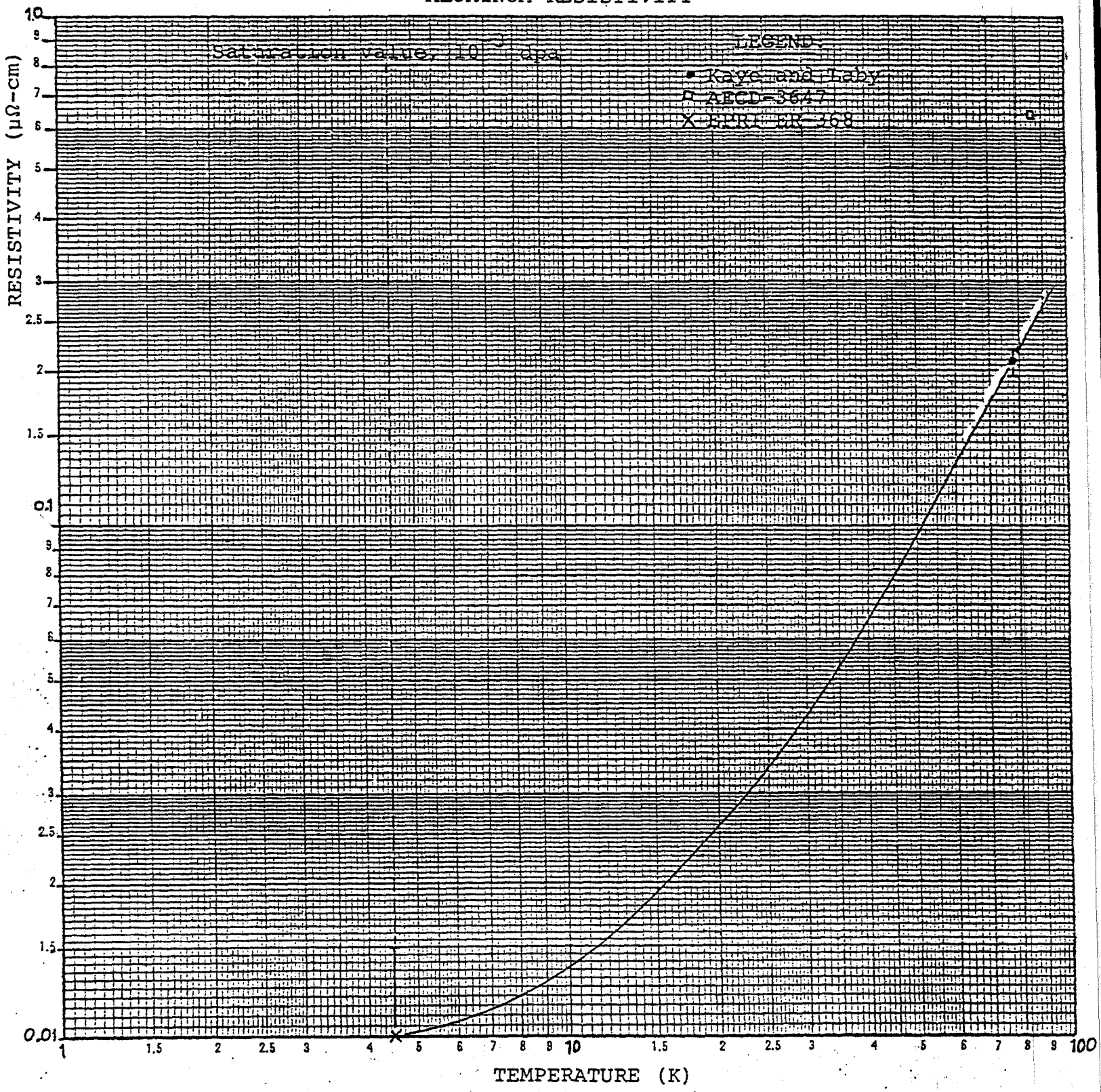

COPPER

FIGURE 3a

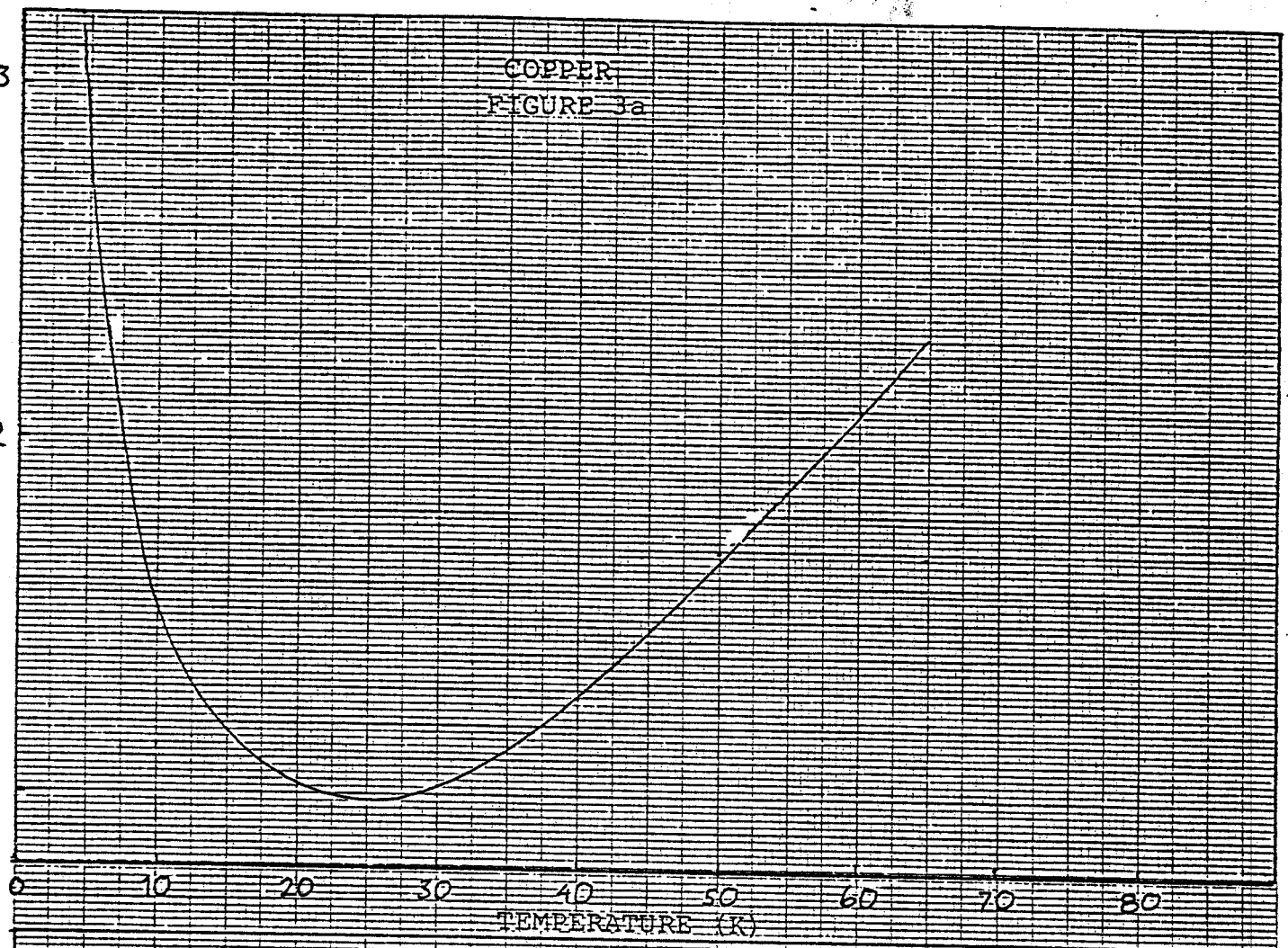

ALUMINUM

FIGURE 3b

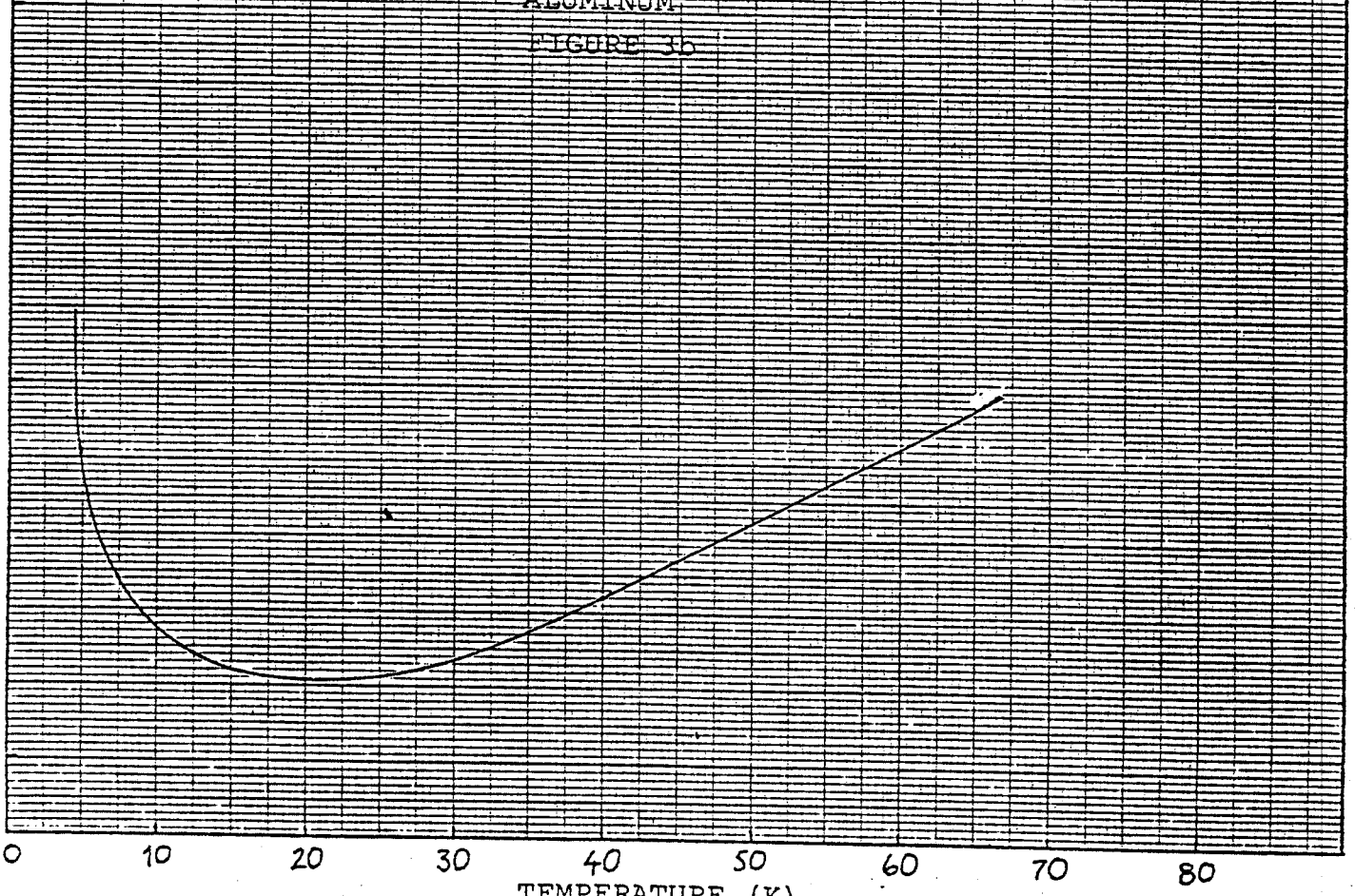

PRODUCT OF THE RESISTIVITY OF 430 RRR HIGH PURITY ALUMINUM AND THE REFRIGERATION FACTOR AS A FUNCTION OF TEMPERATURE.

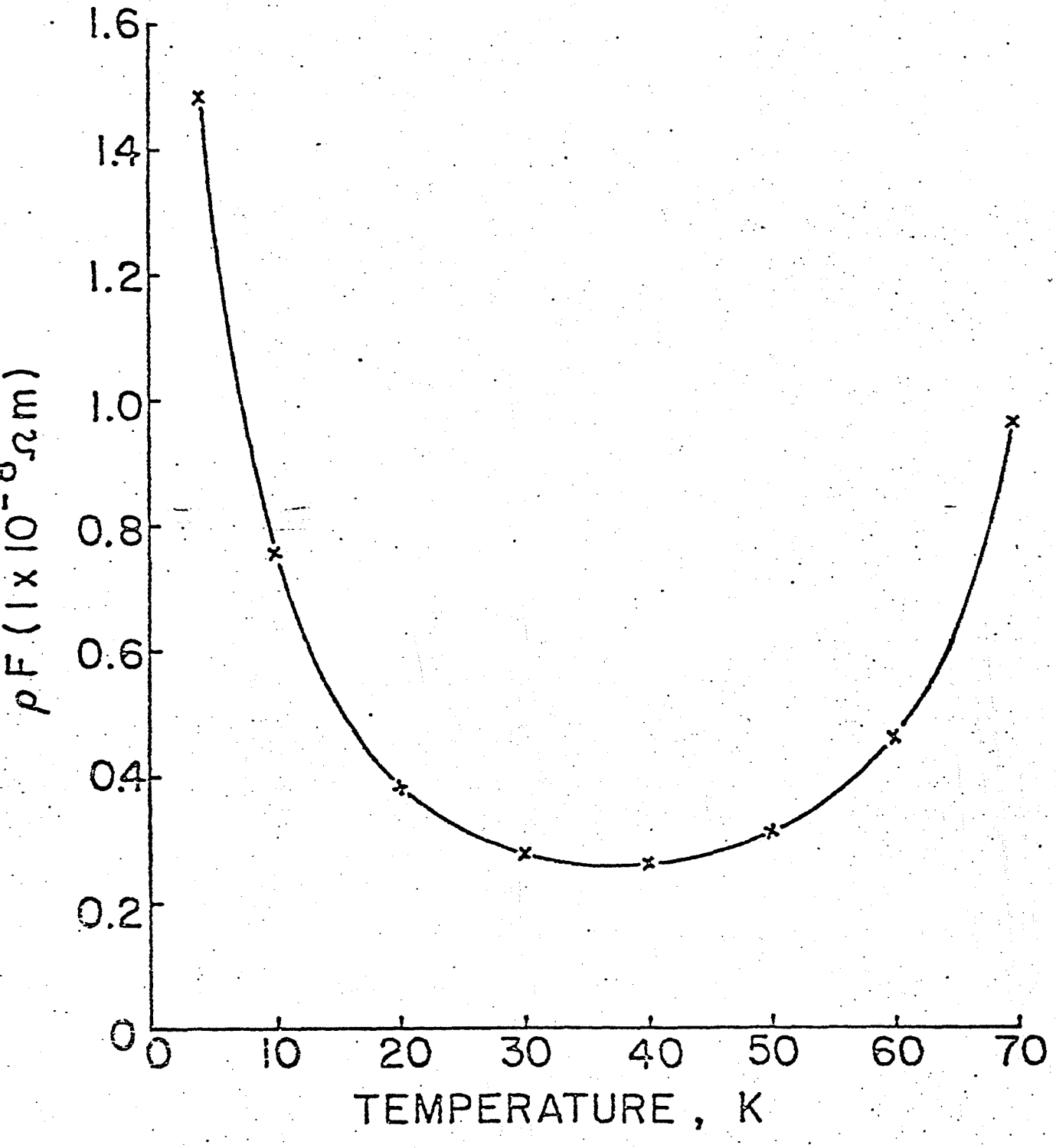

FIGURE 4: From NUWMAK study, Fig. VI-D-4.

REFERENCES:

1. G.C.Haselden, "Cryogenic Fundamentals", Academic Press, New York, 1971.

2. G.Kaye and T.Loby, "Tables of Physical and Chemical Constants", 14th ed, Longman Co., 1973, p.124.

3. UWFDM-68, Vol.1, "UWMAK-I, Tokamak Reactor Design", p.VII-A-21.

4. EPRI ER-368, Vol.II, "UWMAK-III, Noncircular Tokamak Power Reactor Design", p. 9-149.

5. OFHC Copper data book, p.12.

6. The Reactor Handbook, Vol.3 Materials, Section 1 General Properties, USAEC, March 1955, AECD-3647.

7. NUWMAK Reactor, University of Wisconsin

6.0 Bundle Divertors for ISX-B and ISX-C

6.1 The Design and Fabrication of ISX-B Bundle Divertor

Due to the experimental success of DITE bundle divertor [1] and the success of designing such a divertor for reactor, there is a vast interest in bundle divertor. Many improvement concepts have been proposed in the past year.[2,3] To understand the physics in the higher β regime the ISX-B bundle dibertor was proposed and to be built at ORNL. A very detailed design has been done by the Culham Laboratory.[4] A brief design study has been carried out by Westinghouse.[5] These two studies form the basis for the present final design at MIT. The conventional two coil configuration was chosen because of the existing tight space of ISX-B. The final configuration was chosen based on the considerations of lower magnetic field ripple, larger flux expansion and better engineering design without paying the penalty for additional complexity.

The plane view of the ISX-B TF coil and bundle divertor coil layout is shown in Figure 1. The key parameters of ISX-B are R_o = 92 cm, a = 20 cm and the scrape-off layer thickness is 7 cm. The designed value of B_o is 1.8 T. The selection of this final magnetic configuration is described below.

The original DITE divertor is two solenoid system. The current density is 25 kA/cm^2/Tesla. Consequently the magnetic stress concentration is very higher. The new Culham design uses large radius to reduce the current requirement thus the current density has been reduced to 7.6 kA/cm^2/Tesla. However, the ripple is still above 2%. The use of toroidal ripple has also been proposed by ORNL. This is not

desirable because the periodical toroidal ripple is found to have a deleterious effect on the confinement of energetic particles. A pair of vertical axiliary coils to reduce the field intensity to be nulled by the divertor was suggested in the Westinghouse study. This will add the undesirable complexity. The method used here is to spread out the conconductor to reduce the current density. This can be accomplished by increasing the radius of each turn while being moved away from the null point. Each divertor coil is now a sectional conical shape instead of solenoid. A current density of 7.6 kA/cm^2/Tesla has also been achieved. The ripple is lowest among all the methods discussed. It is generally conceded that the optimal divertor angle is 45° when adequate space is available. Because of the very limited space in ISX-B a 30° angle was chosen. The consideration of such a choice is given below.

In search for the flux pattern given in Figure 1, a series of configurations for various coil sizes and angles have been computed. Three typical flux patterns are presented in Figure 2. The corresponding divertor angles are 40°, 35°, and 30°. The radius of the coils is constrained by placing the outside edge of the coils along the center lines through the TF coils while the front corner closest to the first wall is fixed at R = 122 cm. For the angle larger than 40° or larger radius the fluxes will run into structure. This figure demonstrates that a very thick scrape-off layer in the divertor can be produced as long as space is available. The fluxes in figures 2a and b are still interfering with the structures. Figure 2c is the best choice. For

angles less than 30° the expansion is too small and the current requirement and ripple will go up.

As has been pointed out in the culham design[4] the poloidal field will cause the diverted flux bundle drifted upward and partially intercepted by the coil structure. To study the plasma stability in the divertor we would like to correct this deviation. The resultant field lines were computed by taking into account of poloidal field coil and plasma current. The poloidal field coil arrangement and filamentary representation of the plasma current are shown in Figure 3. The bundle divertor is interfering with the neighboring EF coils. they are bent locally to bypass the divertor as shown by the side view. The typical field lines projected on the midplane, on the vertical plane on the divertor center line and on the R-θ plane are shown in Figure 4. To see whether they will interfere with the structure the points of intersection of the field lines with the cross sectional planes at five locations as shown in Figure 4 are plotted in Figure 5. The circles in Figure 5 represent the inner structures of the divertor assembly. None of the points actually falls on the structure. More detailed study of the scrape-off layers in the tokamak and divertor are in progress. The divertor assembly structure and assembly method are shown by Figure 6. The divertor coils are inserted into the housing and sealed by a cover from the back side.

The force and torque are shown by Figure 7. The torque is contained by the divertor housing of a monolithic structure milled according to the designed contour by numerical control. The whole assembly is tied to the two neighboring TF coils so that translational forces are balanced. The divertor assembly is shown by Figure 8. The finished coil winding and housing are shown by Figure 9. The conductor configuration and cooling are given in Table 1 and Figure 10. A detailed three dimensional stress analysis has been carried out. A partial stress analysis model is shown by Figure 10. The stress highest level is well within the design limit and there is no dangerous stress concentration. The estimated thermal growths during the pulse are given in Table 2. The construction of divertor house and winding has been completed and in the process of being tested.

6.2 Conceptual Design of ISX-C Bundle Divertor

ORNL has also contracted MIT to carry a conceptual design of the bundle divertor for ISX-C to be built at ORNL. The advanced divertor system developed at MIT (Section 3.0) is considered. The design study is under way.

References

1. P. E. Stott, C. M. Wilson, A. Gibson, Nuclear Fusion 475 (1977) and references cited.
2. J. Sheffield, R. A. Dory, ORNL-TM6330 (1978).
3. T. F. Yang, et al, WFPS-TME-104 (1978).
4. K. M. Plummer, et al, Culham Report, CLM/02/1 (1979).
5. T. F. Yang, WFPS-TME-075 (1978).

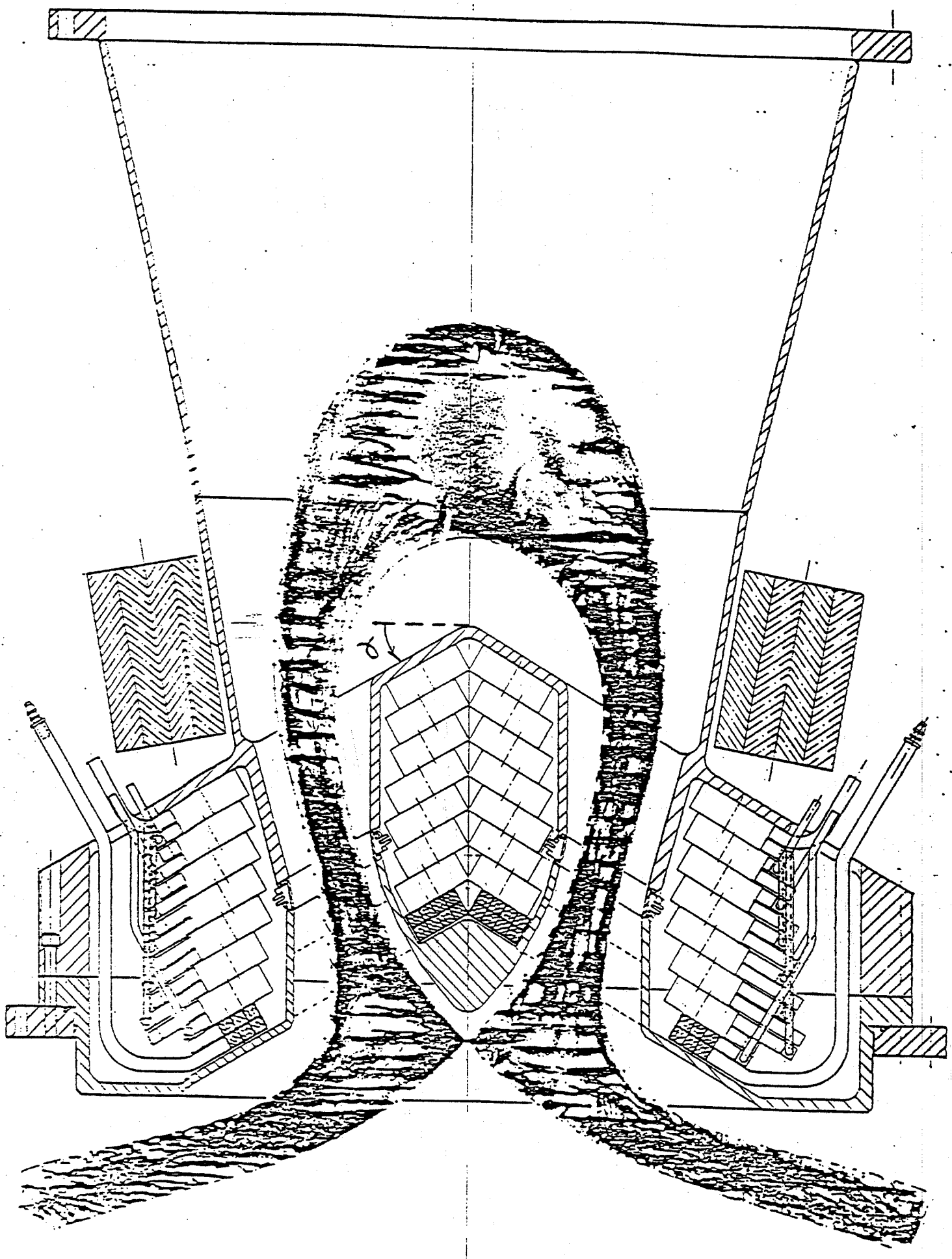

Figure 1. ISX-B Bundle divertor projected on midplane divertor angle $\alpha = 30°$.

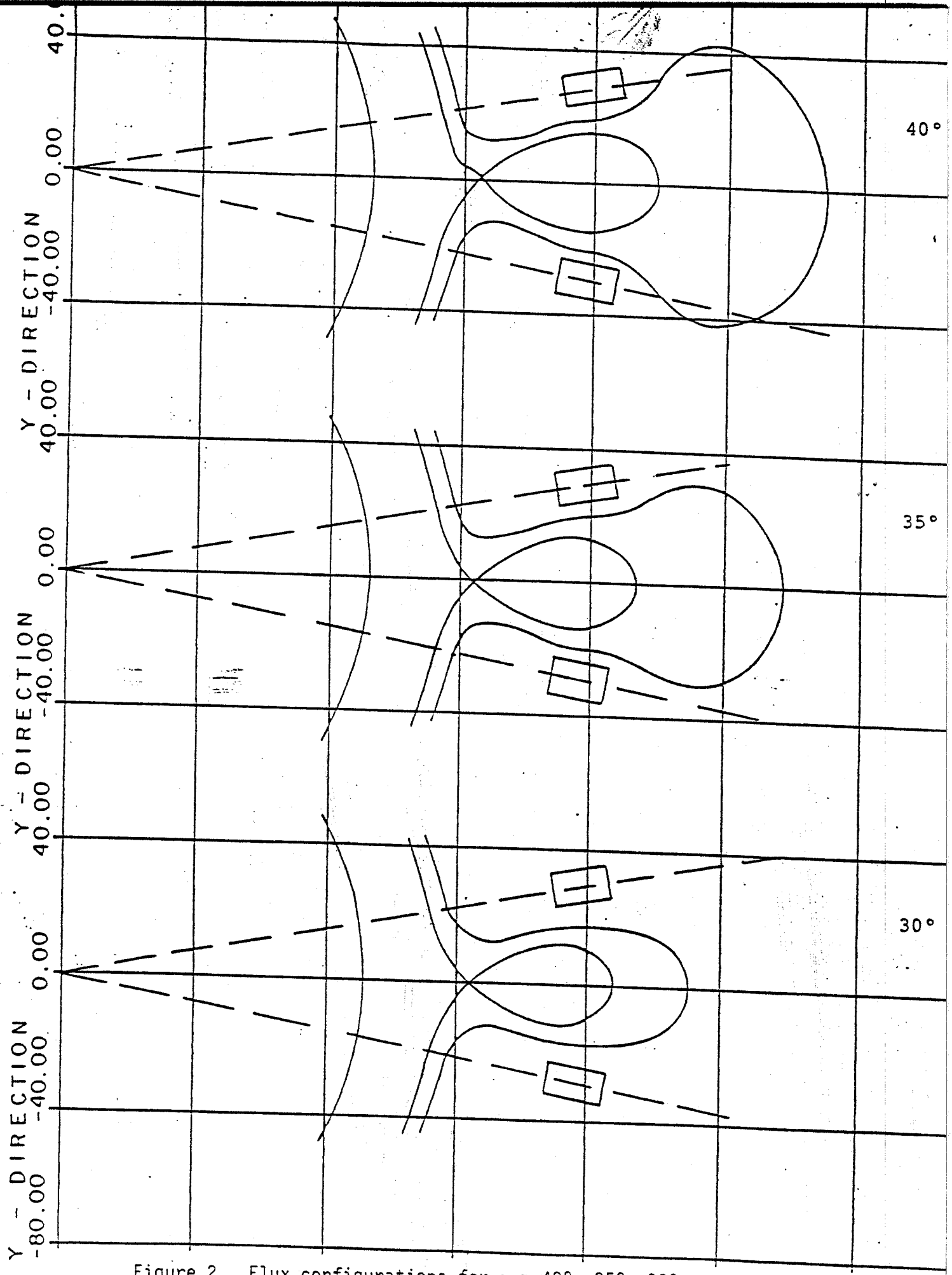

Figure 2. Flux configurations for α = 40°, 35°, 30° on midplane.

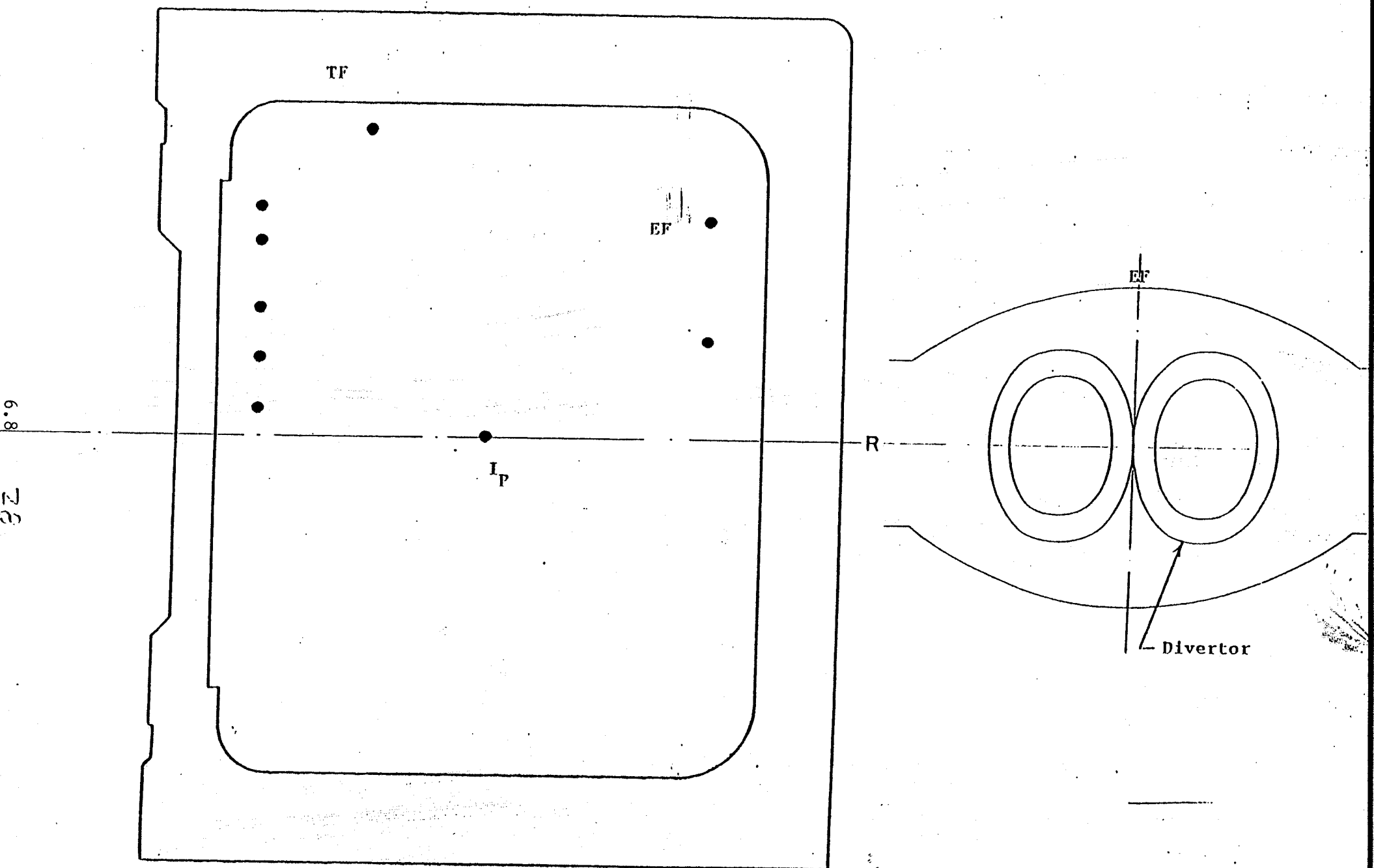

Figure 3. Model of the Equilibrium Field coils (cross-sectional view)and the section of the equilibrium coils around divertor (side view) for computation.

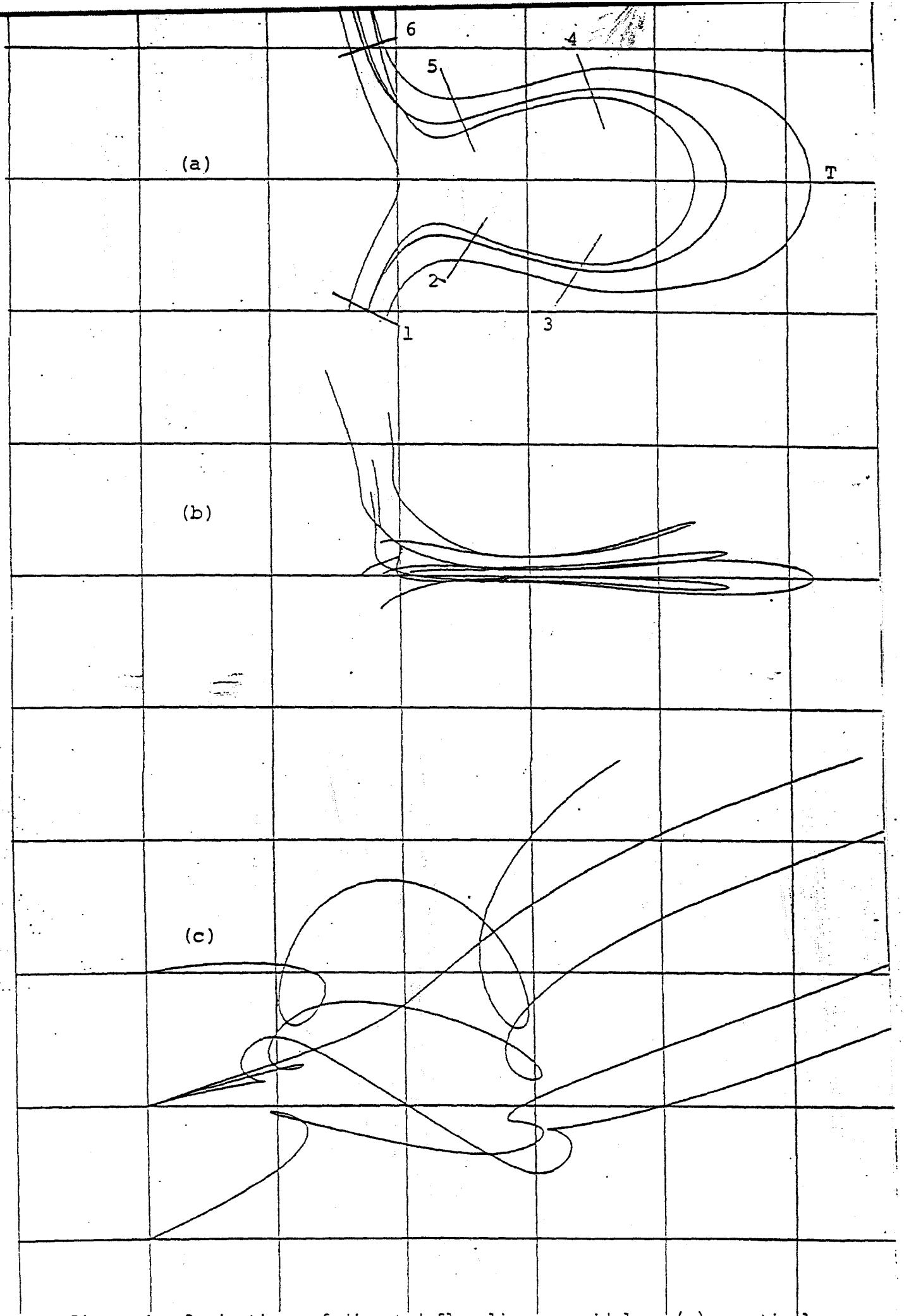

Figure 4. Projections of diverted flux lines on midplane (a), vertical

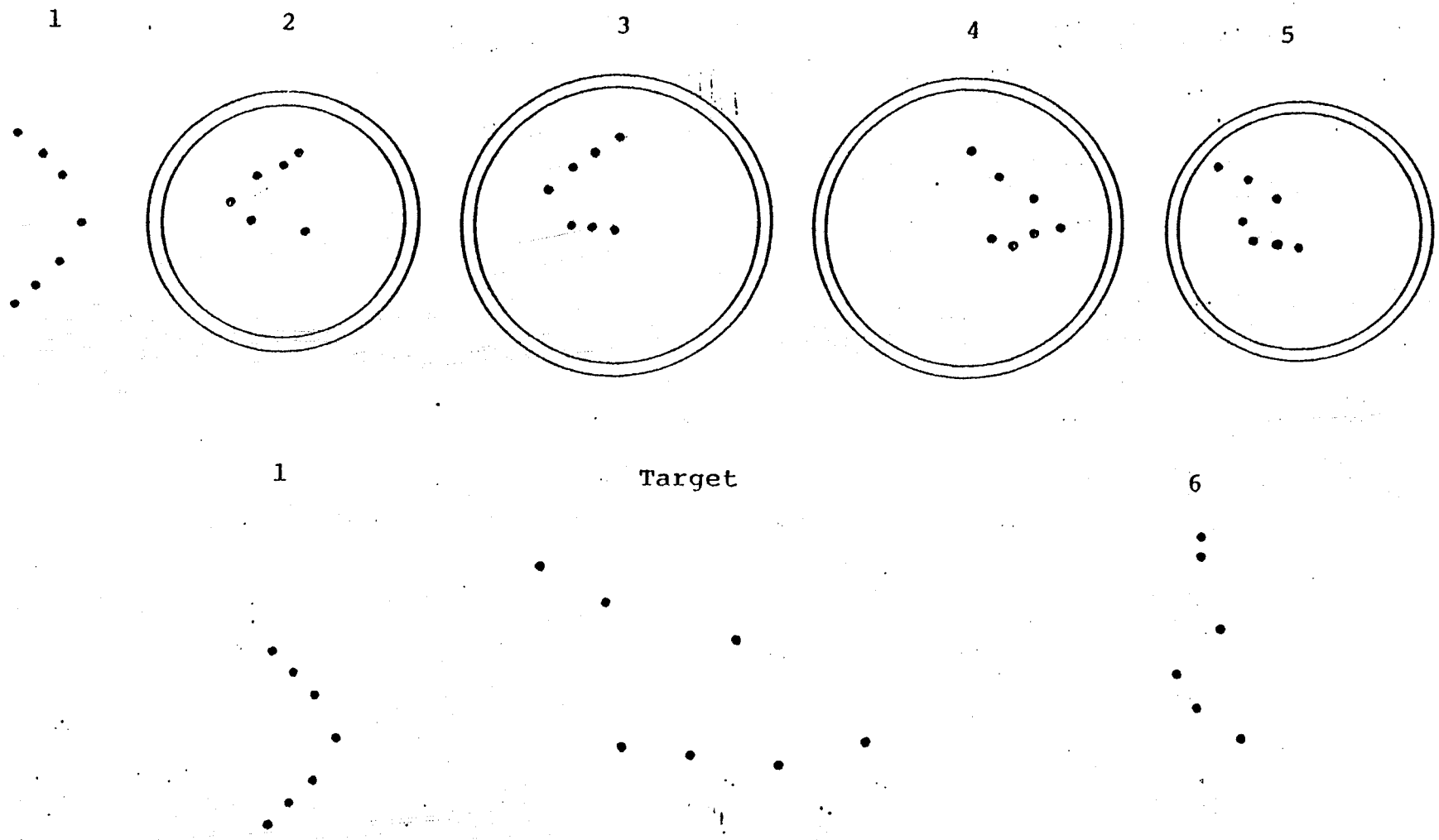

Figure 5. Intersections of the flux lines with cross-sectional planes 1 through 6 of Figure 4a.

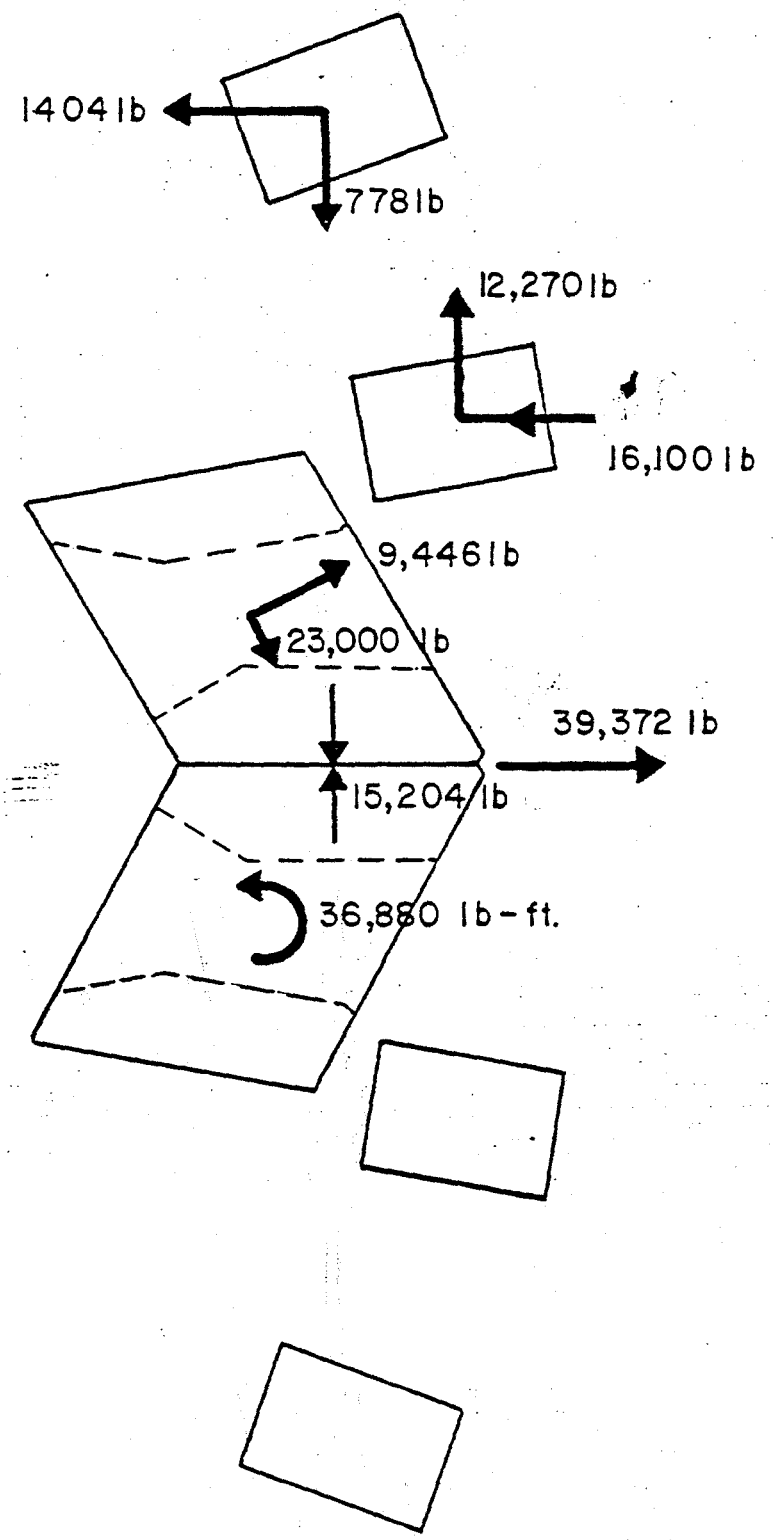
14041b
7781b
12,2701b
16,1001b
9,4461b
23,000 lb
39,372 lb
15,204 lb
36,880 lb-ft.

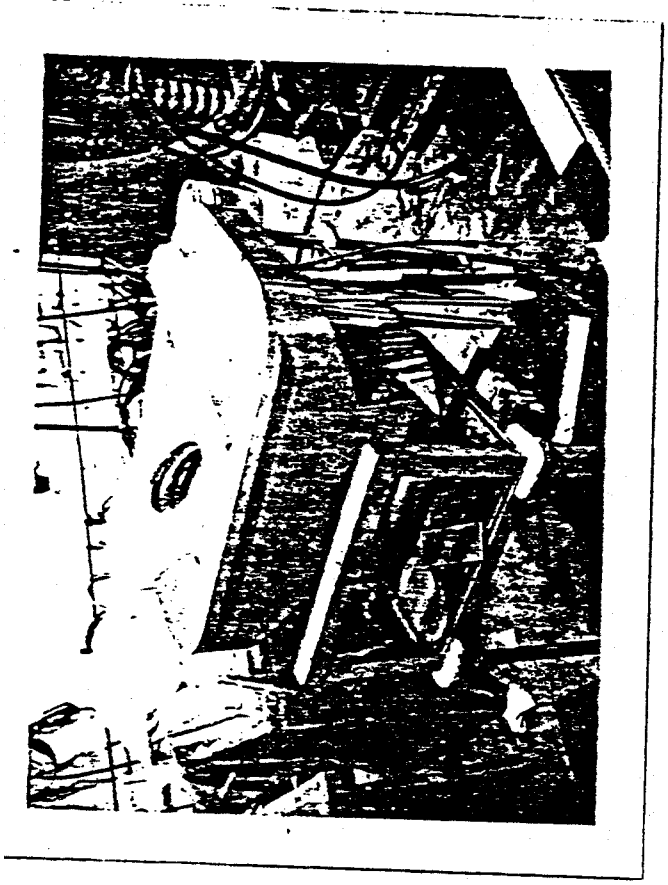

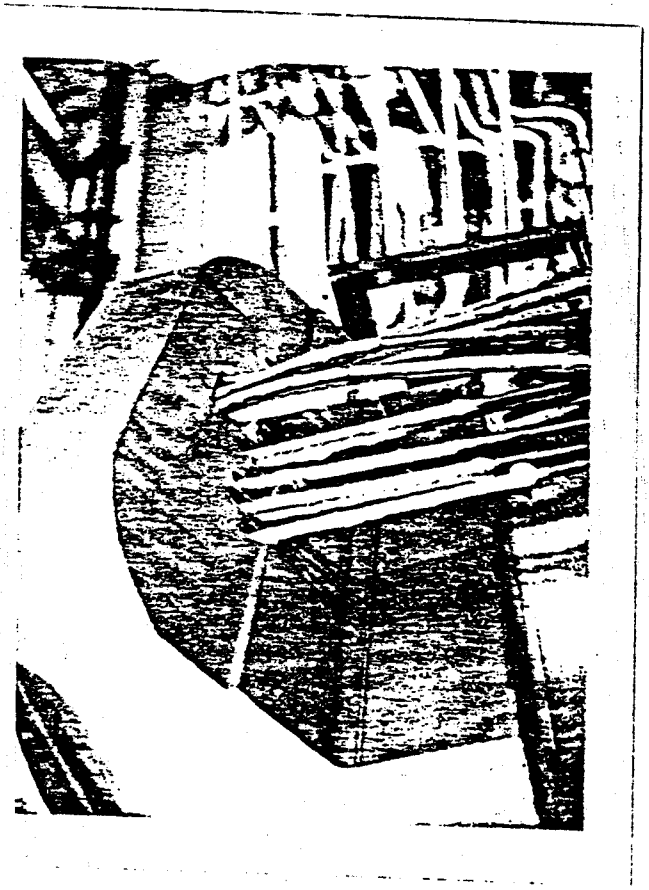

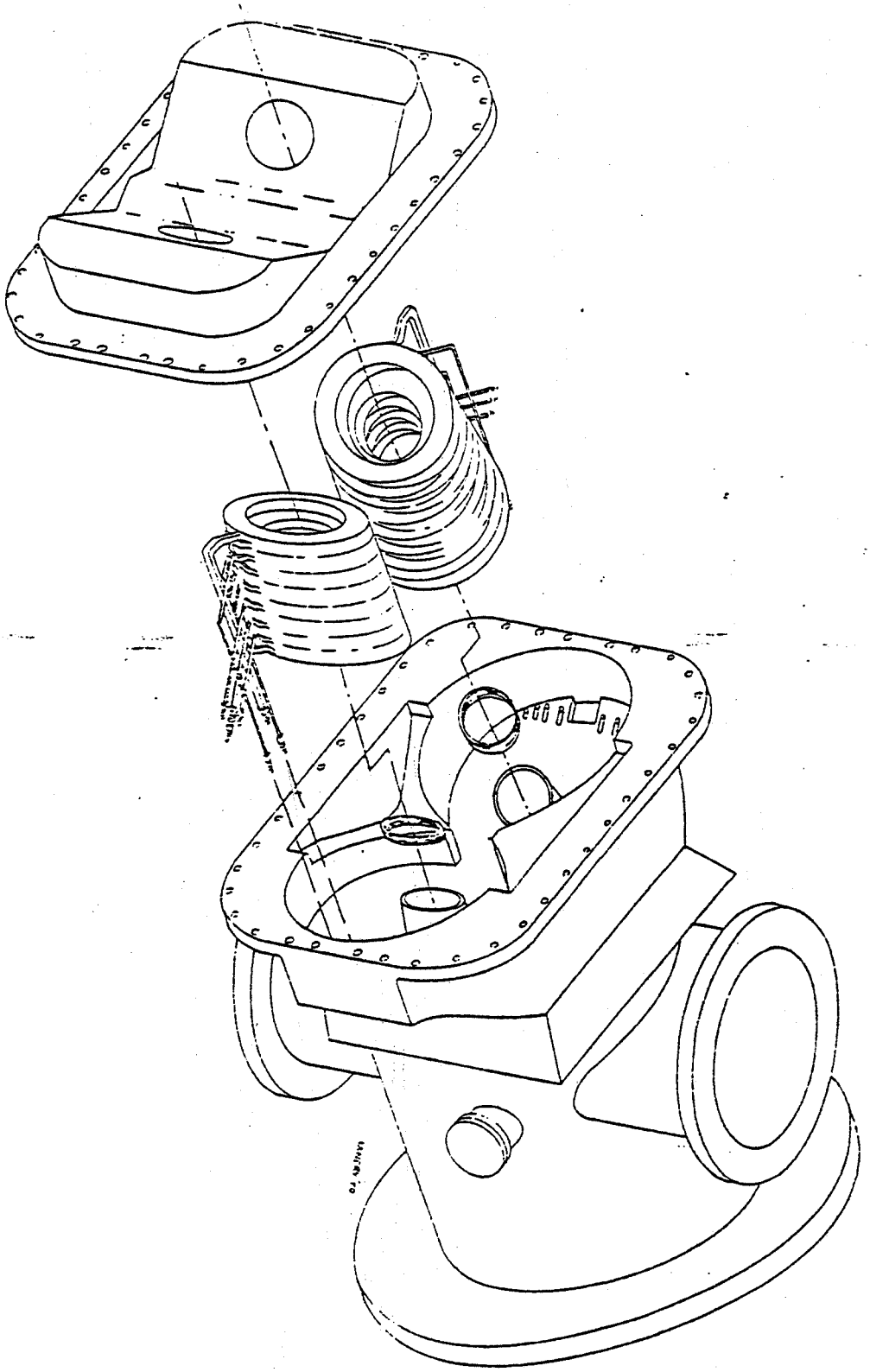

COIL COOLING:

I. CONDUCTOR: 1.1 CM SQ. X 0.4 CM ROUND HOLE.
DOUBLE LAYER PANCAKES
LENGTHS: 381 CM (12.5 FT) TO
751 CM (24.6 FT)

II. WATER FLOW:
16 PANCAKES = 26 GPM AT ΔP = 150 PSI

III. COIL CONDITIONS
- COIL ADIABATICALLY HEATED 27° C.
- ENERGY TO BE REMOVED ~1070 B.T.U.
- TIME AVAILABLE FOR COOLING COILS ~5 MIN.

IV. PANCAKE INTERLAYER SHEAR STRESSES
- IF $(T_{OUT} - T_{IN}) = 24^{\circ}$ C:
$\tau \approx$ 1000 TO 5800 PSI

Conductor:

Supplier: Kabelmetal (from Eltek)

Type: SE-Cu Drawn and Annealed Deoxidized High Conductivity Cu

Conductivity: 100% IACS

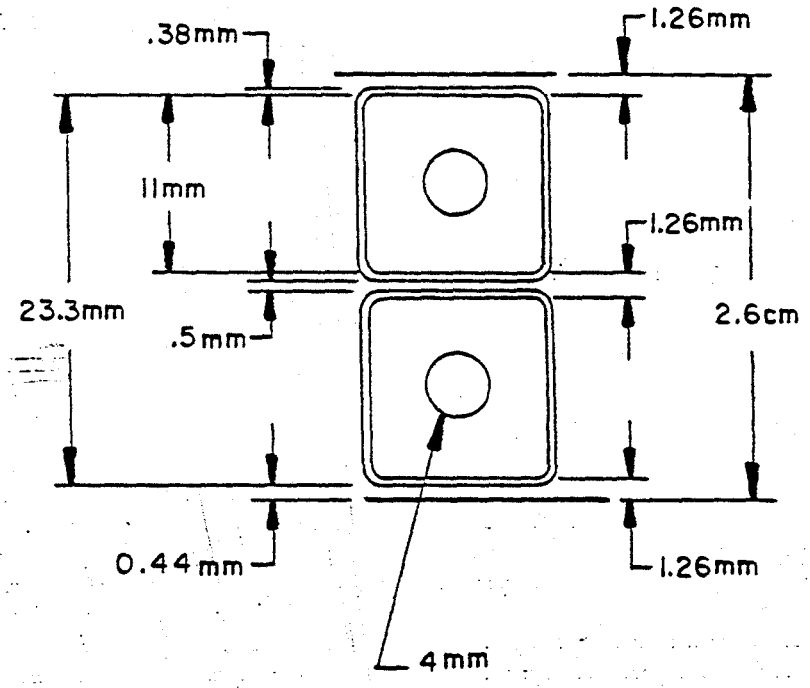

TWO CONDUCTOR STACK

scale- 2:1

Isometric: Layer 8
Case, Coil, Epoxy

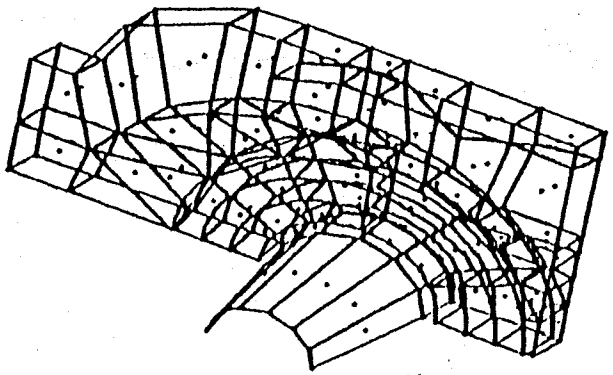

ELEMENTS TO BE DRAWN = G100-G900

THERMAL STRESSES

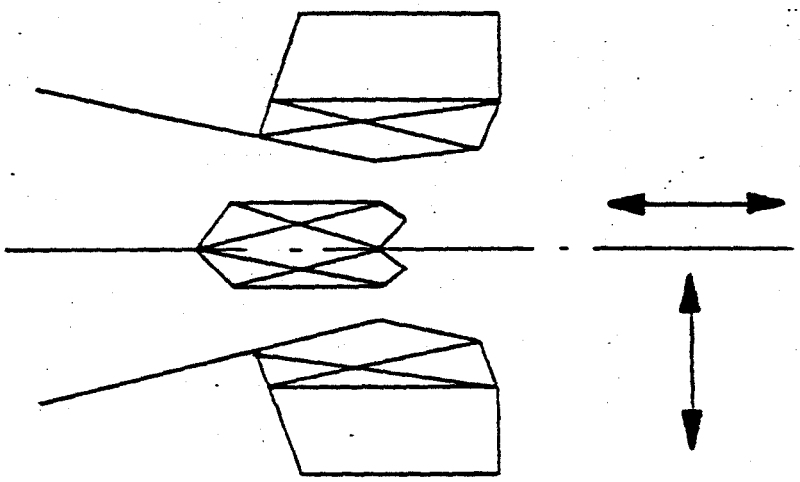

I. AXIAL GROWTH

4 mils in 8 inches accommodated by shimmed gap

II. RADIAL GROWTH

6 mils in 12 inches

- Accommodated by compression of coil; by compression of potting compound; by hoop tension of structure.
- Estimated adiabatic thermal local pressure varies from 200 to 500 psi.
- Hoop stress in structure – 24,000 psi.

7.0 Simulation Source

7.1 Plasma Source Using Random Electrostatic Deceleration of Intense Ion Beams

This section studied the possibility of using intense ion beams as a plasma source for a divertor test facility. Based on, for example, 10^{24}/s 1 keV H^+ ions passing through 100 m^2 divertor throat, the plasma flux is about 0.2 A/cm^2 and the ion heat load is 0.2 kW/cm^2. Presently developed duoPIGatron beam sources such as the PLT injectors can reliably produce about 0.2 A/cm^2 10 to 45 keV H^+ ion beams, over 300 cm^2 and 0.5 s.

The problem is to reduce the ion energy to a Maxwellian spectrum around 1 to 2 keV. Specifically, firing the beam through a gas cell with a retarding potential was considered.

Method

A Monte Carlo computer approach was used to determine the optimal ion beam and gas cell parameters. Incident monoenergetic protons were tracked through a constant-density background gas. Over the range 1 to 30 keV explored, the dominant interactions are charge exchange neutralization and ionization. In H_2 and most other gases, the neutralization interaction is dominant. However in helium, the two cross-sections are comparable, although neutralization is still much more likely.

The problem is essentially 1-D since the incident ions have little angular divergence and since the scattering associated with charge exchange is small - calculations indicated less than a few percent error in direction and energy with this assumption.

Incident ions are tracked through a 55x55 matrix, one axis representing energy and the other for axial position. For the calculations presented, the axial step size was always less than 10% of the interaction mean free path (mfp). In proceeding from

step to step, the probability of interaction was calculated and compared with a random number. This determined whether the particle became neutralized or ionized (depending upon its initial charge state). During charged motion, the retarding potential was applied to reduce the particle's energy. Even if an interaction occured, an average amount of retardation was computed to account for the fraction of the axial step spent in the charged state. When this amount accumulated to over one step size, the particle was transferred to the next lower energy group.

Below 1 keV, the interaction mfp becomes long compared to gas cell dimensions. In the program, these particles were not explicitly followed. However, the number of these "lost" particles was recorded since, for a Maxwellian ion distribution around 1 to 2 keV, about 20% of the ions should be below 1 keV.

For retarding potentials larger than the incident ion energy, some particles may be accelerated back. These particles were also not tracked. This was a small effect in this study since only retarding potentials less than or slightly greater than the incident ion energy were considered.

The particular parameters investigated were incident ion energy (10 - 30 keV), neutral gas (H_2 and He) and density (0.6 to 4.0 $x10^{14}$ $/cm^3$) and retarding potential (typically within 1 keV of incident ion energy). Since changing the cell length was equivalent to changing gas density - they both determine the number of interactions - a 54 cm long gas cell was arbitrarily chosen.

Results

The final result was charged and neutral particle energy distributions at the end of the gas cell, and density distributions along the gas cell. Typically, about 25,000 particles were followed for each case. Table 1 summarizes the results, and some ion and neutral energy distributions are shown in Figures 1 to 6.

TABLE 1: ION EXIT ENERGY DISTRIBUTION

Incident ion energy (keV)	Background gas	Gas density ($\times 10^{14}$ /cm^3)	Retarding potential (keV)	Ion peak energy (keV)	Nbr particles at peak (x100)	Distribution shape
20.	H_2	0.6	19.	1.	20.	Peaked
		1.0		1. 14.	3. 1.	Double peaked
		3.0		15.	2.	Maxwellian
		7.0		16.	4.	Maxwellian
10.		1.0	9.	1. 8.	2.5 1.	Double peaked
		2.0		9.	1.4	Maxwellian
		3.0		9.	1.6	Maxwellian
20.	He	3.0	19.	1.	50.	Peaked
		7.0		1. 10.	3.4 4.0	Double peaked
		20.		12.	8.	Maxwellian
10.		10.	9.	1.	1.6	Peaked
		20.		3.5	8.	Maxwellian
		30.		4.	12.	Maxwellian
		40.		4.5	11.	Maxwellian
		30.	10.	3.	12.	Maxwellian
			11.	2.	12.	Maxwellian
			11.5	1.7	12.	Maxwellian (10% below 1 keV)

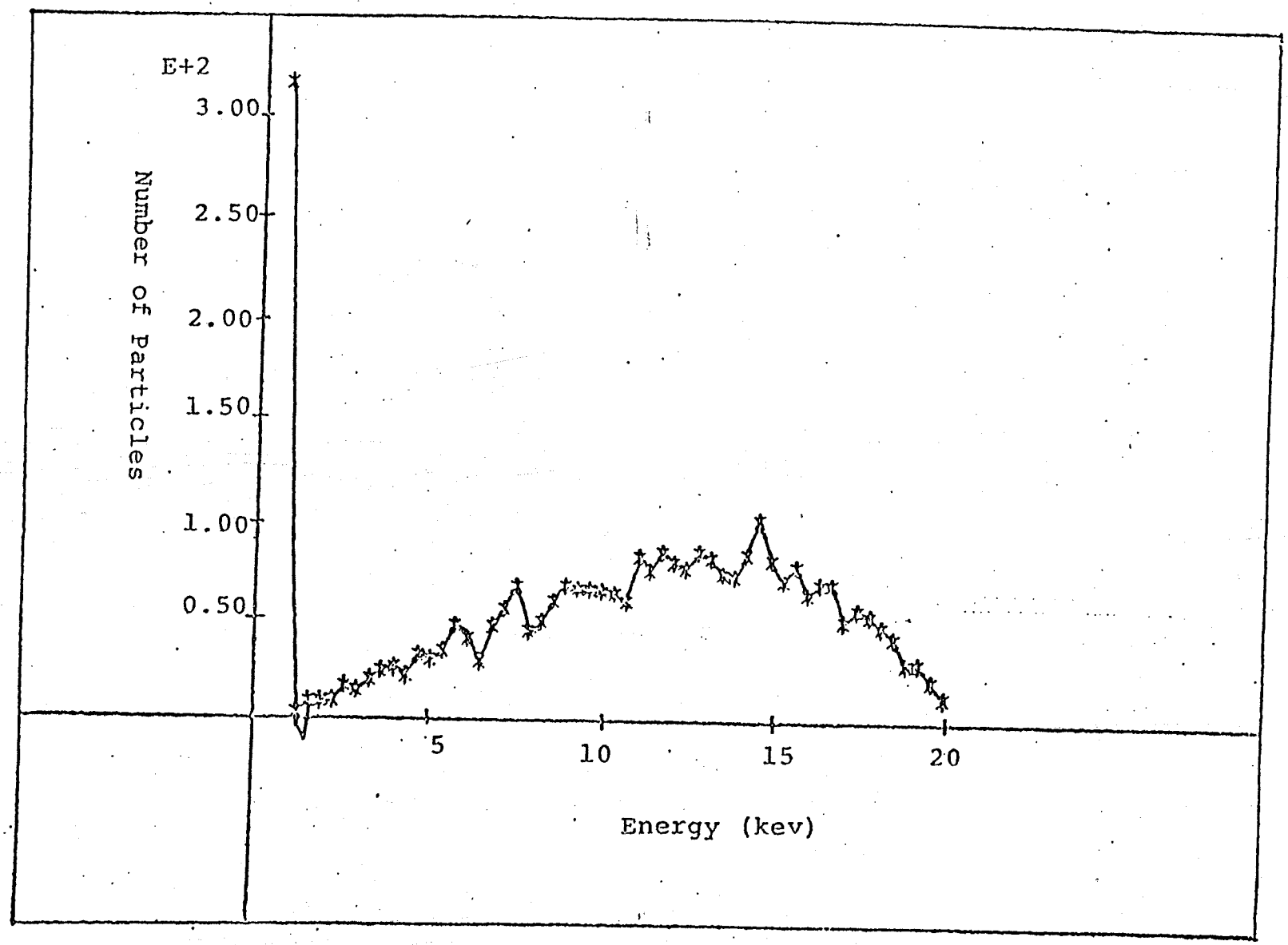

Figure 1 . Ion Energy Distribution for 20 Kev Ion Beam Incident on a 10^{14} cm^{-3} Hydrogen Gas Density and Influenced by a 19 Kev Potential.

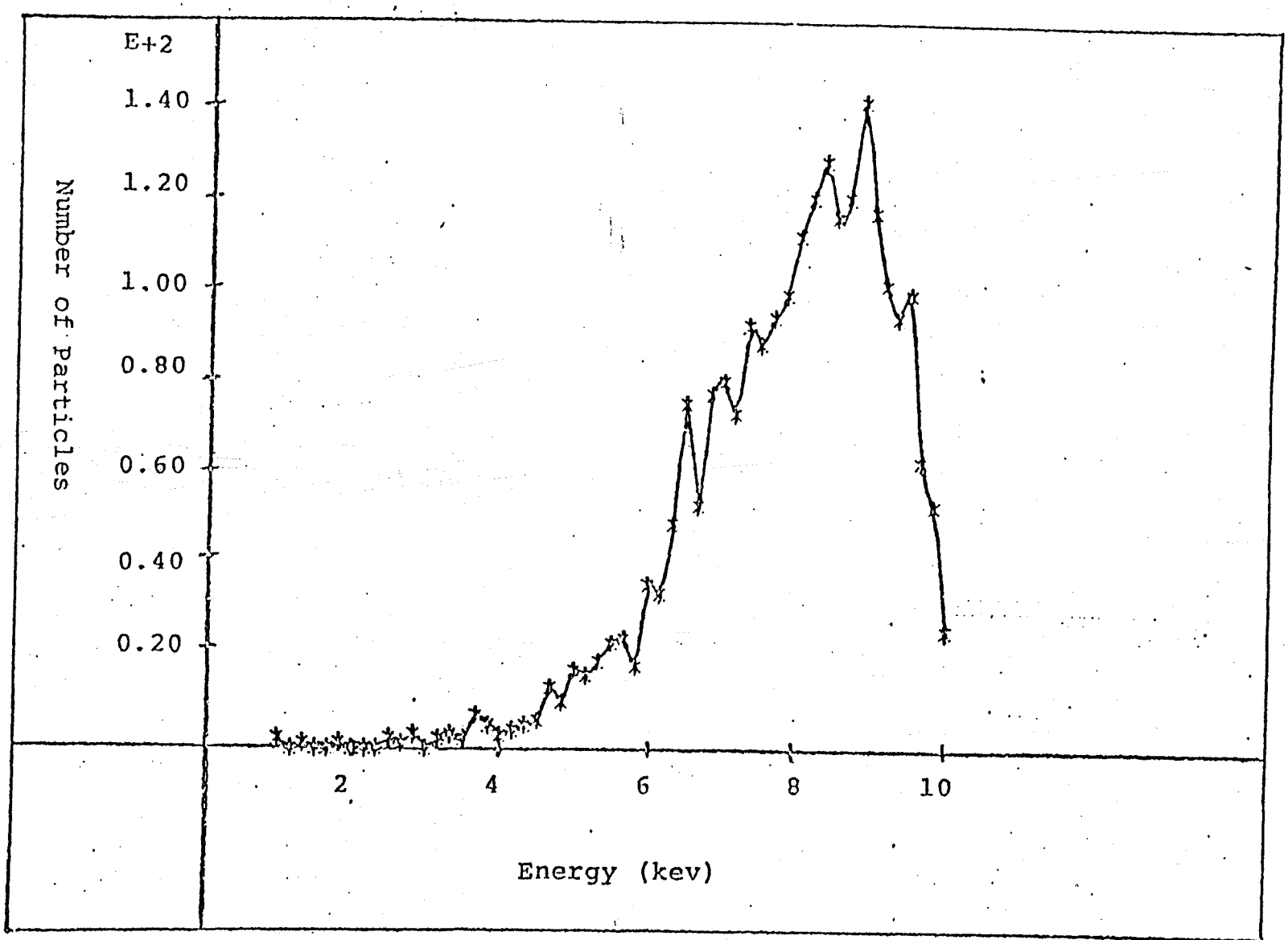

Figure 2. Ion Energy Distribution for a 10 Kev Ion Beam Incident on a 2×10^{14} cm^{-3} Hydrogen Gas Density and Influenced by a 9 Kev Potential.

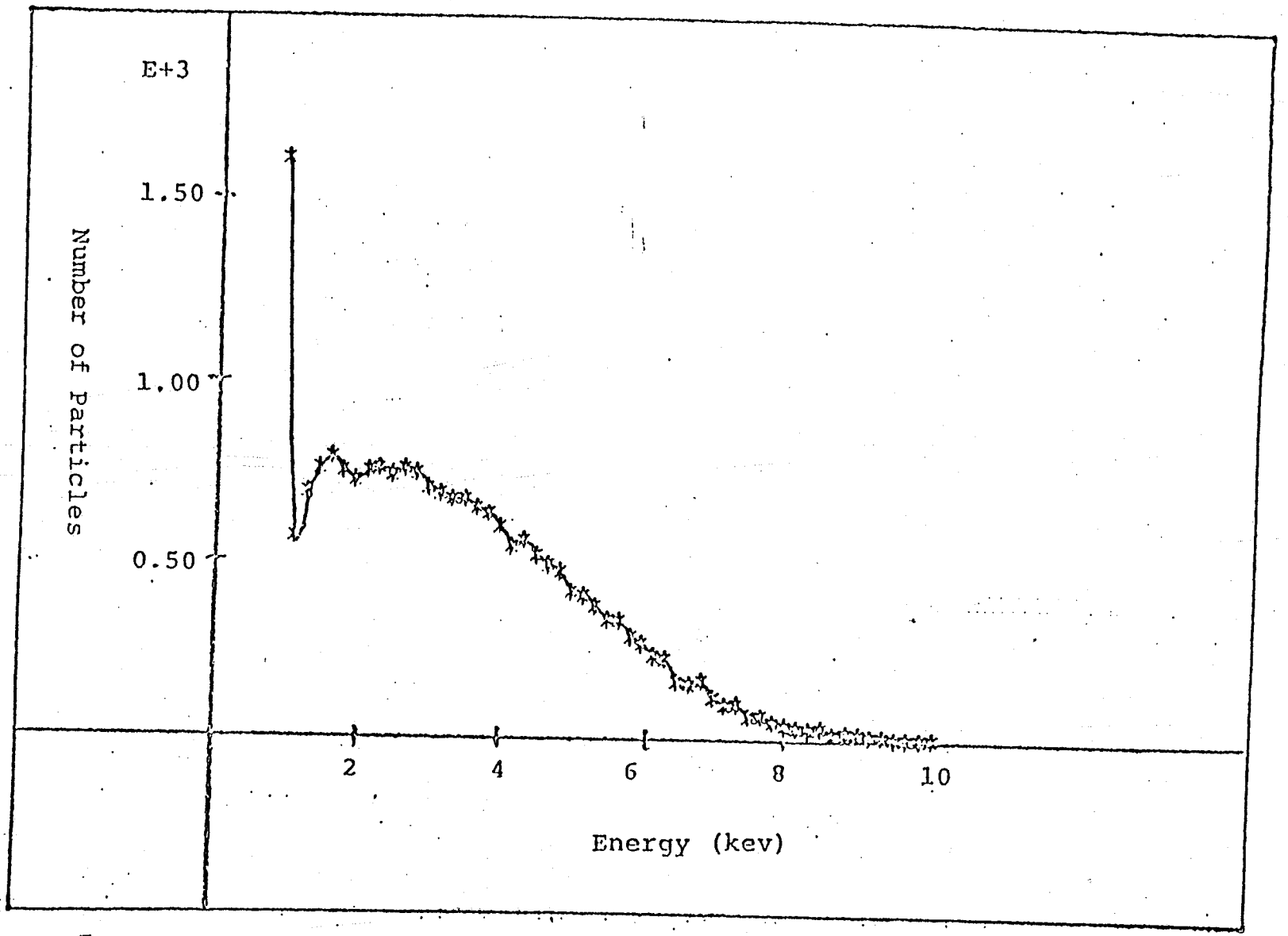

Figure 3. Ion Energy Distribution for a 10 Kev Ion Beam Incident on a 10^{15} cm^{-3} Helium Gas Density and Influenced by a 9 Kev Potential.

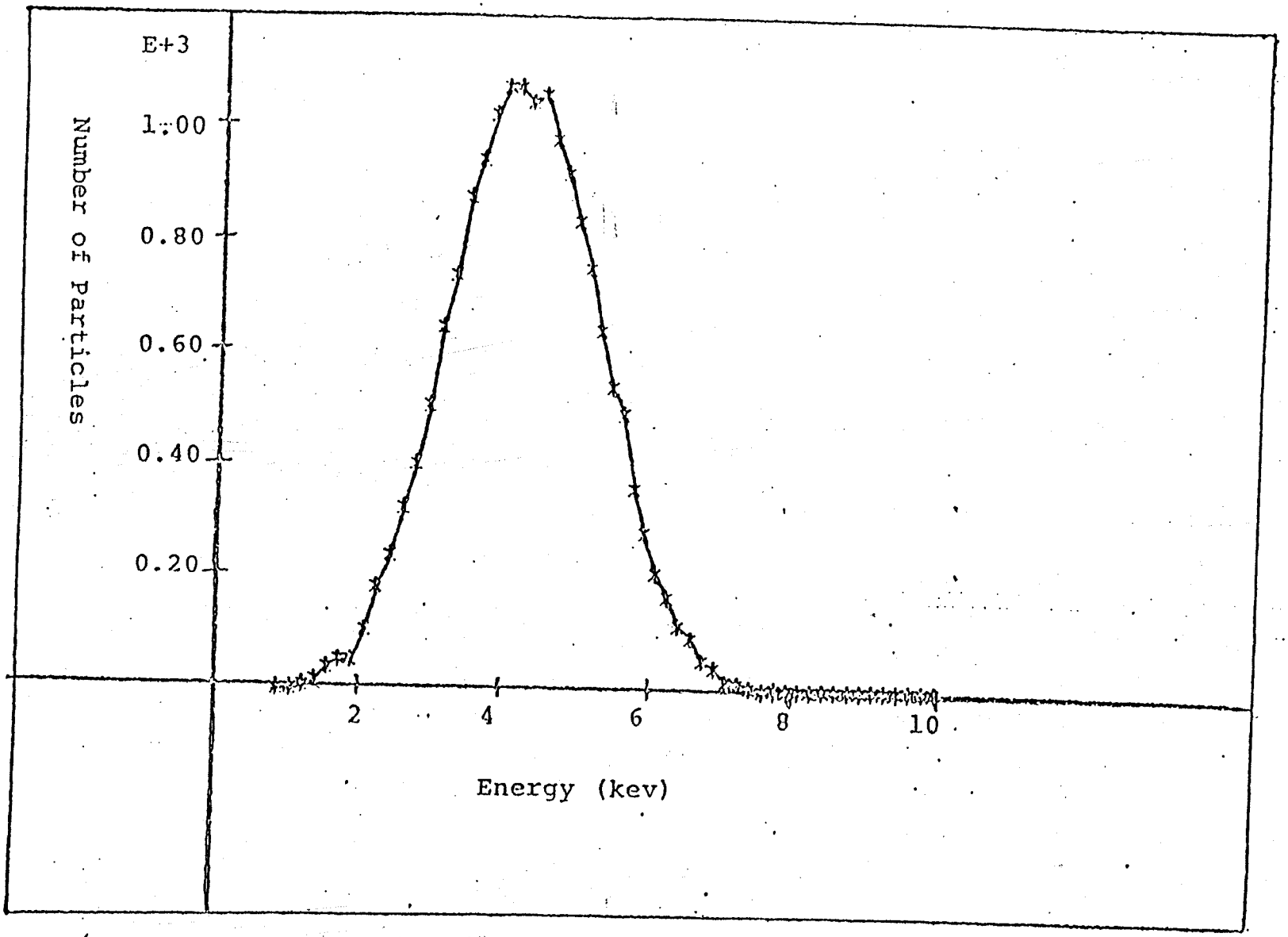

Figure 4 . Ion Energy Distribution for a 10 Kev Ion Beam Incident on a 4×10^{15} cm^{-3} Helium Gas Density and Influenced by a 9 Kev Potential.

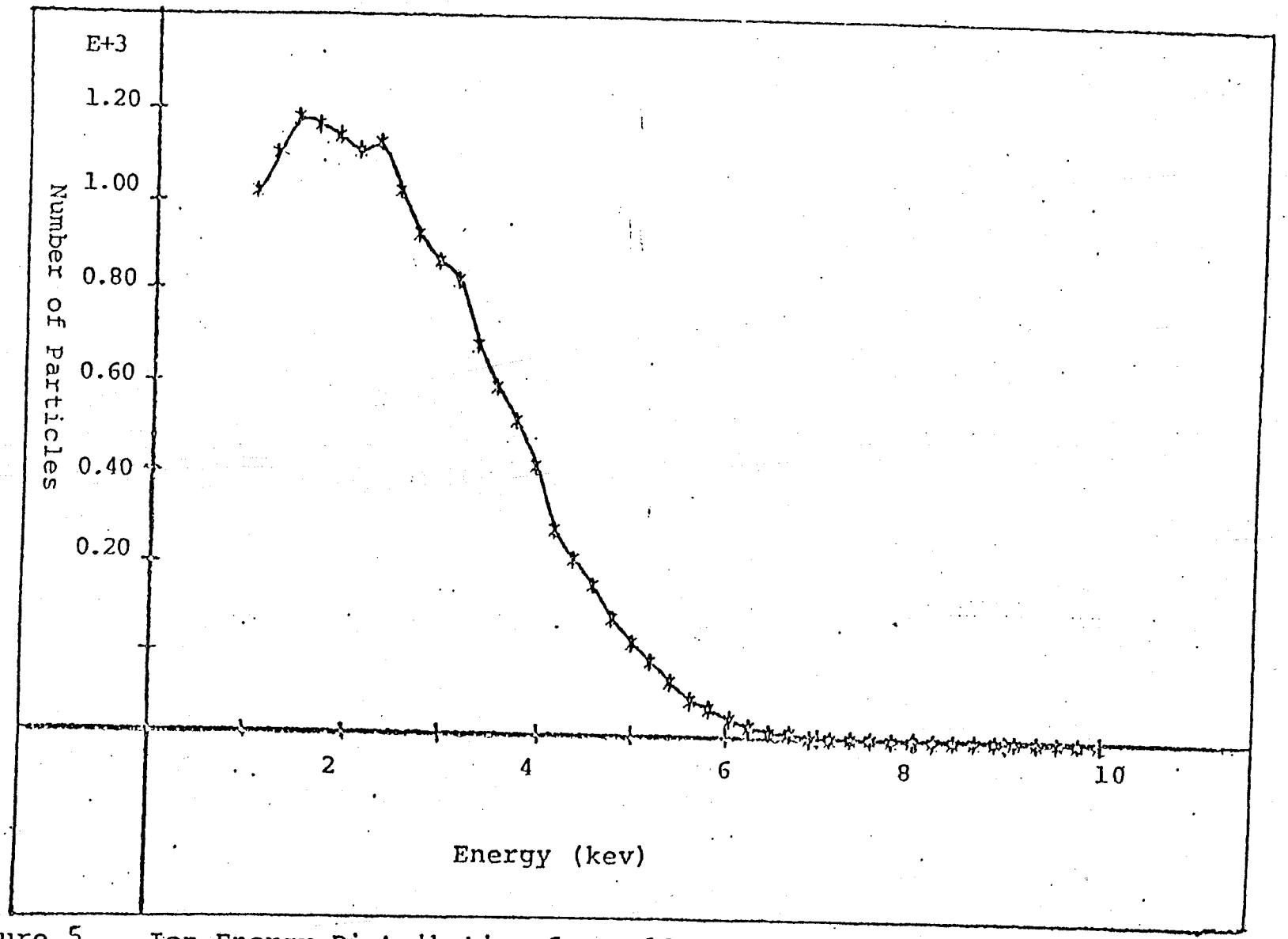

Figure 5 . Ion Energy Distribution for a 10 Kev Ion Beam Incident as a 3×10^{15} cm^{-3} Helium Gas Density and Influenced by a 11.5 Kev Potential.

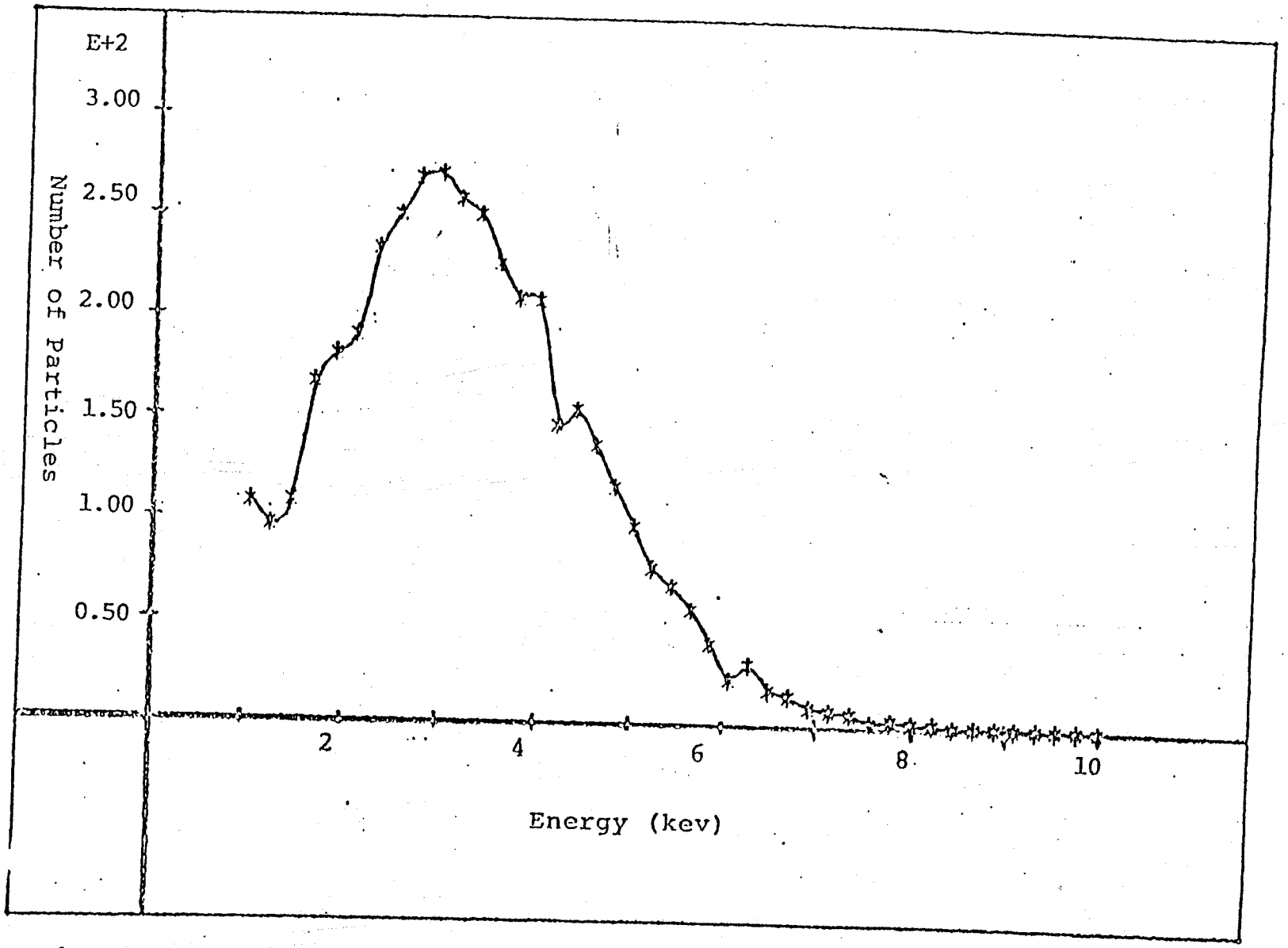

Figure 6 . Neutral Energy Distribution for a 10 Kev Ion Beam Incident on a 3×10^{15} cm^{-3} Helium Gas Density and Influenced by a 11.5 Kev Potential

The trends shown by these figures can be understood as follows:

1) Gas density: For low densities, the neutral mfp is large. Thus incident ions tend to pass through without any interactions (leaving at the incident minus potential voltage) or with a single neutralizing interaction. The resulting ion energy distribution is monoenergetic. As the density increases, a Maxwellian ion energy distribution forms as sufficient interactions occur in the gas cell. The peak of this distribution is higher than at the monoenergetic ion exit energy since the fraction of time spent as neutrals is spent without the retarding potential. Thus increasing the density, while it does better thermalize the spectrum, is limited in its ability to reduce the peak energy to the desired 1 to 2 keV.

2) Incident Ion Energy: Decreasing the ion energy lowers the Maxwellian energy peak simply because the starting energy is less. The lower bound here is set by the practical requirements for producing 0.2 A/cm^2 beams.

3) Gas: For gases such as H_2, the neutralization cross-section is much larger than the ionization cross-section. Consequently, the interacting particles spend much more time as neutrals than as ions, feel the retarding potential less, and thus produce a Maxwellian energy distribution at higher energies than desired. No gas seems to have a dominant ionization cross-section, but in helium the ionization and neutralization cross-sections are relatively comparable over 1 to 30 keV.

4) Retarding potential: Increasing the potential will reduce the ion energy. Increasing it too much will cause backstreaming.

Conclusions

Based on the numerical trials, it was found that a 10 keV H^+ ion beam passing through a 0.54 cm He gas cell at $3.0 \times 10^{15}/cm^3$ with a 11.5 keV retarding potential would produce a roughly Maxwellian energy distribution peaked at about 1.7 keV, with only about 14% particle loss as neutrals or back-accelerated ions.